A STUDY OF ECHELON FRACTURE SETS IN THE KILLARNEY IGNEOUS COMPLEX, KILLARNEY, ONTARIO

A STUDY OF ECHELON FRACTURE SETS IN THE KILLARNEY IGNEOUS COMPLEX, KILLARNEY, ONTARIO

By

PAULA MACKINNON

A Thesis

Submitted to the School of Graduate Studies

in Partial Fulfilment of the Requirements

for the Degree

Master of Science

McMaster University

August, 1988

MASTER OF SCIENCE (1988) McMASTER UNIVERSITY
(Geology) Hamilton, Ontario

TITLE: A Study of Echelon Fracture Sets in the Killarney Igneous Complex, Killarney, Ontario

AUTHOR: Paula MacKinnon, B.Sc. (Queen's University)

SUPERVISOR: Dr. P.M. Clifford

NUMBER OF PAGES: ix, 164

Abstract

The igneous rocks of the Killarney Complex, Killarney, Ontario exhibit numerous echelon fracture sets near their contact with mylonites of the Grenville Front. The echelon fracture sets are younger than the Grenville Front mylonites and are therefore part of the late brittle history of the Grenville Province. These fracture sets are confined to a small (5 km^2) area but display a wide range of orientations and morphologies. They can be divided into four peak orientations and these can be compared with inferred stress states for several periods in the tectonic history of the Grenville Province from 1200 Ma to the present. Based on these orientations and other observations it is suggested that the echelon fracture sets formed over a period of time spanning the end of the Grenvillian Orogeny (1000 Ma) to the beginning of Ottawa-Nippissing rifting (post 575 Ma).

Measurement of the geometrical characteristics of the echelon fracture sets and comparison with those quoted in the literature has led to the conclusion that the geometry of an echelon fracture set does not unequivocally indicate its origin or mode of formation.

Current models using fracture-zone angle and overlap ratio for the classification of echelon fracture sets seem to be unapplicable to the echelon fracture sets examined in this study and must be used with caution. The echelon fracture sets studied here are interpreted to have formed in "shear zones" and to consist of dominantly tensile fractures. Some of the fractures have originated as shear fractures or have undergone shearing at some point in their history.

Acknowledgements

I would like to thank Dr. P. M. Clifford for supervising this thesis and for his support and help throughout its preparation. Much thanks go to my office mates, John Ferguson and Bill Buhay, and to Franco Marcantonio who have kept my spirits up throughout the last two years with many trips to the pub. I would also like to thank Gordon Kribs for his capable assistance in the field.

My thanks go to all the people at Erindale who have allowed me to hang around, become semi-computer literate, and participate in many stimulating discussions. Dr. G. W. Pearce, Dr. R. M. Stesky and Dr. P.-Y. F. Robin have all freely lent their expertise concerning matters ranging from microcomputers to philosophy. I would especially like to thank Dr. R. M. Stesky for many enlightening discussions on fracturing and for the use of his circular histogram program.

For all his help, patience, and his frequent reminders of "Don't Panic" I am particularly indebted to Frank Fueten.

This research was supported by an NSERC research grant to Dr. P.M. Clifford.

Table of Contents

List of Figures

List of Tables

1.0 Introduction

1.1 Purpose

Fractures are present in nearly all rocks. The patterns they create are often complex and may be due to a long history of brittle deformation. Fractures and joint sets have frequently been used as indicators of regional stress directions in the reconstruction of tectonic histories (Price 1966, Engelder et al 1980). However, the process of fracturing, from a microscopic to a macroscopic scale, is not fully understood. An example of this is the controversy surrounding the interpretation of echelon fracture sets. Several mechanisms have been proposed for the formation of echelon fracture sets and their interpretation in terms of local or regional stress directions is dependent on how they are perceived to form. Studies of echelon fracture sets to date have largely been confined to echelon vein arrays occurring in sedimentary rocks (Shainin 1950, Roering 1968, Hancock 1972, Beach 1975, Rickard and Rixon 1983, Ramsay and Huber 1983, and Bahat 1986). This study deals with echelon fracture sets in volcanic/plutonic rocks of the Killarney Igneous Complex at their contact with gneisses of the Grenville Province.

The purpose of this study is to examine in detail a group of echelon fracture sets. Particular attention has been directed at the geometry of the echelon fracture sets as well as their orientations. The fracture sets represent a brittle phase of the tectonic history of the Grenville Province and as such they may provide additional information about this history. More generally, this study may provide further information regarding the formation and interpretation of echelon fracture sets.

1.2 Regional Geology

The study area is located on the boundary between rocks of the Killarney Igneous Complex and gneisses of the Grenville Province (Fig. 1.1). This boundary, known as the Grenville Front, is locally expressed as mylonites which are the result of thrusting of Grenville Province rocks over the Killarney Complex between 1650 Ma and 1150 Ma (Davidson, 1986).

The Killarney Igneous Complex, which consists of volcanic and silicic-plutonic rocks, intrudes Huronian metasedimentary rocks at its northwest margin and is itself deformed at its southeast margin by activity on the Grenville Front. The Killarney Complex, dated at 1740 Ma (Davidson, 1986), was deformed prior to the Grenvillian Orogeny. This is inferred from foliation and lineation attitudes within the Killarney Complex which differ sharply from those in the Grenville Province but which swing into strike parallelism with Grenville age structures as the Grenville Front mylonites are approached. The Killarney Complex has been interpreted as a high-level volcanic-plutonic association similar to other middle Proterozoic terranes in mid-continental North America (Davidson, 1986).

Fractures within the Killarney Complex post-date the Grenvillian Orogeny since they are found cutting mylonites of the Grenville Front. The fractures and echelon fracture sets may be correlated with major lineaments in the Grenville Province (Stesky and Bailey-Kryklywy, 1988). This may allow interpretations to be made about their origin relative to the tectonic history of the Grenville Province from 1200 Ma to the present.

1.3 Location, access and methodology

The study area is located on the north shore of Georgian Bay, Ontario, approximately 10 kilometres east of the village of Killarney (Fig. 1.2). It consists of

Figure 1.1

Regional geology and location of study area.

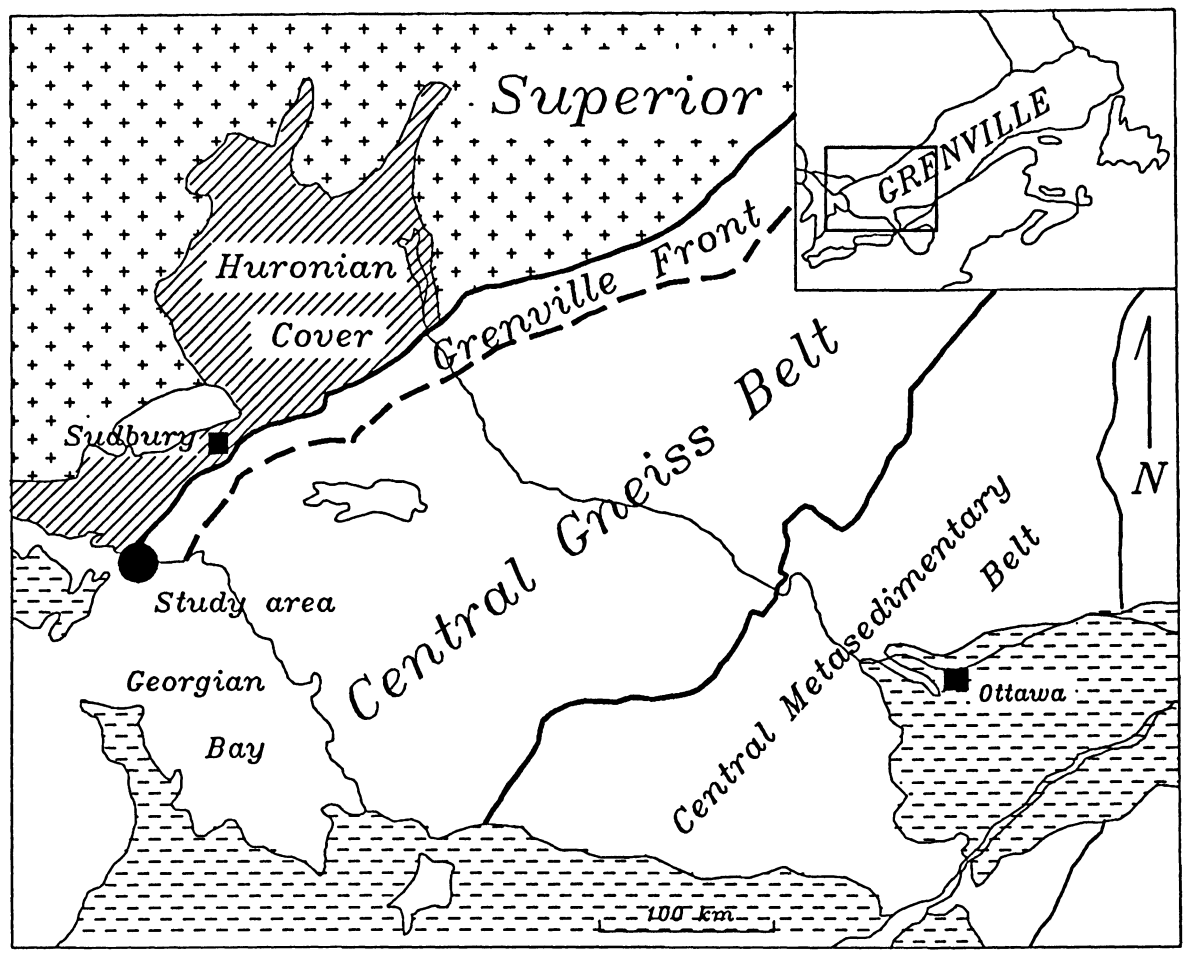
Superior
Huronian
Cover
Grenville Front
GRENVILLE
Sudbury
Central Gneiss Belt
N
Study area
Georgian
Bay
Central Metasedimentary
Belt
Ottawa
100 km

Figure 1.2

Geological map of the area around Killarney, Ontario.

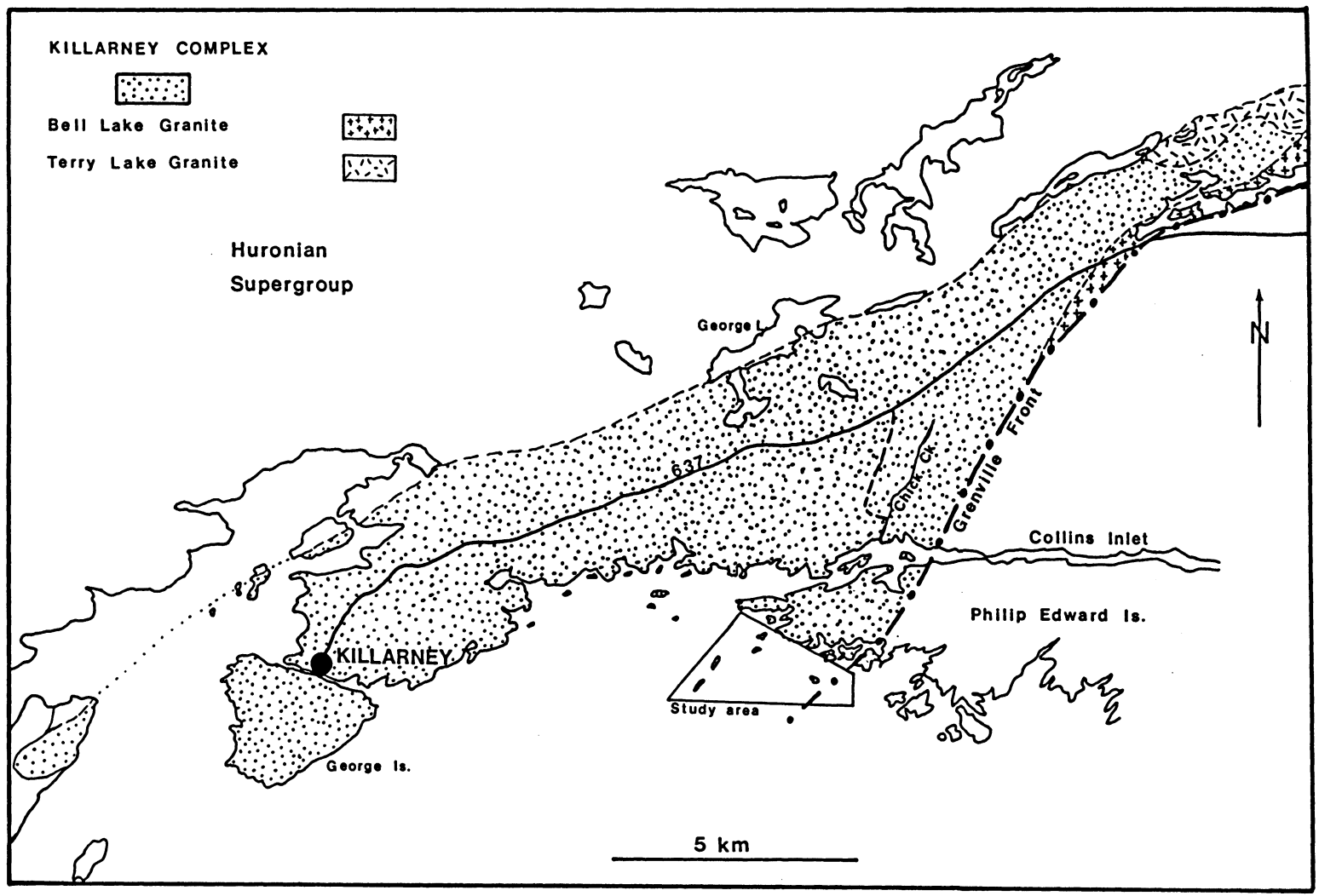
KILLARNEY COMPLEX
Bell Lake Granite
Terry Lake Granite
Huronian
Supergroup
George L.
637
Chiek Ck.
Grenville Front
N
Collins Inlet
Philip Edward Is.
KILLARNEY
Study area
George Is.
5 km

several small islands scattered over an area of roughly 5 square kilometres, at and around the Grenville Front mylonites. The outcrops are smooth and clean due to glacial erosion and water action and provide excellent exposure. An added bonus is the beauty of the scenery which competes with the geology for attention (Fig. 1.3).

Access to the study area was by outboard motor boat through Chickanishing Creek and Collins Inlet (Fig. 1.2). Exposure on the islands is close to 100% and detailed mapping of fractures was possible. Some of the islands contain numerous echelon fracture sets. Twenty-three stations were established where detailed fracture measurements were made (Fig. 1.4).

There are some general problems associated with mapping fractures. A common problem is the overwhelming abundance of fractures. Accordingly, there are several approaches to mapping a specific area. The first is to randomly measure fractures within the area. Given the fact that any sampling is never completely random, this approach may or may not produce a representative group of measurements for a given area. It does not provide detailed information on the relationship between various fractures. Another approach is to measure all fractures that cross a given line or that are contained within a given circle. This allows greater objectivity in mapping and ensures that a better distribution of fractures will be measured. The most comprehensive approach is to measure and produce a detailed map of all the fractures present within a given area. This is by far the best method but it is not practical for mapping large areas. The methodology used in this study was to produce detailed fracture maps on a selected number of outcrops. Mapping of the rest of the area was accomplished by measurements of selected features.

Another problem with mapping fractures is the degree of three-dimensional exposure. If the outcrops are primarily sub-horizontal surfaces, as is the case at Killarney, then there is the possibility that many sub-horizontal fractures will go unmeasured. Fortunately, the majority of fractures at Killarney are sub-vertical which allows them to

Figure 1.3

A typical wave-washed outcrop in the study area.

Figure 1.4

Map of the study area with station locations.

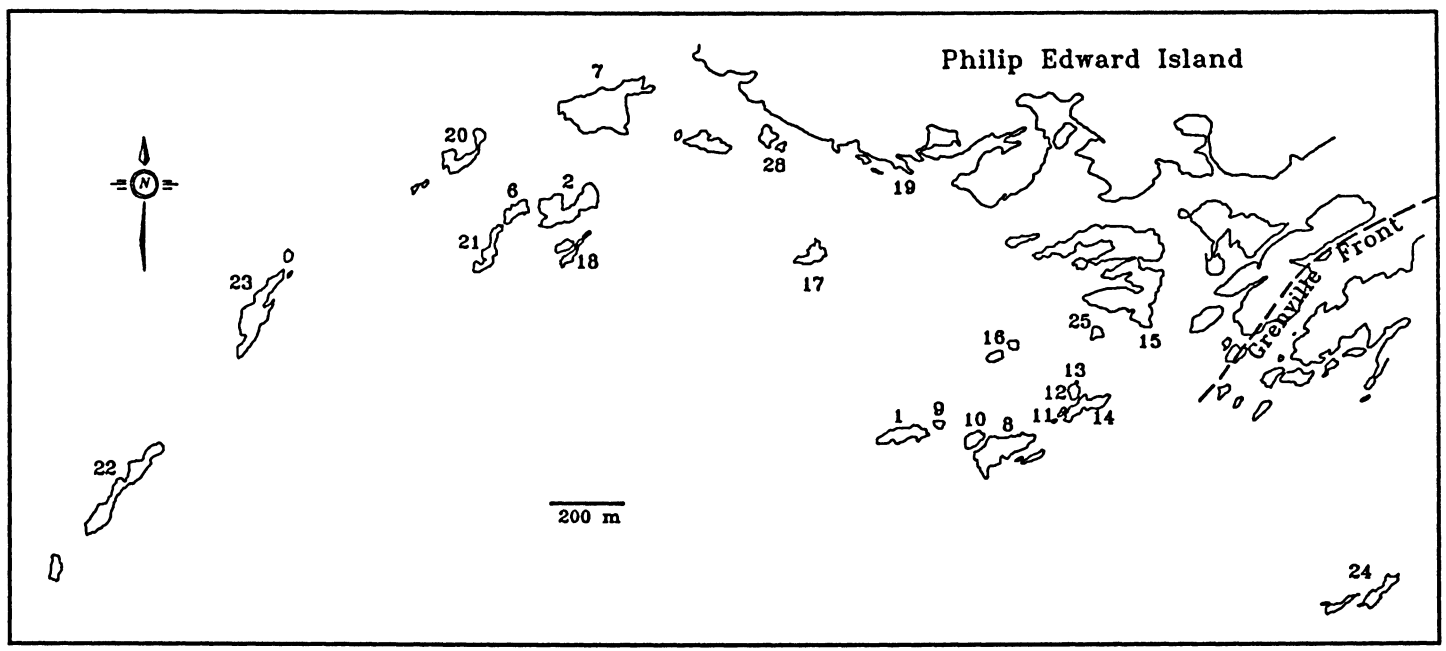
Philip Edward Island
N
7
20
28
19
6
2
21
18
17
23
25
15
16
Grenville Front
13
12
11
14
1
9
10
8
22
200 m
24

be mapped as traces on sub-horizontal surfaces. With smooth sub-horizontal outcrop surfaces the measurement of fracture strike is relatively easy but fracture dip is not. In many cases the fracture surface was partially exposed due to weathering and this allowed a straight edge to be placed along the surface and the dip measured. The measurement of the attitude of the echelon fracture sets themselves was also complicated by the lack of vertical exposure in Killarney. This will be discussed further following an outline of the definitions used in measuring echelon fracture sets.

An echelon is a steplike arrangement of units with each unit stepping to the left or right of the one in the rear. If each unit is planar then the echelon will have one general direction but individual planar units will be parallel to each other and at an angle to the general direction. In order to describe completely the characteristics and orientation in space of an echelon of planar elements a precise terminology must be adopted. The following classification and description for fractures arranged en echelon is modified from Pollard, Segall and Delaney (1982).

For the purposes of this study, fractures of approximately equal dimensions, spacing and orientation arranged en echelon will form an echelon zone (Fig. 1.5). Each zone is itself a planar feature having a strike or a trend on the outcrop surface. A zone is defined as right-stepping (Segall and Pollard, 1980) if successive fractures step to the right when viewed along the strike of an individual fracture. In left-stepping zones successive fractures step to the left. The acute angle between the trend of the zone and the strike of individual fractures is defined as the fracture-zone angle; this is arbitrarily positive for right-stepping zones and negative for left-stepping zones. The length of fractures, step or spacing between fractures, and overlap of fractures are defined as shown in Figure 1.5. Using this terminology the geometry of an echelon array may be described without implying a particular origin for the array.

The basic information recorded for every echelon fracture set mapped in the field was: 1) the trend of the fracture set on a sub-horizontal outcrop surface, 2) the average

Figure 1.5

A schematic diagram of echelon fracture sets.

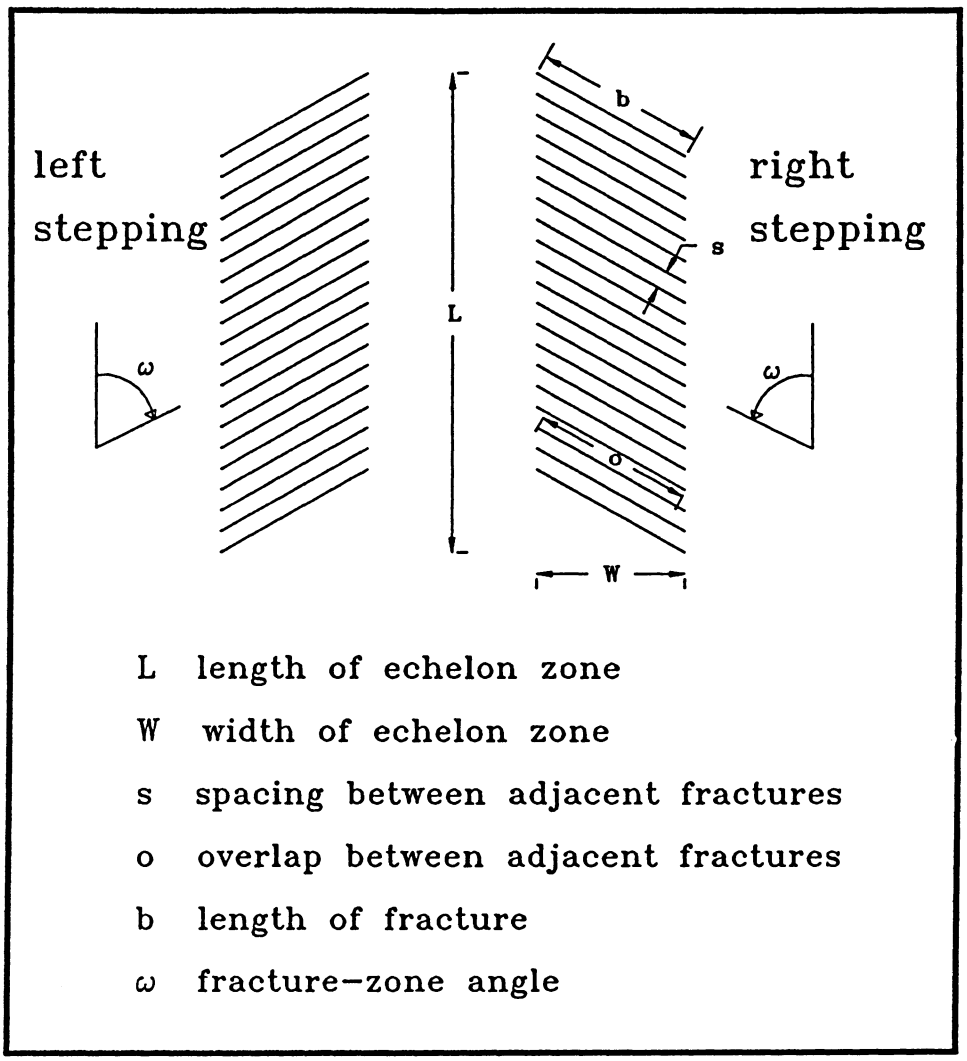

L length of echelon zone

W width of echelon zone

s spacing between adjacent fractures

o overlap between adjacent fractures

b length of fracture

ω fracture–zone angle

orientation of its fractures, and 3) its sense (right-stepping or left-stepping). An echelon fracture set is a planar feature but lack of vertical exposure prevented complete measurement of its attitude. Where echelon fracture sets were exposed in vertical outcrops they appeared to be sub-vertical in attitude.

Additional measurements were made on selected echelon fracture sets. The parameters commonly measured included: length of the echelon fracture set, width of the set, a representative fracture length or several fracture lengths, a representative fracture step or several fracture steps, and a representative fracture overlap or several fracture overlaps. Observations included the nature of fracture terminations, sense of shear on individual fractures, the degree of hematite staining surrounding fractures, the dilatancy of the fractures, and the nature of the fracture filling.

In addition to echelon fractures sets, measurements routinely were made of isolated fractures or fracture sets, shear fractures, ductile shear zones, foliation, dykes, and quartz veins. At some localities, survey grids were laid out by Brunton compass where it was felt a detailed map of all the fractures present would be useful. These areas were mapped at a scale of 1:50. Still more detailed surveys were made of individual fracture sets at a scale of 1:5.

Samples of rock containing fractures were obtained when possible. Several samples were drilled using a portable hand-held drill. This proved useful only on fracture sets more resistant to weathering with intact fracture fill. In general the wave-washed nature of the outcrop inhibited sampling but allowed for excellent photographic opportunities.

2.0 A Review of Fracturing and Echelon Fracture Sets

2.1 Fracturing

2.11 Introduction

Fractures at the macroscopic scale are generally considered to initiate and propagate from pre-existing microcracks. The orientation and geometry of fractures may reflect the orientation and magnitude of macroscopic stresses (or strains). This chapter reviews the initiation and propagation of fractures and controls on their geometry. This will involve a consideration of microcracks, their formation and growth, fracture mechanics and its application to crack propagation, the fracture process zone, fracture geometry, and the growth of fracture sets.

2.12 Microcracks

Microcracks in rock have been extensively studied and this literature has been comprehensively reviewed by Kranz (1983). Microcracks can be defined as openings in rock less than 100 microns in length with an aspect ratio of less than 10^{-2}. They can be classified into four types: grain boundary cracks, intracrystalline cracks, intercrystalline cracks, and cleavage cracks. The formation of microcracks is dependent on local stresses induced mechanically or thermally.

There are at least six mechanical mechanisms that produce microcracks and they include the following: 1) twin interactions, 2)kink bands and deformation lamellae, 3) cleavage separations, 4) stress concentrations at grain boundaries and cavities, 5) elastic differences between adjacent grains, and 6) grain translations and rotations. Microcracks are also produced by differential thermal expansion between grains of varying anisotropy orientations or varying thermal properties. For granites, thermally induced microcracking

begins above a critical temperature of 70°-75°C. The majority of microcracks appear to be extensional since shear offsets along microcracks are rarely observed. It seems likely that microcracks will be ubiquitous in all polycrystalline rock and will serve as loci for fracture growth in subsequent tectonic stress regimes.

The response of microcracks to changes in the stress field has been documented. If hydrostatic pressure is increased porosity will decrease and microcracks will close. For dry rocks, hydrostatic pressures exceeding 100-200 MPa will effectively close all microcracks (Kranz, 1983). The effect of imposing hydrostatic pressure on a deviatoric stress field is to decrease the deviatoric stresses near crack tips and increase friction between crack surfaces. This inhibits crack propagation and means that microcracks are more stable under higher hydrostatic pressures. If a deviatoric stress field is imposed on microcracks then their orientation becomes important in determining which cracks propagate. The principles of fracture mechanics can then be applied to the growth of isolated microcracks.

2.13 The stress state around a microcrack

Stresses acting at a crack tip can be modelled using fracture mechanics. The simplest model assumes linear elastic behaviour and considers the case of the "mathematic crack". This is a flat, sharp crack of zero thickness (Jaeger and Cook, 1976). Applied stresses can be broken down into stress components acting on the crack tip. By definition, the Z direction is parallel to the crack tip, the Y direction is perpendicular to the crack plane, and the X direction is perpendicular to the crack tip but within the crack plane. The stress components are inversely proportional to the square root of the radial distance, r, from the crack tip.

Under loading, there are three modes of distortion that can be imposed on a crack tip. Mode I is displacement in the Y direction (tensile). Mode II is displacement in the X direction (in-plane shear). Mode III is displacement in the Z direction (anti-plane

shear) (Fig. 2.1). The magnitude of the stress components for a particular mode are given by the stress intensity factors, k_I, k_{II}, and k_{III}. These are scaling factors which are dependent on the applied stress and the crack length. Therefore a stress component is equal to a distribution function multiplied by a stress intensity factor.

An alternative approach is to consider the crack extension force, G, or strain energy release rate. This is defined as the loss of elastic strain energy and potential energy of the loading system per unit of new crack surface area formed for an increment of crack extension (Atkinson, 1987). The crack extension forces for the three modes of crack tip distortion under plane strain are G_I, G_{II}, and G_{III}.

Through stress intensity analysis or crack extension force analysis, the distortion and stresses acting on a crack tip may be modelled. This then allows an evaluation of the conditions necessary to initiate propagation of the crack.

2.14 Critical parameters for crack propagation

There are two regimes under which crack growth may occur. The first is the equilibrium condition which requires that cracks grow stably or unstably at speeds approaching that of sound when some critical value of a fracture mechanics parameter is reached. The second is the kinetic condition in which the crack grows at a rate that is dependent on the crack driving force. This occurs at subcritical values of fracture mechanics parameters and is known as "subcritical crack growth" (Atkinson, 1987).

For equilibrium crack growth, the critical parameters commonly used in fracture mechanics are critical stress intensity factors, k_{Ic}, k_{IIc}, k_{IIIc}, and critical crack extension force, G_c (Atkinson, 1987). Critical stress intensity factors can be determined experimentally which allows them to be used to compare the "fracture strength" of different materials (Paterson, 1978). The critical crack extension force can be expressed in terms of the critical stress intensity factors. In this assessment the crack is considered to be growing in equilibrium and dynamic effects due to the kinetic energy of the

Figure 2.1

Mode I, II and III distortions on a crack tip (modified after Paterson 1978).

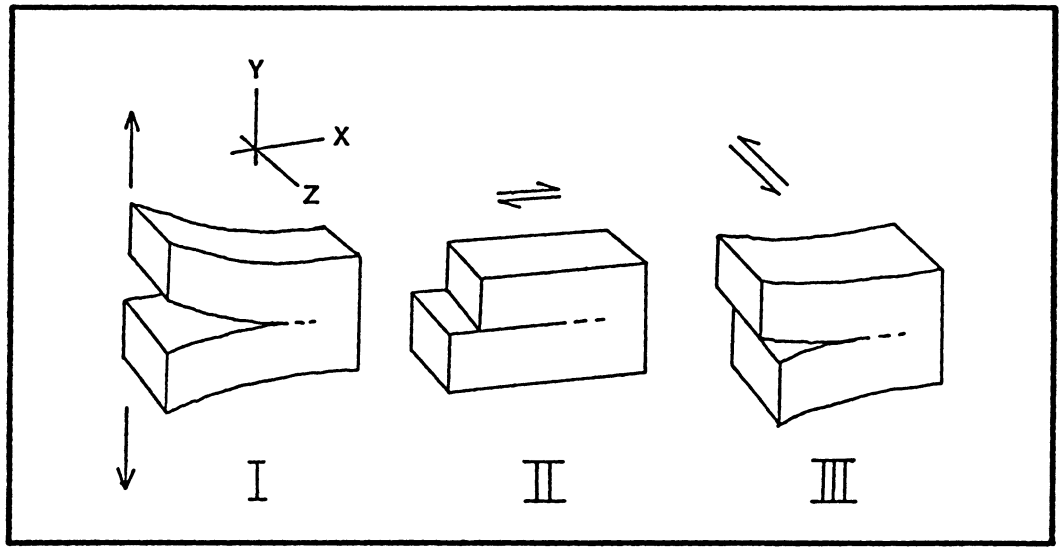
Y
X
Z
I
II
III

propagating crack are not considered. If dynamic effects are to be considered this involves the use of dynamic stress intensity factors (Paterson, 1978).

Subcritical crack growth does not take place in equilibrium and occurs at values of k and G below their critical values. The most common mechanism considered to induce subcritical growth is stress corrosion. This process is the chemical weakening of the crack tip through hydration. For silicate/water systems the reaction may be:

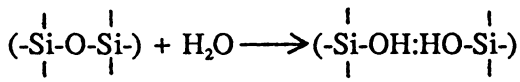

(Atkinson, 1982). In this reaction the Si-O bonds are replaced by weaker H-H bonds. This effectively reduces the energy required to propagate the crack tip. The rate of crack growth will be dependent on the rate limiting step in the process of stress corrosion. The steps in stress corrosion are: 1) migration of reactants to the crack tip (limited by permeability and diffusion rates), 2) adsorption of the reactants (limited by diffusion rate), 3) the hydrolysis reaction (limited by kinetics of the reaction), 4) migration of products away from the crack tip (limited by permeability and diffusion), and 5) breaking of the hydrogen bonds (Anderson, 1977). It is still unclear which is the rate-limiting step in this process (Anderson, 1977). What can be stated is that the velocity of subcritical crack growth is some function of the stress intensity and crack extension force and that the form of the function is dictated by the chemistry of the stress corrosion process (Atkinson, 1987).

The discussion until now has considered only linear elastic fracture mechanics although it is clear that non-elastic processes may be acting at the crack tip (ie. stress corrosion). It may be advantageous, therefore, to consider non-linear elastic behaviour at the crack tip, such as that which occurs in the fracture process zone.

2.15 The fracture process zone

The inelastic region at an advancing crack tip is known as the fracture process zone (Labuz et al, 1987). The inelastic behaviour can be caused by microcracking in the crack tip region or by plasticity (Atkinson, 1987). The fracture process zone has been observed on a macroscopic scale with dyke intrusion (Rogers and Bird, 1987) and has been measured on a microscopic scale in experiments (Labuz et al 1987, and Atkinson 1987).

If the process zone is large enough relative to the crack length, then linear elastic fracture mechanics must be modified to compensate for energy used in creating the process zone (Labuz et al, 1987). This is done by considering an effective crack length, which includes a portion of the process zone, when calculating fracture mechanics parameters.

Atkinson (1987) shows how microcracking in a process zone influences fracture propagation. With increasing tensile stress, microcracking becomes intense in the process zone and some microcracks link up. This allows propagation of the fracture by linking of the microcracks. The fracture process zone migrates ahead of the advancing fracture and a cloud of microcracks is left along each side of the newly formed fracture.

Labuz et al (1987) have measured the fracture process zone in granite by ultrasonic probing and acoustic emmision. They found that the length of the process zone depended on the grain size of the fractured rock. For a granite with an average grain size of 1 mm the process zone was 40 mm long and for a grain size of 10 mm the process zone was 90 mm long.

At the outcrop scale, Rogers and Bird (1987) observed a greater abundance of fractures close to dyke margins. They interpreted these fractures as coeval with dyke emplacement. They modelled the stress distribution around a propagating dyke for specific loading conditions and determined the size of the tensile stress zone, analogous to the fracture process zone, around the dyke tip. This zone is elliptical in cross-section and extends for 1 to 5 metres into the host rock perpendicular to the trend of the dyke.

This discussion indicates the importance of a fracture process zone to fracture propagation. The process zone can occur at all scales and the linking of smaller fractures to form larger throughgoing fractures has been documented (Segall and Pollard, 1983).

2.16 Fracture propagation and resultant geometry

The growth of an individual fracture

Often the terminations of fractures or the structures on fracture surfaces give an indication of the history of fracture propagation (Engelder 1987, Ryan and Sammis 1978, Hodgson 1961). Structures on fracture surfaces indicate that fractures propagate from a point source or nucleus (Hodgson, 1961). In granitic rocks the nucleus of fracture propagation may be a large microcrack or a small fracture (Segall, 1984). A fracture may terminate in several ways. If the fracture is propagating at a critical high velocity it may branch, bifurcate, or form a hackle zone of en echelon cracks (Engelder, 1987). The hypotheses are that 1) a fracture propagating at terminal velocity distorts the stress field at its tip which causes the fracture to branch and propagate into a new plane or 2) at terminal velocity local stress intensity at the fracture tip is high enough to cause the formation of secondary fractures (Engelder, 1987). Branching and bifurcation of fractures at high velocities has been observed in experiments on glass (Lawn and Wilshaw, 1975). At the outcrop scale, branching of fractures into hackle zones of echelon cracks has been observed where fractures terminate at the boundaries of sedimentary beds (Hodgson 1961, Bahat 1986). This can be interpreted as branching of the fracture into a reoriented stress field that is induced locally by the sedimentary bed surface (Engelder 1987, Bahat 1986). Therefore it seems that fracture terminations do not unequivocally indicate the conditions existing during fracture propagation and must be used with care.

The propagation of fracture sets

Given a polycrystalline rock with a uniform distribution of randomly oriented microcracks, the problem of predicting the geometry of fracture sets resulting from the imposition of a stress field on the rock is complex. The local stresses acting on an individual crack subjected to a remote stress field can be modelled using fracture mechanics but the problem becomes complicated when more than one crack is involved. Numerous studies have been conducted that relate joints and faults to tectonic stress fields but with variable success. The complications result from the variability of rock properties and environmental conditions and the variability of the stresses involved, both in space and time.

One study that has been successful was conducted on regional joint sets on the Appalachian Plateau (Engelder and Geiser, 1980). The basic premise is that the joints propagate along the regional stress trajectories normal to the least principal stress. The success of the study is largely due to the fact that the tectonic and strain history of the area is well known through large scale structures and mesoscopic strain indicators. The timing of deformation is well constrained as the rocks are sedimentary and span a relatively short deformation history.

In general, far more studies have been done of joints and fractures in relatively undeformed and unmetamorphosed igneous and sedimentary rocks than in metamorphosed or complexly deformed rocks. This is not suprising. Extensive models have been devised to account for orientations of fractures in sedimentary basins and in folded sedimentary strata.

Joints are often found in sets which are defined as a group of two or more joints having a common characteristic, usually orientation (Engelder and Geiser, 1980). If their orientation is attributable to the stress field then one of the fundamental problems still to be addressed is what dictates the spacing of joints in a set.

In sedimentary rocks the spacing of joints may be linearly related to the thickness of the sedimentary bed they are contained in (Ladeira and Price, 1981). Ladeira and Price (1981) have compared bed thickness to fracture spacing in the bed and have divided the resulting curves into two components. The first is a linearly increasing relationship between fracture spacing and bed thickness (for bed thicknesses under a metre) that they attribute to traction at the interface between competent and incompetent layers. The second is a constant linear relationship in which fracture spacing is independent of bed thickness above a bed thickness of about a metre. They suggest this relationship results from hydraulic fracturing.

In a compressive stress regime hydraulic fracture occurs when the difference between the least compressive stress and the fluid pressure equals or exceeds the tensile strength of the rock. If a fracture forms in a sedimentary layer it will produce a fluid pressure gradient around it that will be dependent on the velocity of fracture propagation and the permeability of the unfractured rock (Ladeira and Price, 1981). This will inhibit the formation of fractures close to the first formed one as they will only form in a region far enough away to have sufficient fluid pressure for fracturing. Thus rocks with low permeability will have a narrow region of reduced fluid pressure surrounding a fracture and hence fractures may be closely spaced. Rocks with high permeability will have wider zones of decreased fluid pressure surrounding fractures resulting in widely spaced fractures (Ladeira and Price, 1981). This theory may hold for rocks with significant permeability, such as sedimentary rocks, but seems less likely to be applicable to massive rocks like granite. Given that any granite will have a finite, although low, permeability this theory predicts that fracture spacing will be small in the granite.

Joint sets in granitic rocks may also exhibit a regular spacing that cannot be readily attributed to any one factor (Segall and Pollard 1983). Segall (1984) has addressed the problem of what controls final fracture set geometry by modelling the formation and growth of a fracture set using linear elastic fracture mechanics. This is a simplified

approach to a very complex problem as many closely spaced fractures will have non-linear elastic interactions.

Segall and Pollard (1983) have described subvertical joint sets that are well-exposed in granitic rocks of the Sierra Nevada. These joint sets contain fractures of apparently dilatant origin that have similar orientations. The wall rock surrounding the joints is hydrothermally altered indicating that the fractures may have been filled with fluids as they formed (Segall and Pollard, 1983). They found no evidence of branching of fracture terminations and concluded that the fractures propagated slowly (at less than terminal velocity). These observations form the basis for Segall's (1984) assumption that the fractures propagated by subcritical crack growth due to stress corrosion of the fracture tip by aqueous fluids.

Segall models the conditions for crack growth using the parameter crack extension force, G. A crack will propagate if it reaches a critical value of crack extension force that is equal to or greater than the fracture surface energy per unit area, Γ (Segall, 1984). However, stress corrosion of the fracture surface will decrease the fracture surface energy term to a value given by Γ^*. This gives a range of values of crack extension force that result in subcritical crack growth; given by the expression:

$$2\Gamma^* \leq G \leq 2\Gamma$$

If $G > 2\Gamma$ then dynamic (equilibrium) crack growth occurs with fractures propagating at high velocities. An expression for G can then be derived for an individual crack within a system.

The system is modelled as an array of cracks of equal length, $2c_o$, contained in an elastic medium which is subjected to a constant displacement (2-D plane strain) in one direction. All of the cracks are oriented perpendicular to the applied extension direction. This means each crack is subjected to mode I (tensile) displacements only. To represent the effect of other cracks on an individual crack, the other cracks can be separated into a

local group, which interacts with the crack in question, and a remote group, which can be represented as an orthotropic medium with an effective Young's modulus, $\tilde{E}$. The effect of the local group of cracks is represented by the stress intensity factors, k_I and k_{II}, that account for the crack interactions. Now the crack extension force, G, for any crack in this system with a half length c can be expressed by the following equation:

$$G_{(c)} = \frac{\pi(1-\nu^2)}{E} (k_I^2 + k_{II}^2) \left[\frac{\tilde{E}\Delta\epsilon}{(1-\nu^2\tilde{E}/E)} + \Delta p \right]^2 c$$

$\Delta\epsilon$ = change in remote strain

ν = Poisson's ratio

E = Young's modulus of unfractured rock

$\tilde{E}$ = effective Young's modulus of fractured rock

Δp = change in internal fluid pressure

c = 1/2 crack length

(Segall, 1984).

Once crack propagation begins, G is dependent on five variables: 1) increase in crack length (c), 2) change in applied strain ($\Delta\epsilon$), 3) changing elastic interactions with adjacent cracks ($k_I^2 + k_{II}^2$), 4) change in internal fluid pressure (Δp), and 5) changing effective stiffness of the system with crack growth ($\tilde{E}$) (Segall, 1984). These factors serve to increase or decrease G. With continued crack growth: crack length increases, change in strain is positive, elastic interactions vary, effective stiffness (Young's modulus) decreases and internal fluid pressure decreases (Segall, 1984). This means that generally G will increase with crack length and applied strain but will decrease with decreasing effective stiffness and decreasing fluid pressure. Segall suggests that the combined effect of these factors is to keep G more or less constant thus enabling subcritical crack growth to occur even after fracture lengths are long.

To model the effect of initial crack densities on the final geometry, the system just described can be modified. The initial assumptions are that all fractures have the same length at the same time, there are no crack interactions and that the internal fluid pressure is constant. For a given set of parameters, an arbitrary applied extension and $G = 2\Gamma^*$, Segall (1984) derives an expression for the equilibrium crack length. The result indicates that a change in crack length from an initial state to a final state depends on applied strain and initial crack density. This means that for a given strain the equilibrium crack length increases with decreasing initial crack density (Segall, 1984).

From this analysis Segall presents a scenario for the growth of fracture sets in extension. The initial state is of a rock containing randomly oriented and distributed microcracks with the internal fluid pressure equal to the least compressive stress. If a remote stress is imposed on the system, local stresses acting on the microcracks will vary and those microcracks with sufficient crack extension force will grow slowly. Eventually the cracks will be larger than the grain size of the rock and will form a subparallel array of cracks similar to the initial state of cracks in the above model. These cracks will then individually behave according to the equation given for crack extension force (Segall, 1984).

2.2 Echelon Fracture Sets

2.21 Introduction

A common geometry for fractures, veins and dykes in outcrop is echelon arrays. This geometry has been noted by many authors although there is no clear concensus as to their origin. Veins and dykes may be thought of as filled fractures so the essential problem is one of generating fractures in an echelon configuration. There are several different mechanisms proposed by different authors to explain observed geometries of echelon fracture arrays.

Echelon arrays can be divided into two categories: 1) echelon arrays derived from the branching of a parent fracture or dyke as it propagates into a reoriented stress field, and 2) echelon arrays that formed in a zone of localized strain. The first mechanism, proposed by Pollard et al (1982), considers a parent fracture propagating due to mode I (tensile) loading. The individual echelon fractures that form as the parent fracture propagates into a reoriented stress field are also tensile in origin (Nicholson and Pollard 1985, Bahat 1986). The second mechanism assumes the existence of a zone of localized strain. Within this zone conditions exist that cause the formation of echelon fractures of tensile or shear origin (Shainin 1950, Roering 1968, Lajtai 1969, Hancock 1972, Beach 1975, Rickard and Rixon 1983, Ramsay and Huber 1983). The mechanisms just described form a framework for a more detailed look at the echelon array geometries recorded in the literature and the mechanisms proposed for their origin.

2.22 Echelon arrays from parent fractures

Echelon fractures associated with parent fractures have been observed as hackles on the fringe of a joint face (Hodgson, 1961) and, in experiments with glass, as fracture lances from a main fracture (Sommer, 1969). They have also been described in the field by Bahat (1986). Pollard, Segall and Delaney (1982), based on the geometry of echelon dyke segments in Ship Rock, New Mexico (Delaney and Pollard, 1981) and a hand

sample of shale containing echelon fractures with a parent fracture, have analysed the breakdown of a parent fracture into an echelon array.

The starting assumption is of a parent fracture of a fixed length and infinite width contained in an elastic medium and subject to remote principal stresses. The fracture is oriented such that it lies in the principal plane containing σ_1 and σ_2 and is perpendicular to σ_3, the least principal compressive stress. The crack tip is then subjected to mode I deformation as it propagates. The next assumption is that the fracture propagates into a region where the remote stresses have rotated through some angle about an axis parallel to the propagation direction. This imposes a shear stress in the fracture plane and the crack tip is now subjected to mode I and mode III deformation. Near the crack tip the local minimum compressive stress has been rotated. As the fracture grows it will attempt to grow perpendicular to this local minimum stress. This involves twisting the entire fracture through some angle to realign it with the remote principal stresses. The surface area of an array of echelon cracks is less than the surface area of an intact fracture rotating through the same twist angle. Therefore it is energetically easier for the fracture to branch into an array of echelon cracks to accomplish this rotation (Pollard et al, 1982).

Pollard et al (1982) model the echelon fractures as helicoidal surfaces. By surface energy considerations there is theoretically no upper limit on the number of echelon cracks produced. However, they suggest that heterogeneities in the rock will produce a finite number of cracks. The formation of left or right-stepping arrays is dictated by the sense of rotation of the remote principal stresses. Looking in the direction of propagation of the parent crack, left-stepping arrays are formed with a clockwise rotation of the remote principal stresses and right-stepping arrays with a counter-clockwise rotation (Pollard et al, 1982) (Fig. 2.2). Observed twist angles of echelon fractures from parent fractures are rarely greater then 30° for both field and laboratory studies (Pollard et al 1982, Bahat 1986). Lateral propagation of echelon fractures is controlled by energy

Figure 2.2

Echelon fracture arrays propagating from a parent crack.

a) A left-stepping array (when viewed in the propagation direction) resulting from a clockwise rotation of σ_3.

b) A right-stepping array resulting from a counter-clockwise rotation of σ_3.

Figure 2.3

A schematic diagram of a dextral shear zone. The theoretical orientations of the incremental strain ellipse, extension fractures and shear fractures are shown. E represents the orientation of tension fractures. R and R^1 are the orientations of Riedel and conjugate Riedel shear fractures. C is the orientation of a shear fracture in the shear plane and A is the orientation of an antithetic shear (modified after Hancock 1985).

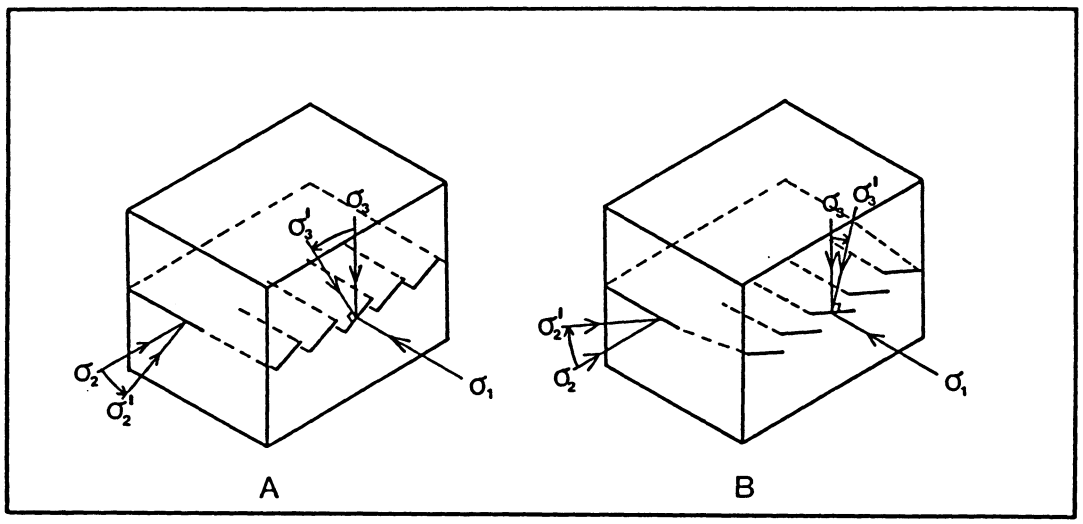
σ3
σ'3
σ2
σ'2
σ1
A
σ3
σ'3
σ'2
σ2
σ1
B

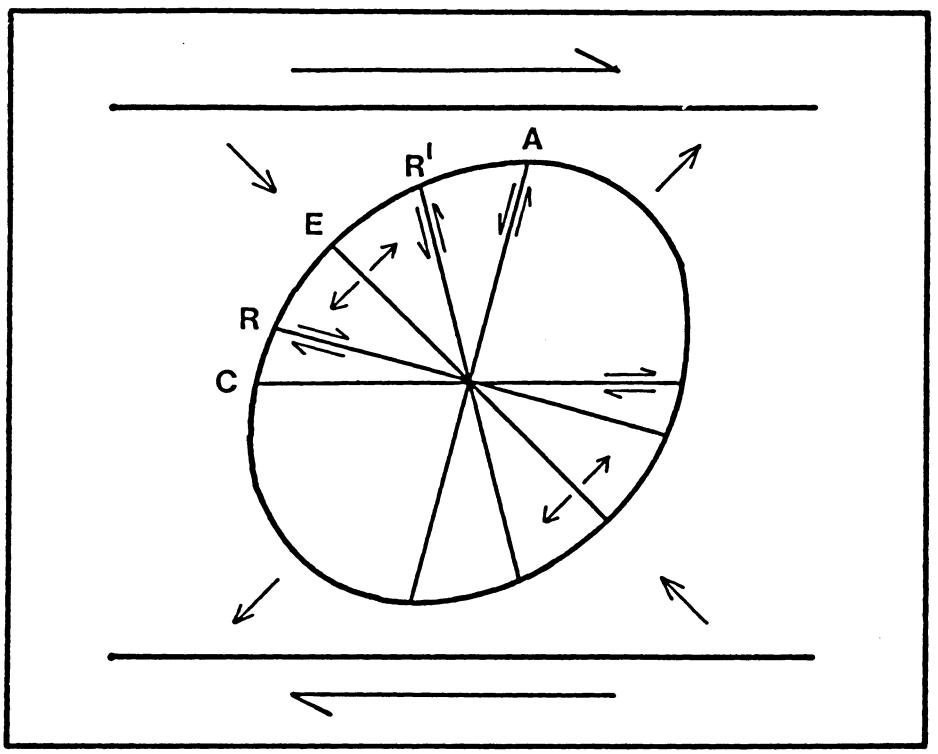
A
R'
E
R
C

constraints, dilation of the fracture and its proximity to adjacent fractures (Pollard et al, 1982).

A field example of echelon fractures branching from a parent crack has been documented by Bahat (1986). Bahat measured vertical joints and subvertical echelon crack arrays in Middle Eocene chalks near Beer Sheva, Israel. The joints are interpreted as having developed due to a horizontal NNE-SSW compression. The echelon crack arrays that accompany each joint are interpreted as tensile fractures occuring due to unloading of the compression. It was observed that the echelon arrays are restricted to an area of about one square kilometre and their formation seems to be controlled by the horizontal bedding. Due to abundant vertical exposure, Bahat was able to document the orientation and dimensions of echelon cracks as they branched from parent joints. This allowed several important observations to be made. The echelon cracks occur in both right-stepping and left-stepping sets. They are found branching both above and below a parent joint and from either side of a parent joint as seen in a horizontal surface. There is often a bimodal distribution of echelon crack sizes with both usually having the same orientation. The twist (fracture-zone) angles between echelon cracks and parent joints ranges from 7° to 37°. There seems to be a linear correlation between vertical length of echelon fractures and step.

2.23 Echelon arrays as zones of localized strain

Echelon fractures and veins that occur in shear zones have been recognized by many authors (Shainin 1950, Hancock 1972, Beach 1975, Rickard and Rixon 1983, Ramsay and Huber 1985). Shear zones are planar zones of rock that have been the locus for an accumulation of shear strain. The fractures may form as a brittle response to incremental shear strain (Ramsay and Huber 1985, Rickard and Rixon 1983, Hancock 1972) or as a response to second order stresses within the shear zone (Latjai 1969,

Tchalenko 1970, Hancock 1972). Presumably the remote principal stresses or the imposed strains determine the orientations of these zones of weakness.

Each shear zone has a particular geometry relative to the remote principal stresses. The orientation of the principal stress, σ_1, relative to the shear zone determines the sense of motion on the shear. For the case of exclusively simple shear, (no flattening across the shear zone) one can look at the development of strain within the shear zone. Figure 2.3 indicates the orientation of the strain ellipse for a small amount of strain in a dextral shear zone. This is known as the incremental strain ellipse and, in theory, the brittle response of the rock within the shear zone is dependent on its orientation (Ramsay and Huber, 1983). It can be shown that the long axis of the incremental strain ellipse is always oriented at 45° to the shear direction (Ramsay and Graham, 1970). Tension fractures are considered to form perpendicular to the maximum extension direction and to dilate parallel to it. Therefore, tension fractures will initiate perpendicular to the maximum incremental extension direction, at 135° to the shear direction (a fracture-zone angle of 45°), and will propagate in this direction (Ramsay and Graham, 1970).

Shear zones of low shear strain could contain, in theory, arrays of tension fractures at 45° to the shear zone walls. The arrays would be left-stepping for a dextral shear zone and right-stepping for a sinistral shear zone (Fig. 2.4). If there is a large strain gradient across the shear zone, fractures may become rotated into the shear direction with continued shear and subsequently dilated. The crack may become a vein as it is infilled with quartz, calcite or other minerals. The central portion of the vein may be rotated with increasing shear strain in the centre of the zone while the vein tips continue to grow perpendicular to the maximum incremental strain direction leading to the development of sigmoidal veins (Ramsay and Huber, 1983). This type of echelon vein array has been frequently documented (Roering 1968, Hancock 1972, Beach 1975, Rickard and Rixon 1983, Ramsay and Huber 1983).

Figure 2.4

Right-stepping and left-stepping echelon fracture arrays in conjugate shear zones.

Figure 2.5

The relationship of fractures in echelon arrays to the principal (primary) stresses as given by Roering (1968) (modified after Roering 1968).

a) Two parallel sets of shear fractures.

b) Two conjugate sets of shear fractures. The fractures in one set are parallel to the trend of the conjugate set.

c) Two conjugate sets of tensile fractures.

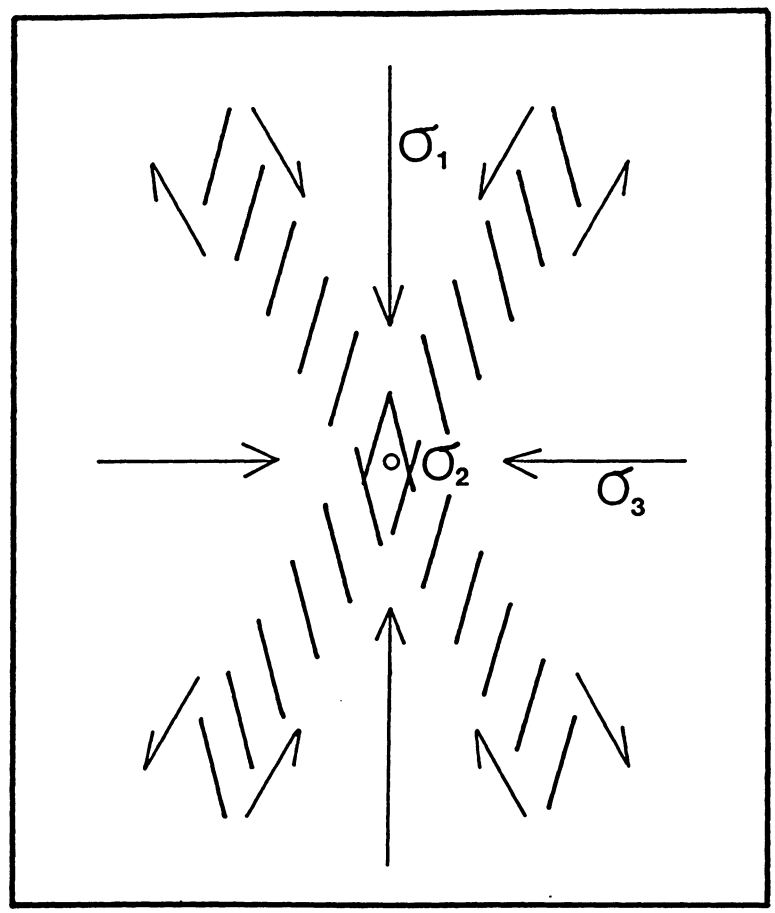
σ1
σ2
σ3

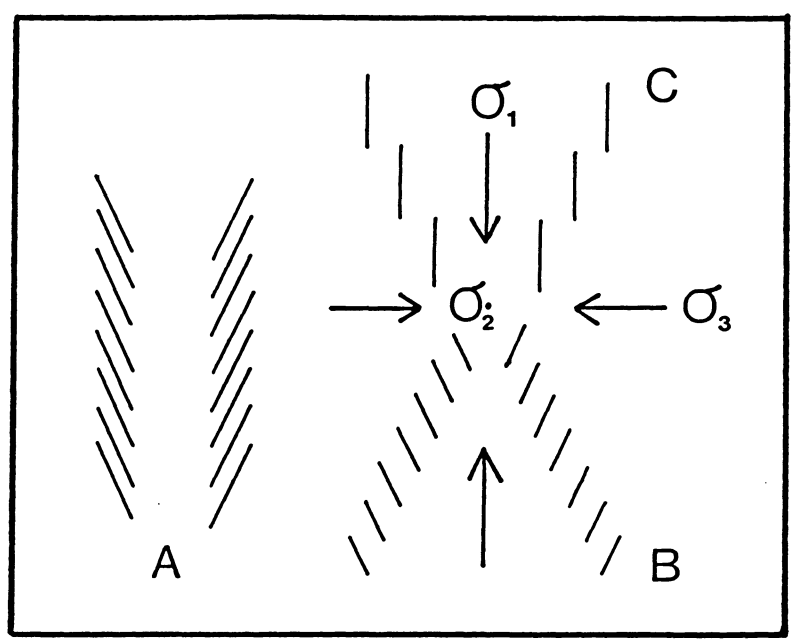
σ1
C
σ2
σ3
A
B

The origin of these echelon vein arrays may not be as simple as the model just described. The angles echelon veins make with the boundaries of the shear zone and the growth directions of vein mineral filling cannot always be explained by the above model.

This suggests there may be other ways in which echelon fractures or veins form within a shear zone. If the fractures form as shear fractures rather than tension fractures their relationship to stress or strain directions becomes more complicated. Direct shear experiments with clay cakes have been done by Riedel (1929) and Cloos (1928); and more recently by Tchalenko (1970). They have documented the formation of sets of shear fractures known as "Riedel shears". Within a shear zone the minimum incremental strain direction may be called the "secondary maximum principal stress direction" and is oriented at 135° to the shear direction. Riedel shears form as conjugate shears to this secondary maximum principal stress direction. If an angle of internal friction for the rock of 30° is assumed then Riedel shears and conjugate Riedel shears will form at 165° and 105° (fracture-zone angles of 15° and 75°), respectively, to the shear direction (Hancock, 1985) (Fig. 2.3).

Hancock (1972) measured echelon veins within 40 arrays in greywackes and found a range of fracture-zone angles from 10° to 46° with two weak maxima at 15° to 20° and at 25° to 30°. Crystal vein fibres, third order veins and minor faulting within the arrays indicated a component of shear acting on veins with fracture-zone angles less than 40°. Accordingly, Hancock has classified undeformed echelon veins in shear zones on the basis of their orientation; veins occupying a fracture-zone angle of 10° to 20° belong to the Riedel shear field, veins at 40° to 50° to the shear zone boundary are extension fractures, and veins between 20° and 40° are hybrid fractures or surfaces transitional between shear and extension fractures (Hancock 1985).

Another factor influencing the angles veins make with a shear zone is dilation. Ramsay and Huber (1983, 1987) argue that for shear zones undergoing positive dilation the maximum extension direction makes a higher angle with the shear direction. Thus

tension veins will initiate at angles of less than 45° in a positively dilating shear zone. Similarly, shear zones undergoing negative dilation will produce tension veins at angles greater than 45°. This is supported by Rickard and Rixon (1983) who observed quartz filled tension veins oriented at 40° to shear zone boundaries.

Roering (1968) measured the orientations of veins in echelon arrays in a quartzite. For thirteen measurements of right-stepping, presumed sinistral shear, arrays the angle between veins and the array ranged from 28° to 52° with a mean of 39°. This shows quite a variation in orientation from the expected 45° angle. Roering attributes this to the veins having formed as shear fractures in response to the primary stress field (Fig. 2.5). Since the angle between these conjugate arrays of left-stepping and right-stepping fractures is 40°, fractures in one array are parallel to the conjugate array and vice versa.

Regardless of the angle that echelon veins or fractures make with the boundaries of the zone, several problems still remain. If the shear zone hypothesis is considered, a mechanism for the localization of shear strain must be produced. If the fractures form as shear fractures in response to the primary stress field then some mechanism for why they nucleate in arrays of left-stepping or right-stepping fractures must be considered. This has been accurately summarized by Latjai (1969): "Any hypothesis postulated for the origin of en echelon fracture systems must provide 1) an explanation for the zonal arrangement of echelon cracks, and 2) a state of stress within such a zone that could lead to fracture either in tension or in shear.". One mechanism that has been postulated (Latjai 1969) is that zones of high shear stress, within which cohesive yielding has occured, will induce a local state of stress that is different from the regional stress. If the local stress state allows fractures to grow they will propagate from pre-existing microcracks and their orientation will reflect the local stress state and not the regional stress field (Latjai 1969).

3.0 Description of Fractures and other Structures

3.1 Rock type, foliation and lineation

The Killarney Igneous Complex consists of granite, porphyritic felsite and inferred ash flows. The study area is located within a weakly deformed version of the ash flows. The rock is relatively homogeneous but contains a few larger clasts. There is a weak foliation defined by the sub-parallel alignment of platey biotite and by the long axes of felsic clasts. The poles to foliation, for all stations, form a broad girdle distribution indicating that the foliation strikes generally eastnortheast--westsouthwest and dips moderately to the north or south (Fig. 3.1). Through the Grenville Front the foliation acquires the dominant Grenville orientation; northeast--southwest striking and steeply to moderately dipping to the southeast. There is a mineral lineation that is only weakly developed in the granite/porphyry. In the Grenville Front and in gneisses of the Grenville province there is a down-dip stretching lineation defined by mineral aggregates of quartz and feldspar. The foliation is crosscut by all other structures but appears not to have influenced the orientation or development of these younger structures.

3.2 Dykes

Dykes of several types can be found in the study area and they prove useful as relative age indicators and as indicators of offset on shear zones. All of the dykes crosscut the foliation and are themselves non-foliated except where they have been deformed by shear zones. Most of the dykes are steep to moderately dipping and the majority strike around 150° to 170° (Fig. 3.2).

Figure 3.1

Poles to foliation in the study area. A contoured equal-area, lower-hemisphere net.

NOTE: All orientation data were counted using the method described by Robin and Jowett (1986).
N = number of points;
k = kurtosis of the Gaussian counting function;
E = expected value of the counts if the N data points were drawn from a population uniformly distributed over the hemisphere;
s = σ = standard deviation about the expected value for counts of the same uniformly distributed population;
Peak value = count at the mode, i.e. the highest count;
Peak position = mode = orientation of the counting point with the highest count; for planar data, the peak position is that of the poles;
Contours are every 2 σ, starting from E.
The kurtosis, k, is a function of N chosen such that E = 3 σ (Robin and Jowett, 1986).

Figure 3.2

Poles to dykes in the study area. A contoured equal-area, lower-hemisphere net.

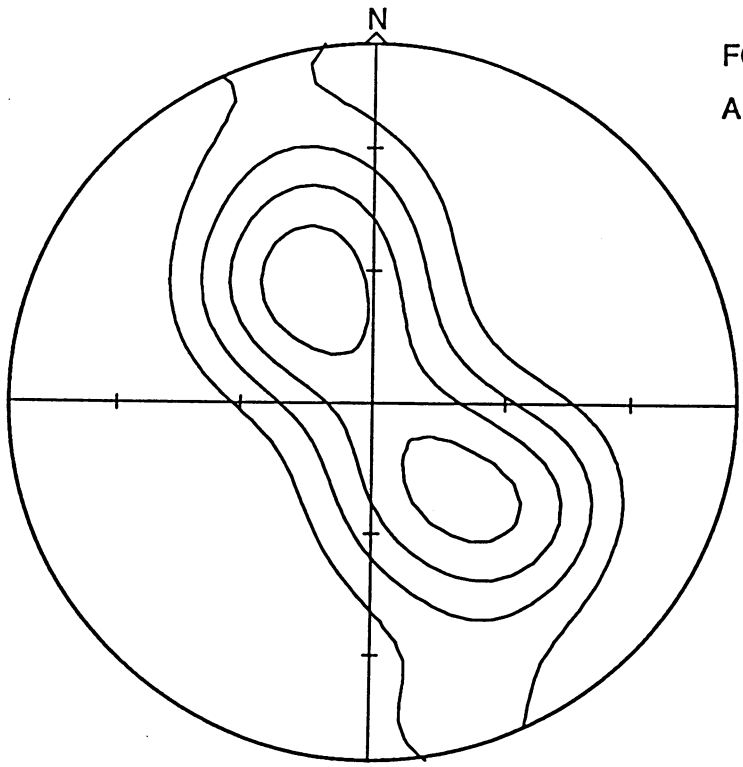

FOLIATION

ALL STATIONS

N 46
k 12.2
E 3.8
s 1.3
Peak: value 13.3
position 333°/ 59°

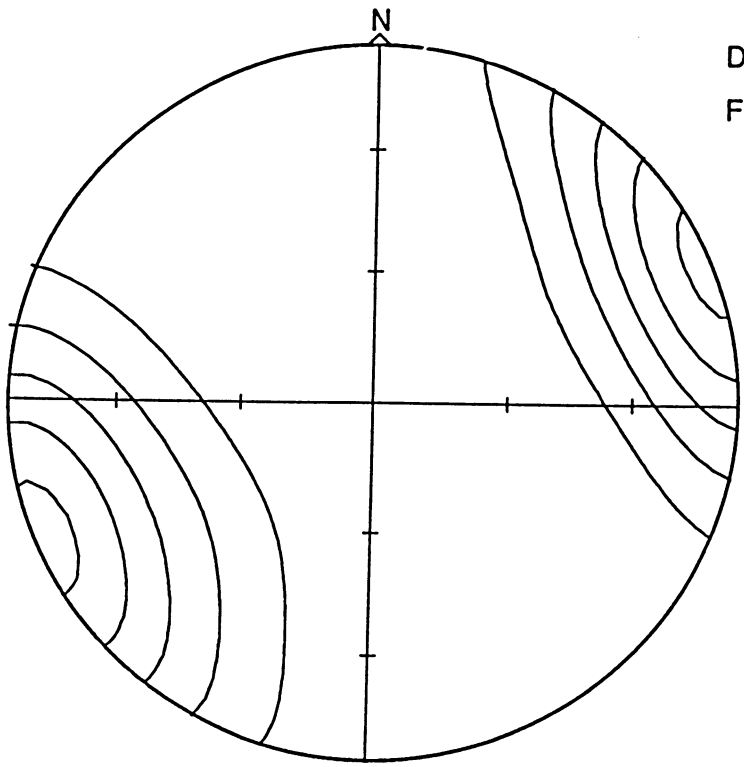

DYKES

FELSIC AND PEGMATITE

N 23
k 7.1
E 3.2
s 1.1
Peak: value 12.7
position 248°/ 2°

Stations in the northwest of the study area contain a series of narrow felsic dykes ranging from one to two millimetres to several centimetres in width and often traversing the entire width of the outcrop. The dykes contain mostly fine-grained feldspar and quartz with some mafic material such as biotite, chlorite, amphibole and sulphides. The felsic dykes often appear veinlike and may pinch out into a fracture. The dykes may also make sharp changes in direction and orientation of up to 35° over a distance equivalent to their width (Fig. 3.3). Another unusual feature is the segregation of material in some vein-like dykes into quartz, feldspar, or mafic-rich areas. This may suggest either more than one phase of dyke injection or some kind of metamorphic segregation after dyke formation.

Pegmatite dykes are found throughout the study area but in increasing abundance towards the Grenville Front. Their orientations are dominantly south-southeast striking. Some of the pegmatites are deformed and sheared by shear fractures and shear zones (Fig. 3.4). In some cases the shear zones only deform the margins of the dyke and do not cross the entire dyke.

3.3 Shear zones and shear fractures

Shear zones and shear fractures are generally found in increasing abundance in the study area as the Grenville Front is approached. They all contain chlorite and epidote group minerals which give them a distinctive green colour. They seem to be intimately related in age or origin as they are found together and often offset the same dyke. They are all apparently older than the fractures and echelon fractures which crosscut them.

The distinction between shear zones and shear fractures is often obscure but some generalizations may be made. Shear fractures are defined as filled fractures along which an offset of markers or a deflection of foliation was observed. Shear zones were defined as zones of recognizable width along which a similar offset was observed. Dextral and

Figure 3.3

A felsic dyke with sharp changes in orientation. Hammer (33.5 cm) as scale.

Figure 3.4

A large (1.5 m wide) pegmatite dyke with a sinistral offset by a shear zone. The shear zone is parallel to the hammer handle. Hammer (33.5 cm) as scale.

sinistral strike-offset components of shear were observed on both shear zones and shear fractures with the majority being sinistral.

Shear zones of two distinct types can be recognized. The first type is of short, often one to two metres long, diffuse shear zones which are not often seen to offset or crosscut dykes. Where seen in a vertical exposure the shear zones appear to be subvertical and many of them strike roughly 50° to 70°. These shear zones are recognized by the concentration of chlorite and epidote within them and the obliquity of the foliation within them to the foliation outside the zones. On a horizontal surface, shear zones that are sub-parallel to the foliation trace appear as zones of more intensely developed foliation (Fig. 3.5a). When the same shear zone is viewed on a vertical surface, the foliation within the shear zone can be seen to be oblique to the foliation outside the shear zone (Fig. 3.5b). Shear zones that, on a horizontal surface, are oblique to the foliation trace outside the zone often have one sharp boundary while the opposite boundary is diffuse. Within the diffuse boundary, foliation from outside the shear zone may be deflected left or right into the zone indicating an apparent strike-slip offset (Fig. 3.6). Where this deflection of foliation was observed it most often indicated a sinistral strike-offset.

Another interesting feature of these shear zones is their terminations. One way in which these zones terminate is to simply taper away to nothing along their length (Fig. 3.5a) (Type I termination of Simpson, 1983). Another way they terminate is to branch into a fan-like structure at their ends (Fig. 3.7) (Type II termination of Simpson, 1983). In most of these shears there are no external markers that can be used to estimate shear strain. These shear zones present an interesting three-dimensional problem for which only two dimensions of structural data are readily available.

The other group of shear zones in the study area seem to be associated with shear fractures and are larger than the first group discussed. These shear zones are only found close to the Grenville Front (Stations 1,8,9,10, Fig. 1.4). The shears are subvertical in

Figure 3.5

a) Two shear zones that are parallel to the foliation on a sub-horizontal outcrop surface. These shear zones have tapered terminations. Knife (9 cm) as scale.

b) The same two shear zones as in a). The outcrop surface is sub-vertical. The shear zones exhibit a reverse (left side up) offset of the foliation.

Figure 3.6

A shear zone that is oblique to the foliation on a sub-horizontal surface. There is a sinistral deflection of the foliation. Hammer (33.5 cm) as scale.

Figure 3.7

A shear zone with a fanned termination. Knife (9 cm) as scale.

orientation and strike 55° to 65°, sub-parallel to the Grenville Front. Both dextral and sinistral strike-offset of markers has been observed on these shear zones but the dominant sense is sinistral (Fig. 3.8). Foliation was also seen to bend left into some shear zones indicating a sinistral strike-offset. The width of the shear zones ranges from several centimetres to close to a metre and the shear zones commonly extend the length of the outcrop. Strain within the shear zones is variably developed and shear zone boundaries may be diffuse or sharp. Some shear zones contain glassy ultramylonite while others contain shear fractures. These shear zones may be related to ductile deformation along the Grenville Front.

Shear fractures are filled fractures along which there is a recognizable shear offset. Many fractures may have originated as shear fractures or have undergone a shear offset but this may not be recognized in the field. Shear fractures in the study area are subvertical, strike dominantly 10° to 30°, and exhibit both dextral and sinistral offsets with the majority sinistral (Fig. 3.9). The shear fractures often occur in sets, the majority of which are left-stepping (Fig. 3.10).

3.4 Field description of fractures

Fractures were classified and mapped in two groups: isolated fractures, and echelon fracture sets. Isolated fractures were defined as individual fractures not belonging to an echelon fracture set on the scale of the outcrop. At stations not mapped in detail they were selectively measured if greater than a metre in length. Echelon fracture sets were defined as discrete zones of echelon fractures that were clearly right or left-stepping. This limited the measurement of echelon sets to those that could be resolved at the outcrop scale. To be recognizable as discrete zones, echelon fracture sets were usually less than one metre in width. At stations with fewer than 20 echelon fracture sets all of them were measured. At stations with greater than 20 echelon fracture sets at least 80% of them were measured.

Figure 3.8

A large shear zone with a sinistral deflection of the foliation. Knife (9 cm) as scale.

Figure 3.9

Shear fractures exhibiting sinistral strike-offsets of a felsic dyke. Knife (9 cm) as scale.

Figure 3.10

A left-stepping set of shear fractures. Note the ductile deformation of the foliation in a sinistral sense. Knife (9 cm) as scale.

Figure 3.11

Poles to isolated fractures in the study area. A contoured equal-area, lower-hemisphere net.

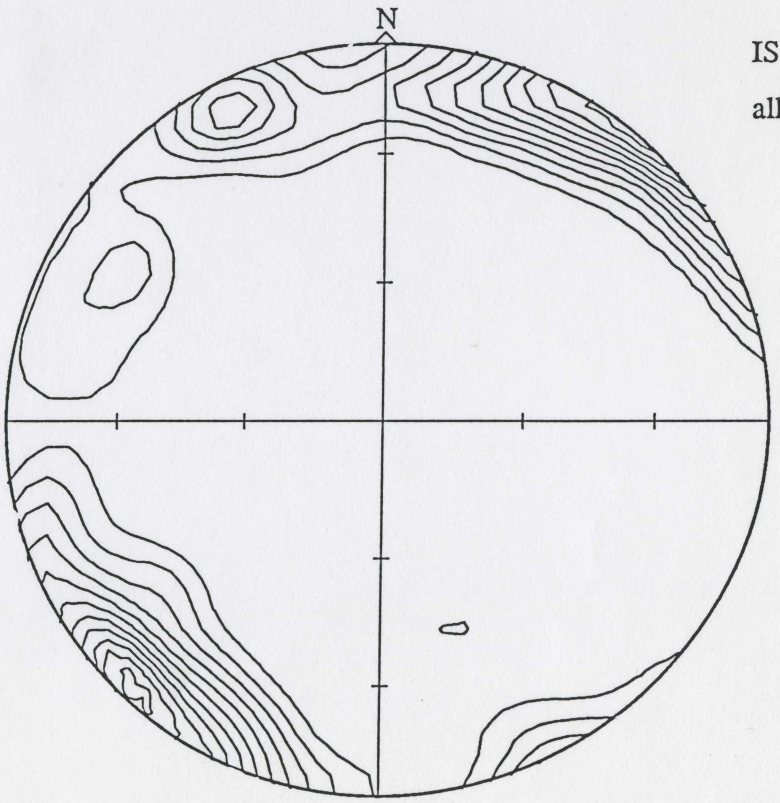

ISOLATED FRACTURES

all stations

N 360
k 82.0
E 4.4
s 1.5
Peak: value 35.5
position 221 / 3

The isolated fractures are generally subvertical in orientation. When plotted and contoured on an equal-area stereonet, two populations can be distinguished (Fig. 3.11). The first and largest population strikes generally northwest--southeast with a peak orientation of 131°. The smaller population is northeast--southwest striking with a peak orientation of 63°. These two populations are evident in the detailed maps produced for several stations. Figure 3.12a-d is a detailed fracture map of a portion of station 6 (Fig. 1.4). It can be seen that southeast striking isolated fractures link up the echelon fracture sets (Fig. 3.12b). Shorter northeast striking fractures are discontinuous and are truncated by the southeast striking fractures (Fig. 3.12c). Generally, foliation, dykes and shear zones do not seem to influence the formation of the fractures. An exception to this may be seen in Figure 3.12d where a pegmatite dyke has controlled the development of fractures.

Echelon fracture sets were classified into right-stepping (RS) and left-stepping (LS) sets (Fig. 3.13). Over the entire study area, RS sets outnumber LS sets by a ratio of 3:1 since 325 RS and 98 LS fracture sets were measured. The fracture-zone angles for RS and LS fracture sets vary greatly. This angle is generally smaller in LS sets than in RS sets. All fractures in the echelon sets are sub-vertical to vertical in orientation and the echelon sets themselves are sub-vertical.

The trends of RS fracture sets (zone orientation) and LS fracture sets have a similar broad distribution in a northwest--southeast direction. The RS zones have a broad distribution peak between 100° and 160°. The LS zones have a broad distribution peak between 90° and 180°. The mean zone orientation of RS sets is 133° and of LS sets is 118°. The fractures in RS sets have a broad peak between 60° and 130°. In LS sets the fractures have a broad distribution between 110° and 200°.

The general characteristics of the echelon fracture sets are as follows. The sets are one to several metres in length and contain fractures from millimetres to several metres in length. The average fracture length of fractures within sets is about 25 centimetres.

Figure 3.12

A detailed map of the east end of station 6.

a) Pegmatite dykes, felsic dykes, segregated veins and quartz veins.

b) Echelon fractures.

c) Northeast trending fractures.

d) Unclassified fractures.

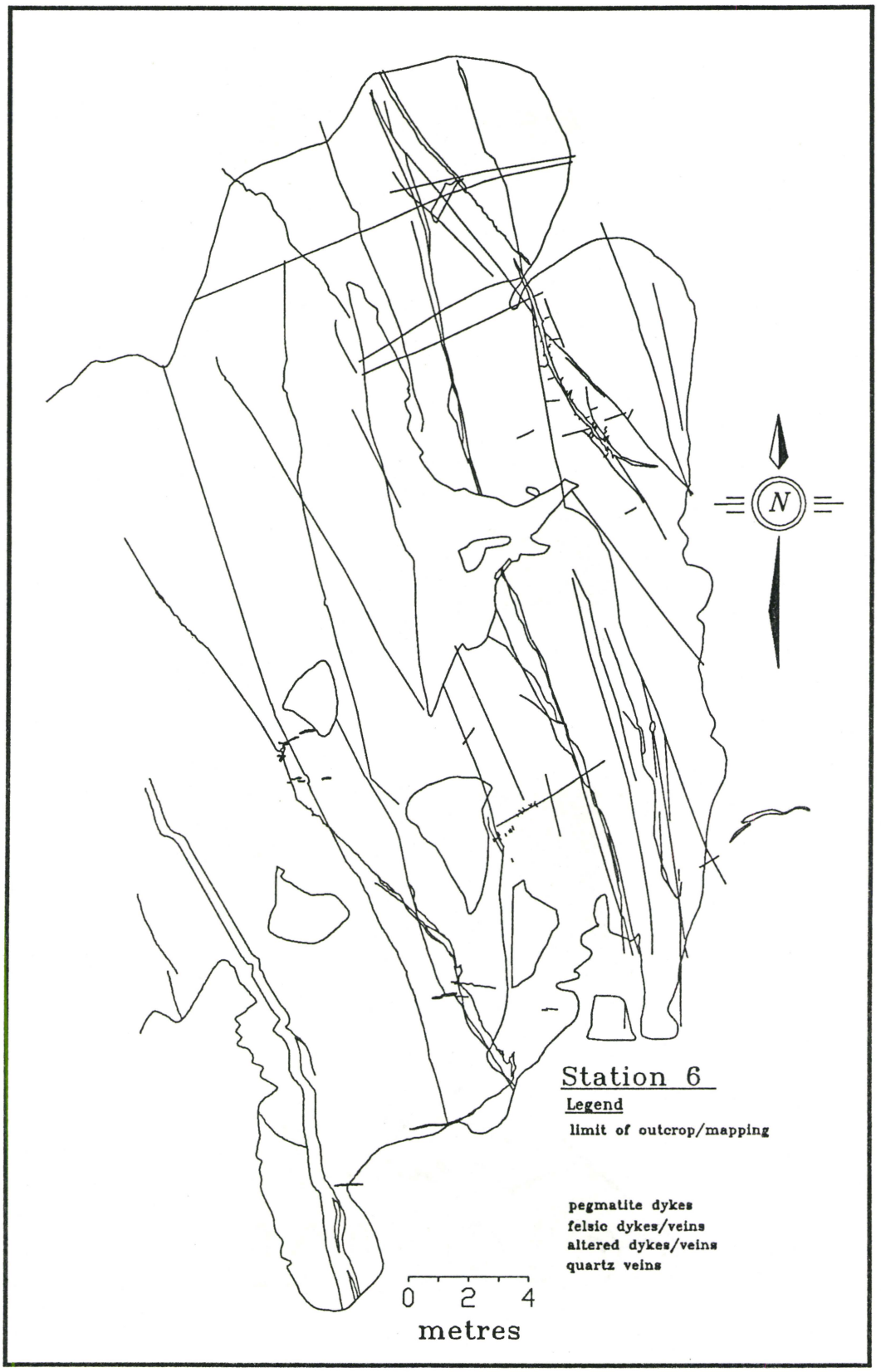
N
Station 6
Legend
limit of outcrop/mapping
pegmatite dykes
felsic dykes/veins
altered dykes/veins
quartz veins
0 2 4
metres

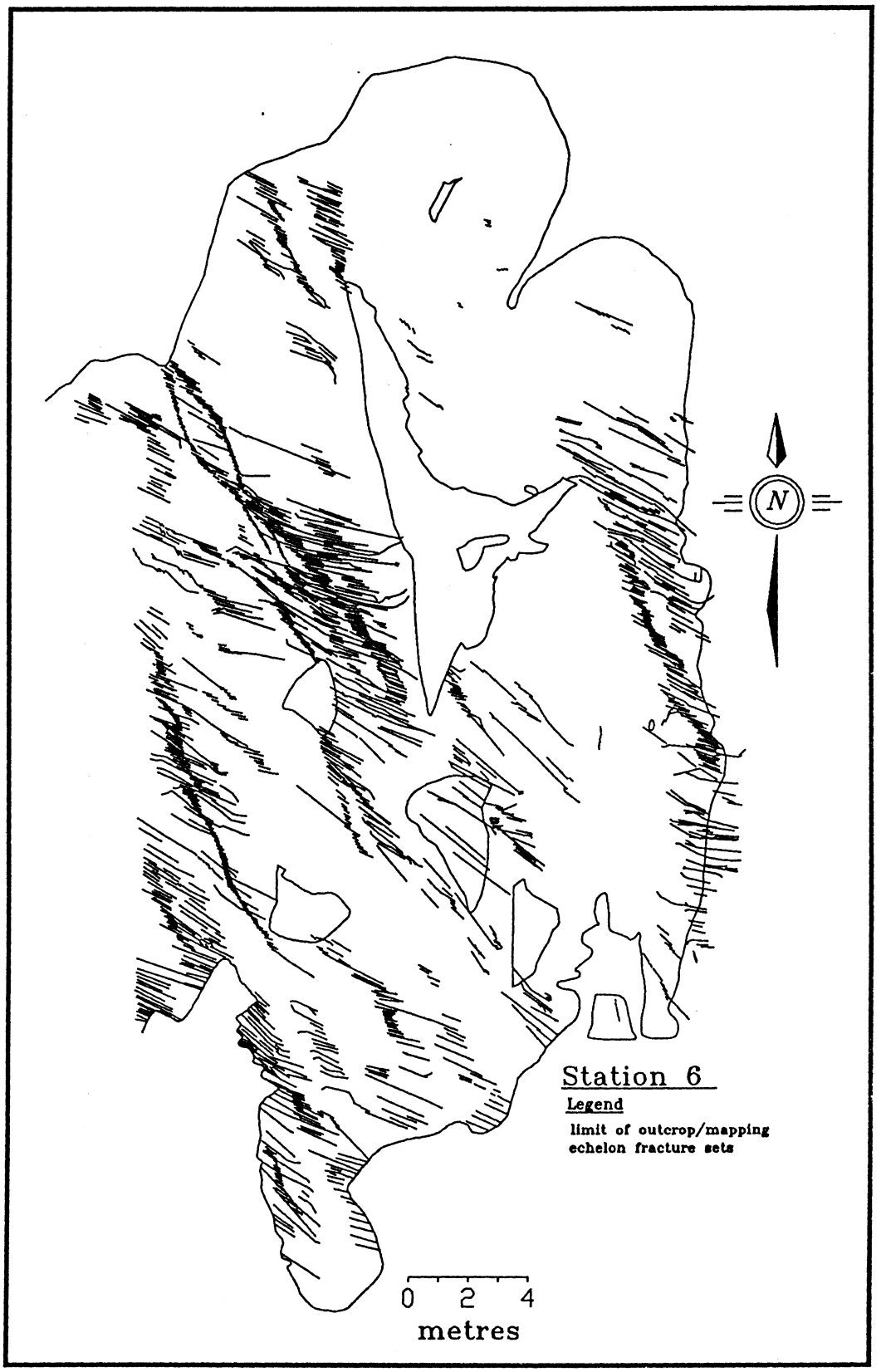
N
Station 6
Legend
limit of outcrop/mapping
echelon fracture sets
0 2 4
metres

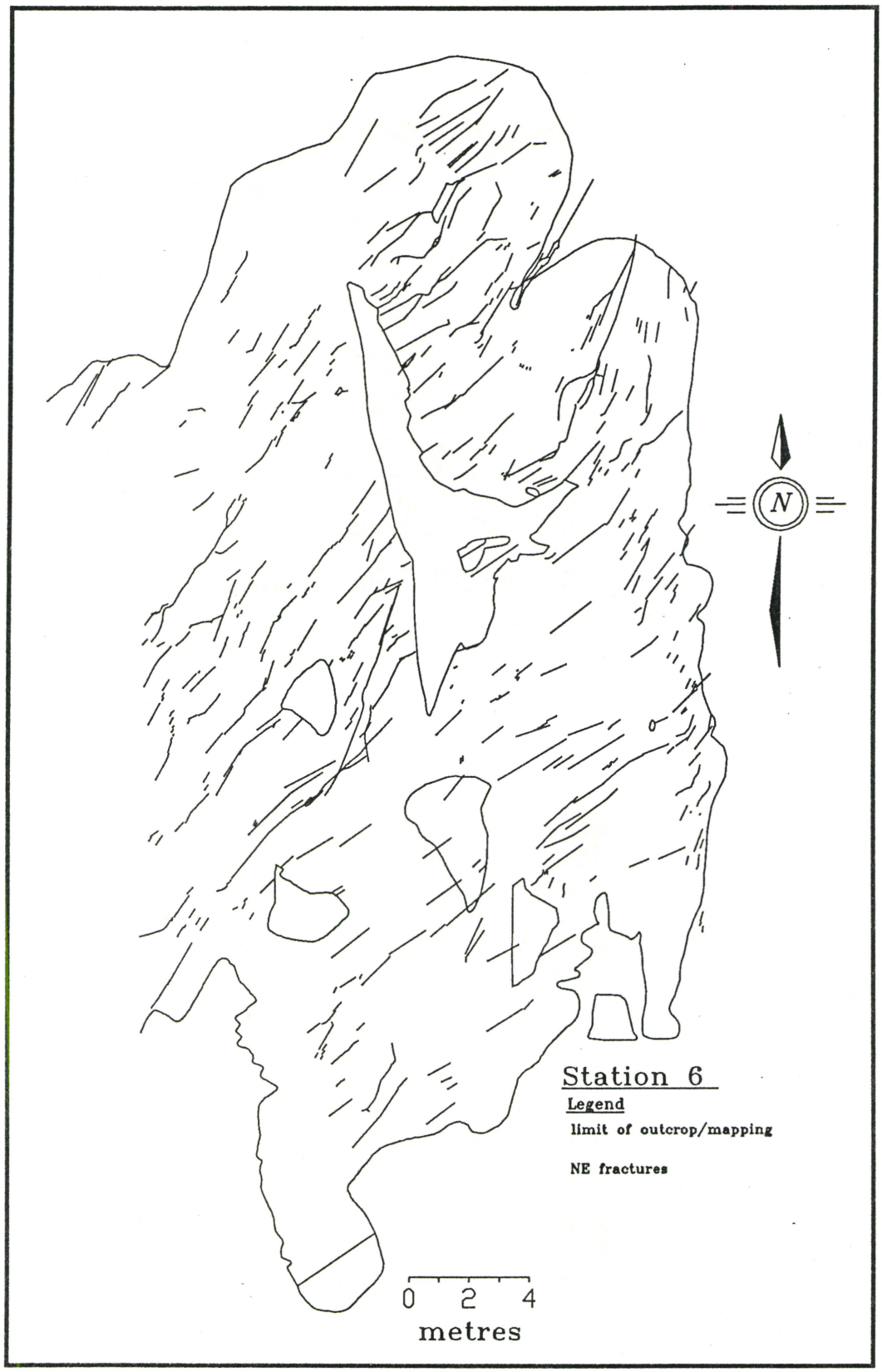
N
Station 6
Legend
limit of outcrop/mapping
NE fractures
0 2 4
metres

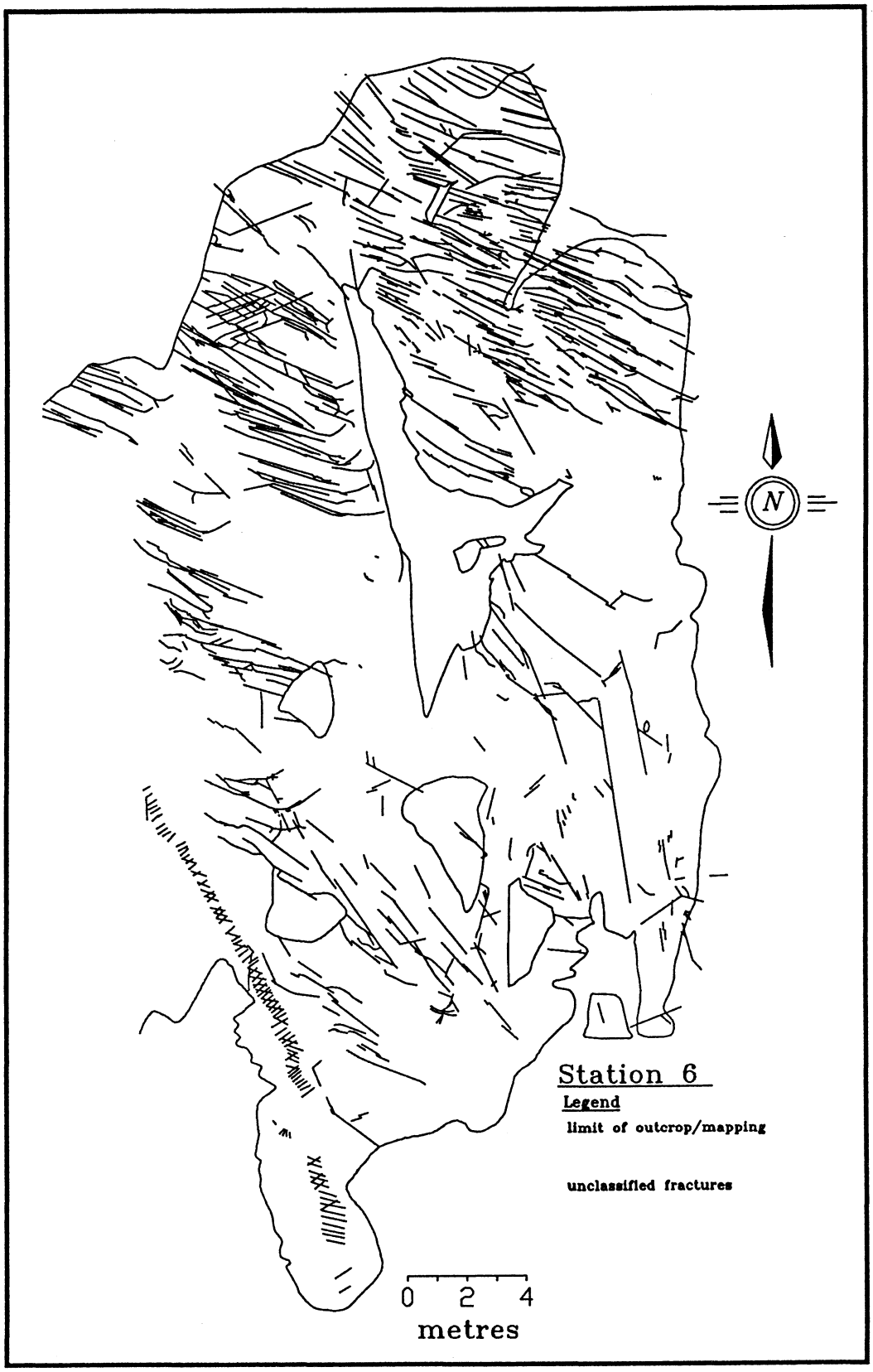
N
Station 6
Legend
limit of outcrop/mapping
unclassified fractures
0 2 4
metres

Figure 3.13

a) A right-stepping echelon fracture set. Hammer (33.5 cm) as scale.

b) A left-stepping echelon fracture set. Knife (9 cm) as scale.

Generally, fractures in LS sets are shorter than fractures in RS sets, although, in both, 75% of the fractures are from 10 to 80 centimetres long. There is often more than one population of fracture lengths in an individual zone (Fig. 3.14). The longer fractures are more widely spaced than the shorter fractures. This leads to the observation that there may be a relationship between fracture length and fracture spacing.

The fracture-zone angle, although variable over the study area, is fairly consistent within an individual zone (Fig. 3.15). Most of the fracture sets show some degree of hematite staining. The fractures may be dilatant up to two or three millimetres but in general the fractures appear as hairline cracks and the nature of fracture fill, if any, cannot be determined at the outcrop (Fig. 3.14).

Some of the characteristics not common to all echelon fracture sets allow them to be further classified on the basis of their field appearance into "straight" sets, "sigmoidal" sets, and "closely spaced" sets. The "straight" sets are moderate to large in size and contain straight fractures with low to moderate hematite staining (Fig. 3.15). The "sigmoidal" sets are less common and are restricted to several small islands in the east end of the study area (Stations 12,13,14, Fig. 1.4). These sets are characterized by the presence of a main fracture that travels the length of the set and bisects all the echelon fractures. Some of the fractures may be offset by the main fracture. The echelon fractures themselves are sigmoidal and curve at their terminations into the direction of trend of the zone (Fig. 3.16). The degree of hematite staining is well developed. Both the "straight" sets and the "sigmoidal" sets have hairline fractures with no discernible fracture fill in hand sample. Some more dilatant fractures were observed but these were often indistinguishable from weathered fractures. The "closely-spaced" sets are characterized by abundant, short, closely-spaced fractures with a high degree of hematite staining. These fractures often appear vein-like and/or have a green chlorite/epidote fracture fill. The closely-spaced fractures may be sigmoidal and curve at their terminations into the zone trend direction (Fig. 3.17). In Figure 3.17 and 3.18 some

Figure 3.14

A right-stepping echelon fracture set with long and short fractures. Knife (9 cm) as scale.

Figure 3.15

A right-stepping echelon fracture set classified as "straight". Hammer (33.5 cm) as scale.

Figure 3.16

A right-stepping echelon fracture set classified as "sigmoidal". Knife (9 cm) as scale.

Figure 3.17

A right-stepping echelon fracture set classified as "closely spaced". Some sigmoidal fractures bound septae of rock that have been rotated in a sense consistent with sinistral shear. Knife (9 cm) as scale.

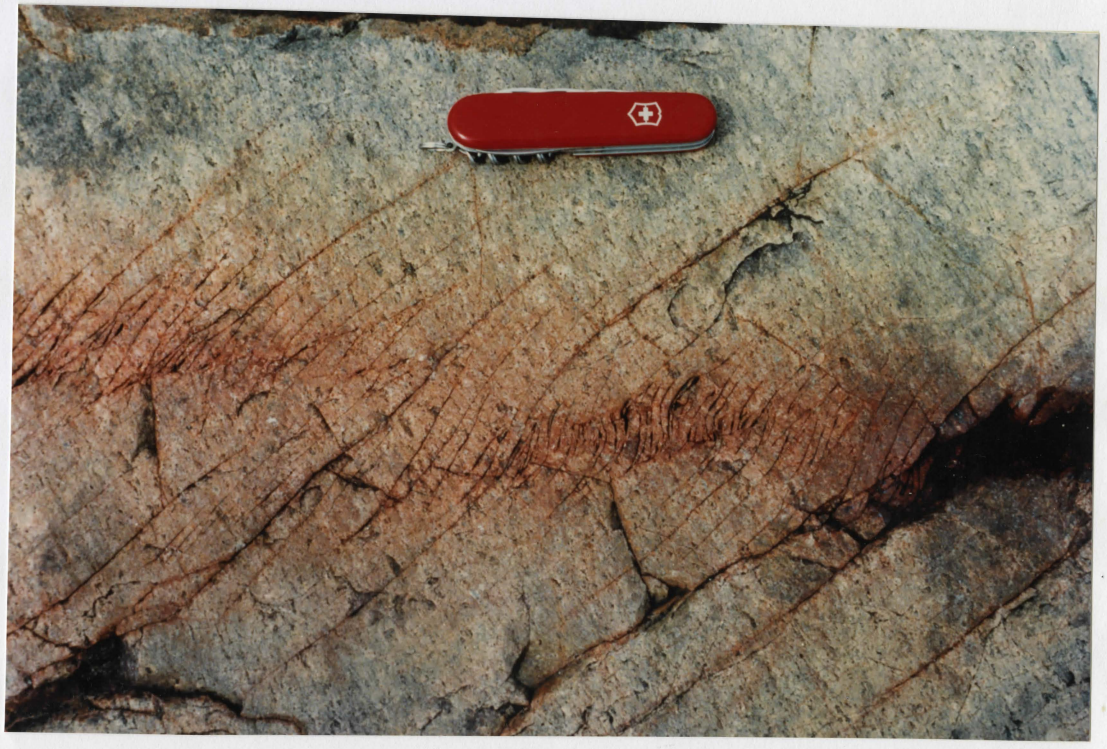

Figure 3.18

A right-stepping echelon fracture set classified as "closely spaced". The rotation of fracture-bound septae has resulted in truncation of some fractures. Knife (9 cm) as scale.

Figure 3.19

Two right-stepping echelon fracture sets that offset felsic veins in both a sinistral and dextral sense as seen in a horizontal outcrop. Hammer (33.5 cm) as scale.

fractures bound septae of rock that have been rotated and truncated in a direction consistent with a sinistral sense of shear in the RS set. Individual fracture sets may offset dykes in both a sinistral and dextral sense as seen in a horizontal plane (Fig. 3.19).

Several of these features need further discussion. The hematitization of fracture surfaces and rock adjacent to fractures must be the result of a flow of fluids through the fractures. This implies that the fractures are dilatant and that the rock surrounding the fractures allows fluid migration. The degree of hematite staining around fractures may be dependent on the fracture process zone. However, there is a large variation in width of the hematitization zone around different fractures despite the similar grain size of the rock. Hematitization has been found with fractures and lineaments that are associated with the Ottawa-Bonnechere-Nippissing graben system (Stesky et al 1988).

The sigmoidal nature of some echelon fractures warrants a brief discussion here. There are two ways in which they could form; through shearing and rotation of a filled fracture (Ramsay and Huber, 1983) or through propagation of a fracture into a stress field of a different orientation. Although shearing and rotation of fractures has been observed in some echelon sets (Fig. 3.17), sigmoidal fractures are observed (Fig. 3.18) with no evidence of shearing or ductile deformation of the rock. Therefore propagation into a stress field of changing orientation is favoured for the formation of sigmoidal echelon fracture sets in this study area.

The shear offsets of dykes observed in some echelon sets cannot be resolved into strike-offset and dip-offset components due to lack of vertical exposure. Both dextral and sinistral strike offsets were observed. Generally LS sets exhibited dextral strike-offsets and RS sets exhibited sinistral strike-offsets. However, some sets had both dextral and sinsistral strike-offsets.

3.5 Microscopic description of fractures

A limited number of samples were examined in thin section to look at the nature of the fractures and their filling, if any. It was found that hairline, hematite stained fractures in hand sample appeared as hairline cracks in thin section. These fractures are not obviously filled or dilatant but acted as a locus for the growth of chlorite, epidote and clinozoisite (Fig. 3.20). Although not seen in Figure 3.20, these fractures are often discontinuous as they pass through some clusters of chlorite and epidote grains. Some shear offsets of grains were also observed.

Chlorite/epidote filled fractures in hand sample appeared "vein-like" in thin section and were filled with fine-grained chlorite and/or epidote (Fig. 3.21). Samples of fractures that offset dykes showed that some of the offsetting fractures were microbreccia zones and some were hairline fractures in thin section (Fig. 3.22). Samples of shear fractures in thin section appeared as shear zones with feldspar porphyroblasts and quartz ribbon pressure shadows (Fig. 3.23).

This microscopic assessment leads to several conclusions. The first is that commonly more than one type or generation of fracture exists within an individual fracture set. The second is that the fractures are not simply two surfaces separated by a fracture filling. Fracture filling is not a reliable indicator for the classification of these echelon fracture sets since many fracture sets or fractures appeared to be multigenerational. Finally, many fractures are recognizable as dilatant or shear fractures in their present form but this does not indicate whether they formed in tension or shear.

Figure 3.20

Photomicrograph of an apparent "dilatant" fracture. The highly birefringent minerals bordering the fracture are chlorite and epidote. The long axis of the photo is 1.2 millimetres.

Figure 3.21

Photomicrograph of a "vein-like" fracture. The highly birefringent minerals are epidote group minerals. The long axis of the photo is 6 millimetres.

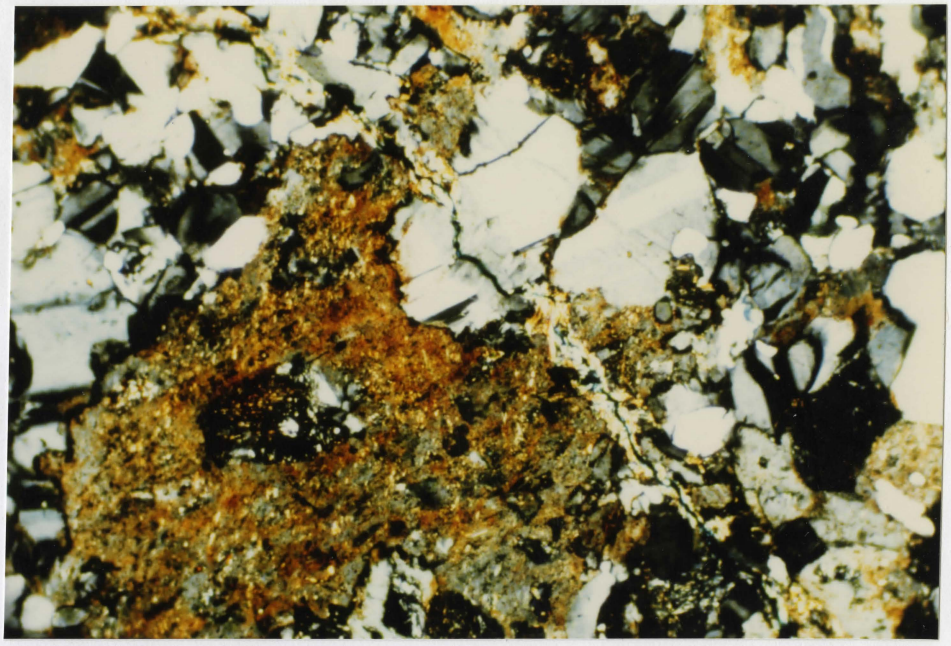

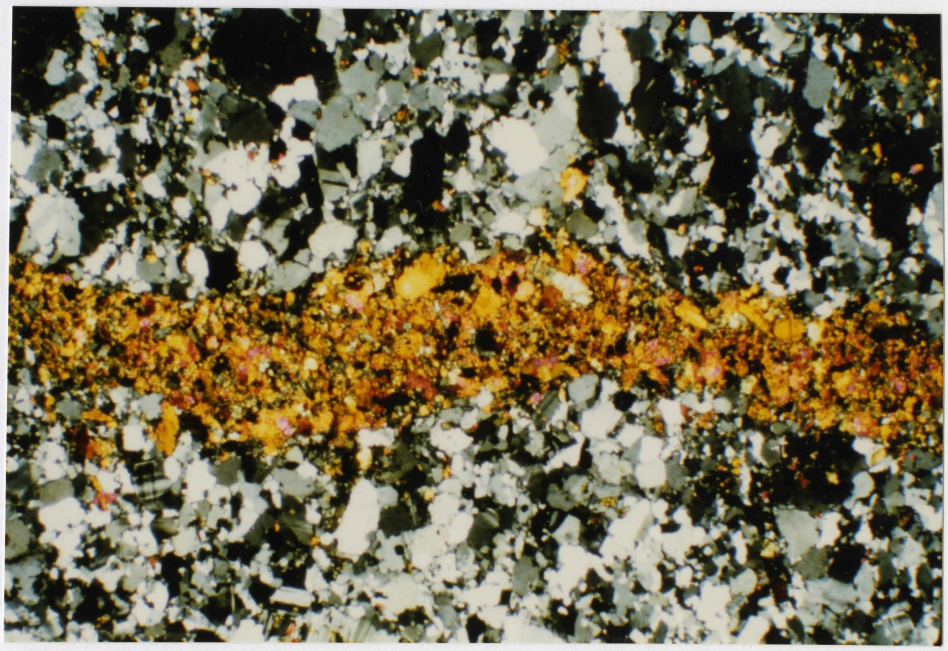

Figure 3.22

Photomicrograph of branching "shear fractures" which offset a quartz-feldspar dyke (as seen in Fig. 3.19). The long axis of the photo is 3 millimetres.

Figure 3.23

Photomicrograph of a shear fracture. This shear fracture is a discrete "shear zone" at this scale. The long axis of the photo is 6 millimetres.

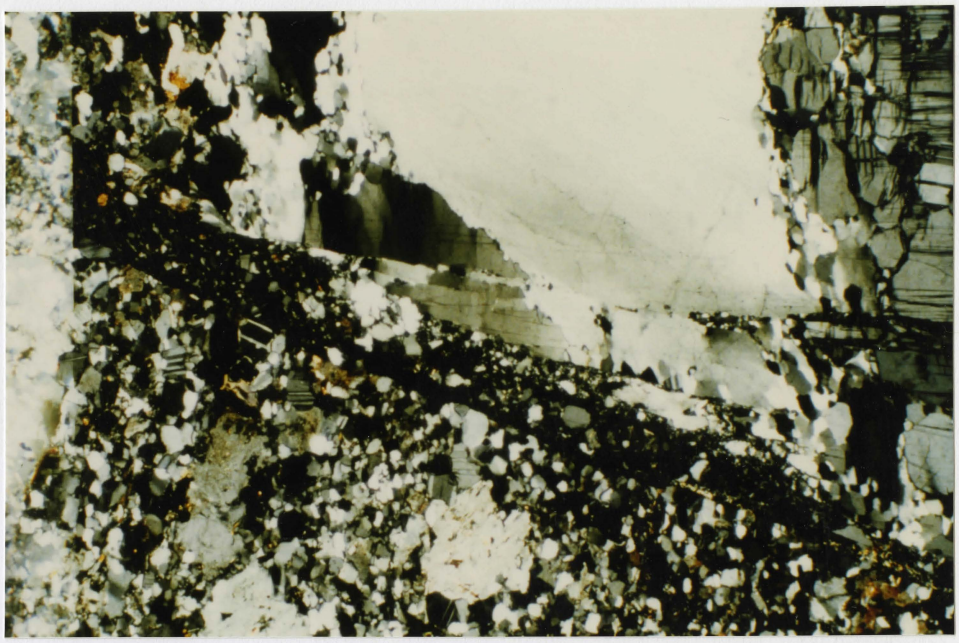

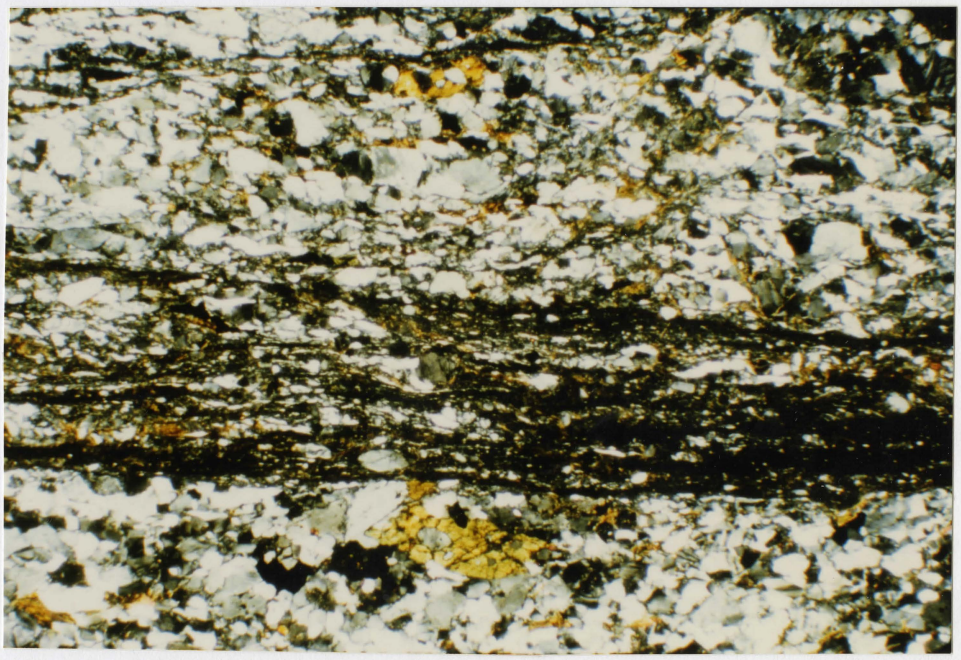

4.0 Geometrical Parameters of Echelon Fracture Sets

4.1 Introduction

The geometrical parameters of echelon fracture sets may provide constraints on the origin of the fracture sets. These parameters include: fracture length, fracture spacing, fracture overlap, twist angle, fracture set length, fracture set width, and spacing between fracture sets. Measurements of these parameters were made in the field and from photos and maps. The data are given in Appendix A. Very few such detailed measurements of echelon fracture sets have been reported in the literature and it is hoped that this study will add significantly to the information available about echelon fracture sets. Accordingly, the frequency distribution of these parameters, the relationships between them, if any, and the significance they have in the formation and growth of echelon fracture sets will be discussed.

4.2 Fracture length

Data, collected in the field, of fracture lengths within echelon sets are generally confined to one "representative" measurement for each set although several fracture length measurements were made for many sets. These measurements, however, do not give an adequate representation of the variation in fracture lengths within a given echelon fracture set. To determine the variation within an individual set, measurements of fracture lengths were made from a detailed (1:5 scale) map of a fracture set (Fig. 4.1). This was compared with variations in fracture lengths within sets obtained from measuring photos. For all three data sets the results were very similar (Fig. 4.2-4.4). The fracture length histograms indicate a very large number of short fractures with some form of decreasing

Figure 4.1

Detailed map of a right-stepping echelon fracture set at station 17.

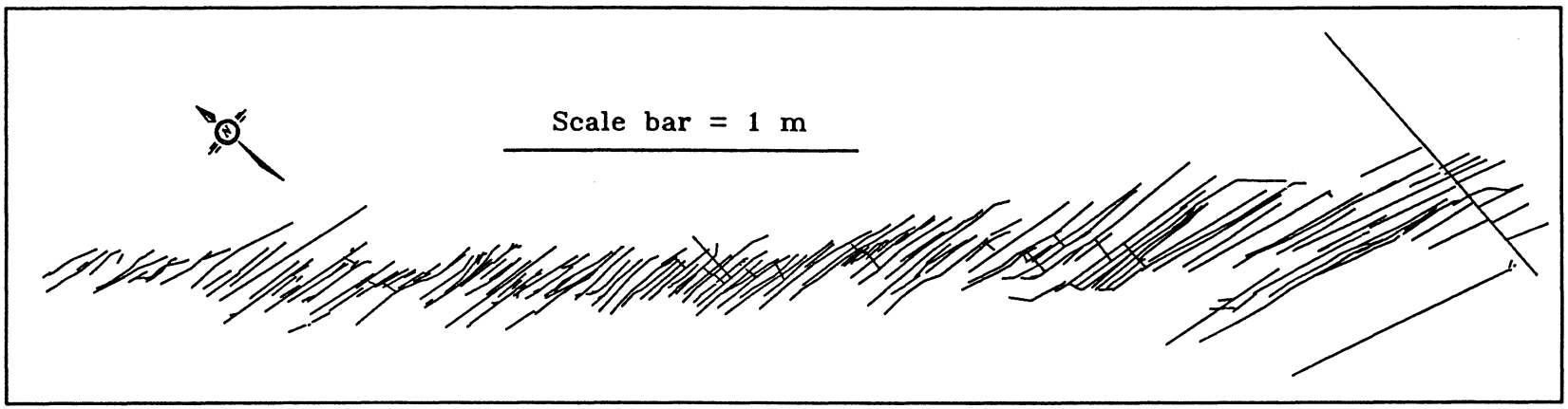
Scale bar = 1 m

Figure 4.2

Histogram of average fracture lengths for all echelon fracture sets.

Figure 4.3

Histograms of fracture lengths measured in echelon fracture sets.

a) All measured fracture lengths in 8 echelon fracture sets (4 RS and 4 LS).

all fracture sets

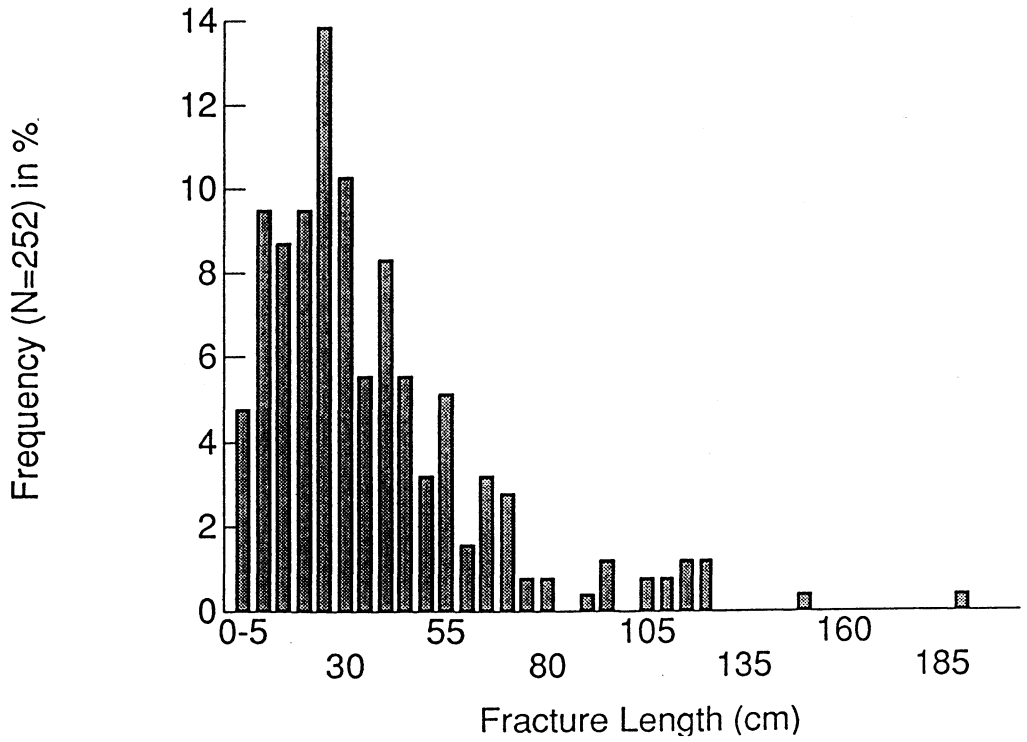

8 sets

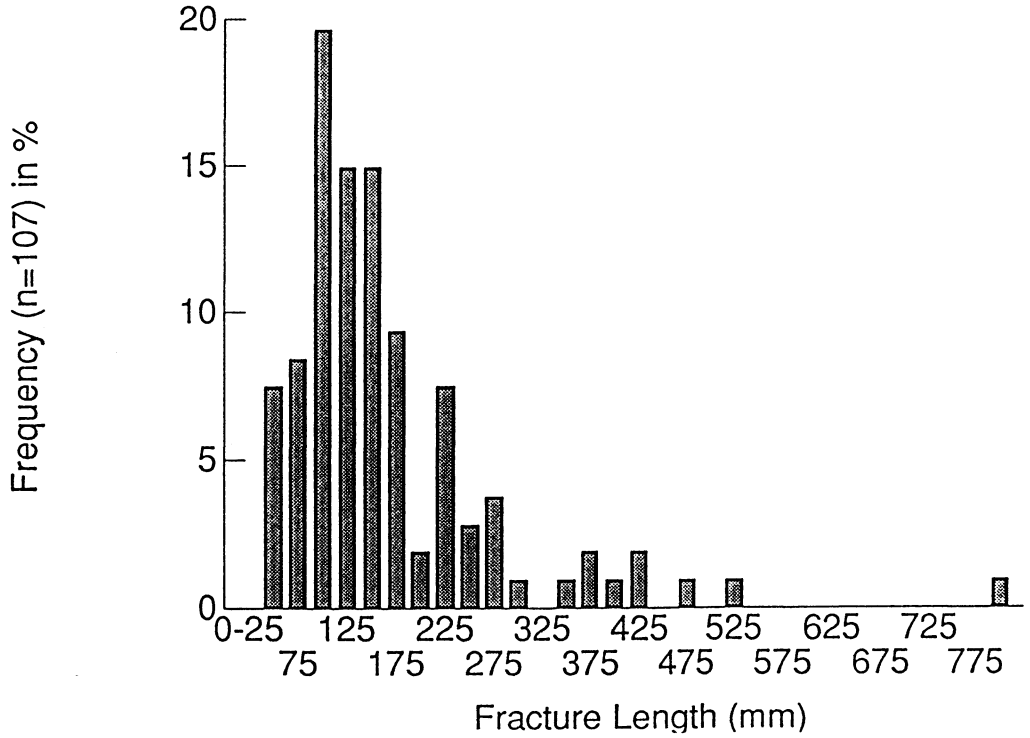

b) All measured fracture lengths in 4 right-stepping echelon fracture sets.

c) All measured fracture lengths in 4 left-stepping echelon fracture sets.

RS (4 sets)

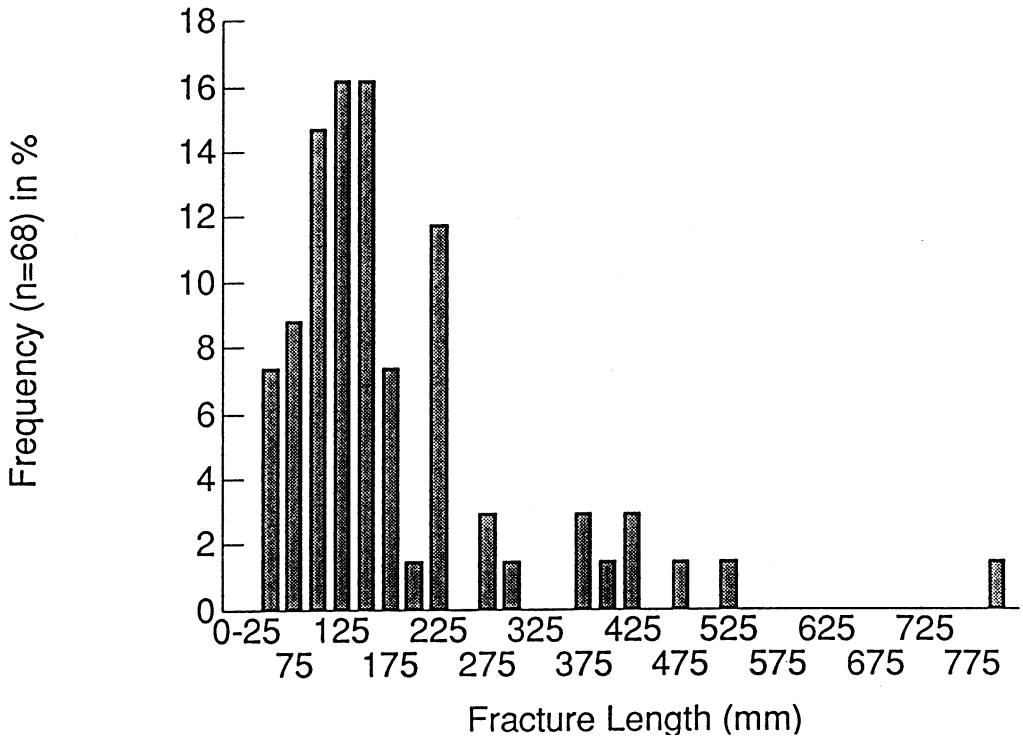

LS (4 sets)

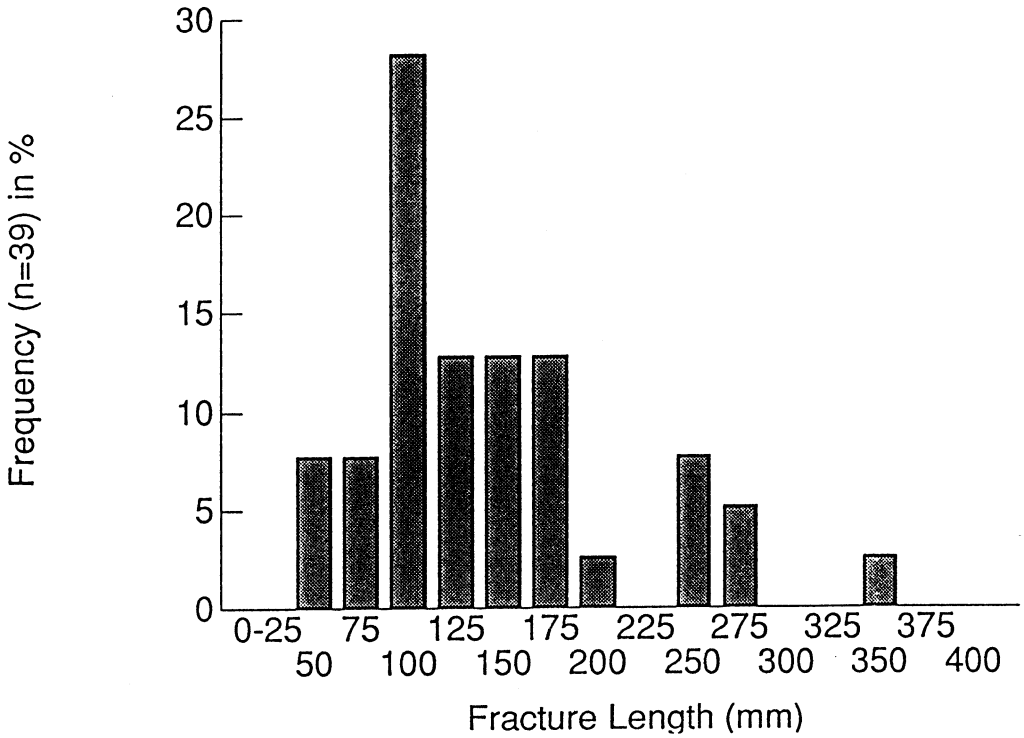

Figure 4.4

Histogram of all measured fracture lengths in a right-stepping set at station 17 (Figure 4.1).

Figure 4.5

Histogram of average fracture spacings for all echelon fracture sets.

RS set (Stn 17)

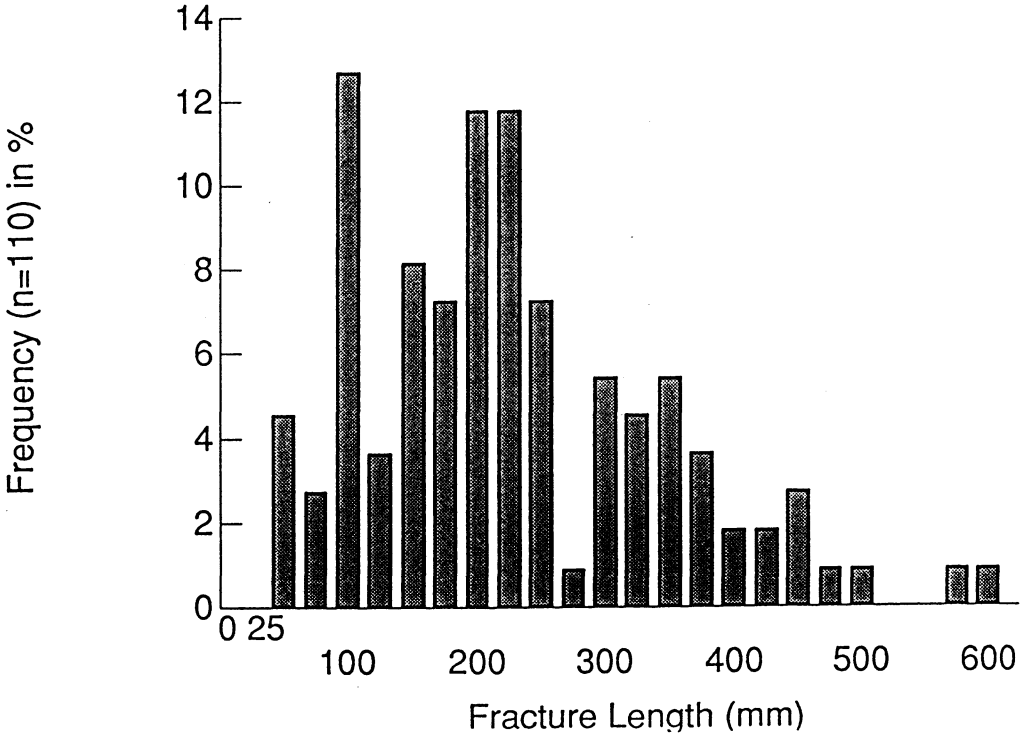

all fracture sets

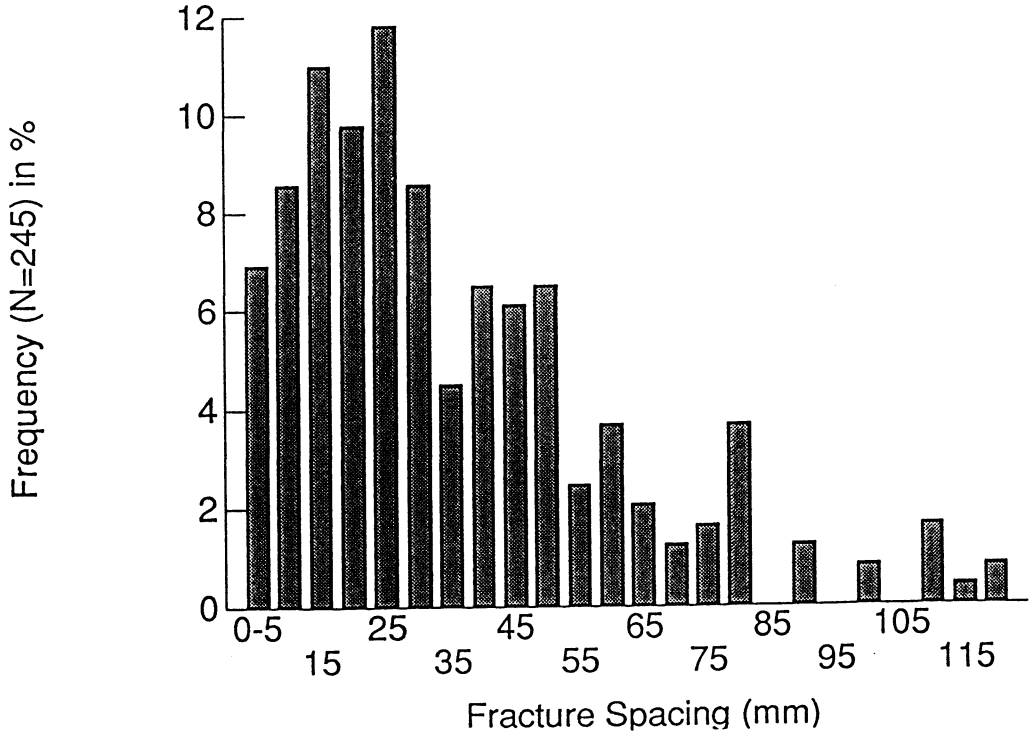

function towards higher fracture lengths. The number of short fractures reaches a peak which falls off rapidly towards the origin.

This distribution is very similar to that of fracture lengths reported by Segall and Pollard (1983) and Gudmundsson (1987). These authors consider the distribution of fracture lengths to fit a power law function having the form:

$$freq = a*length^{-n}$$

where a and n are some constants. They note that the number of short fractures predicted by the power law function exceeds the actual number measured. This can be attributed to the scale of observation. In the Segall and Pollard (1983) study the limit of the mapping resolution was one or two metres and the number of measured fractures less than two metres is smaller than the peak number of fractures. Similarly, the Gudmundsson (1987) study at a smaller scale shows a decrease, relative to the peak, in the number of measured fractures less than 200 metres. In the present study, the limit of mapping resolution is several centimetres. This corresponds to a decrease in the number, relative to the peak, of measured fractures less than about ten centimetres. This leads to the observation that regardless of scale the number of short fractures greatly exceeds the number of long fractures.

There seems to be one reason why this is so and it involves a consideration of fracture mechanics. In Chapter 2 it was noted that the longer a fracture the larger its crack extension force, G, becomes. Because of this one would expect a large number of long fractures (Gudmundsson, 1987). However, this is not the case as short fractures are more abundant. The problem is one of crack interaction. As a fracture grows under tension it relieves the tensile stress around itself to a distance on the order of its length (Nur, 1982). Calculations by Segall and Pollard (1983) indicate that long fractures inhibit the growth of adjacent shorter fractures that are less than 1/2 the longer fracture length away. As the longer fracture grows, the area in which it relieves the tensile stress increases thereby preventing even more shorter fractures from growing further. The result

is many small fractures with very few long fractures. Since adjacent fractures may prevent each other from growing and this depends on fracture length and spacing, a discussion of fracture spacing is important.

4.3 Fracture Spacing

Fracture spacing data are also confined to one "representative" measurement for each echelon fracture set and more than one measurement for several sets. Fracture spacing was also measured from a detailed (scale of 1:5) fracture map (Fig. 4.1) and from photos. It is defined as the perpendicular distance between two adjacent fractures in the plane of the outcrop (sub-horizontal). The frequency histograms of fracture spacing for all sets of data are very similar (Fig. 4.7-4.9). Fracture spacing peaks at relatively low spacings of 10-20 mm but drops towards the origin at spacings less than 10 mm. The distribution falls off gradually towards higher fracture spacings. The drop in fracture spacing towards the origin may be explained by the limit of mapping resolution for fracture spacing which is about 10 mm. Hence, fracture spacings of less than 10 mm may not be adequately represented on the histograms. Measurements of fracture spacings have errors of 2 to 3 mm for the photos and 5 mm for the field measurements and detailed maps. Therefore the use of 5 mm bar increments on the histograms is reasonable. The distribution of fracture spacings in the detailed map of a RS set from Station 17 (Fig. 4.7) ranges from less than 5 mm up to 70 mm. This indicates that there is a large variability in fracture spacing even within an individual echelon fracture set. A comparison of peak fracture lengths and peak fracture spacings within this set gives an order of magnitude difference between the two.

This means that adjacent fractures are well within 1/2 a fracture length of each other and should influence each other's growth. Assuming that the fractures are propagating under tension (mode I), the interaction of two parallel cracks of lengths 2c and 2a and spacing s may be modelled. Segall and Pollard (Fig. 11, 1983) plotted crack

Figure 4.6

Histograms of fracture spacings measured in echelon fracture sets.

a) All measured fracture spacings in 8 echelon fracture sets.

b) All measured fracture spacings in 4 right-stepping echelon fracture sets.

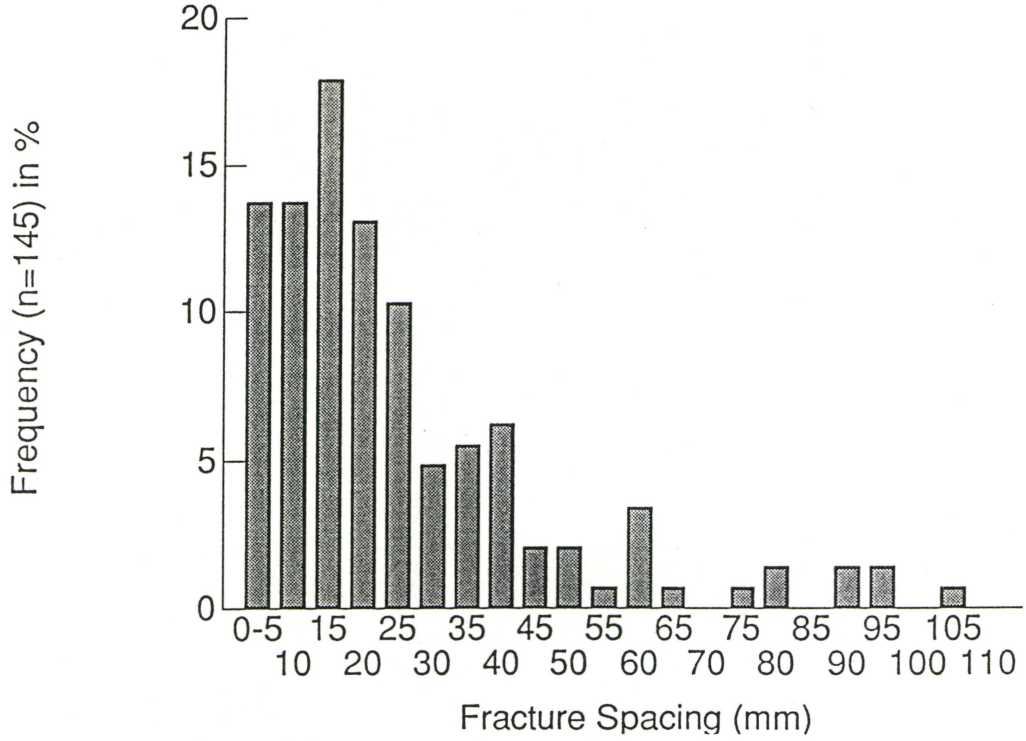
8 sets
Frequency (n=145) in %
20
15
10
5
0
0-5 15 25 35 45 55 65 75 85 95 105
10 20 30 40 50 60 70 80 90 100 110
Fracture Spacing (mm)

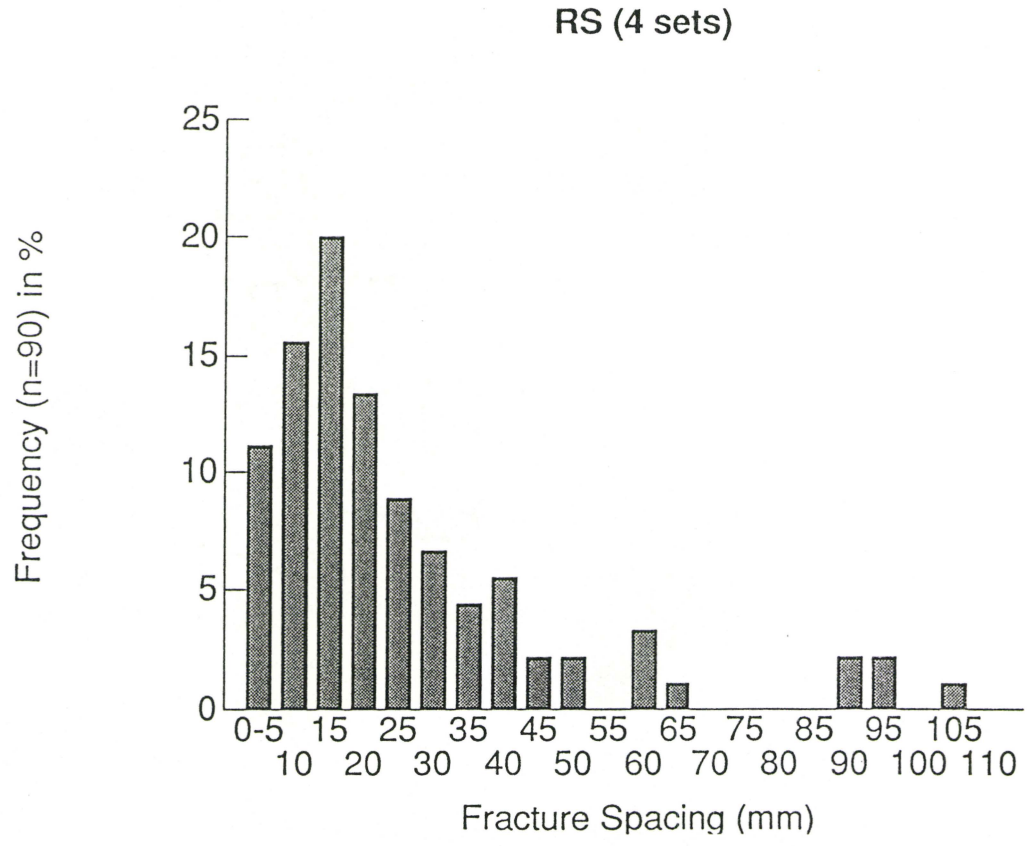
RS (4 sets)
Frequency (n=90) in %
25
20
15
10
5
0
0-5 15 25 35 45 55 65 75 85 95 105
10 20 30 40 50 60 70 80 90 100 110
Fracture Spacing (mm)

c) All measured fracture spacings in 4 left-stepping echelon fracture sets.

d) All fracture spacings in set 2b-8.

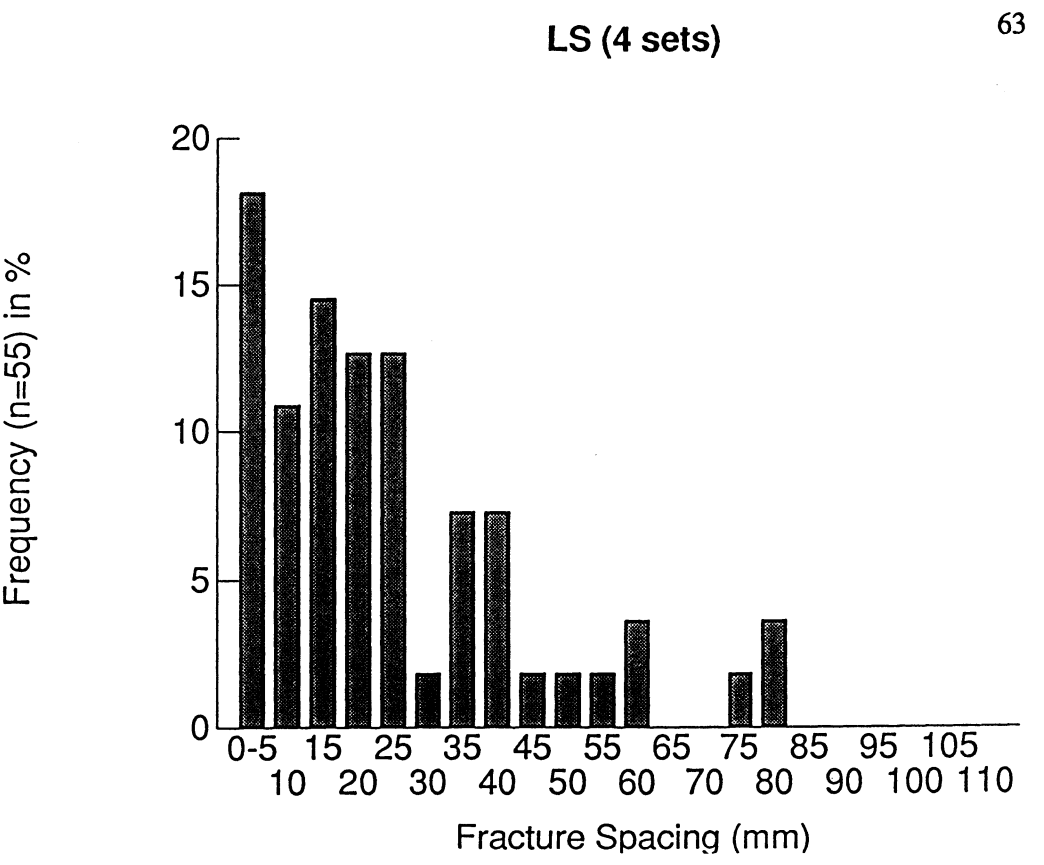
LS (4 sets)
Frequency (n=55) in %
20
15
10
5
0
0-5 15 25 35 45 55 65 75 85 95 105
10 20 30 40 50 60 70 80 90 100 110
Fracture Spacing (mm)

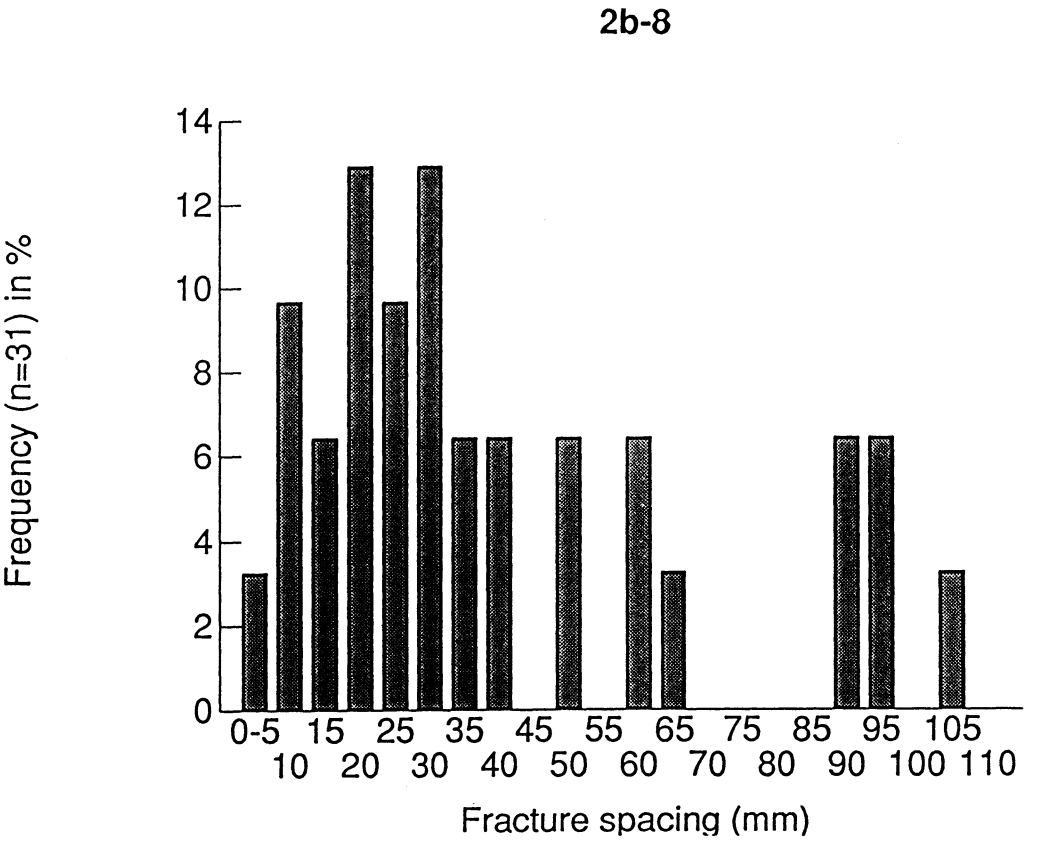
2b-8
Frequency (n=31) in %
14
12
10
8
6
4
2
0
0-5 15 25 35 45 55 65 75 85 95 105
10 20 30 40 50 60 70 80 90 100 110
Fracture spacing (mm)

e) All fracture spacings in set 3-3.

f) All fracture spacings in set 3-2.

3-3

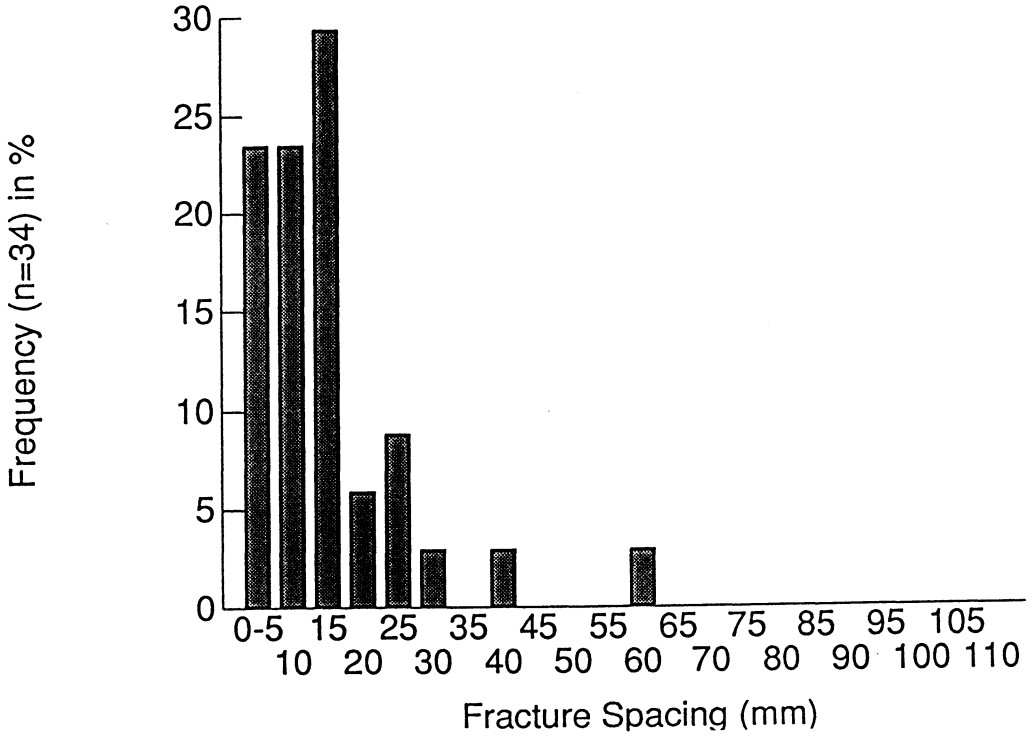
Frequency (n=34) in %
30
25
20
15
10
5
0
0-5 15 25 35 45 55 65 75 85 95 105
10 20 30 40 50 60 70 80 90 100 110
Fracture Spacing (mm)

3-2

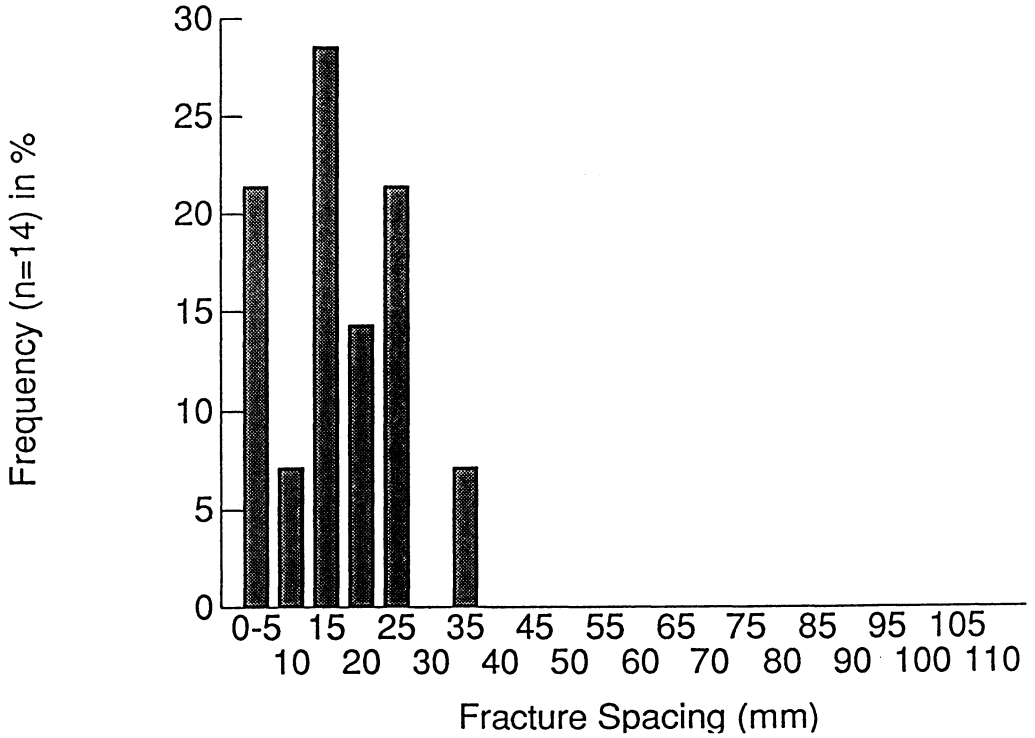
Frequency (n=14) in %
30
25
20
15
10
5
0
0-5 15 25 35 45 55 65 75 85 95 105
10 20 30 40 50 60 70 80 90 100 110
Fracture Spacing (mm)

g) All fracture spacings in set 7-8.

Figure 4.7

Histogram of all measured fracture spacings in a right-stepping set at station 17 (Figure 4.1).

7-8

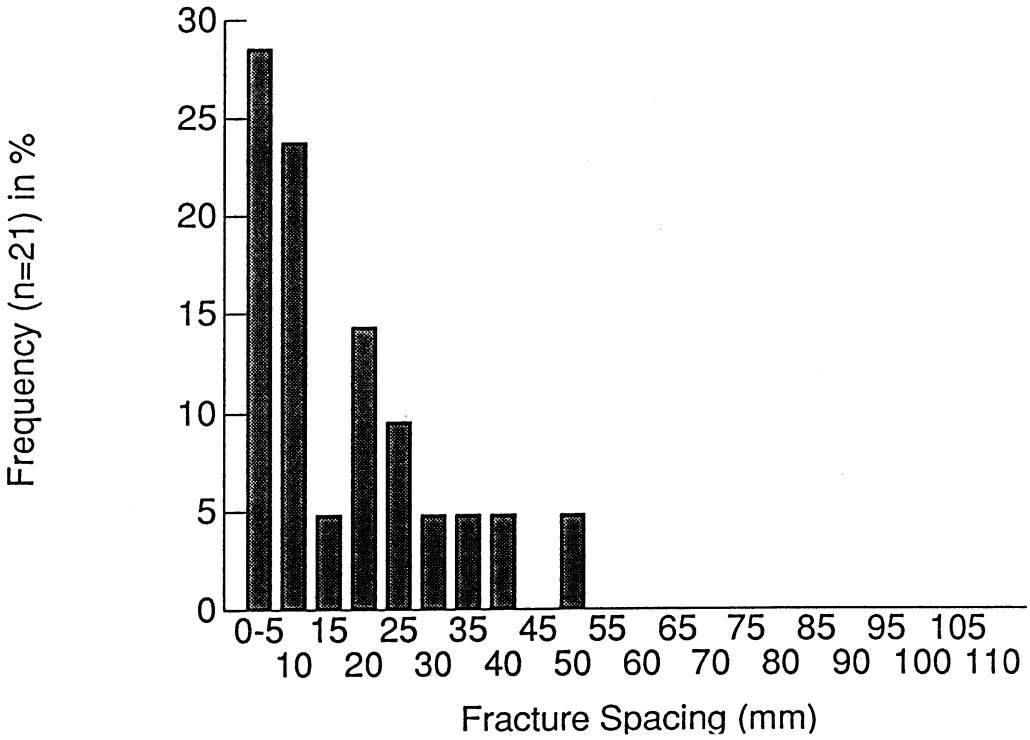

RS set (Stn 17)

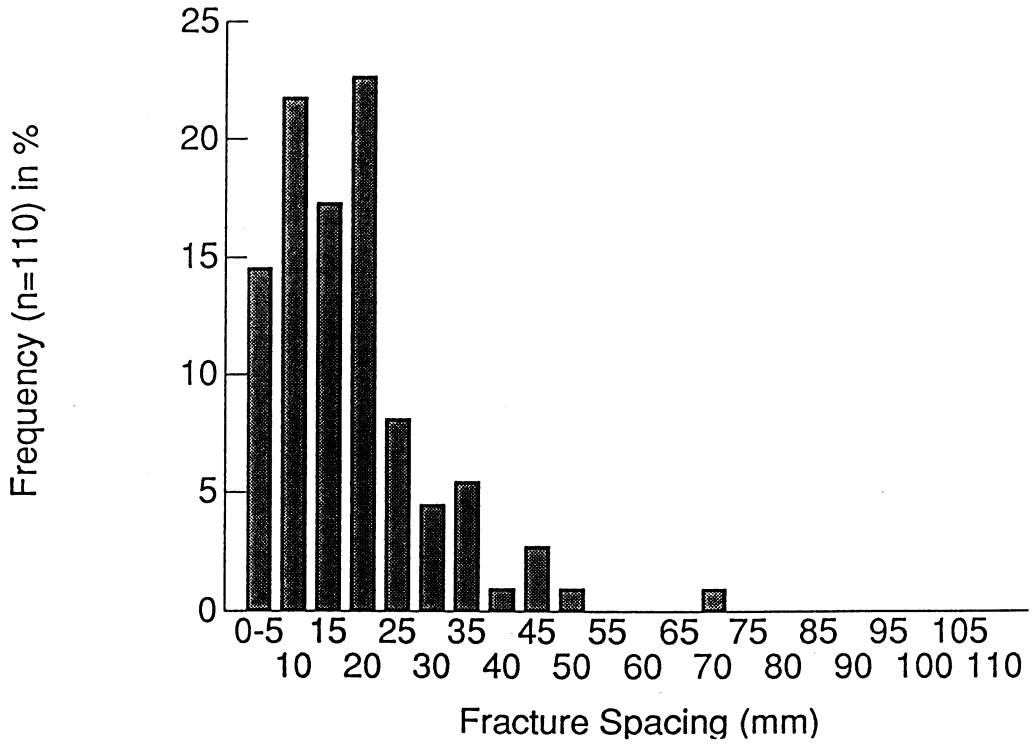

extension force, normalized to its value for an isolated crack, versus the ratio of the two crack lengths (a/c) for different ratios of crack spacing over crack length (s/c). Their graph shows that as the crack length ratio increases, the longer crack behaves more like an isolated crack while the shorter crack has its crack extension force go to zero. At small crack spacings relative to crack length the longer crack has a greater effect in reducing the shorter crack's crack extension force. Two cracks of equal length with a ratio s/c=0.5 will both have about 1/2 the crack extension force they would have as isolated cracks. If one fracture, a, increased its length by 50% it would have the crack extension force of an isolated crack while the other fracture, c, would have a crack extension force of close to zero. Two cracks of equal length that are separated by a distance an order of magnitude smaller than their length will have a ratio of s/c=0.2. If one of these cracks grows only a little longer than the other it will effectively stop the other crack from growing. Closely spaced fractures will greatly influence the propagation of each other even if they are nearly the same length. The echelon fractures in this study are very closely spaced relative to their length. If these fractures were propagating at the same time, they must have grown at very similar rates in order to reach lengths that are an order of magnitude greater than their spacing.

4.4 Relationship between fracture length and spacing

An apparent correlation between fracture length and spacing was observed while mapping echelon fracture sets of this study. It was noted that longer fractures seemed to be more widely spaced then shorter fractures within an individual fracture set. An approximate order of magnitude difference between fracture length and spacing has been established from the fracture length and spacing histograms. Fracture spacing can be plotted against fracture length to determine the nature of the relationship. The results of this for the data sets available are shown plotted in Figures 4.8 to 4.10 and Appendix B.

Figure 4.8

Average fracture lengths plotted against average fracture spacings for all echelon fracture sets. Each average fracture length for an echelon set is plotted with the average fracture spacing for that set. Calculated first order linear regression lines are also plotted with each graph.

a) All echelon fracture sets.

b) An enlargement of the graph in a).

Fracture length vs spacing

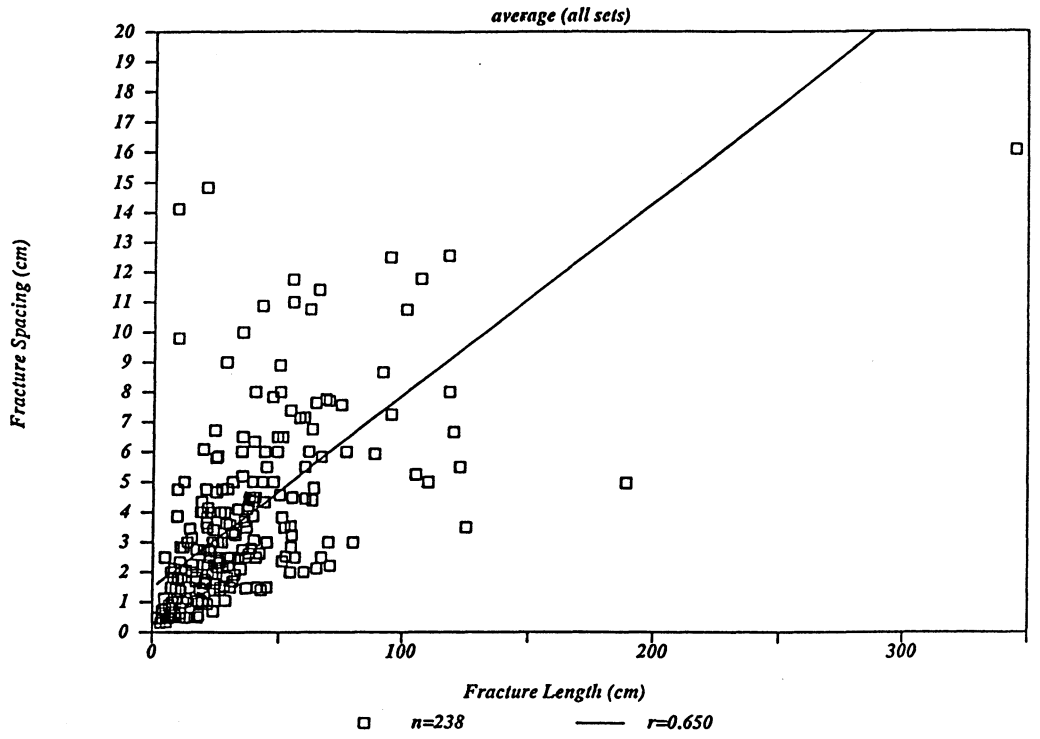

Fracture length vs spacing

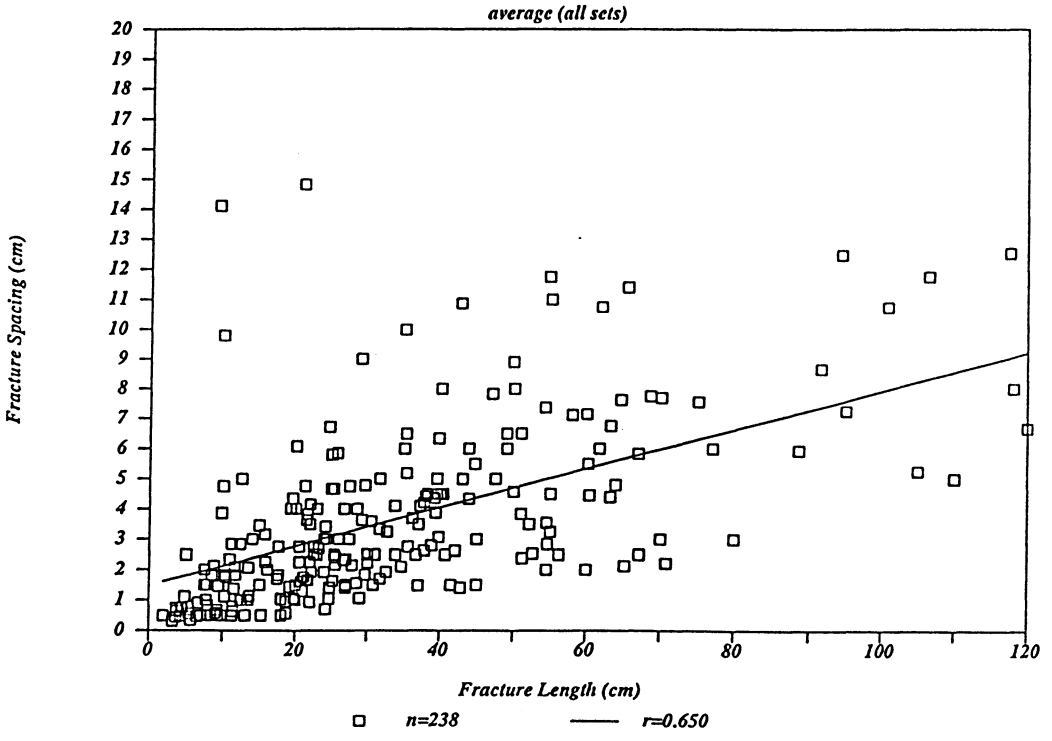

Figure 4.9

Fracture lengths plotted against fracture spacings for 8 echelon fracture sets. Each measured fracture length is plotted with the fracture spacing measured to the next fracture. Calculated first order linear regression lines are also plotted with each graph.

a) All measurements for 8 echelon fracture sets.

b) All measurements for 4 right-stepping echelon fracture sets.

Fracture length vs spacing

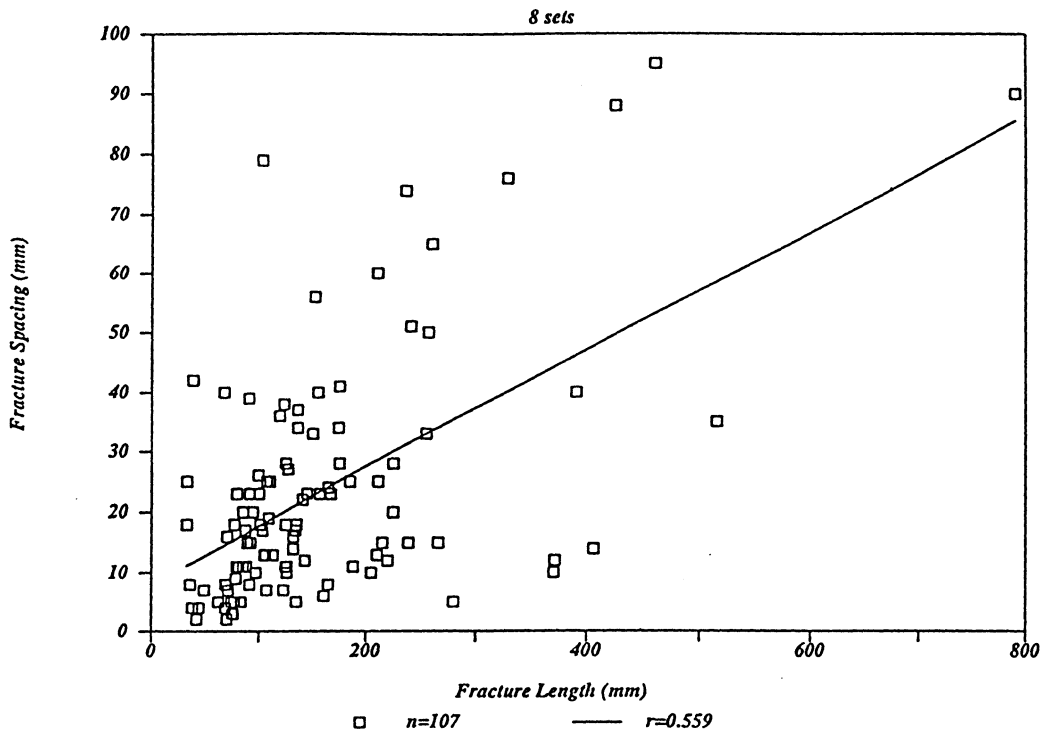

RS (4 sets)

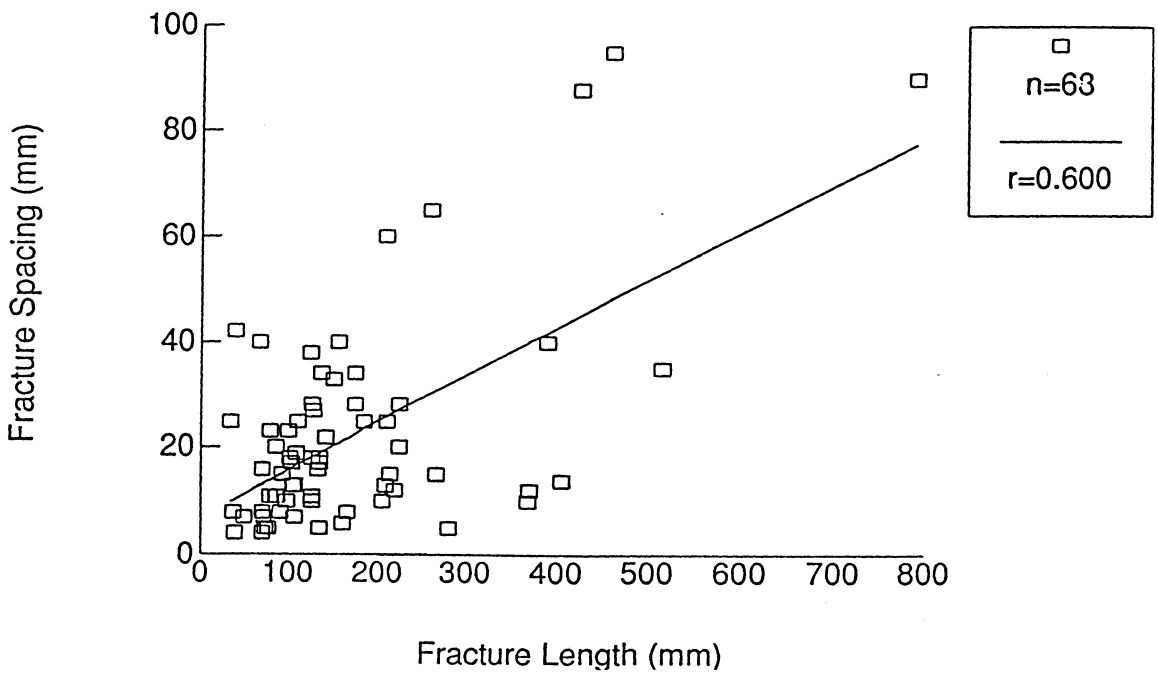

c) All measurements for 4 left-stepping echelon fracture sets.

Figure 4.10

Fracture lengths plotted against fracture spacings for a right-stepping fracture set at station 17 (Figure 4.1).

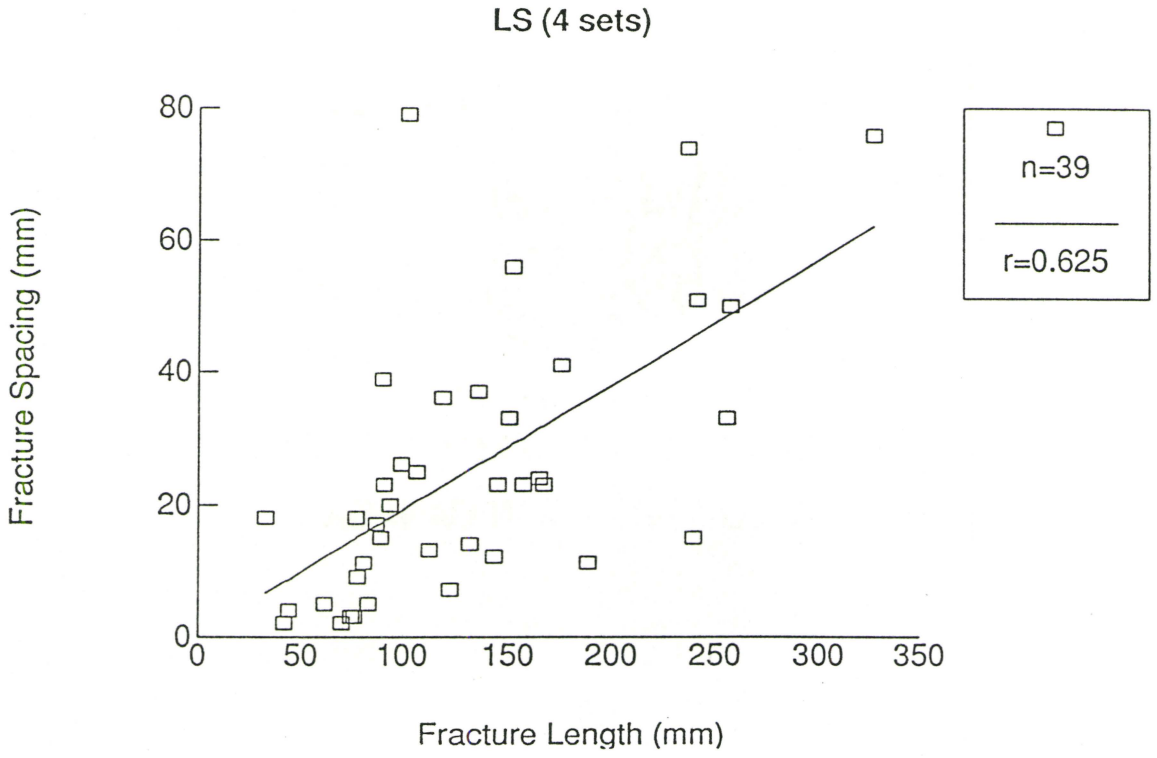

Fracture length vs spacing

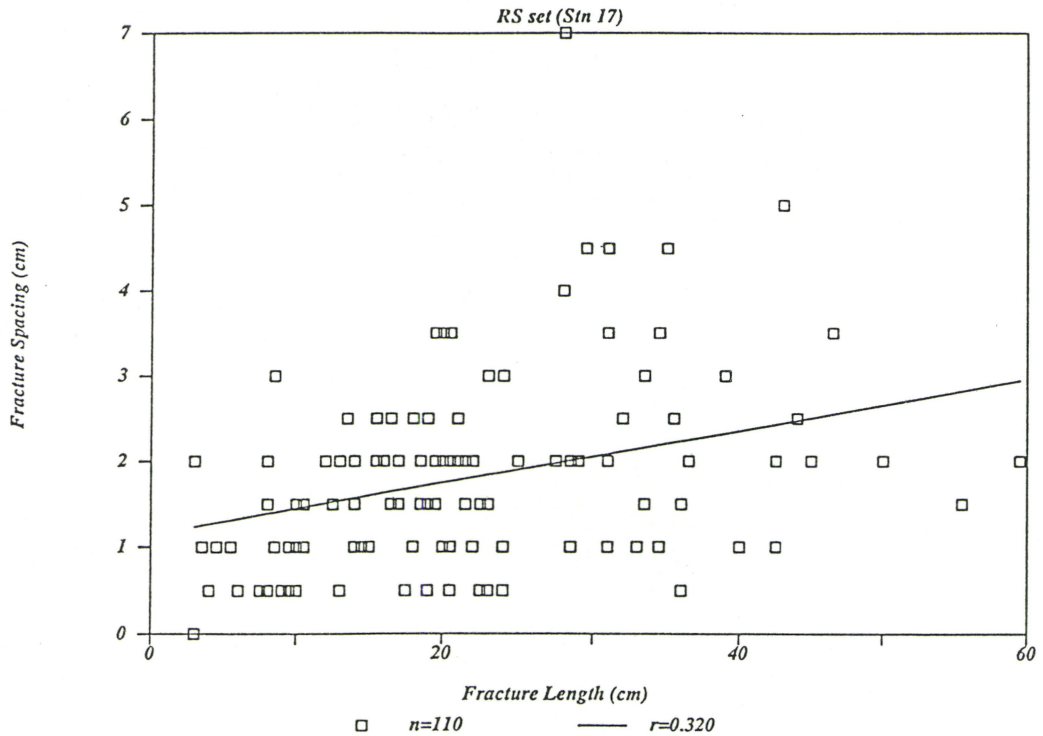

The plotted data show a large degree of scatter on all the graphs. It is unclear from these plots what the nature of the relationship is, if any exists, and there is no theoretical basis to suggest that this relationship must be linear. However, best-fitting straight lines through the data may give an approximation of the true relationship. First order linear regressions were calculated without fixing the Y-intercept and the corresponding correlation coefficients, r, range from 0.213 to 0.702 (Table 4.1). The regression lines were not constrained to pass through the origin because the true relationship may not be linear as it approaches the origin. Second order linear relationships were analysed but the resulting correlation coefficients were not improved and those results are not presented here.

Despite the lack of any clear linear relationship, it was found that the slopes of the regressions in almost all cases indicate an order of magnitude difference between fracture length and spacing. This confirms the general relationship outlined by the fracture length and spacing histograms.

4.5 Fracture-zone angle

The most commonly used parameter in classifying echelon fracture sets is the fracture-zone angle. This is the acute angle between the fracture and the zone it is contained in. In this study it is measured as the acute angle between the trend of the fracture and the trend of the set (or zone) on the sub-horizontal outcrop surface. This angle has been measured for 406 RS and LS echelon fracture sets and is shown plotted as histograms in Figure 4.11.

Both RS and LS sets have a broad Gaussian-like distribution of fracture-zone angles. The LS sets have a peak at about 20°-25° which is a smaller angle then the RS peak of about 30°-35°. These peaks are significantly less than the expected 45° angle for tension fractures in shear zones predicted by Ramsay and Huber (1983) and discussed in Chapter 2. If the fractures are tensile then angles of 20°-35° indicate positively

Table 4.1

Table of regression analysis results for fracture length versus fracture spacing.

REGRESSION ANALYSIS OF FRACTURE LENGTH VERSUS SPACING

Data set		n	slope	constant	corr coef r
All sets		238	0.064	1.48	0.650
8 sets		107	0.098	7.93	0.559
4 RS sets		68	0.089	6.92	0.600
	7-23	11	0.116	3.21	0.509
	2b-8	23	0.105	8.77	0.665
	2-37	13	-0.152	43.3	0.471
	3-3	21	0.012	8.73	0.213
4 LS sets		39	0.189	0.259	0.625
	3-2	10	0.112	4.91	0.564
	2b-16	6	-0.066	23.9	0.232
	7-8	13	0.142	-0.18	0.702
	7-30	10	0.138	24.2	0.439
RS set	Stn 17	110	0.030	1.15	0.320

Figure 4.11

Histograms of fracture-zone angles for all echelon fracture sets.

a) All right-stepping echelon fracture sets.

b) All left-stepping echelon fracture sets.

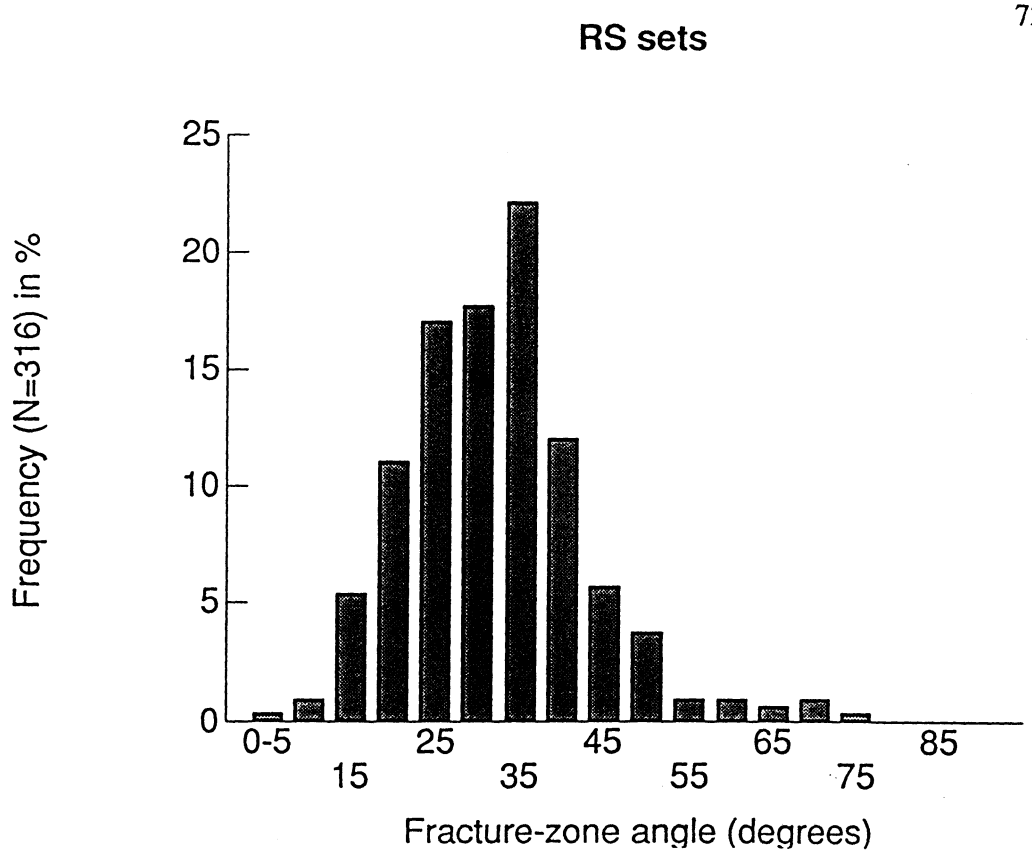
RS sets
Frequency (N=316) in %
25
20
15
10
5
0
0-5
15
25
35
45
55
65
75
85
Fracture-zone angle (degrees)

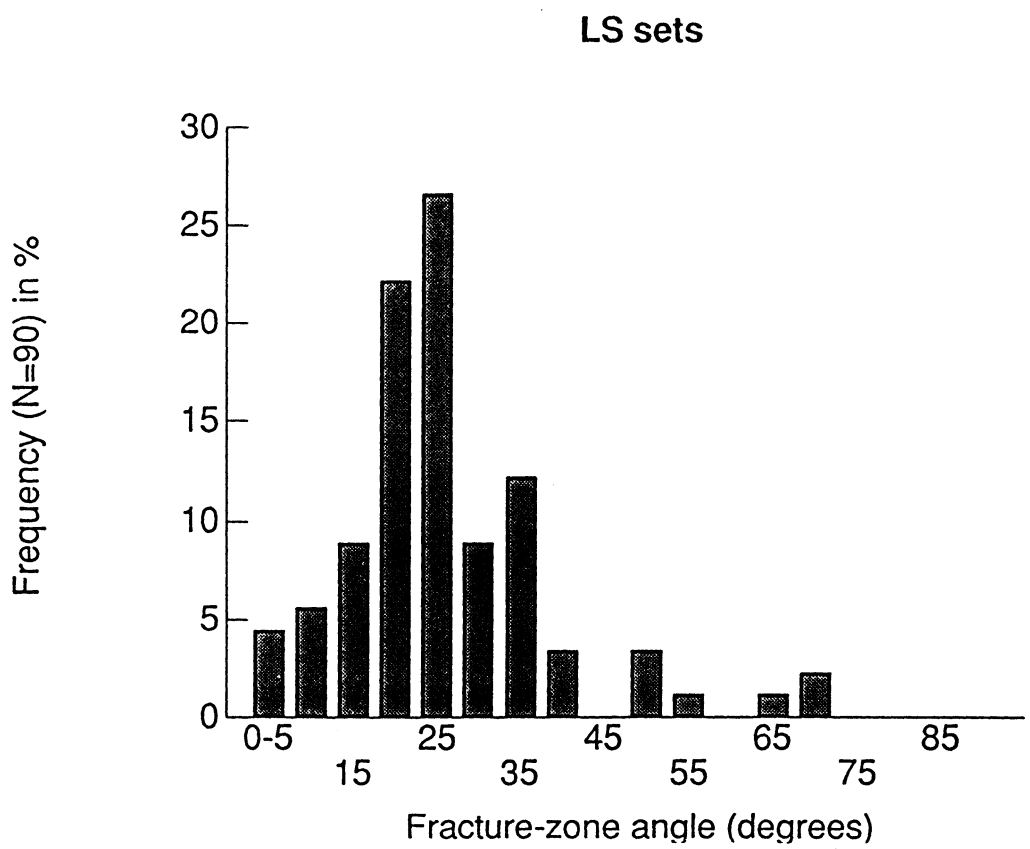
LS sets
Frequency (N=90) in %
30
25
20
15
10
5
0
0-5
15
25
35
45
55
65
75
85
Fracture-zone angle (degrees)

dilating shear zones (Ramsay and Huber, 1987). However, fractures within these echelon sets are not significantly dilatant and the overall apparent dilation of an individual fracture set is at least an order of magnitude smaller than the dilations of the echelon vein arrays considered by Ramsay and Huber's model. Therefore this model does not adequately explain the observed fracture-zone angles in this area.

Hancock's classification (1985) of fractures in shear zones places fractures in the 20°-35° range within the field of hybrid fractures or surfaces transitional between extension or shear. The classification of Rothery (1988) places arrays with fracture-zone angles of 20°-35° at the boundary between extension (propagation from a parent fracture) arrays and shear (shear zone) arrays. Clearly, there is a lack of concensus in the literature regarding the interpretation of fracture-zone angles. There is no systematic variation in fracture-zone angle through the study area or at the outcrop scale. The distribution of fracture-zone angles measured at one station is very similar to the distribution observed over the study area (Fig. 4.12). Figure 4.13 shows the areal distribution of average fracture-zone angles for several locations at different stations. Over an outcrop distance of several metres the variation of fracture-zone angles is not systematic. Therefore the wide range of observed fracture-zone angles cannot be attributed to local systematic variations in features such as foliation or rock type that may influence fracture propagation. It seems likely that changes affecting the entire study area, perhaps of rock properties or stress state, were responsible for producing the range of fracture-zone angles observed.

As noted in Chapter 2, many factors can influence, in theory, the fracture-zone angle. These observations, combined with the broad distribution of fracture-zone angles measured, mean that these echelon fracture sets cannot be classified on the basis of fracture-zone angle alone.

Figure 4.12

Histogram of fracture-zone angles for all right-stepping echelon fracture sets at station 6.

Figure 4.13

Areal distribution of average fracture-zone angles for several stations.

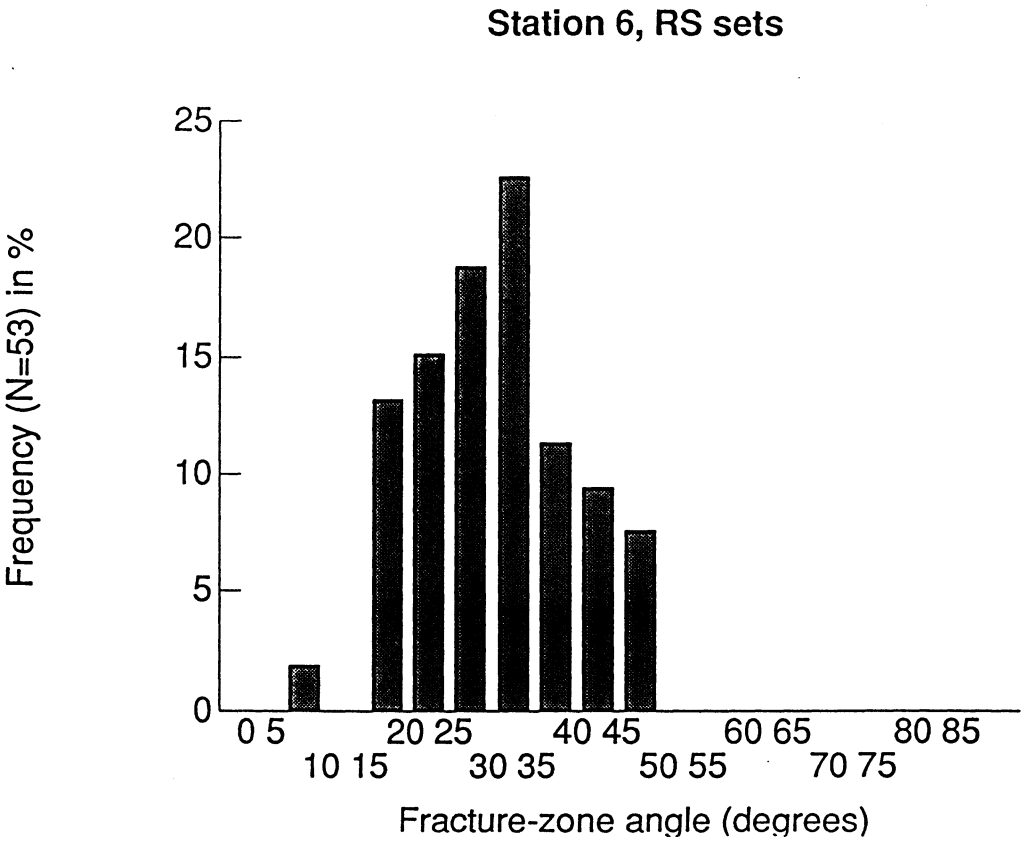
Station 6, RS sets
Frequency (N=53) in %
25
20
15
10
5
0
0 5
10 15
20 25
30 35
40 45
50 55
60 65
70 75
80 85
Fracture-zone angle (degrees)

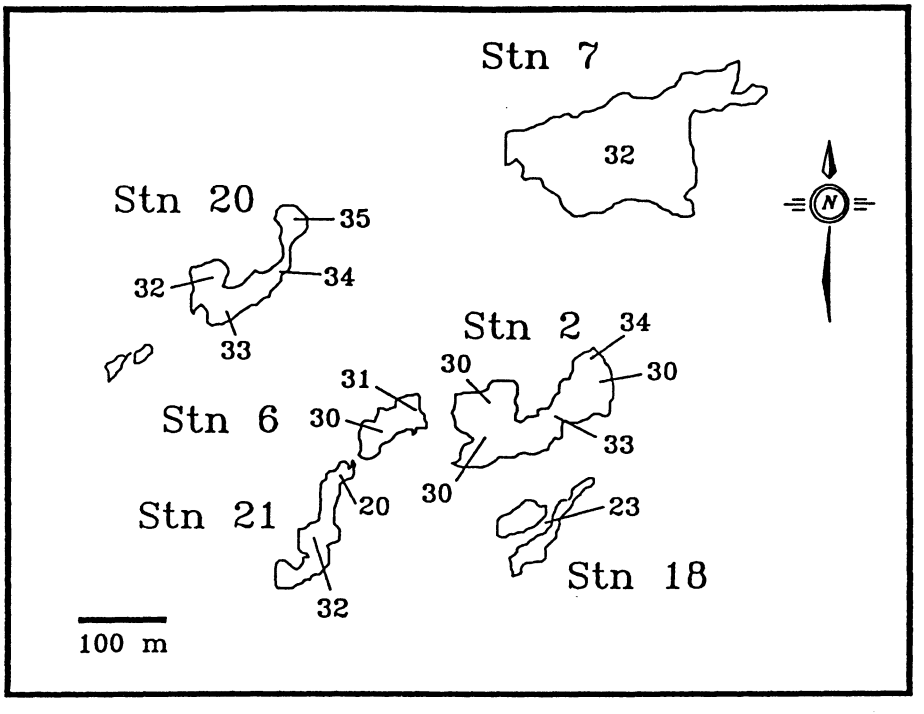
Stn 7
32
Stn 20
35
32
34
33
Stn 2
34
30
30
31
Stn 6
30
33
30
Stn 21
20
23
Stn 18
32
100 m

4.6 Fracture Overlap

Fracture overlap has been defined as the distance one fracture overlaps the next adjacent fracture within the fracture sets and is measured parallel to the fractures. The overlap for each fracture can be normalized to its fracture length and is called overlap ratio. Figure 4.14 is a histogram of overlap ratios for an individual fracture set. It can be seen that there is a wide range of overlap ratios but 80% of the data have overlap ratios greater than 0.5. The wide range is due to variations in fracture lengths and spacings within the set (Fig. 4.1). Overlap ratio has been used as an aid to classification of echelon fracture sets. Pollard et al (1982) report that overlap of crack tips in echelon fracture sets that propagated from a parent crack are approximately equal to the spacing between cracks. Rothery (1988) sets an arbitrary cutoff for overlap ratios of echelon sets that propagated from a parent crack of 0-0.4. On this basis, the echelon fracture sets in this study have overlap ratios significantly greater than the ratios observed for echelon fractures propagating from a parent crack.

Overlap ratio is dependent on the parameters fracture length, fracture spacing and fracture-zone angle (Fig. 4.15). It may be expressed as the equation:

$$OR = 1 - s/L(\tan B)$$

where OR is overlap ratio, L is fracture length, s is fracture spacing and B is the fracture-zone angle. If the ratio of fracture length to spacing is held constant then overlap ratio versus fracture-zone angle is a hyperbolic function (Fig. 4.16). Both Beach (1975) and Rothery (1987) obtained linear relationships between overlap ratio and fracture-zone angle although they do not specify how they accounted for the variables fracture length and spacing. A plot of average overlap ratios and fracture-zone angles for 85 fracture sets within the study area gives a scatter plot with no linear correlation (Fig. 4.17a). These data can be compared with the calculated theoretical curves for constant s/L (Fig. 4.17b).

Figure 4.14

Histogram of overlap ratios for a right-stepping echelon fracture set at station 17 (Figure 4.1).

Figure 4.15

The relationship of overlap to fracture length, fracture spacing and fracture-zone angle.

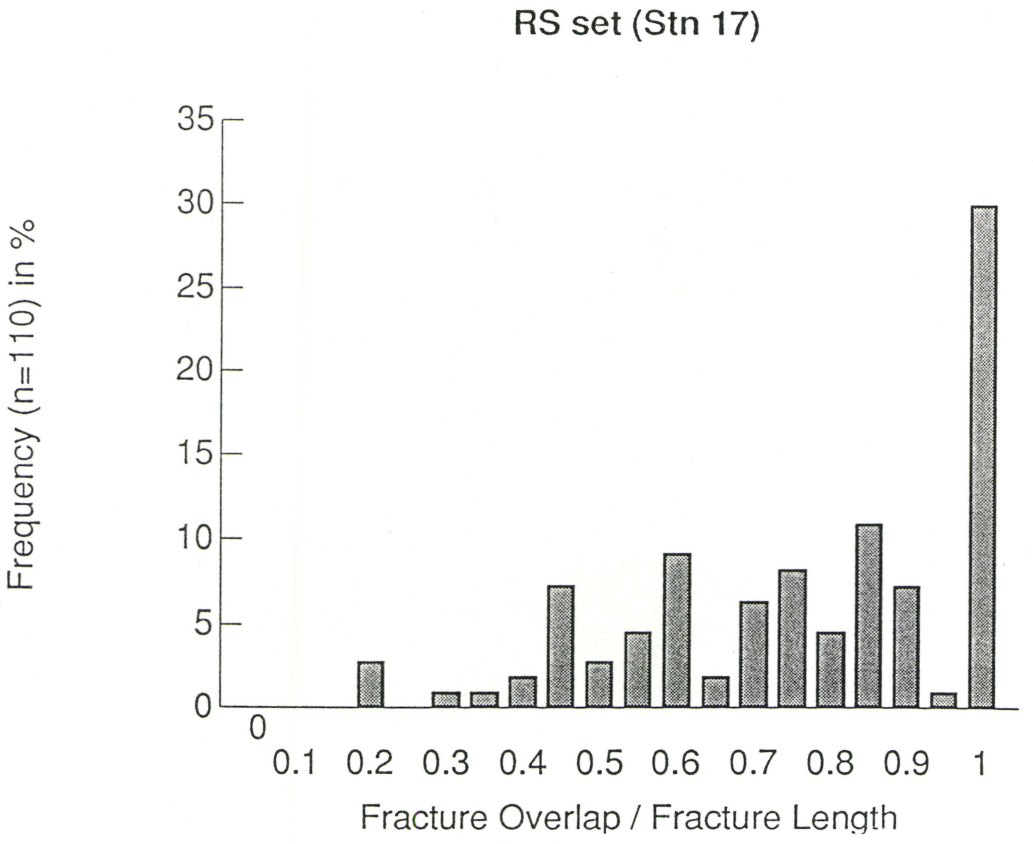
RS set (Stn 17)
Frequency (n=110) in %
35
30
25
20
15
10
5
0
0
0.1
0.2
0.3
0.4
0.5
0.6
0.7
0.8
0.9
1
Fracture Overlap / Fracture Length

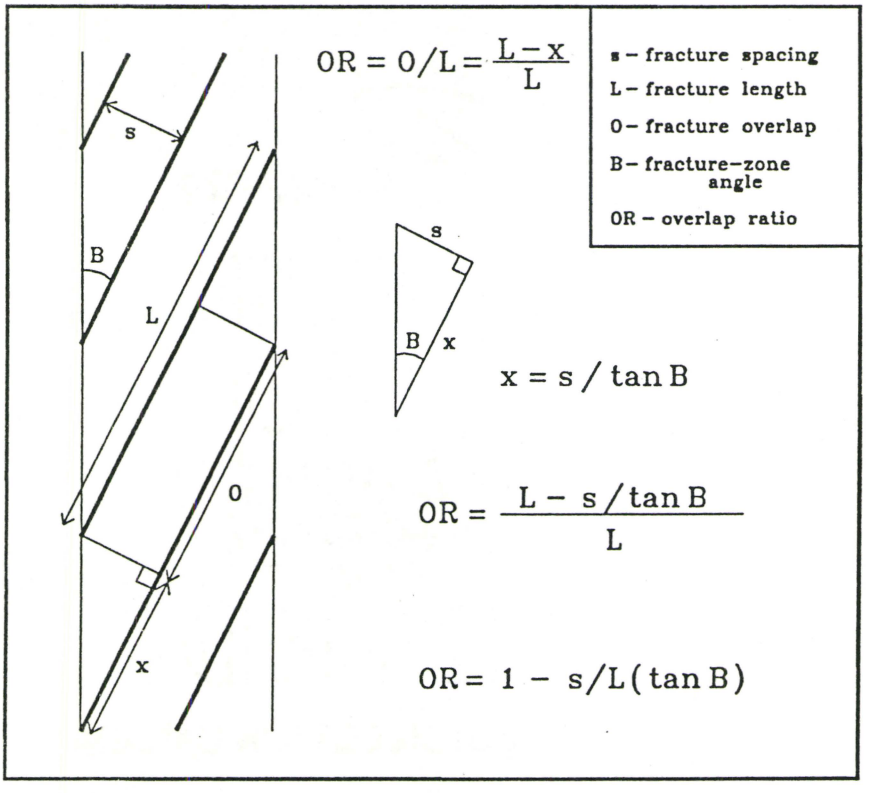
OR = O/L = (L − x)/L
s – fracture spacing
L – fracture length
O – fracture overlap
B – fracture–zone angle
OR – overlap ratio
s
B
L
O
x
B
x
x = s / tan B
OR = (L − s/tan B)/L
OR = 1 − s/L(tan B)

Figure 4.16

Theoretical curves for overlap ratio as a function of fracture-zone angle for constant fracture spacing to fracture length ratios.

Figure 4.17

a) Overlap ratio plotted against fracture-zone angle for all echelon fracture sets. The overlap ratio was calculated by dividing the average overlap by the average fracture length for each echelon set. A calculated first order linear regression line is plotted for comparison.

OR VS FRACTURE-ZONE ANGLE

as a function of s/L

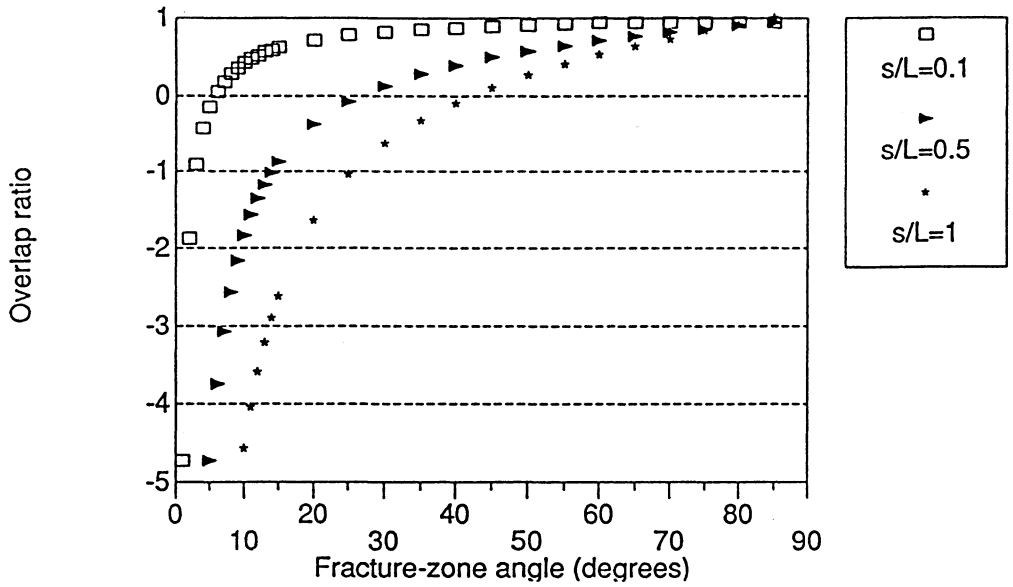

OR VS FRACTURE-ZONE ANGLE

all fracture sets n=85

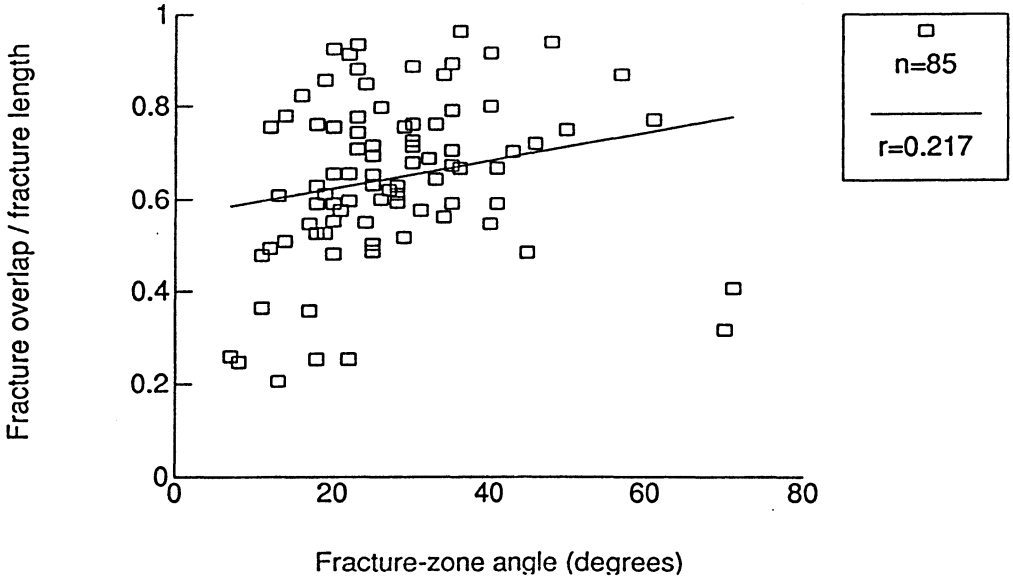

The data do not lie on any one curve but are scattered around indicating a range of s/L values. This is not too suprising given the large variability in fracture lengths and spacings.

4.7 Fracture set length, width and distribution

The dimensions of the echelon fracture sets can be characterized by their zone lengths and zone widths. Zone length was measured along the trend of the zone for the distance it was exposed in outcrop. Many of the fracture sets or zones extended beyond the limits of the outcrop. The zone width was measured perpendicular to its trend and was arbitrarily confined to a width that encompassed the majority of fractures within the set. These two parameters varied considerably but there is no consistent linear relationship between them (Fig. 4.18).

RS fracture sets have been observed to step right into adjacent RS fracture sets (Fig. 4.19). This suggests a heirarchy in that fracture sets themselves may be part of a larger domain of fracturing with a similar geometry at a smaller scale. This could explain the "domainal" nature of echelon fracture sets or why they are abundant in particular areas and absent in others. The echelon fracture sets may also be fairly regularly spaced over the extent of an outcrop (Fig. 4.20). Thus, locally, fracturing can be very intense, although, over the scale of an outcrop or the scale of the study area, the amount of strain accommodated by fracturing is very small.

4.8 Summary

Very little published data is available on the geometrical parameters of echelon fracture sets. The results of this study should contribute significantly to this knowledge and may be summarized as follows. The distribution of fracture lengths within echelon fracture sets in this area is similar to power law distributions reported for larger fractures and fissures in other areas. This supports the notion that smaller fractures are more

b) The same data as in a) with a theoretical curve for overlap ratio shown for comparison.

Figure 4.18

Zone length plotted against zone width for all echelon fracture sets.

OR VS FRACTURE-ZONE ANGLE

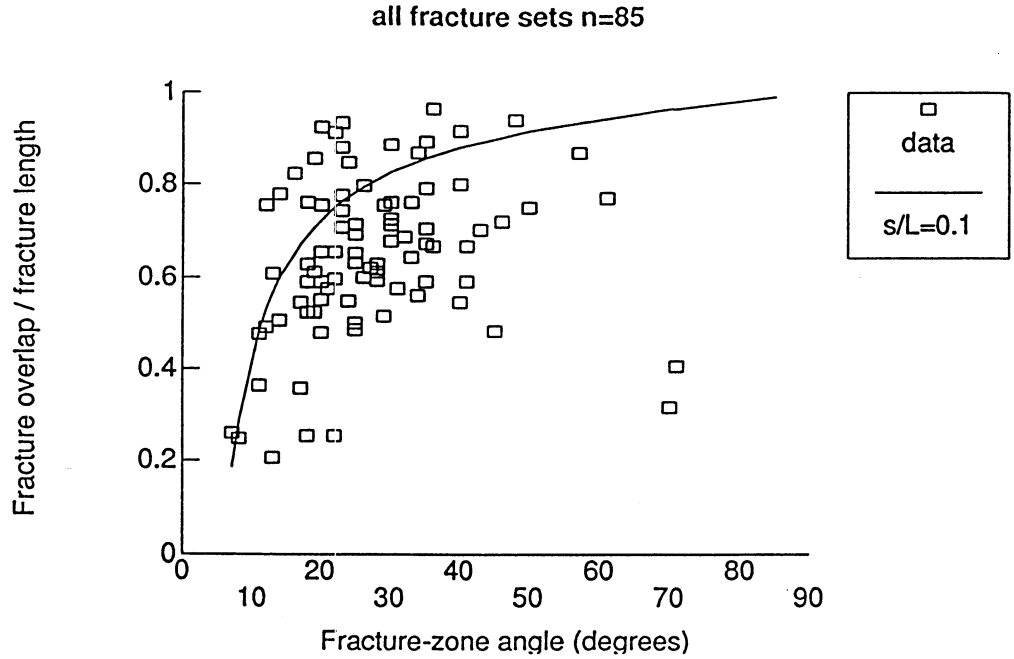

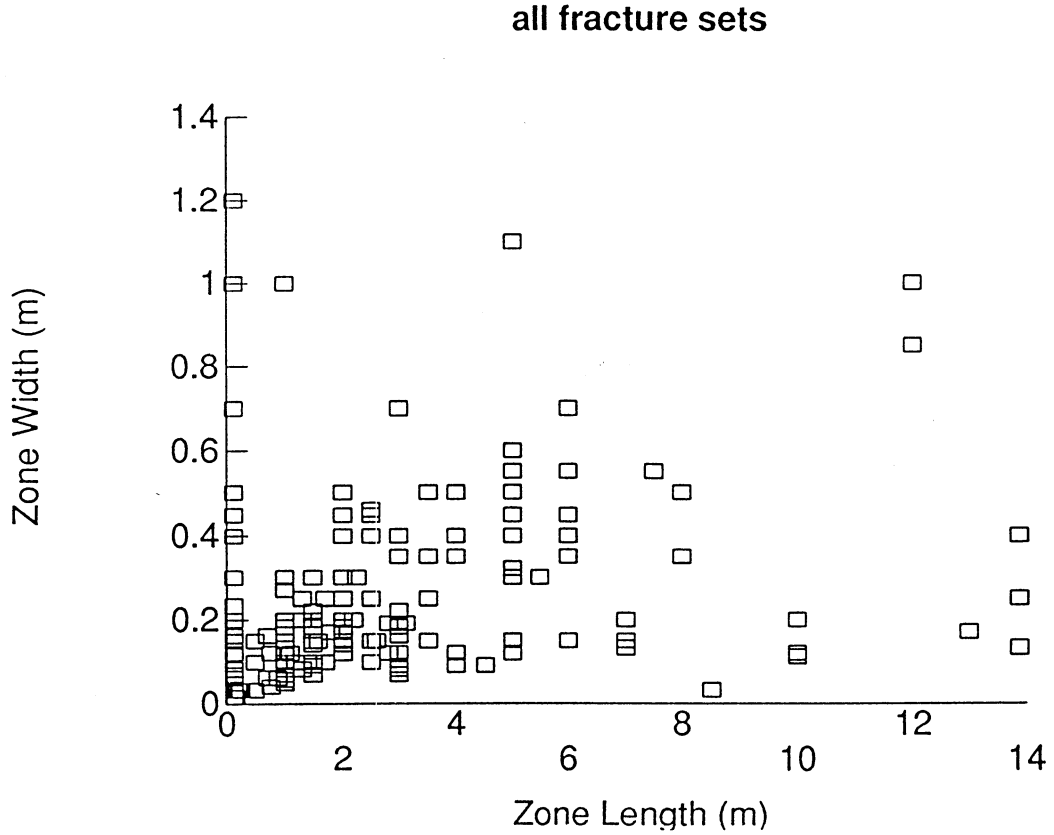

Figure 4.19

A right-stepping echelon fracture set that is composed of smaller echelon sets that step right. Hammer (33.5 cm) as scale.

Figure 4.20

A map of station 6 showing the areal distribution of echelon fracture sets.

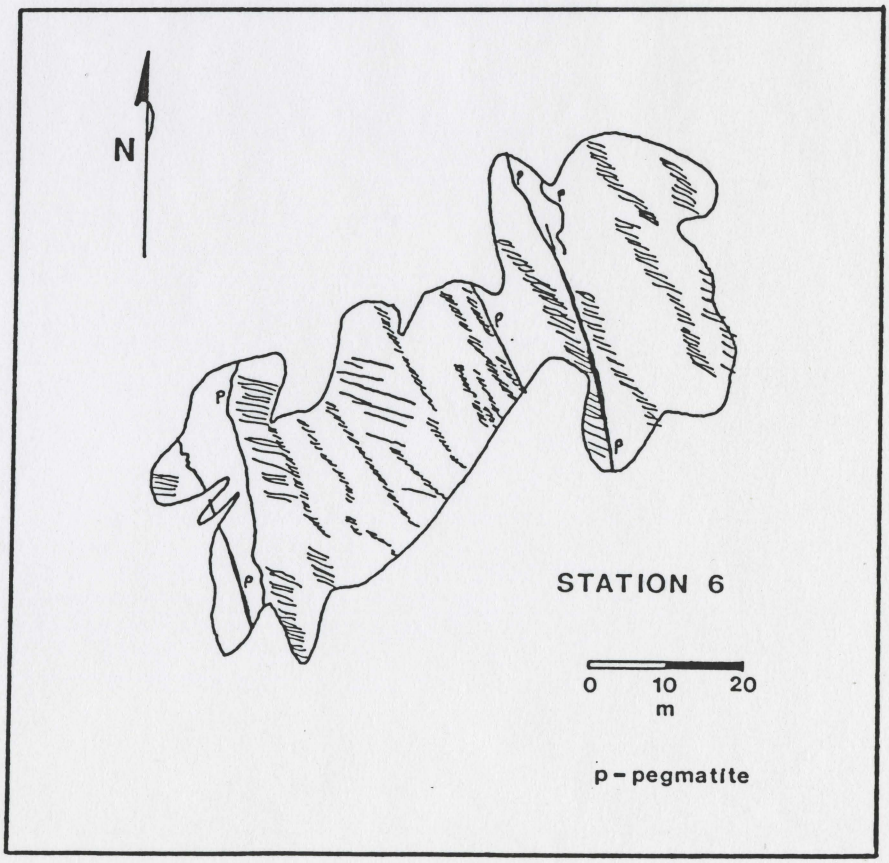
N
p
p
p
STATION 6
0
10
20
m
p - pegmatite

abundant then larger fractures at any scale of observation. Fracture spacing within echelon fracture sets was found to have a distribution similar to that observed for fracture lengths. This suggests the existence of some relationship between fracture length and spacing. Further analysis led to the conclusion that there is an approximate order of magnitude difference between fracture length and spacing. This means fractures are closely spaced relative to their lengths and thus crack interactions are very significant within echelon fracture sets. Fracture-zone angles were found to have a broad distribution and included values that have been attributed, in the literature, to both tension and shear fractures. This angle alone does not provide sufficient evidence to classify the echelon fracture sets. The overlap ratio of fractures within the sets is generally greater than 0.5 which could exclude their formation due to propagation from a parent fracture. And, finally, the echelon fracture sets are part of a heirarchy of fracturing that accommodates very little strain over the scale of the study area.

5.0 Orientations of Echelon Fracture Sets

5.1 Orientation Data

Orientations of isolated fractures, shear zones and shear fractures are shown plotted and contoured on equal-area stereonets in Figure 5.1. Contouring reveals that the poles to isolated fractures form a tight sub-horizontal cluster. Shear zones and shear fractures are also dominantly subvertical. Since the majority of all features described above are close to vertical, their distribution of strikes can be plotted as a circular histogram without loss of geologic significance.

The use of circular histograms allows for a better delineation of peaks than is possible with contoured equal-area stereonets. Accordingly, all subsequent orientation diagrams will be displayed as circular histograms. The orientations are counted at 2.5° intervals on a 360° circle using a continuous weighting function (Stesky per. comm. 1988). The details of the calculations and the weighting function chosen are given in Appendix C. The inner solid circle on the histograms represents the expected value for a uniform distribution of the data. The dashed outer circle represents 1.8 standard deviations above the expected value. This can be considered as the minimum value for statistically significant peaks given 100 data points (Robin, per. comm. 1988). Most of the histograms presented here contain less than 100 data points. However, the purpose of this plotting is to distinguish the location of peaks in the distribution, therefore, regardless of their statistical significance, peaks larger than the expected distribution are here considered geologically significant.

Orientations of LS and RS echelon fracture sets for all stations are plotted in Figures 5.2 and 5.3. There are two histograms for each figure. The first is a plot of the

Figure 5.1

a) Poles to isolated fractures. A contoured equal-area lower-hemisphere net.

b) Poles to shear fractures. A contoured equal-area lower-hemisphere net.

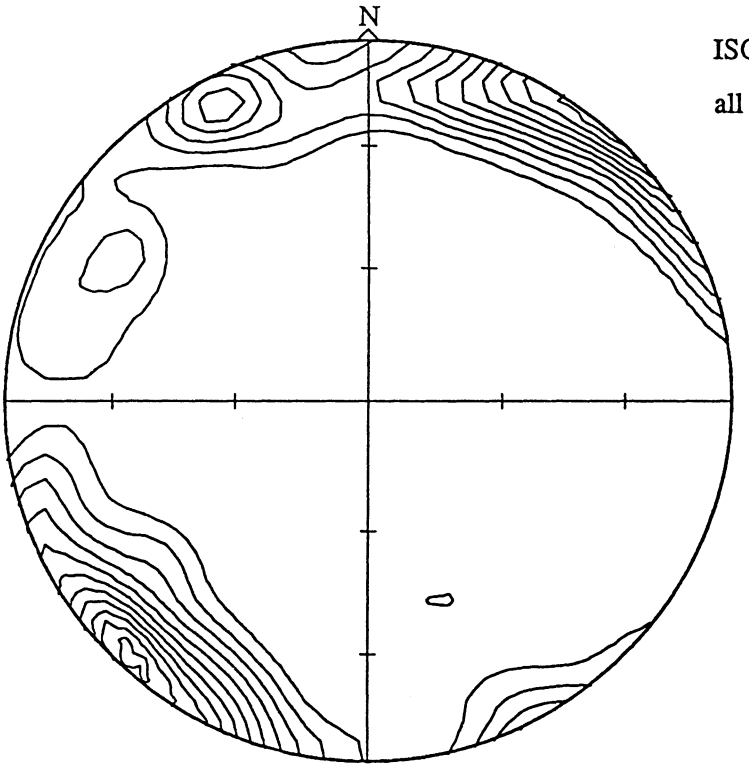

ISOLATED FRACTURES

all stations

N 360
k 82.0
E 4.4
s 1.5
Peak: value 35.5
position 221 / 3

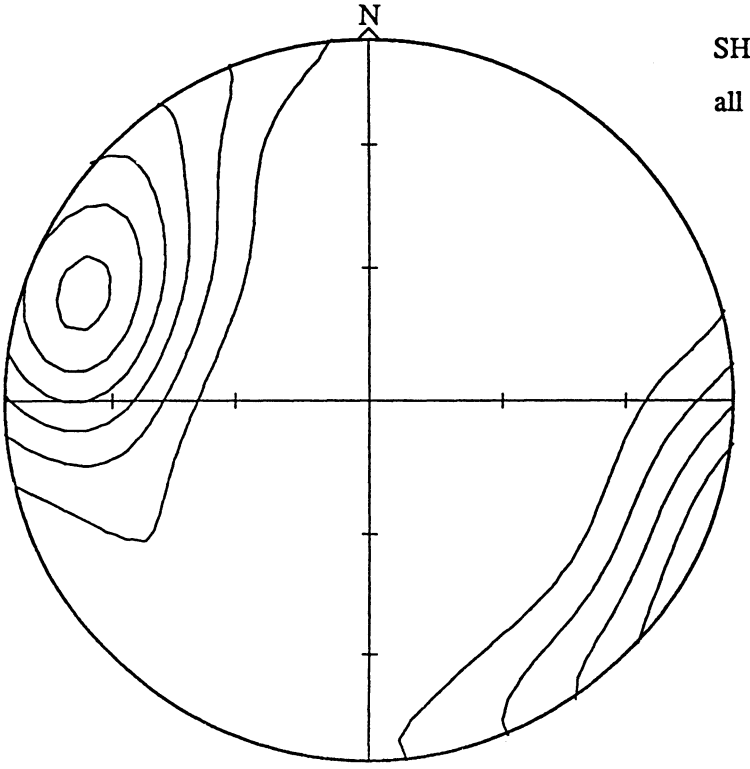

SHEAR FRACTURES

all stations

N 43
k 11.6
E 3.7
s 1.2
Peak: value 16.9
position 290 / 19

c) Poles to shear zones. A contoured equal-area lower-hemisphere net.

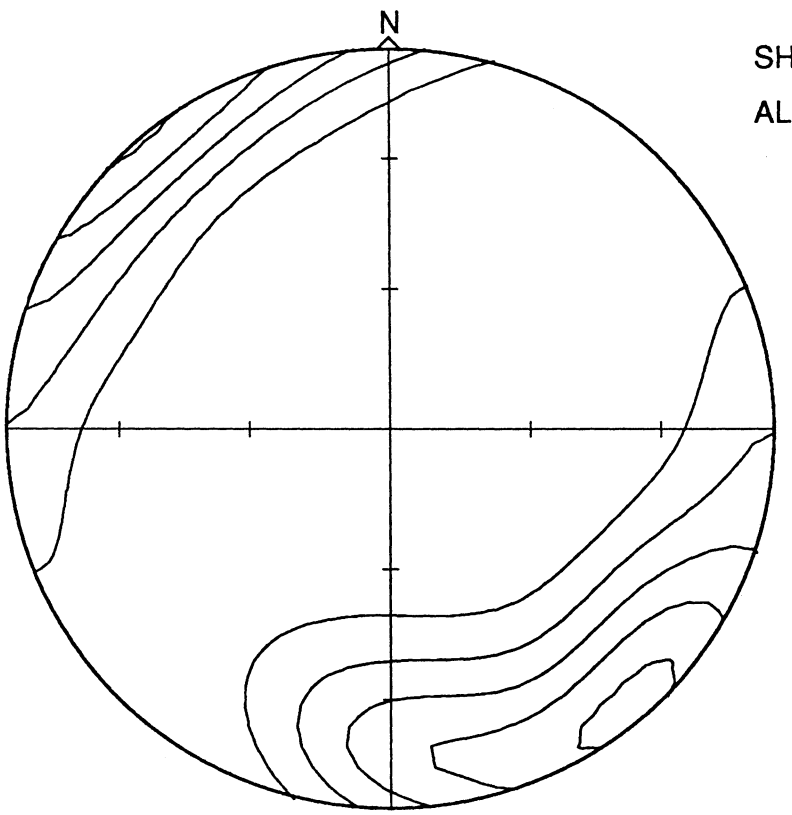

SHEAR ZONES

ALL STATIONS

N 53
k 13.8
E 3.8
s 1.3
Peak: value 14.9
position 139°/ 3°

Figure 5.2

Circular histograms of fracture and zone orientations.

a) All right-stepping zone orientations.

b) Fracture orientations for all right-stepping zones.

NOTE: All orientation data were counted using the method described by Robin and Jowett (1986) which has been modified for circular histograms by Stesky and Bailey-Kryklywy (1988).
N = number of orientations;
k = kurtosis of the Gaussian counting function; set at 100;
E = expected value of the counts for each station if the orientations were uniformly distributed over 180°;
σ = standard deviation about the expected value for the same uniform distribution;
Peak value = the highest count obtained;
Peak orientation = orientation of the counting station with the highest count; i.e. the peak fracture or zone orientation from 1°-180°.

ALL STATIONS

right-stepping fractures

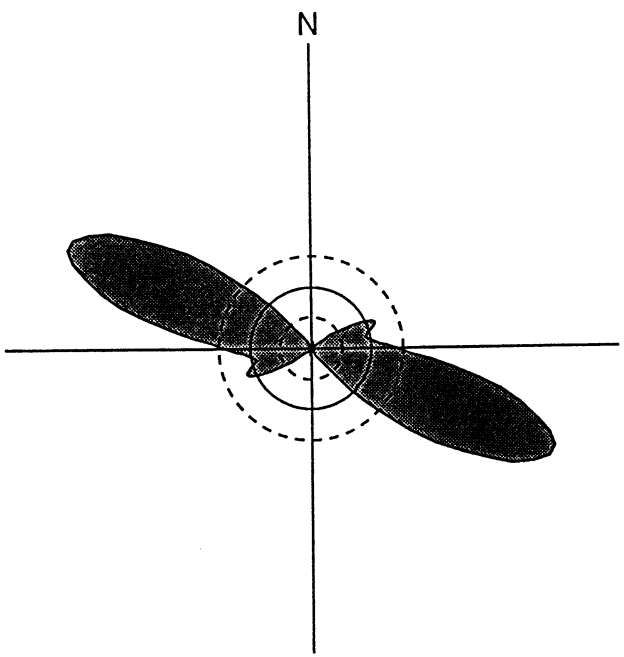

n = 315 E = 25.16 σ = 7.04 k = 100

Peak value = 106.58 Peak Orientation = 112.5°

—— E - - - - E ± 1.8σ

ALL STATIONS

right-stepping zones

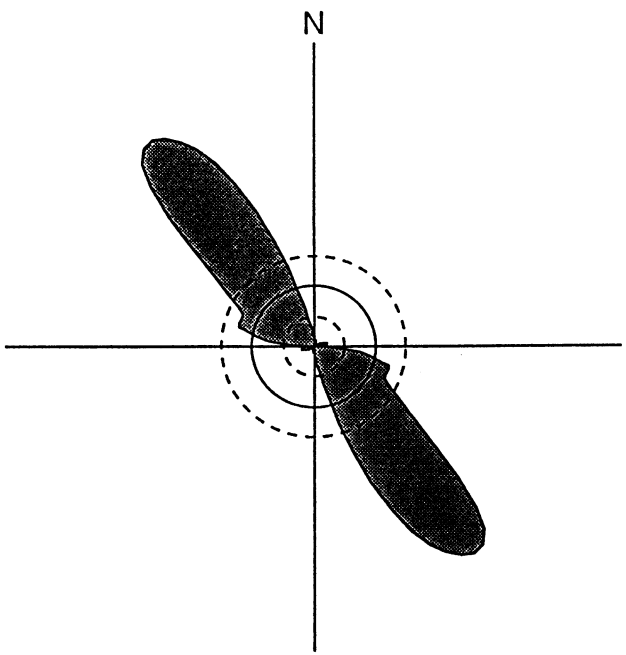

n = 321 E = 25.64 σ = 7.11 k = 100

Peak value = 111.42 Peak Orientation = 142.5°

—— E - - - - E ± 1.8σ

Figure 5.3

Circular histograms of fracture and zone orientations for left-stepping sets.

a) All left-stepping zone orientations.

b) Fracture orientations for all left-stepping zones.

ALL STATIONS

left-stepping fractures

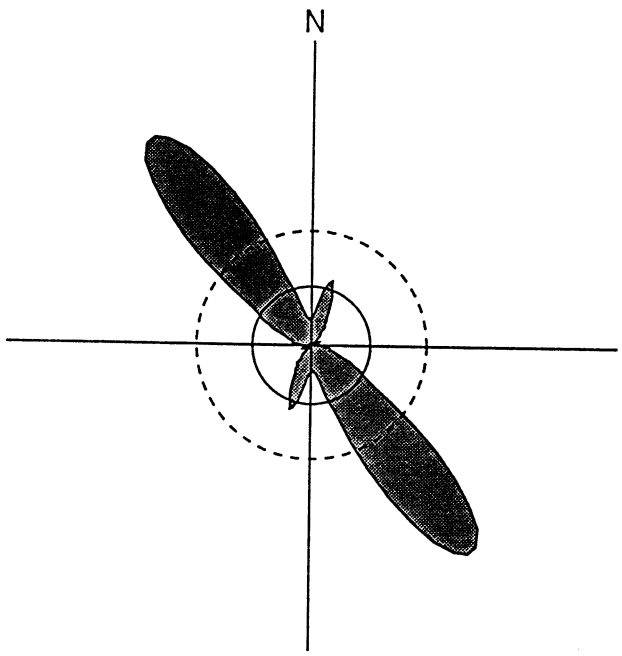

n = 85 E = 6.79 σ = 3.66 k = 100

Peak value = 30.20 Peak Orientation = 142.5°

—— E - - - - E ± 1.8σ

ALL STATIONS

left-stepping zones

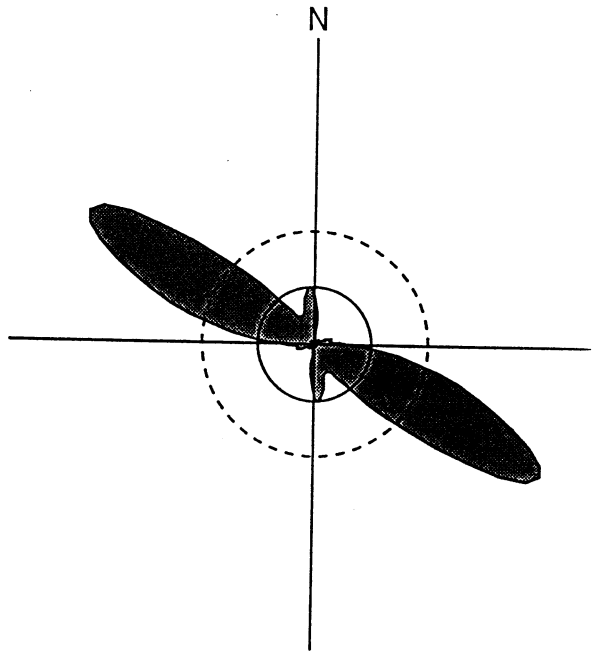

n = 89 E = 7.11 σ = 3.74 k = 10

Peak value = 31.95 Peak Orientation = 120.0

—— E - - - - E ± 1.8σ

orientation of each fracture set measured, called the zone orientation. The second is a plot of the orientation of individual fractures within echelon sets with one representative fracture orientation plotted for each set measured. These orientations are broken down by station(s) in Appendix D. The resulting peaks in distribution are summarized in Table 5.1. For the entire study area, the largest peak orientation of RS zones is 142.5° and of RS fractures in these zones is 112.5°. There is a smaller peak of RS zones at 106° and of RS fractures at 68.5°. The largest peak orientation of LS zones, for the entire study area, is 120° and of LS fractures is 142.5°. There is also a smaller peak of LS zones at 175° and of LS fractures at 18°. These relationships are summarized diagramatically in Figure 5.4. In the following discussion these four orientations of echelon fracture sets will be called A, B, C, and D as labelled in Figure 5.4.

If RS and LS echelon fractures sets are considered as conjugate pairs, then at least four pairings may be made in Figure 5.4. It seems unlikely that these echelon fracture sets can be directly correlated with one stress or strain field. It may be advantageous, therefore, to look at variations in echelon fracture and zone orientations from station to station.

RS echelon fracture sets are pervasive throughout the study area. At all of the stations, RS zones and fractures are present as peaks that are within 20° of the overall peak orientation represented by set B (zones at 142.5° containing fractures at 112.5°). The peak orientation of set D (zones at 106° containing fractures at 68.5°) is less common but occurs throughout the study area. This orientation shows as a small peak at stations 22, 23, 20, and (11,12,13,14) and as a large peak at stations 19, (1,8), and (15,16,25).

LS echelon fractures sets are much less common than RS echelon fracture sets and are absent from many stations. The greatest numbers of LS sets are present at stations 22, 23 and 24 with the remainder scattered throughout the study area. The peak orientation represented by set C (zones at 120° containing fractures at 142.5°) can be

Table 5.1

Summary table of orientation data.

STATION	ISOLATED FRACTURES N	ISOLATED FRACTURES PEAK	ECHELON FRACTURES right-stepping fractures N	right-stepping fractures PEAK	right-stepping fractures SS	right-stepping zones N	right-stepping zones PEAK	right-stepping zones SS	left-stepping fractures N	left-stepping fractures PEAK	left-stepping fractures SS	left-stepping zones N	left-stepping zones PEAK	left-stepping zones SS	SHEAR FRACTURES N	SHEAR FRACTURES PEAK	SHEAR ZONES N	SHEAR ZONES PEAK
West																		
22	25	128	25	117.5 x 75.5		26	135.0 x 102.0		20	135.0 x		20	110.0 x		0		0	
23	23	117	22	100.0 x 65.5		29	135.0 x 100.0		13	142.5 x		17	122.5 x		12	12.5 x 48	10	47.5 x
20	77	140 72	20	102.5 x 66.0		20	140.0 x 108.0		6			6			10		0	
21	21	135	13	115.0 x		13	145.0 x		0			0			0		0	
6	20	118	51	120.0 x		51	150.0 x		6			6			1		0	
2	33	118	51	115.0 x		51	150.0 x		6			6			0		3	
18	12	68	5			5			0			0			0		0	
7	18	115	6			6			2			2			0		3	
Mid																		
28	3		0			0						1			0		1	
17	5	142	13	107.5 x		13	140.0 x		0			0			8		10	65 x 17
19	14	124	18	67.5 x 117.5 x		17	102.5 x 122.5 x 140.0 x		6	130.0		6	120.0		0		1	
East																		
1	11	106	32			32			1			1			6		31	22.5 x 87
9	3		0			0			0			0			4		17	57.5 x 85
10	5	90	0			0			3			3			1		7	
8	21	144	11			11			6			6			6		34	97.5
16	1		2			2			0			0			0		0	
11,12,13,14	27	117	21	127.5 x 68.0 7.5		19	152.0 x 117.5 x 67.5		2			2			4		12	162.5
15	2		5			5			0			0			1		5	
25	7	135	4			4			6	147.5 x		6	120.0 x		0		0	
Grenville																		
24	18	117	16	100.0 x		16	137.5 x		7	155.0 x		8	135.0 x		3		1	
Combinations																		
7,18			11	115.0 x		11	140.0 x											
2,6,7,20									20	137.5 x		20	122.5 x					
6,20															11	17.5 x		
1,8			43	110.0 x 88.0 x		43	140.0 x 106.5 x											
1,8,9,10															23	17.5 x 55		
1,8,10,11 15,16,25			11	112.5 83.0		11	140.0 x 110.0 x		13	17.5 x		13	177.5 x					
ALL	360	131	315	112.5 x 68.5		321	142.5 x 106.0		85	142.5 x 18.0		89	120.0 x 175.0		62	12.5 x 50	132	35 x

N is the number of measurements
x denotes peaks of value >1.8 standard deviations above E (expected)
adjacent stations containing few data have been combined for ease of plotting

Figure 5.4

Schematic diagram of the peak orientations of the echelon fracture sets. The sets labelled B and C are more abundant. The inset for set A shows the sinistral offset observed on fractures of this orientation.

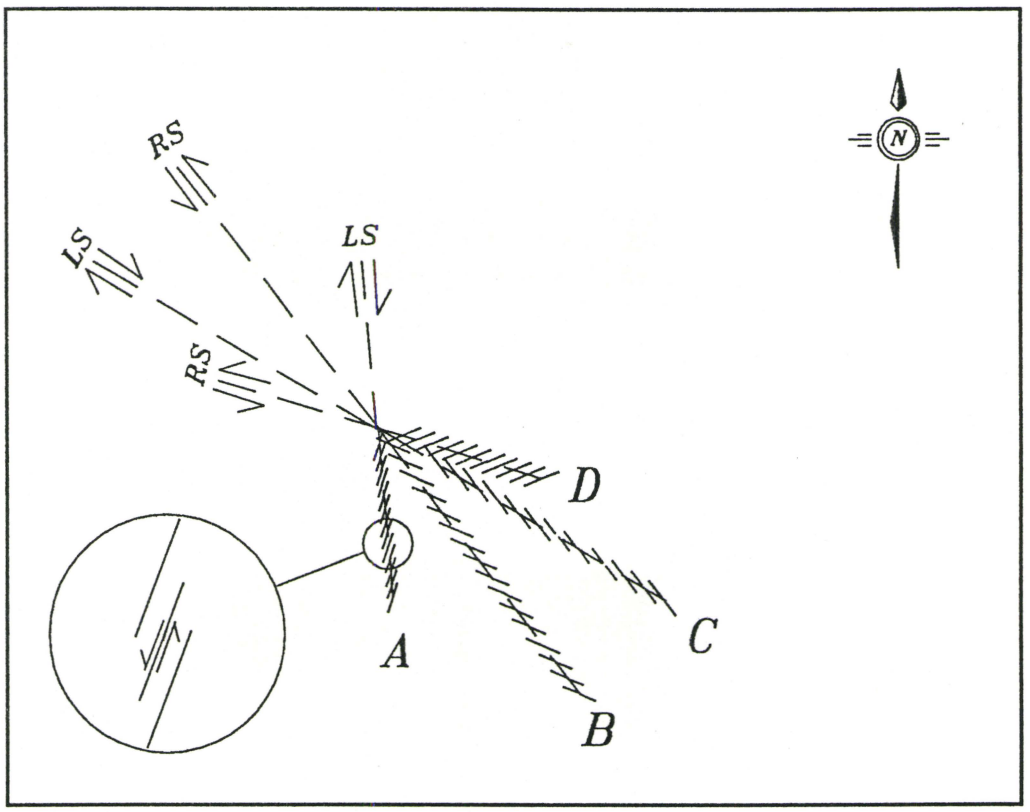
RS
LS
LS
RS
N
D
C
A
B

observed at stations 22, 23, (2,6,7,20), 25, and 24 (ie. throughout the study area). The peak orientation of set A (zones at 175° containing fractures at 18°) can be observed at stations (1,8,10,11) (ie. adjacent to the Grenville Front).

Additional structural data such as isolated fractures, shear zones and shear fractures can also be examined station by station. The orientations of shear zones and shear fractures are plotted as circular histograms in Figure 5.5 and Appendix E. The orientations of isolated fractures by station are also displayed in Appendix E. These data are summarized in Table 5.1. The relationship of isolated fractures to echelon fracture sets of orientation B may be seen in Figure 3.12 and has been briefly discussed in Chapter 3. RS echelon fracture sets of orientation B are connected to adjacent sets by longer through-going fractures belonging to the 131° isolated fracture peak. The isolated fractures are parallel or sub-parallel to fractures within the RS sets. Although not seen in Figure 3.12, these isolated fractures are also parallel or sub-parallel to fractures within LS echelon fracture sets of orientation C. On the basis of peak orientations, the isolated fracture peak of 131° bisects the acute angle between fracture sets B (142.5°) and fracture sets C (120°). This suggests that fracture sets B and C may be conjugate sets that are coeval with isolated fractures of peak orientation 131°. This conjugate relationship was never observed in outcrop.

The majority of shear zones are found at stations 1, 8, 9, and 10 (stations closest to the Grenville Front). The peak orientation of the shear zones is 35° (sub-parallel to the Grenville Front). Shear fractures have a peak orientation of 12.5° and often occur in left-stepping sets. This is very similar to the orientation of fractures within LS sets A. Echelon fracture sets of this orientation are only found adjacent to the Grenville Front in the study area. A closer examination of these echelon sets has shown them to be similar in appearance to shear fractures that occur in sets (Fig. 5.6). This means that some LS sets of shear fractures that do not exhibit shear offsets have been classified as echelon fracture sets.

Figure 5.5

a) Circular histogram of shear fracture orientations.

b) Circular histogram of shear zone orientations.

SHEAR ZONES

all stations

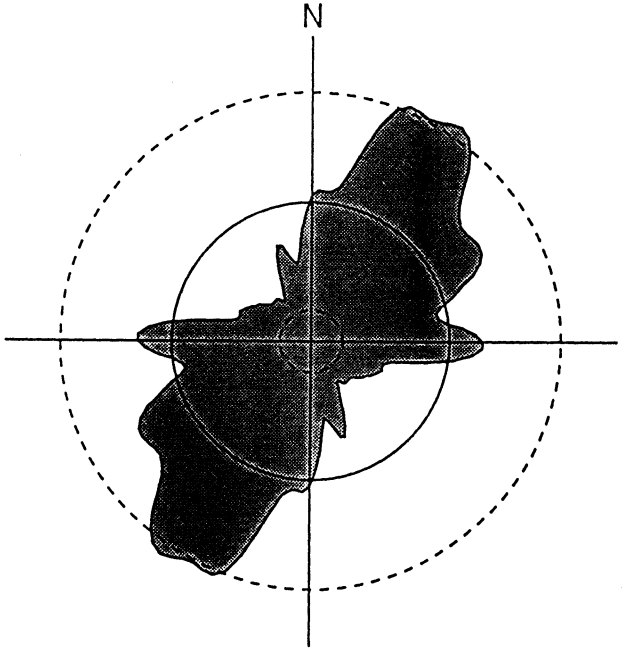

n = 132 E = 10.55 σ = 4.56 k = 100

Peak value = 19.73 Peak Orientation = 35.0°

—— E - - - - E ± 1.8σ

SHEAR FRACTURES

all stations

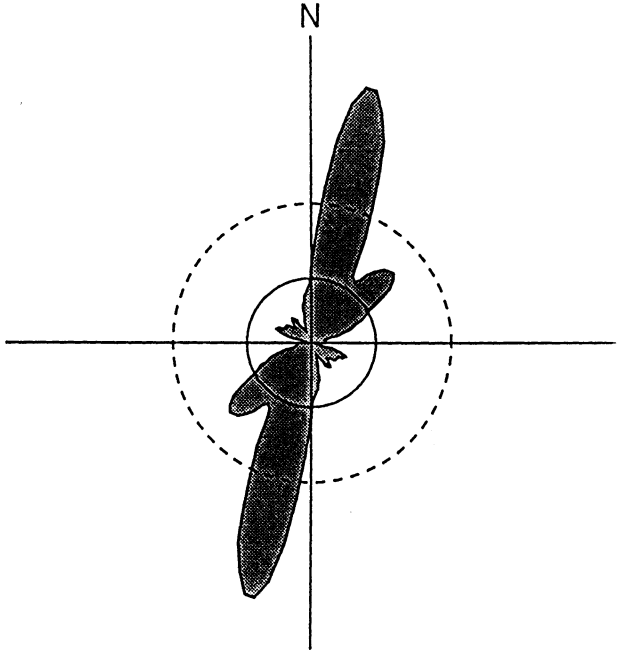

n = 62 E = 4.95 σ = 3.12 k = 100

Peak value = 19.93 Peak Orientation = 12.5°

—— E - - - - E ± 1.8σ

Figure 5.6

A left-stepping shear fracture set of orientation A.

5.2 Discussion of Orientations

Four distinct orientations of LS and RS echelon fracture sets have been observed in the study area (Fig. 5.4). There are many ways in which these echelon sets may be interpreted given that they may be any age from 1200 Ma to the present. The tectonic history of the Grenville province (Stesky and Bailey-Kryklywy, 1988) in addition to geological data may help to provide a working hypothesis of their formation.

The tectonic history of the Grenville Province from 1200 Ma to the present can be divided into several periods. From 1200 Ma to 1000 Ma the region was subjected to NW-SE compression associated with the Grenvillian Orogeny (Davidson, 1986). This period has an inferred stress state, for thrusting at the Grenville Front, of a horizontal, NW-SE trending σ_1, a vertical σ_2 and a horizontal σ_3 (Fig. 5.7). From 1000 Ma to 500 Ma the region was dominated by N-S and NE-SW extension responsible for the formation of the Grenville diabase dyke swarm, dated at 575 Ma (Fahrig and West, 1986) and the Ottawa-Bonnechere graben system. The inferred stress state for the diabase dyke swarm is not well constrained since the dykes are vertical. The least compressive stress, σ_3, must have been horizontal and NE-SW to N-S trending while σ_1 could have been horizontal or vertical (Fig. 5.8). The formation of the Ottawa-Bonnechere graben system is believed to postdate the diabase dykes (Kretz et al, 1985) and has an inferred stress state of a vertical σ_1, a horizontal, NE-SW to N-S trending σ_3 and a horizontal σ_2 (Fig. 5.9). From 500 Ma to 350 Ma there was NW-SE compression due to uplift of the Algonquin and Frontenac Arches. The period from 350 Ma to 200 Ma was quiet and was followed by NE-SW extension and rifting from 200 Ma to 50 Ma. The period from 50 Ma to the present is dominated by subsidence and glacial uplift. This is a complex history with many of the major events active in the same directions.

The orientations of fracture sets A and their distinct nature as shear fractures allows them to be considered separately from the other fracture sets. Based on cross-cutting

Figure 5.7

Schematic diagram of echelon fracture set orientations with the inferred stresses for the Grenville Orogeny.

Figure 5.8

Schematic diagram of echelon fracture set orientations with the inferred stresses for the formation of the Grenville dyke swarm.

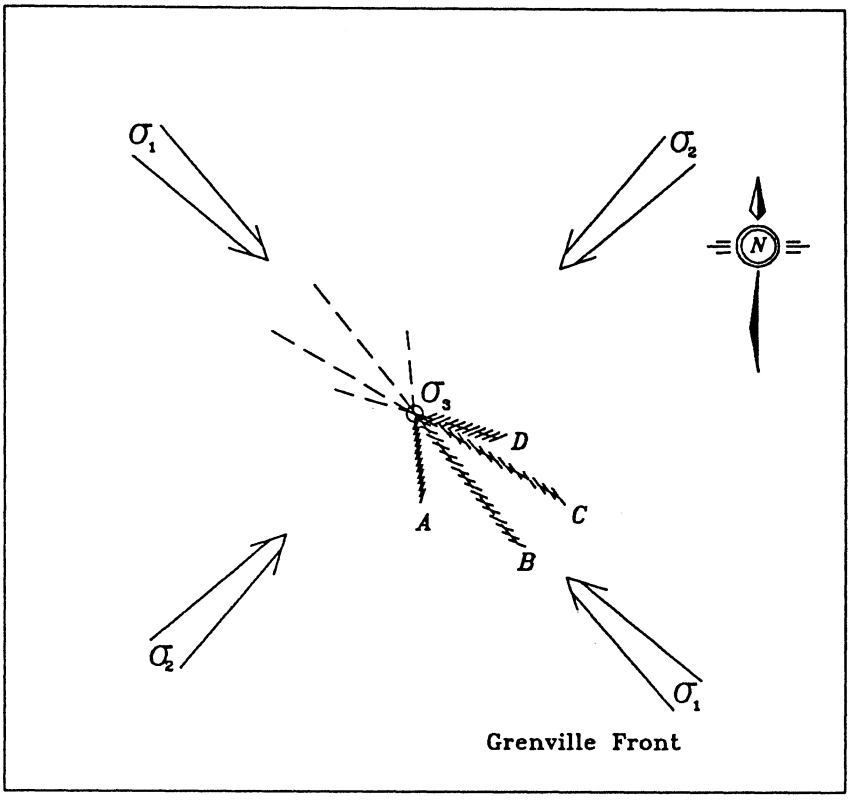
σ1
σ2
N
σ3
D
C
A
B
σ2
σ1
Grenville Front

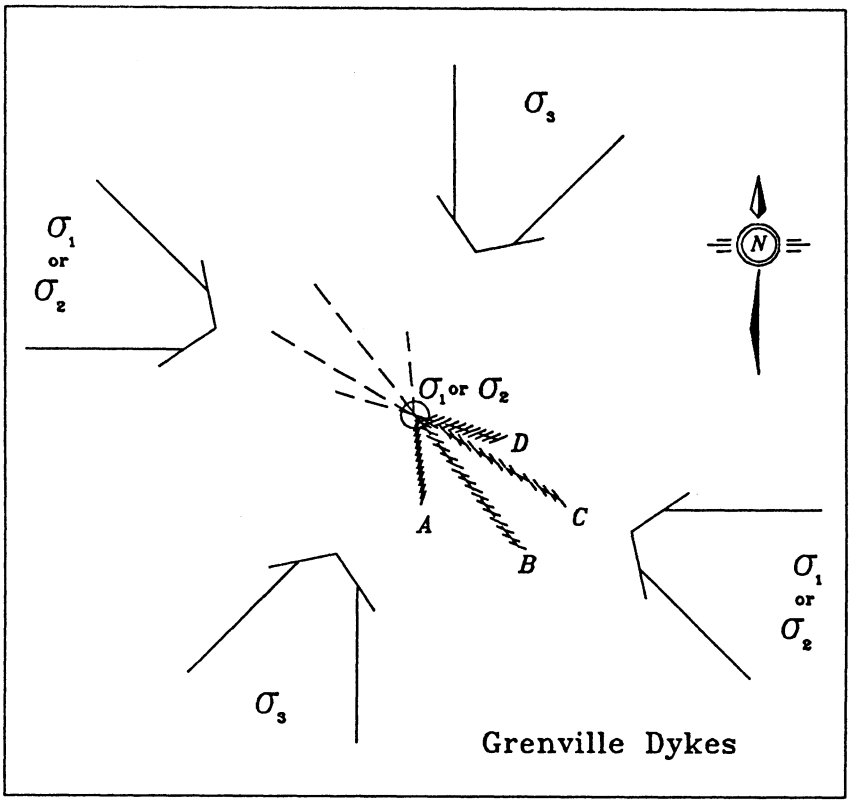
σ3
σ1
or
σ2
N
σ1 or σ2
D
C
A
B
σ1
or
σ2
σ3
Grenville Dykes

Figure 5.9

Schematic diagram of echelon fracture set orientations with the inferred stresses for the formation of the Ottawa-Nippising graben system.

Figure 5.10

Schematic diagram of echelon fracture set orientations with the inferred stresses for their formation.

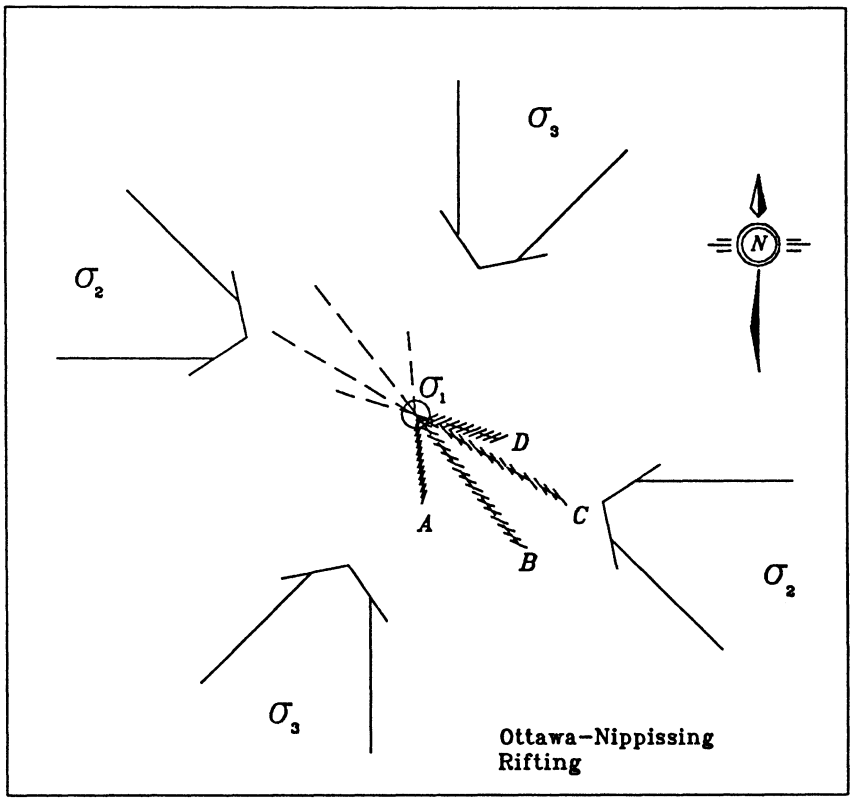
σ3
σ2
N
σ1
D
C
A
B
σ2
σ3
Ottawa–Nippissing
Rifting

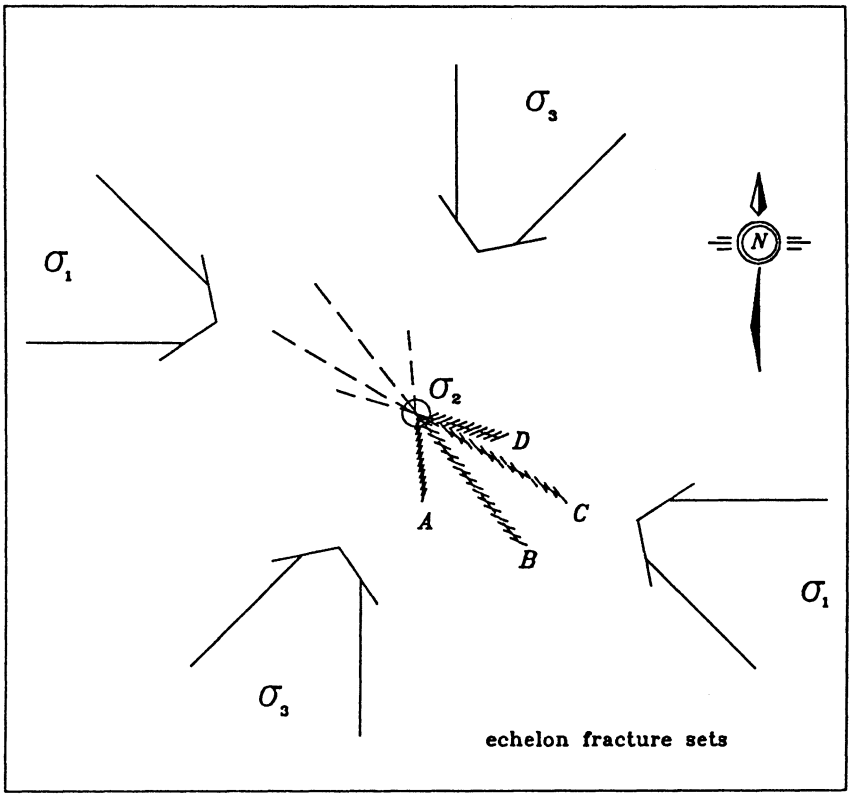
σ3
σ1
N
σ2
D
C
A
B
σ1
σ3
echelon fracture sets

relationships, these fracture sets are younger than, or coeval with, the non-echelon shear fracture sets and ductile shear zones but older than the echelon fracture sets B, C and D. Shear zones and shear fractures in the study area are oriented obliquely to the Grenville Front and hence obliquely to the NW-SE compression. The dominant strike-offsets observed on these zones and fractures are sinistral. Although there may be a significant dip-offset that cannot be measured, the sinistral offset is compatible with a NW-SE compression. If the LS fracture sets of orientation A were considered to be shear zones containing tension fractures, then they would indicate a dextral sense of shear. However, these sets have been interpreted as shear fractures and are therefore also compatible with the NW-SE compression (Fig. 5.7). Shear zones, shear fractures and LS echelon fracture sets A are therefore seen as the result of NW-SE compression from 1200 Ma to 1000 Ma that produced the Grenville Front mylonites and they may represent a ductile to brittle transition during that deformation.

The dominant echelon fracture sets B and C include fracture sets with the field classifications of "straight" and "closely-spaced". Some of the fracture sets in these orientations exhibit shear offsets and others do not. If sets B and C are considered as conjugate sets then their orientations and sense of shear imply a stress state with a horizontal σ_1, trending on average NW-SE, a vertical σ_2 and a horizontal σ_3 (Fig. 5.10). This is based on the peak orientations of the fracture sets and an implied conjugacy for sets B and C. There is no systematic change in the peak orientations of these sets throughout the study area and the range of orientations represented by the peaks is similar at all stations. This implies that the large range of orientations is the result of changes in orientations of the principal stress directions through time. It should also be noted that the predominance of RS sets over LS sets may imply a rotation of the maximum compressive stress, σ_1 (Ramsay and Graham, 1970).

The absolute age of these echelon fracture sets cannot be determined as yet but their inferred stress directions can be compared to the inferred stress directions for the

tectonic history of the Grenville Province. Grenville fracture lineaments striking 90° to 120° have been correlated with E-W striking faults of the Nippissing Graben that have intense hematitization and brecciation (Stesky and Bailey-Kryklywy, 1988). These lineaments are similar in orientation to the isolated fracture peak of 131° and echelon fracture sets B, C and D. Although an absolute date for the hematitization is unknown and it may not be coeval with the hematitization in the study area, it may be reasonable to assume that these echelon fracture sets are older than or coeval with the 90°-120° fracture lineaments. The inferred stress state for fracture sets B and C then fits into the transition period from 1000 Ma (post Grenville Orogeny) up to but not including the time of formation of the Ottawa-Nippissing graben system (post 575 Ma ?). These fracture sets may predate, be coeval with, or postdate the formation of the Grenville diabase dykes. Their formation may well span this entire period with earlier formed fracture sets becoming reactivated or progressively deformed with the rotating/changing stress field. This period involved major changes in the stress state from a horizontal σ_1 and vertical σ_3 (Grenville Front thrusting) to a vertical σ_1 and horizontal σ_3 (Ottawa-Nippissing rifting).

The orientations of echelon fracture sets D are compatible with the inferred stress state for this transitional period but are not coeval with fracture sets B and C. The fracture sets D are hematite stained and include sets classified as "straight" and "sigmoidal" but they do not display shear offsets. A possible explanation for the lack of shear offsets is that fracture sets D are younger than B and C. This is compatible with a counter-clockwise rotation of σ_1 through the transition period discussed. If these fractures are tensile in origin, they indicate an approximately E-W trending, horizontal σ_1.

The possibility of the echelon fracture sets B, C and D having formed after 500 Ma has not been excluded. However, there are reasonable arguments to suggest that they may postdate the Grenville Orogeny but predate the Ottawa-Nippissing rifting. To complicate the interpretation, once the echelon fractures have formed they may become

reactivated during later tectonic events. This may lead to growth of new fractures in already weakened zones of echelon fractures.

6.0 Discussion

6.1 LS fracture sets of orientation A

The LS echelon fracture sets of orientation A (Fig. 5.4) are distinct from the other fracture sets in both morphology and orientation and their origin has already been discussed in Chapter 5. The nature of the fractures within sets A, in outcrop and in thin section, is that of shear fractures. The orientations of the fractures in sets A are similar to the orientations of shear fractures in the area that are isolated and in sets. This has led to the tentative conclusion that these fracture sets formed as part of the ductile to brittle deformation resulting from NW-SE compression associated with the Grenville Front. These fracture sets are a minority of the total number measured and will now be excluded from the discussion of the remaining fracture sets.

6.2 Echelon fracture sets from a parent fracture

There are four reasons that suggest that the echelon fracture sets in this study did not propagate from a parent fracture. The first is that this relationship was never observed in outcrop. The second reason is the large number of echelon fracture sets with a fracture-zone angle greater than 30°. Pollard et al (1982) suggest fracture-zone angles for echelon fracture sets propagating from a parent crack rarely exceed 30°. Rothery (1988) suggests a maximum fracture-zone angle of 27° for classification of echelon fracture sets as originating from a parent fracture. Another reason is the high overlap ratio of these fracture sets (80% > 0.5). This ratio exceeds that observed and predicted for echelon fracture sets propagating from a parent fracture (Pollard et al 1982, Rothery 1988). Finally, isolated fractures tend to be sub-parallel to fractures within the most

abundant echelon fracture sets (set B) and oblique to the fracture sets themselves. These arguments lead to the conclusion that the echelon fracture sets in this study did not form as echelon arrays that propagated from a parent fracture.

6.3 Tensile versus shear origin of fractures

In any examination of fractures the problem of determining a tensile versus shear origin for fractures arises. Often fractures are classified as tensile or shear on the basis of their relationship to known or inferred stress directions. Tensile fractures are considered to form parallel to the maximum compressive stress or perpendicular to the maximum tensile stress while shear fractures are considered to form at some acute angle to the maximum compressive stress. Implicit in this is that shear fractures form in a compressive regime while tensile fractures can form in either an extensional or compressive regime. The characteristics of a fracture such as dilatancy or shear offsets can be used to classify it as a tensile or shear fracture but this is a categorization of its present state which may or may not be connected with its origin. Both tensile and shear fractures propagate by the linking of microcracks and small fractures so it is unclear how they may be distinguished from each other if there is little or no dilation or shear offset of the fracture surfaces.

Despite these problems in interpretation, the following arguments favour the dominant origin of fractures in these echelon sets as tensile. The majority of fractures in outcrop and thin section were continuous hairline cracks with no shear offsets. Although the variability of the fracture-zone angle includes values that have been attributed to tensile and shear fractures, the consistency of that angle within "straight" echelon sets indicates that the fractures within that set formed by the same mechanism. Shear fractures formed in experimental shear zones are found in several orientations with cross-cutting relationships (Tchalenko, 1970). This morphology was not observed in echelon fracture sets except those exhibiting shear offsets.

Sigmoidal fractures have been discussed briefly in Chapter 3 but will be elaborated on here. Consider a RS echelon fracture set within a sinistral "shear zone" (Fig. 6.1a). There are two types of sigmoidal fractures that may be produced by sinistral shear of these pre-existing fractures. The first type is "Z"-shaped fractures which are produced by shearing of the fracture tips (Fig. 6.1b). This type of sigmoidal fracture is not very common in echelon fracture arrays. The second type is "S"-shaped fractures which are formed by rotation of the fractures during simple shear (Fig. 6.1c). With sufficient shear strain, filled tension fractures that originally propagated at 45° (for shear zones of zero dilation) to the shear zone boundaries will be rotated in the centre of the zone into the shear direction while the fracture tips continue to propagate at 45° (Ramsay and Huber, 1983). This type of sigmoidal fracture is common in some echelon vein arrays (Beach 1975, Rickard and Rixon 1983) but is unlike the sigmoidal fractures in this study area (Fig. 6.1d) or those within other documented echelon arrays (Shainin 1950, Roering 1968).

Any rotation of tensile fractures in simple shear will cause shear offsets along the fractures. Where this degree of simple shear was observed in echelon fracture sets of this study, fracture-bound septae of rock were rotated into the shear direction and their bounding fractures were truncated instead of becoming sigmoidal fractures. The majority of echelon fracture sets containing sigmoidal fractures do not show this evidence of rotation or shear. In general the shear strain accommodated by the echelon fracture sets is very small as the sets have close to zero dilation and no visible shear offsets. This leads to the assumption that the sigmoidal fractures must have propagated as sigmoidal fractures.

The formation of these sigmoidal fractures can be explained by the following model. Consider the localization of an echelon fracture set along a zone of weakness (Fig. 6.1e). An initial relief of shear stress along this zone of weakness, perhaps through microcracking, will cause the local maximum compressive stress, σ_1^1, within the zone to

Figure 6.1

Schematic diagram of the formation and growth of sigmoidal fractures.

a) Two right-stepping fractures in a sinistral "shear zone".

b) The formation of sigmoidal "Z" fractures by sinistral shearing of the fracture tips.

c) The formation of sigmoidal "S" fractures by sinistral shearing of the fractures in the centre of the shear zone or by growth of the fractures during sinistral shear.

d) The appearance of the majority of sigmoidal fractures in right-stepping sets in the study area.

e) The growth of sigmoidal fractures by reorientation of the remote principal stresses within the "shear zone". The local extension direction, E_L, within the zone is non-coincident with the regional extension direction, E_R.

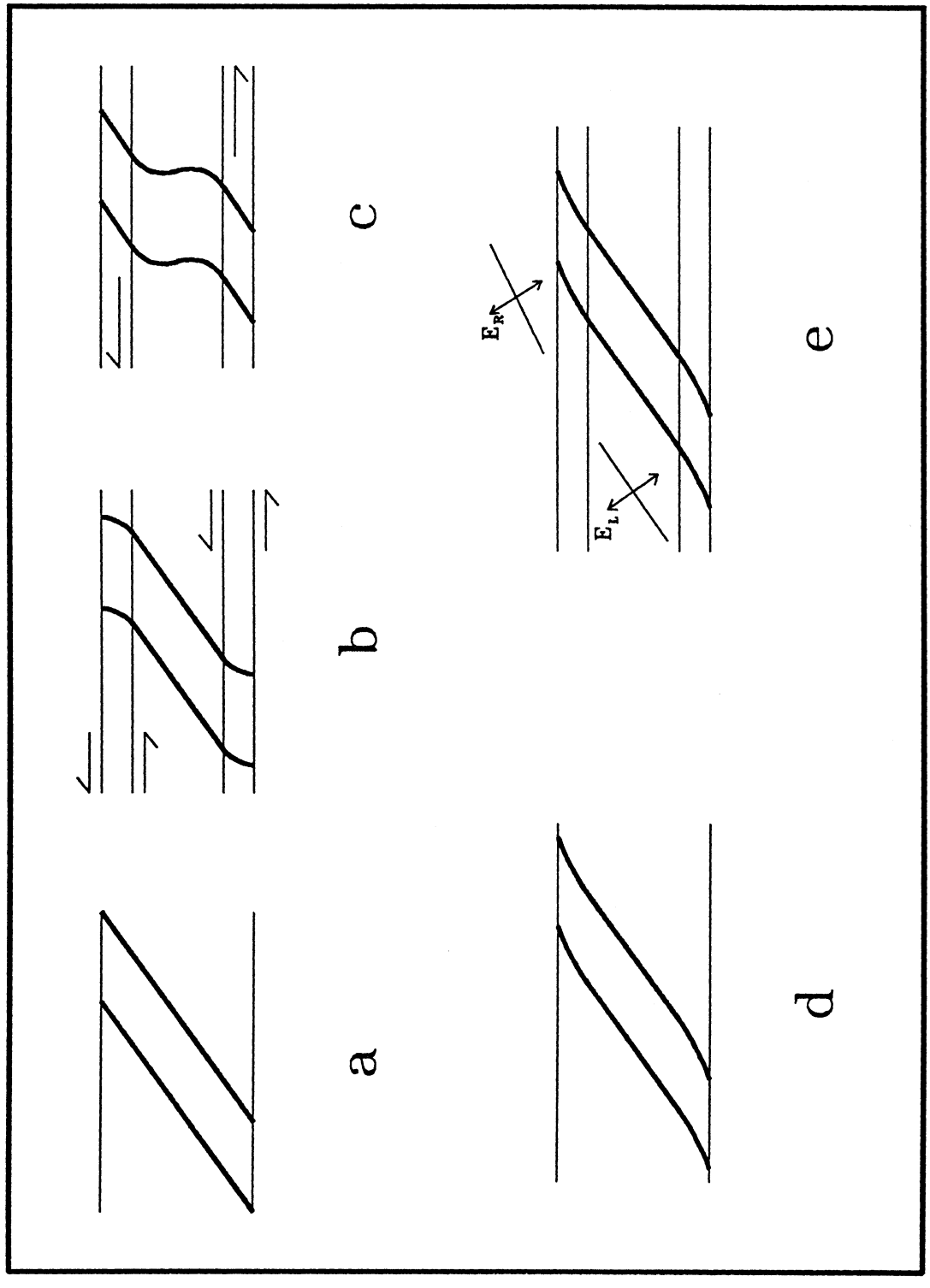
a
b
c
d
e
E_R
E_L

be non-coincident with the regional maximum compressive stress, σ_1. For a sinistral "shear zone" there is a counter-clockwise rotation of σ_1^1, within the zone, relative to σ_1, outside the zone. Tensile fractures within the "shear zone" will propagate parallel to σ_1^1. If fracturing is more intense towards the centre of the zone and less intense at the boundaries there will be a progressive rotation of σ_1^1 into parallelism with σ_1 as the boundaries of the zone are approached. Therefore tensile fractures that propagate to a sufficient length will be sigmoidal with their tips parallel to the regional maximum compressive stress, σ_1 (Fig. 6.1e).

The existence of sigmoidal fractures of a tensile origin within these echelon fracture sets is a strong argument for a tensile origin of the majority of these echelon fractures. This does not preclude the formation of shear fractures or the shearing of pre-existing tensile fractures within some echelon sets later in their history.

6.4 Relationship of fractures to local and regional stresses

It has been established that the majority of the fractures within these echelon sets are most likely tensile in origin. These fracture sets may be thought of as localized zones of strain or "shear zones". The relationship of these fractures to the regional stresses can be discussed.

The model described above to explain sigmoidal tensile fractures can be applied to all tensile fractures within a discrete "shear zone". This means that tensile fractures within a set will be parallel to the local maximum compressive stress, σ_1^1. Therefore tensile fractures within an echelon set may be in a different orientation then isolated tensile fractures outside the echelon set which are parallel to the regional maximum compressive stress, σ_1.

6.5 Significance of the fracture-zone angle

This study has shown that tensile fractures can have a range of fracture-zone angles from <5° up to 75° in "shear zones" with little to no apparent dilation. This has several implications. The first is that the fracture-zone angle cannot be used unambiguously to classify echelon fractures as "tensile" or "shear" fractures. The second is that the angle tensile fractures make with the "shear zone" may not be dependent on dilation which contradicts the model of Ramsay and Huber (1983, 1987) and Durney (1985). A possible explanation for this is that their model depends on having significant ductile deformation of the non-fractured rock within the "shear zone" which is not observed here. It is still unclear, however, why their strain based model does not appear to be applicable to the echelon fracture sets in this study.

The implications of this study are that the fracture-zone angle is dependent on the angle the "shear zone" makes with the regional σ_1 and the degree of reorientation of σ_1 within the "shear zone". This dependency of fracture-zone angle on zone orientation has been noted by Rothery (1988) in an area where the inferred principal stress directions are constrained by other geological data. Unfortunately, the variability of the inferred stress states responsible for the echelon fracture sets in this study do not allow for a meaningfull assessment of the dependence of fracture-zone angle on zone orientation.

6.6 Localization of fractures in sets

One of the fundamental questions yet to be answered about fracture sets and echelon fracture sets in particular is why they form in sets. If the rock is heterogeneous then fractures may be localized by pre-existing weaknesses in the rock but this does not explain the formation of fracture sets in a strictly homogeneous rock. The problem can be restated as solving the question of why strain localizes in zones rather than homogeneously distributing itself throughout the rock. This phenomenon is not confined to fracturing as the same problem exists with shear zones, cleavage development, pressure

solution, and dislocations, to name only a few. One answer to this may be that it is energetically easier to accommodate strain in a few localized areas rather than evenly throughout the medium. This idea is expressed in dislocation theory which states that dislocations find it energetically easier to move and form tilt boundaries rather than remain distributed throughout a crystal (Hobbs et al 1976). Thus it may be energetically easier for fractures to localize in discrete zones or sets to accommodate strain. Another possibility is that a chance concentration of microcracks will act as a zone of weakness and favour the propagation of larger fractures. However, chance concentrations of microcracks are not likely to be regularly spaced so they cannot be the only mechanism acting to form fracture sets. This is clearly a complex problem that will not be readily solved.

6.7 Relationship of fracture sets to Grenville Province tectonics

A correlation of the echelon fracture sets with Grenville Province tectonics has been attempted in Chapter 5. There are several problems with attempting a correlation of regional stresses with locally distributed fractures. The most significant is that regional stresses may acquire a local orientation over the scale of the study area due to the presence of major faults or other anisotropies that affect the entire study area. However, it is expected that the misorientation of local stresses with regional stresses will be less than 90°. In this study area the local stress state for the area should be within the range of orientations inferred for the regional stress state.

Another problem is the lack of observed conjugacy for LS and RS sets and the dominance of RS sets. This has led to the inference of principal stress directions for the sets based on the peak orientations of LS and RS sets. The large range of orientations of LS and RS sets and the overlap in orientations of RS and LS sets indicates a large variability in principal stress directions. These factors combined with the complexity of the known tectonic history of the Grenville Province makes this correlation tenuous.

The inferred stress states for the echelon sets and the geologic evidence correspond reasonably well to a period of transitional stress states starting at the end of the Grenville Orogeny (1000 Ma) and progressing through to the beginning of rifting and formation of the Ottawa-Bonnechere-Nippissing graben system.

7.0 Conclusions

The echelon fracture sets in the Killarney Igneous Complex display a range of orientations and characteristics that indicate more than one orientation of the principal stress directions responsible for their formation. These echelon fracture sets have been interpreted as dominantly tensile fractures contained within "shear zones" rather than the product of a propagating parent fracture. The "shear zones" do not exhibit ductile deformation but some zones contain brittle shear fractures with strike-parallel offsets.

The majority of these "shear zones" have very small dilation and shear components of strain yet they exhibit a large range of fracture-zone angles. This contradicts an established model relating fracture-zone angle to "shear zone" dilatancy (Ramsay and Huber 1983, 1987). It has been suggested in this study that the fracture-zone angle is dependent on the orientation of the zone relative to the principal stress directions and the degree of reorientation of these stresses within the "shear zone".

The results of this study indicate that the correct use of the geometrical parameters fracture-zone angle and overlap ratio for classification of echelon fracture sets is far from resolved. This is largely due to the conflicting array of models present in the literature for fracture propagation and formation of echelon sets. Many of these models are based on specific examples that are often contained in sedimentary rocks. Suggestions for further study include the measurement and documentation of echelon fracture sets in all rock types and tectonic regimes and the careful consideration of the geometrical parameters that describe these sets.

References

Anderson, O.L. and Grew, P.C. 1977. Stress corrosion theory of crack propagation with applications to geophysics. Reviews of Geophysics and Space Physics, **15**, pp. 77-104.

Atkinson, B.K. 1982. Subcritical crack propagation in rocks: theory, experimental results and applications. Journal of Structural Geology, **4**, pp. 41-56.

Atkinson, B.K. 1987. Introduction to fracture mechanics and its geophysical applications. in Fracture Mechanics of Rock, B.K. Atkinson ed., Academic Press, London, 534 p.

Bahat, D. 1986. Joints and en echelon cracks in Middle Eocene chalks near Beer Sheva, Israel. Journal of Structural Geology, **8**, pp. 181-190.

Beach, A. 1975. The geometry of en-echelon vein arrays. Tectonophysics, **28**, pp. 245-263.

Davidson, A. 1986. Grenville Front relationships near Killarney, Ontario. in The Grenville Province, ed. J.M. Moore, A. Davidson and A.J. Baer, Geological Association of Canada Special Paper, **31**, pp. 107-117.

Durney, D.W. 1985. Attitude variation of en echelon fractures in generalized Riedel experiments. Abstract in Journal of Structural Geology, **7**, pp. 491-492.

Engelder, T. 1987. Joints and shear fractures in rock. in Fracture Mechanics of Rock, B.K. Atkinson ed., Academic Press, London, 534 p.

Engelder, T. and Geiser, P. 1980. On the use of regional joint sets as trajectories of paleostress fields during the development of the Appalachian Plateau, New York. Journal of Geophysical Research, **85B**, pp. 6319-6341.

Fahrig, W.F. and West, T.D. 1986. Diabase dyke swarms of the Canadian Shield. Geological Survey of Canada, Map 1627A, Scale 1:4,873,900.

Gudmundsson, A. 1987. Tectonics of the Thingvellir fissure swarm, SW Iceland. Journal of Structural Geology, **9**, pp. 61-69.

Hancock, P.L. 1972. The analysis of en-echelon veins. Geological Magazine, **103**, pp. 269-276.

----------1985. Brittle microtectonics: principles and practice. Journal of Structural Geology, **7**, pp. 437-457.

Hodgson, R.A. 1961. Classification of structures on joint surfaces. American Journal of Science, **259**, pp. 493-502.

Jaeger, J.C. and Cook, N.G.W. 1976. Fundamentals of Rock Mechanics, 2nd Edition, Chapman and Hall, London, 585 p.

Kranz, R.L. 1983. Microcracks in rock: a review. Tectonophysics, **100**, pp. 449-480.

Kretz, R. et al 1985. Petrology of the Grenville swarm of gabbro dykes, Canadian Precambrian Shield. Canadian Journal of Earth Sciences, **22**, pp. 53-71.

Labuz, J.F., Shah, S.P. and Dowding C.H. 1987. The fracture process zone in granite: evidence and effect. Int. J. Rock. Mech. Min. Sci. and Geomech. Abstr., **24**, pp. 235-246.

Ladeira, F.L. and Price, N.J. 1981. Relationship between fracture spacing and bed thickness. Journal of Structural Geology, **3**, pp. 179-183.

Lajtai, E.Z. 1969. Mechanics of second order faults and tension gashes. Geological Society of America Bulletin, **80**, pp. 2253-2272.

Lawn, B.R. and Wilshaw, T.R. 1975. Fracture of Brittle Solids, Cambridge University Press, 204 p.

Nicholson, R. and Pollard, D.D. 1985. Dilation and linkage of echelon cracks. Journal of Structural Geology, **7**, pp. 583-590.

Nur, A. 1982. The origin of tensile fracture lineaments. Journal of Structural Geology, **4**, pp. 31-40.

Paterson, M.S. 1978. Experimental Rock Deformation - The Brittle Field, Springer-Verlag,
New York, 254 p.

Pollard, D.D., Segall, P., and Delaney, P.T. 1982. Formation and interpretation of dilatant echelon cracks. Geological Society of America Bulletin, **93**, pp. 1291-1303.

Price, N.J. 1966. Fault and Joint Development in Brittle and Semi-Brittle Rock, Permagon Press Ltd., London, 176 p.

Ramsay, J.G. and Huber, M.I. 1983. The Techniques of Modern Structural Geology, Volume 1, Strain Analysis. Academic Press, London.

Ramsay, J.G. and Huber, M.I. 1987. The Techniques of Modern Structural Geology, Volume 2: Folds and Fractures. Academic Press, London, 700 p.

Rickard, M.J. and Rixon, L.K. 1983. Stress configurations in conjugate quartz-vein arrays. Journal of Structural Geology, **5**, pp. 573-578.

Robin, P.-Y.F. and Jowett, C.E. 1986. Computerized density contouring and statistical evaluation of orientation data using counting circles and continuous weighting functions. Tectonophysics, **121**, pp. 207-223.

Roering, C. 1968. The geometrical significance of natural en-echelon crack-arrays. Tectonophysics, **5**, pp. 107-123.

Rogers, R.D. and Bird, D.K. 1987. Fracture propagation associated with dyke emplacement at the Skaergaard intrusion, East Greenland. Journal of Structural Geology, **9**, pp. 71-86.

Rothery, E. 1988. En echelon vein array development in extension and shear. Journal of Structural Geology, **10**, pp. 63-71.

Ryan, M.P. and Sammis, C.G. 1978. Cyclic fracture mechanisms in cooling basalt. Geological Society of America Bulletin, **89**, pp. 1295-1308.

Segall, P. 1984. Formation and growth of extensional fracture sets. Geological Society of America Bulletin, **95**, pp. 454-462.

Segall, P. and Pollard, D.D. 1980. Mechanics of discontinuous faults. Journal of Geophysical Research, **85 B**, pp. 4337-4350.

Segall, P. and Pollard, D.D. 1983b. Joint formation in granitic rock of the Sierra Nevada. Geological Society of America Bulletin, **94**, pp. 563-575.

Shainin, V.E. 1950. Conjugate sets of en echelon tension fractures in the Athens limestone at Riverton, Virginia. Bulletin of the Geological Society of America, **61**, pp. 509-517.

Simpson, C. 1983. Displacement and strain patterns from naturally occurring shear zone terminations. Journal of Structural Geology, **5**, pp. 497-506.

Sommer, E. 1969. Formation of fracture lances in glass. Engineering Fracture Mechanics, **1**, pp. 539-546.

Stesky, R.M. and Bailey-Kryklywy, K.A. 1988. Lineaments, faults and the tectonics of the Grenville Province, Ontario. submitted to Canadian Journal of Earth Sciences.

Tchalenko, J.S. 1970. Similarities between shear zones of different magnitudes. Bulletin of the Geological Society of America, **81**, pp. 1625-1640.

Appendix A

Fracture Data

STAT #	zone trend	S	L m	W m	FRAC STRK	FRAC DIP	fracture length (cm)										fracture spacing (cm)										fracture overlap (cm)							page #
1	135	R			110																													21
1	120	R	1.3	0.2	103																													23
1	148	R	1.3	0.08	115																													16
1	140	R		0.15	285	78	19	12	17	19	23	18	26	30	25	23	2.5	1.75	1.5	1	0.75	1	2	1.5	1	1.5	19	15	12	14	14			23
							28	23	31	10	20	15	17				1	1.25	0.75	1	1.5	0.75												
1	172	R	2.2	0.2	132		63	41	48	12	12	71	8	20	45	10	6.5	8.5	5.5	6.5	5	4	5	2	2.5	2.5								16
							23	24.5	21	19	27	18	32	20	27	38	3.5	3.5	2.5	2	4	4	3	2.5	9	13.5								
							43																											
1	20	R	3.1	0.19	310	59	81	20	32	92	75						6	6	5	9	6	10	8				19							23
1	115	R	2	0.25	85		53	28																										21
1	105	R	1	0.27	70																													23
1	125	R	3.5	0.5	105		95										6	8.5									88							21
1	140	R			110																													23
1	130	R			110																													21
1	105	R	1.7	0.25	250	76	23	25									3										19							21
1	135	R			105																													23
1	160	R			120		15																											21
1	117	R	6	0.7	87		154	111	97	108							14.5	22	8	6	7	14	13	15.5	12	13.5	80	96	76					21
1	134	R	5	0.55	280	87	112	112	104	109	130	98	80				12	13.5	11	15	12	12.5	10	9	11		72	80	96	121	94			23
1	140	R			108																													21
1	140	R			115																													23
1	148	R	1.8	0.17	130		39	31	33	23	30	37	23.5	127	26	63	5	3.5	4	2	6	2.5	1.7	2.3	3.3	2	14	23	23	18.5	23	23.5	15	16
							24	21									1.5										15	42.5	11					
1	102	R		0.12	90		36	38									3	4																23
1	115	R	2.25	0.3	270	78	38	60	49								3	10									33	29						16
1	140	R	1.2	0.1	105		20										4																	23
1	125	R	2	0.25	85		22	27	31								1.5	1.5	3	3	2.5													21
1	7	R			136	48																												23
1	140	R			110																													21
1	140	R	10	0.2	292	80																												23
1	103	R	2.6	0.15	265	75	21	31	12	29	40	9	17	41	29	15	5	2.2	1.5	1	2.5	2	2.5	1.5	2	2	8	22	-4	12	7	2.5	-6.5	16
							50	10	11	21							1.5	0.3	1								13	5	2					
1	140	R			295	75																												23
1	105	R	6	0.4	265	84																												21
1	105	R		0.23	90																													21
1	150	R			115																													21
1	140	R			105		15	40									2.5	7																23
1	6	L	1.6	0.15	28		8	9	4	4	15	19	5	15	50	20	8.5	2	6	4.5	0.5	1.5	4.5	2	1.5	3.5	15	3	4	7	3.5	0.5	2	23
																											-2	1						
1		L		0.08	30		45										1.5																	25
2	135	R	1	1	100	73																												32
2	150	R	2	0.45	117		50										8																	33
2	140	R	6	0.15	115	75	7	8	9								0.5										4							29
2	156	R			110																													30
2	153	R	14	0.4	115	82	105	40	8								6	4	1.5															30
2	125	R			111																													27
2	145	R		0.5	110	76																												30
2	162	R	30		130	78																												33
2	121	R			100																													27
2	157	R	4		125												1																	33
2	135	R	5	0.45	110		35	30	21	28							5	2	3	5.5														29
2	98	R			62		43										10																	28
2	135	R		0.4	100	78	55	69	40								7	1.5	0.5	1	6.5	0.5												29
2	130	R			105																													28
2	135	R			105																													29
2	145	R	7.5	0.55	110	78	67	67	85	60	64						10	4	7	6	9	10.5												28
2	125	R			90																													29
2	153	R			125												4																	33
2	115	R	0.5	0.15	85												1.5																	29
2	145	R	0.5	0.1	120		21	23	12	12	59						4.5	2.5	2	2	1.5						15	10	12					28
2	133	R	1		97	75																												29
2	154	R			122	87																												29
2	146	R	2		303	87	39	34	24	10							4										25							29
2	155	R			115																													29
2	148	R	20	0.13	125		12	14	10	10	5						1	2	3	1	2	2					9							32
2	155	R			120	90																												29
2	153	R			122																													32
2	151	R			113	77																												30
2	161	R	10	0.11	130		13										0.5										7.5							32
2	139	R			107																													27
2	148	R			125																													32
2	122	R	0.7	0.16	65		23										4										20							28
2	144	R	4	0.5	105		58										9										46							32
2	133	R	12	0.85	113	83	260	190	200	120	175						4	2	7	3.5	11	3.5	7	8	4.5	3.5								28
																	5.5	2	2.5	4.5	6													

2	142	R	12	1	112	80	118									8										90							32
2	139	R			112											4																	33
2	150	R			102																												27
2	135	R			123	84																											29
2	160	R	3	0.22	120		15									1	2									12							32
2	145	R	6	0.45	115	78	88	93	21	30						12	11	3	2.5														30
2	147	R	5	0.15	120		18									0.5																	32
2	112	R			98																												27
2	129	R	2	0.15	105		20									1	2									17							32
2	154	R			130																												28
2	145	R	25	0.25	118	80																											32
2	150	R			115																												29
2	165	R			134																												32
2	96	R		0.4	63																												28
2	155	R			124	80										5																	33
2	165	R	4	0.12	135	84	24	26	9	5	18	29	22	12	15	16	2	1	1	1.5	2.5	2	0.5	0.5	2.5	1.25	8	12.5	18	6	12	10	12	29
																	1.5	1	6.5	2	1.5						24	7	10					
2	142	R			112																												32
2	156	L			138																												27
2	91	L			114																												27
2	118	L			130																												28
2	124	L			132																												27
2	132	L	0.18	0.03	151		12.5	9	5	3	5.5	5				1	1	1.25	0.6	0.7						6.5	5	1.5	3	4	4.5		28
2	124	L			133																												27
6	150	R			127		7	0.5																									109
6	149	R	3	0.4	113	80	57	73	48	37	30	18				7	9.5	3	11	3.5	3	5				23	25	30	36	32			105
6	156	R	4	0.4	108	80	77	53	48	60	25					3.5	4.5	1	1	5	0.2												105
6	135	R	1	0.2	115	85	51	68	49	49						7.5	9	7.5	5.5							33	40	17					107
6	150	R	6	0.15	128	90	22	36	25	34	18					3	3.5	3	1.5	0.7													105
6	131	R			96	72																											116
6	156	R	2	0.25	126		25	20	43	26	10	11				2.5	4	1.5	2	1	4	3	4			23	28	18					105
6	134	R		0.16	110	80																											116
6	154	R			122	78	51	55	14	29	32					7	2	2.5	2	5													105
6	144	R			114																												107
6	146	R	8	0.5	112	80	145	53	113	43						13	16	7	1.5	1.5	0.5	6	2										105
6	156	R			306	75																											115
6	135	R	2	0.17	113	76	40	44	31	40	30					3	1	0.4															106
6	132	R	2	0.18	99	74	34	36	26	26						5.5	4.5	3	2	2	4.5					32	25	18	18				115
6	150	R	7	0.15	115	86	28	49	20	26	56	6				0.5	2.5																106
6	150	R		0.07	122	85																											114
6	158	R	1	0.055	124		3.5	3	5.5	3.5	12	8	2			0.3	0.3	0.4	0.5	0.3	0.6	0.9	1.6	1.4	1.6	4	3	4	3	2	2		106
6	149	R	10	0.12	108	66	29	1.5								0.5																	108
6	144	R	3	0.4	121	85	56	85	11	52	52	51				1.5	4	2	0.5	3	1	1	6										106
6	144	R	3.5	0.35	113	71	20	31	53							3	3	1	1.5	2													114
6	138	R			296	86																											
6	142	R	1.5	0.18	123	90	18	44	27	29	54	19	3	4		0.9	0.5	0.6	1.1	0.8	0.8	1.2	2.5										106
6	150	R		0.03	130	74	25									7	5.5	6	6	4.5													108
6	151	R	2.8	0.12	110		11	15	17	36	31					4.5	7	3.5	6	4	2.5	1.5				17.5	17	14	14	11			113
6	156	R	12		287	87																											112
6	149	R	1.5	0.09	130		11	9	12	18	6					4	4	2	2	3.5	1.5					17	9	8	6	8			113
6	144	R			301	82																											
6	155	R	8	0.35	121	87	44	28	115	60						7	9	4	4	18													105
6	141	R	3	0.18	119	87	76	24	31	47	39																						112
6	152	R	2	0.3	136	86	15	31	20	54						2.3	3.1	2.7	1.5	1.5													107
6	165	R			325	82																											112
6	110	R			68																												116
6	140	R			133	70																											112
6	140	R			303	88																											115
6	155	R	3	0.12	306	84	18	10	4.5	3	15	31				2	1.5	2	0.8	0.5	0.6	0.5											111
6	157	R	4.5	0.09	110	81																											114
6	160	R	8.5	0.03	125	82	3	3	2.5	4	9					0.5	0.7	0.5	0.2														111
6	147	R	2.8	0.19	298	88	34	31	35	61	12	30				2.5	2.5	2	1	2.5	4.5												113
6	144	R	0.22	0.03	104		7	10	4							0.5	0.4	0.5	0.5	0.6													111
6	142	R	14		107	73	5	13	6.5	50						0.4	0.9	0.5	0.3	0.7	0.6												108
6	163	R			126	79																											111
6	138	R			102	81	290	400								33	16	15	7	11.5	14	16											107
6	155	R	3	0.07	127	64																											110
6	115	R			68	82																											116
6	145	R	5	0.4	103	78	80	45	68	115						3	6	6	6	5	10												110
6	156	R	4	0.09	298																												114
6	153	R			304	80	4.5	5	4	2	10	6.5	2	1.5	1	0.7	0.8	1.1	0.6	0.5	0.7	0.8	0.4	0.2			3.5	2	0.5	1	1.5	3		110
6	155	R			114	87	250										25	30															104
6	151	R			124	77																											109
6	150	R	2	0.3	118	72	49	39	33								5	4	3	4	6.5						22	27	25	37				115
6	142	R	6	0.55	112	79	46	44	54	72	86	101					2	1.5	1.5	6.5	0.5	5.5	1.5	1										106
6	158	R	7	0.13	298	85																											113
6	151	R			117																												109
6	109	L			115		31	6	19	29																							107

6	112 L	0.7	0.06	148																													114
6	130 L			148		17	19	9	4	29																							110
6	149 L			40		8	9	11	9							11	11	17	17.5							2	6	5	2				113
6	123 L	1	0.07	159		12	17	7	11.5	7						3.5	3	2.5	1.5	2.5	1					13	11	11	7				112
6	119 L			139		16.5	7	18	4	8.5	7	20				0.5	0.8	0.7	1.2	6	3.4					9	5	9	12	3			107
7	144 R	0.16	0.007	124		6	2.2	2.5	0.7	4	6.5					0.5	0.4	0.1	0.2	0.3	1.1					1.6	1.5	0.7	3.2				41
7	136 R	6	0.35	110	88	65	50	42	43	36	34	42	39			8	1	4	3	10	2	4.5	2.5	4	5	31	25	23					38
																6	2																
7	165 R	2	0.45	305	85	34	42	34	60	70	65	60				1.5	2.5	1	5	7	4.5	3				65	62	58	30	24			42
7	141 R	2	0.5	112		76	64	46	75	56	63					4.5	4	5.5	4.5	3.5	7	12	13			56	33	55					40
7	150 R	5	0.5	116	85	40	7	8	16	22	58	49	33	25	130	7	2	5	4.5	3	1	2	2	1	0.5								40
7	139 R	5	1.1	98		95	147	68	105	89						12	10	20	4	9	10	10	11			89	30						38
7	139 L	1	0.09	182		12	9	11	8	7	8	13	11	9		3	8	5	4	2.5	2	3.5	2.8	4	3.8	8	9	6	8	7	6	6	41
																										5							
7	111 L	0.9	0.06	125		8.5	5	16.5	12	9	18					2	1.5	0.5	0.8	2.6	0.7	1.8	1.2	1.2		4	6.5	2.5	7	9	6		42
7	149	4	0.35			120										8	6	6															41
8	156 R																																179
8	105 R	1.5	0.3	70		40										8										27							50
8	171 R			153		60										2																	179
8	101 R	1.3	0.25	74		37	57	53								6																	51
8	155 R			296	84	66	58									11.5	10																178
8	180 R	5	0.3	315	77	110	55	27	65	45						3	8	2	4	7	2	3	6.5	6	3	25	35	24	33				52
8	110 R	0.5	0.03	89												1	2																69
8	145 R	1	0.15	120	84	23										2	3									16							54
8	150 R			139		15	20	40								3	5	6															179
8	145 R			250	73	37	27	64								12	7	4.5	20														179
8	140 R			289	81																												179
8	110 R			260	85																												63
8	164 L			195	56	70										3																	55
8	145 L			1	78																												179
8	175 L	1	0.18	195	76	22										3.5										13							52
8	180 L	2	0.5	35	82	39	55	50	40	51	52	62				16	18	7.5	4	6	6.5	13	6	4.5	7.5	27	48	40	56	54	42		51
8	150 L	1	0.2	110		14	24	28	40	11	17	34	29			6.5	9	7	9.5	8	3.5	3	6	8		10	20	11.5	8	20	11		54
8	170 L	5	0.6	197	85	60	70	50	110	100	95	175				10	6	13	7	19	22	16	11	8.5		90	140	70	107				52
9	140 R	1	0.1	298	62	20	19	18	18	13						3.5	2	1.5	4							14	7						55
10	141 R	1		289		25	26	25	27							7	6	5	4	4	6	9											56
10	1 L	1.5	0.22	193		67										0.5	7	10															58
10	175 L	1.5	0.14	199		35										6																	58
10	160 L	1.5	0.2	187	60	35	45	38	73	18	26					6.5	6.5	3.5	7	2	2	3											57
11	147 R	0.5	0.15	302	77	50	33	32	38							5.5	4	4															64
11	154 R	5	0.4	307	67											1	2																64
11	155 R	1	0.2	305	75	39	29	21	25							3.5	4	5	4.5	3													64
11	152 R			300	64																												64
11	155 R	1.5	0.1	116												0.5																	63
11	175 L	2	0.12	17		27	10	4	8	8	24	38	41			0.5	6.5	10.5	5.5	9	4.5												64
11	180 L	5	0.15	200	88	11	30	8	3	4						0.5																	64
13	121 R	2	0.4	283	83																												65
13	106 R	2.5	0.1	65																													66
13	134 R	3	0.35	289	70	83	56	50	52							10	1									50	38	30	39				66
13	109 R	2.5	0.1	65																													66
13	115 L																																66
14	68 R			186																													72
14	65 R			134																													74
14	72 R			128																													74
14	324 R	5		254	66																												71
14	80 R			130																													74
14	R			264	69																												72
14	297 R			294	85																												74
14	59 R			130																													74
14	297 R		0.06	249	51											2	2.5	4	1.5	5.5	1.5	4	3.5	1.5	1.5								73
																1.5	1.5	1.5	1.5	2	1	2	1.5	1									
14	300 R			188	64																												72
14	301 R			286	71																												74
14	R			262	50																												72
14	100 L																																74
14	85 L		0.7	129												8	15	7	7	6	5												73
15	109 R	5	0.32	70	72	50	76	58	19	12	10	24				0.5	5																76
15	110 R			83																													76
15	109 R	2	0.18	86	89	33	24	13	61	11	15	19	28			4.5	1	3	1.5	2													77
15	154 R	1.5	0.07	146		36	28	42	28	12						2	4	4.5	4							6	9	6	8				75
15	111 R	2.5	0.45	80	85	37	29	11	61	51						4	2	1.5	1.5	3	2	2	5										75
16	117 R			96		18	14	20	15																								77
16	112 R	3	0.08	280	78	18	14	20	15																	7	6	10	10				77
17	133 R			105	79	101	30	6	124							0.5	2	2	3	3.8	5.2	3.2	1.7	2.1	0.7								80
																0.6	0.7																
17	142 R			296	84											0.5																	78
17	125 R			112	86	92	14	37	17	54						0.5	0.9	0.5	0.4	1.7	1.2	1.1	2.3	1	4.5								80
17	147 R	3	0.16	95		29	16	30	27	24						2	1	1.5	2	0.75	2.7	2	1										78

17	136 R	3	0.7	100		5	10							2.5	0.5																78
17	124 R			106																											81
17	144 R	3.5	0.15	263	82	26	17	9	8	20	28	37		2.3	0.3	0.5	1.5	0.7	2.2	1.7	1.5	1.4	4	14	13	17	16	20	16		79
17	146 R	1.5	0.1	111		18	38	10	20	32	9			0.5	3																78
17	128 R			110		29	16	30	27	24																					78
17	135 R		0.2	107	85	46	12	5	19	5	17	6		5	4.5	1.5	0.8	4													78
17	149 R	5.5	0.3	114	75																										79
17	122 R	5	0.4	280	88	56	49	54	124					0.7	0.9	2.1	2	5	1	1.5	4.5										78
17	137 R			106		29	16	30	27	24																					78
17	70 L	1	0.05	257	72	18	7.5	21.5	20	19	12	4	5.5	3	1.5	3.5	2.5	2.5	1	0.5				1	1.5	4.5	8	5.5	2	2	82
18	139 R	1	0.3	116		73	76	71	60					9.5	9	7	7	6						60	53	59	46				84
18	154 R	3	0.09	129		11	10	13	2	72				3	0.3																82
18	136 R	1.5	0.1	116		16	29	23	10	7	77			1.5	1	1.5	1.5	1	2.5					30	37	16	8	11			82
18	81 R	1.5	0.1	58		25	26	32	16	5				21	25	12	22	5	4												83
18	156 R			132										1.5	2																83
19	120 R			63	73																										85
19	106 R			65		24								3	4	2															87
19	100 R	4	0.4	66	75	52	57							2																	87
19	99 R	4	0.35	75	86	80	30							5	1.5																87
19	140 R		0.45	120	81	15	100	200						0.5	10																85
19	158 R	2.5	0.15	323	79	33.5	18	4	56					0.3	4																87
19	126 R			103	77																										85
19	145 R	1.5	0.1	115		19	23	21	14					4										10	18	12	16				88
19	140 R		0.3	295	86	61	55	74						2	3	4.5	2	3	6	9	7	3									86
19	125 R			105																											87
19	142 R			120																											86
19	79 R			53																											87
19	120 R	1.5	0.15	99	82	26								3										15							88
19	103 R			81	53																										87
19	104 R	1	0.1	76		18																									87
19	136 R	2.5	0.25	120		61	55	78						11.5	5	6	8								52	50	53	78	34			86
19	R			68	70	100	200																								88
19	118 R	4	0.4	64	75	52	57							5	5	5	0.7	2													87
19	69 L	1.1	0.12	99		22	16	9	16					3	1.5																87
19	105 L			127	89	55								4.5										36							84
19	45 L	0.5	0.15	69	71	21								0.5	3																86
19	91 L			129	90																										86
19	118 L			327	81																										86
19	121 L	2	0.2	139	86	56	42	35	73	79	15			7	3.5	4.5	6	2.5	1	7.5				31	37	22	28				84
20	148 R			102	72	15	30							2	3									18	14	16	17				101
20	313 R			74	64	70	40	80	35					2	2.5	1	3	4													93
20	156 R			139	84	100	150							3	4																90
20	134 R			115	78	15	30	65						2	3																93
20	160 R			130		3	20	5						0.5																	101
20	94 R			64	80	25	30							3																	93
20	139 R			111	55	55								10	12																92
20	127 R			95	74																										103
20	143 R			115	78	110	52	140	64					5	9	12								48	55	60					101
20	143 R			302	80																										101
20	107 R			61	86																										91
20	153 R	1	0.3	103	43	35	45							4	5									30							101
20	164 R			131	88	65	14							4	5																95
20	145 R			303	88																										92
20	138 R	0.75	0.12	103	79	30								2	3									18	13	15	25				101
20	107 R			69	68																										91
20	110 R			62	79	54	48							5	8									48							91
20	125 R			102		5	20							1																	99
20	136 R		1.2	102	74	110								5																	94
20	139 R			96		48	31							2	3	10															91
20	125 L			135	90	30	130							3																	92
20	166 L		1	20	74	45	200							1	10																96
20	132 L	0.75	0.04	336	84	3	7	9	4																						104
20	122 L			322	87	13	70							1	2																92
20	120 L			145	82	53	42							4.5	3.5	7								39	29						92
20	100 L			119		45								3										24	17	30					99
21	134 R	0.24	0.03	103																											118
21	154 R	1.7	0.1	117	90																										118
21	159 R	13	0.17	301	86									1.7	1	0.5															119
21	151 R	1	0.13	133	66	47	39	40	33					9.5	6	3.5								34	35	22					118
21	136 R	2.5	0.4	98	70	18	19	30	18	39	54			4.4	1.9	1	1	1.7	0.9												119
21	139 R	3.5	0.25	115	89	44	65	17						3.5	4	2	1														118
21	135 R	0.5		115																											120
21	145 R	2.2	0.2	118	84	22	19	25	22																						118
21	164 R			129	90																										119
21	144 R	2	0.14	295	87	19	25	34	19	14				2.5	1.5	1.5	2	2	2												117
21	144 R	5	0.12	287	89																										119
21	148 R	2.5	0.46	111	88																										119
21	150 R	7	0.2	286	84	22	32	24	16	14	12	14		1	0.4	1	0.6	1.2	2.4	2.9	2.1	1.4	2								117

													1.1	1.9	0.6	1.5										
21	129 L			156																						120
22	166 R			303	80																					121
22	154 R			297	71																					121
22	116 R			103	40	10	15	23					2	1	3	2					11	4	14	10		145
22	110 R			254	88	42	22																			149
22	137 R			125	90	20	26	20					3.5	1	3	1.5					19	11	20			144
22	147 R			295	86																					155
22	133 R			122		20	31						2	3	1.5						9	8	11			146
22	136 R			119	90	20	34	30	7	72			3	1.5	4	1	1.5	0.5								155
22	102 R	0.7		252	86	8.5	10	3	18				3	5	7	11	23				7.5	10				143
22	144 R			295	77																					154
22	19 R			6		36	35	30	40				7	6.5	6						17	11	-6			142
22	18 R																									152
22	125 R			92	85	6	11	7	6				2.5	2	1.5						5	5	4.5			147
22	95 R			66																						150
22	120 R			76	80	9	3	5	4	6			1	0.1												149
22	135 R	1		112	89	28	22	26					4.5	2.5	7						24	17	13			151
22	74 R	0.5		57		14							3								5					144
22	135 R			101	88																					151
22	104 R			80		20	32	21					3	2	3	4					16	17	7			143
22	135 R			294	83																					151
22	134 R			103	90	60	76	52	74				8.5	12.5	15	7	14									151
22	135 R			100																						151
22	102 R			74	80	17	27	26	38	13			1	5.5	5	4	2	3			12	18	16	15		143
22	178 R	0.7		167	16	15	10	10	6				1.5	0.5	1.5	1					7	4	6	4	3.5	145
22	130 R			92	85	18	11	10	9	4			1.5	1	2.5	2										147
22	135 R			92																						151
22	110 L			140		58	53	74	28	21	10	3	9.5	5	5	8	4	5.5	3	1.5						146
22	111 L			135	87	33	36	26					3	3	4											150
22	98 L			302	82	13	16	16	25	39			2	1.5	1.5											152
22	113 L			313	85	26	14	17	22				1.1	1	0.7	0.5	2									150
22	109 L	4		129	90	38	74	80					10	2	7	3	2									152
22	104 L			315	78	130	29	22	10																	149
22	111 L	5		320	82	43	40	51					4	5.5	7											153
22	110 L	1.7		136	90	21	13	7	14	54	77		4	1	0.5	3.5	4.5	1	3							149
22	110 L			149	86	70							10													153
22	113 L			135	87	44	40	34					7	3	2.5	3					35	37				147
22	73 L			98																						154
22	106 L			312	85	39	40	44	29				2.5	3.5	4	4	5.5	7			25	39	27			147
22	95 L			132	82	27	36	32					5	5.5	4.5											150
22	115 L			318	22																					147
22	117 L	4		322	80	22	28	34	43				1.5	1.5	2	2	1.5									153
22	115 L			142		27	24	15	27				1	3	1.5	2.5	5.5				13	17	15	13	14	147
22	100 L			317	86	40	34	24					3	2	4	4										150
22	135 L			115	90																					154
22	102 L			130	88	20	22	23					4	3.5	4						21	7	12	13		152
22	120 L			145	88	21	24	33	17	29			1	1.5	3	1	0.5									145
23	149 R	0.5		132		16	17	15					1.5	2	3	1.5					6	8	10	11		157
23	124 R																									163
23	127 R			104	85																					174
23	145 R			120																						157
23	155 R																									174
23	139 R			100	88																					159
23	76 R	4	0.25	60	80																					172
23	124 R			90	84	27	11	9	10	10			1	0.8	1.2	1										156
23	135 R																									172
23	134 R			105	81	13	8	47	29				1.2	1	0.8	0.3	0.4	0.5								161
23	97 R			54	78																					168
23	133 R	0.5		110		10	9	10	9	9			1.7	1.5	1.4	1.2					7	7	7.5	6.5		157
23	94 R	1.1		70	80	28	15	17	8	19			1.5	2.5	3	1	0.5									164
23	135 R			114	86																					161
23	145 R																									164
23	150 R			293	85																					162
23	135 R																									164
23	138 R	2	0.14	99	78	15	16	25					0.5	0.6	0.7	2										158
23	135 R			93	85	57	54	57	51				15	13	12	7										164
23	127 R			100	90																					160
23	125 R			90	75																					165
23	138 R			110																						157
23	135 R																									165
23	95 R																									167
23	105 R	3		66	79	110	73	100	67	46	54		12.5	12	9	7	10.5	3	2.5	4						165
23	142 R			97	86																					156
23	102 R	0.5		88	78	20	21						2.5	3							16					156
23	135 R			306	86	61	31	16	27				4	4	6	2.5	4									161
23	105 R			65	82	20	22	24					1.5	0.8	0.5											166
23	128 L			166	85	20	19						6	3	4											156

23	119 L		151		10	12	15					2.5	3	3											163
23	121 L		140	81																					161
23	123 L																								163
23	134 L	0.5	171		13	14	8					1.5	1.8	2.2											157
23	100 L																								163
23	118 L		146	82	37	63	13	10	12			1.5	0.5	1	1.5	2.5									161
23	125 L																								174
23	125 L		154		5	8	11	15				0.6	0.5	0.4	0.5										156
23	120 L		140																						174
23	105 L		145	84	13	12	9					0.6	0.8	0.5											161
23	102 L																								163
23	122 L	1.5	320	85	59	33	41	35	28	41	27	7	3.5	3.5	7	4	2.5	2	23	17	26	27	27	22	159
23	125 L		145	76																					174
23	125 L		151	77																					174
23	110 L		138	85																					164
23	115 L		322	83	77	26	19					1.5	2	3.5	4	1.5									159
24	335 R		120																						183
24	135 R		281	84																					185
24	142 R		280																						185
24	147 R		111		9	9	7.5					2	2.5	1											181
24	134 R		100																						181
24	330 R		313	66																					183
24	132 R		102		120	122						31	24												182
24	120 R		270	58																					183
24	140 R		116																						182
24	305 R		90																						184
24	150 R		110																						183
24	325 R	10	120																						184
24	320 R		271	61																					182
24	135 R		100																						185
24	125 R		90																						186
24	125 R		280	57																					186
24	171 L		323	54																					185
24	135 L																								182
24	124 L		335	32																					184
24	80 L		310	39	15	4	6	12				0.5	0.7	1	0.5										186
24	134 L		170																						181
24	104 L		338	39	6	5	4					3	2												184
24	140 L		155																						182
24	122 L		150																						181
25	137 R		295	64	42	34	65					8	9	6.5											189
25	320 R		306	72	20							1													191
25	140 R		290	75																					188
25	142 R		112	69																					189
25	118 L		330	75	5	4.5	2	6				0.6	0.7	0.2	1.5										188
25	128 L		335	50	10	9	8	8				2	3	1	2.5										190
25	120 L		330	77	5	4	3	6				0.8	0.9	0.6	0.7										188
25	121 L	1	326	67	4	7	6	14				1													190
25	132 L		325		10							8.5	1												190
25	118 L	4	325	70	7	6	5	3	3	5		0.5	0.5	0.6	1	2	2.5	0.7							190
28	117 L																								192
28	50 L		70		10	15						5													192

FRACTURE SET DATA MEASURED FROM PHOTOGRAPHS

photo	fracture length	fracture spacing	fracture overlap (mm)	R or L	zone trend	fracture orient	station
2b-16	90	39	90	L	125	111	7
	188	11	31				
	87	17	87				
	132	14	37				
	143	12	54				
	76	3	3				
		20					
		32					
		37					
2b-8	135	18	105	R	136	110	7
	205	10	90			105	
	125	28	85				
	225	28	105				
	150	33	110				
	155	40	125				
	135	5	23				
	85	20	85				
	210	60	180				
	210	13	100				
	110	25	100				
	175	28	165				
	225	20	65				
	100	23	150				
	185	25	185				
	260	65	260				
	390	40	370				
	425	88	350				
	370	10	305				
	460	95	215				
	215	15	215				
	790	90	515				
	515	35	515				
		30					
		50					
		18					
		105					
		95					
		10					
		60					
		50					
2-37	67	40	67	R	149	118	6
	141	22	87				
	127	27	96				
	136	34	98				
	174	34	112				
	125	11	74				
	134	17	101				
	101	18	74				
	125	18	74				
	109	19	94				
	123	38	71				
	161	6	4				
	38	42					
		44					
3-2	44	4	26	L	124	155	6
	33	18	33				
	113	13	63				
	81	11	62				
	89	15	62				
	62	5	30				
	91	23	78				
	78	9	69				
	167	23	107				
	107	25	91				
		31					
		5					
		18					
		12					
3-3		4		R	145	122	6
		8					
		4					
		3					
	69	8	60				
	88	11	88				
		12	104				
	126	10	126				

	135	5	69				
	69	4	52				
	91	8	71				
	71	7	71				
	126	11	107				
	107	7	8				
	36	8	36				
	74	5	74				
	280	5	33				
	33	25	33				
	165	8	110				
	371	12	132				
	132	16	132				
	266	15	266				
	406	14	211				
	211	25	135				
		14	165				
	220	12	77				
	77	5	8				
		15					
		60					
		22					
		16					
		15					
		30					
		38					
7-23	79	23	33	R	133	110	23
	70	16	36				
	92	15	70				
	106	13	61				
	85	11	54				
	97	10	57				
	103	17	59				
	105	13	52				
	79	11	34				
	49	7	29				
	38	4	25				
7-30		58		L	123	158	23
	152	56	129				
	150	33	122				
	145	23	109				
	119	36	119				
	157	23	94				
	102	79	94				
	241	51	160				
	236	74	226				
	327	76	175				
	175	41					
7-8		20		L	115	142	22
	75	3	9				
		4	7				
	70	2	4				
	99	26	99				
	239	15	138				
	165	24	114				
	136	37	136				
	257	50	182				
	255	33	123				
	123	7	11				
		7					
		22	33				
	94	20	48				
	77	18	40				
	83	5	15				
	42	2	0				
		4					
		9					
		10					
		9					

RIGHT-STEPPING ZONE, DETAILED MAP, STATION 17

zone orientation 144
fracture orientation 263 /82

fracture length	fracture spacing	fracture overlap
21	2.5	21
55.5	2	20
25	2	25
59.5	1	34.5
34.5	4.5	28.5
43	2.5	29.5
31	2.5	30.5
39	1	39
46.5	2	36.5
36.5	3	24
24	0.5	23
36	1.5	36
50	1.5	42.5
42.5	2	29
33.5	3.5	12
12	1.5	12
42.5	5	7.5
15.5	2.5	15
23	0.5	6.5
22.5	1.5	22.5
35.5	0.5	6.5
8	2	4
23	1.5	20.5
29	4.5	29
33	3	14.5
14.5	1	8.5
35	2.5	17
17	0.5	14
14	1	8
8	1	8
44	2	32
32	1	14
14	1.5	14
31	2	27
28	4	23
4.5	1	4.5
12.5	0.5	5
8.5	0.5	6.5
9	0.5	6.5
8	0.5	6.5
40	1	28.5
28.5	2	23.5
36	2	23.5
10	1	10
24	1	16
20.5	1	18
20.5	2	17
22.5	0.5	20.5
20.5	0.5	16.5
24	1	13.5
13.5	1.5	13.5
24	2	17
18.5	2	18.5
29.5	1	16.5
16.5	2	14
17	1.5	9.5
9.5	1.5	9.5
21.5	1.5	14
16	1.5	15.5
19	1.5	19
22.5	3	19
21	2	17.5
18	1.5	13
13	2.5	13
20.5	2	18
28.5	2	21.5
21.5	2	11.5
15.5	2	15.5
20	1	10
23	3	23
4	1	4
10	1	10
34.5	1	15
15	2	13
17.5	1	7.5
7.5	1.5	6.5
8	1.5	8
18.5	0.5	11.5
22	0.5	7.5
10.5	1.5	5.5

14	2	12.5
18	2.5	14
14	1	8
27.5	7	17.5
6	0.5	4
8	1.5	3.5
3.5	0.5	3.5
9.5	1	8.5
10	0.5	8
13	2	13
33.5	1.5	19.5
19.5	3.5	19
19	2.5	15.5
19.5	2	19.5
31	4.5	17.5
28	1	16.5
16.5	2.5	16.5
3	1	1.5
8.5	1	1.5
5.5	0.5	5.5
45	3.5	19
19	1.5	14
20	2	8.5
8.5	3	8.5
31	3.5	14.5
20	3.5	9.5
22	1	15.5
3	2	3
10.5	2	7.5
19.5	3.5	14.5

Appendix B

Fracture Length versus Spacing Graphs

for 8 echelon fracture sets

Fracture length vs spacing

2b-16

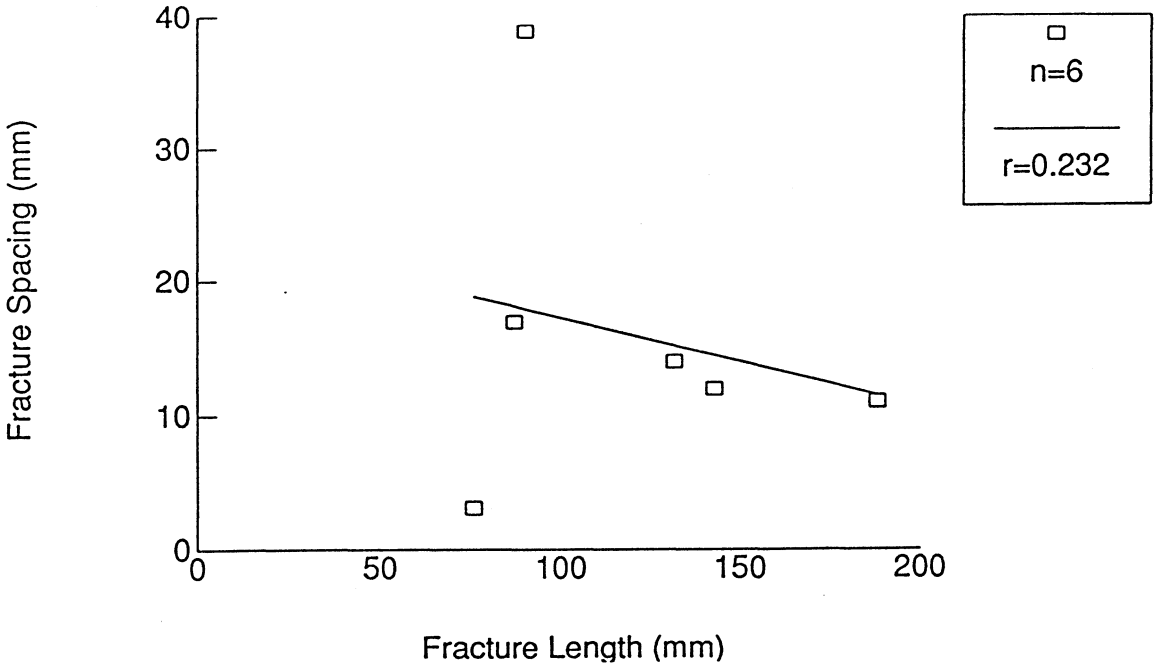

2b-8

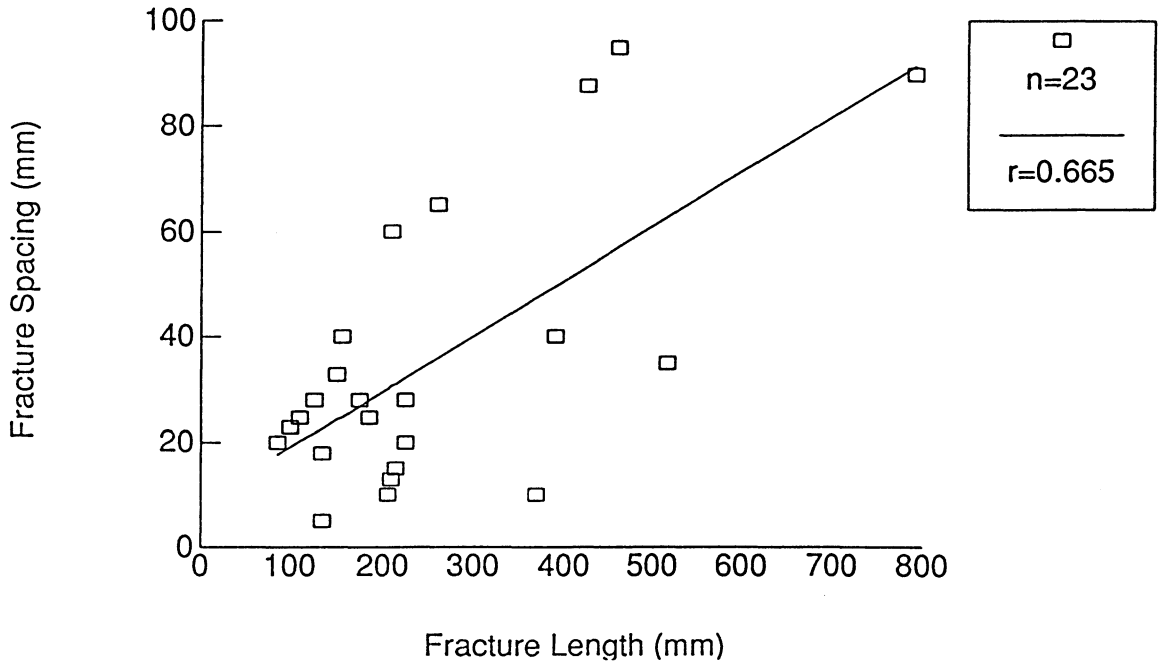

Fracture length vs spacing

2-37

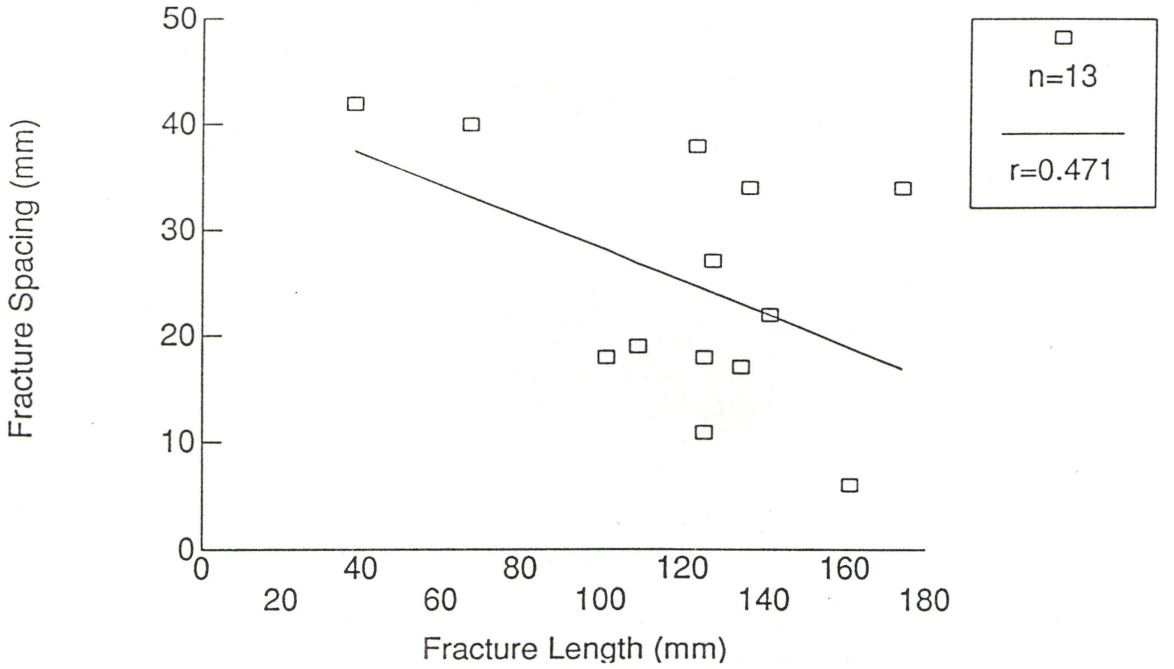

3-2

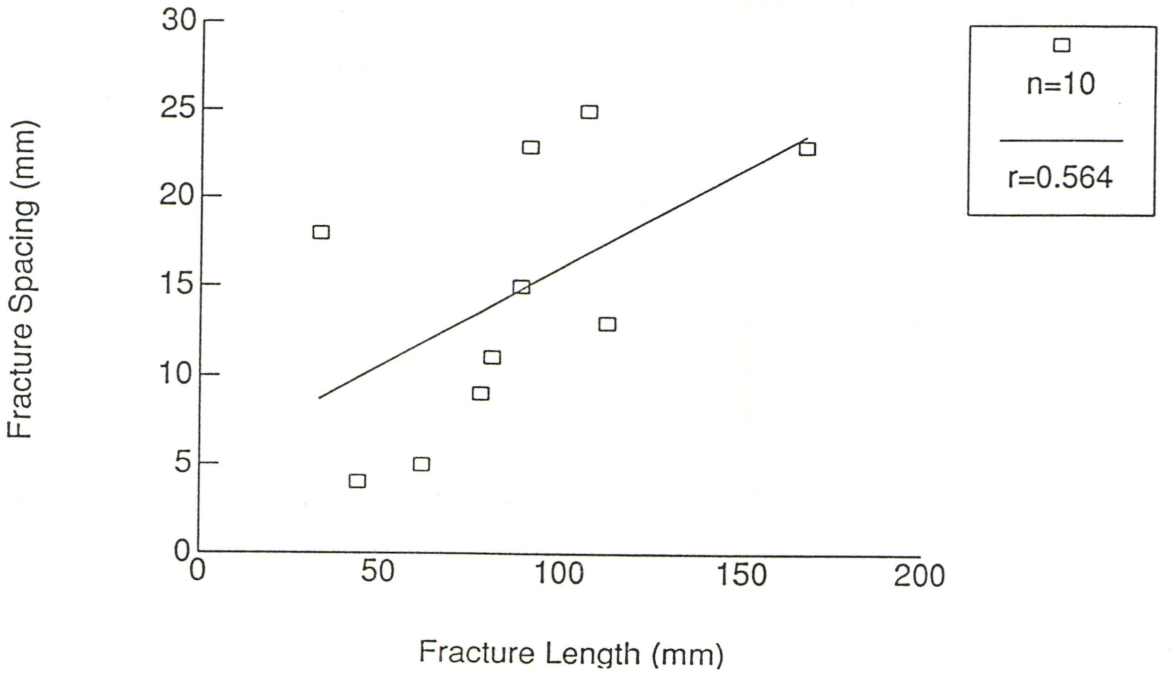

Fracture length vs spacing

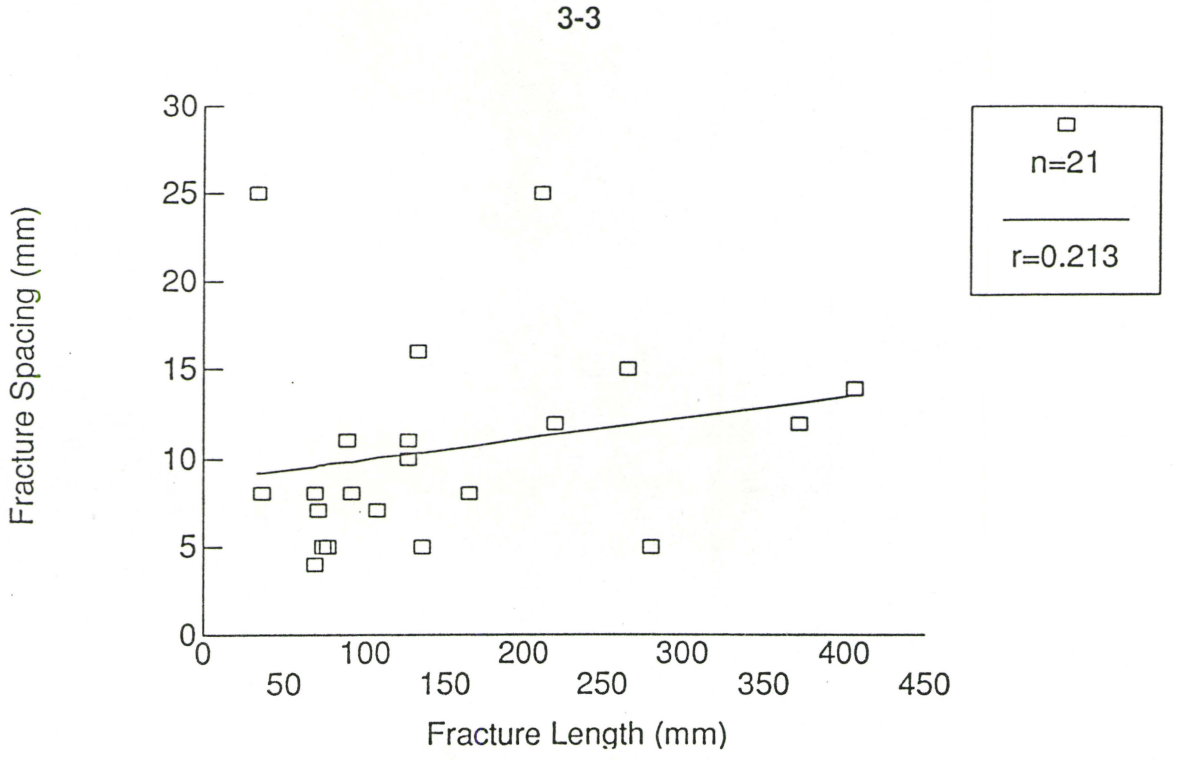

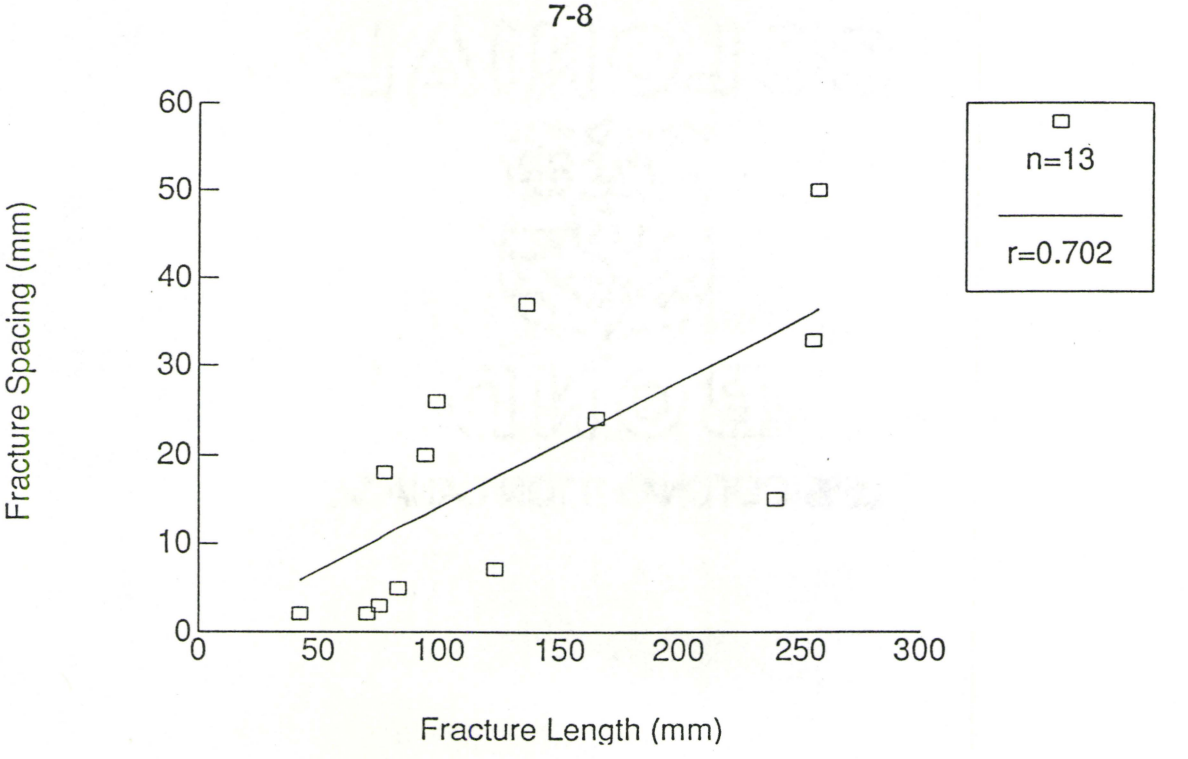

Fracture length vs spacing

7-23

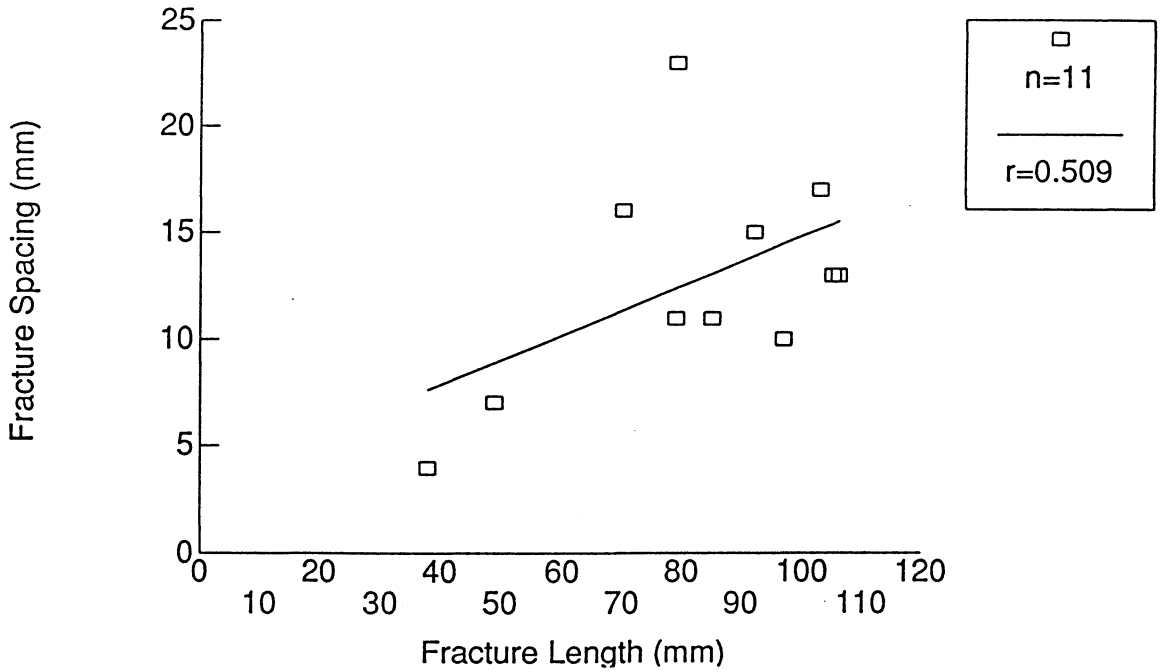

7-30

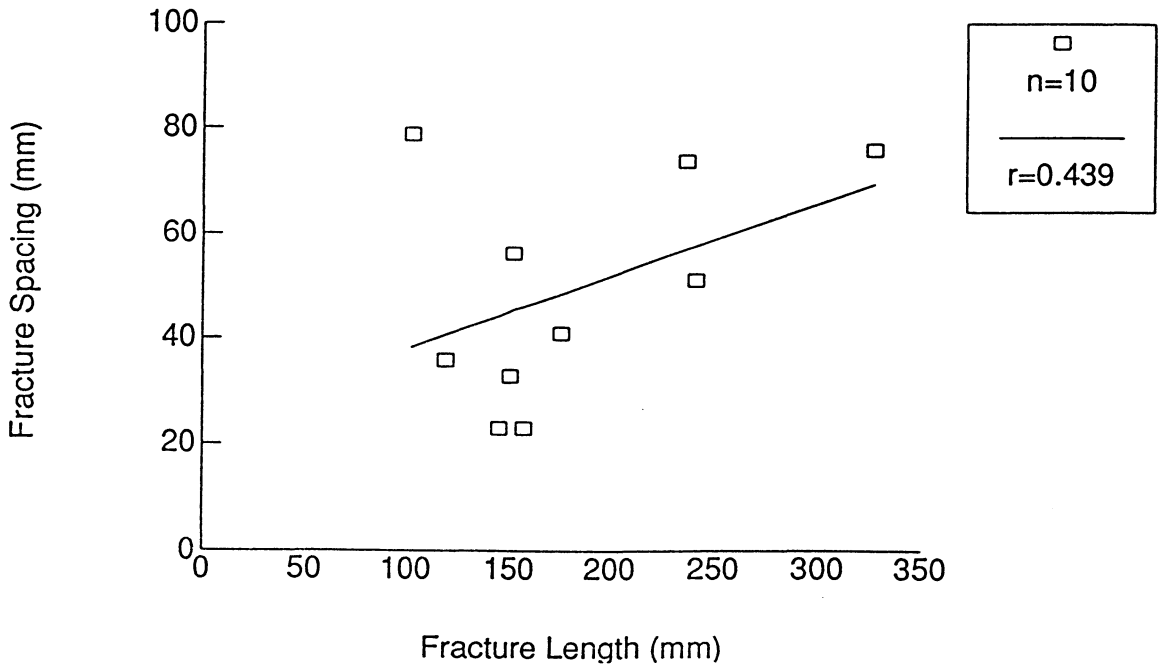

Appendix C

The Gaussian Weighting Function for the Circular Histograms

The weighting function chosen has a kurtosis of 100. This function was chosen with a high kurtosis so that only data close to the counting station are weighted significantly. Data in orientations greater or less than about 7° from the orientation of a counting station do not add significantly to the count for that station. The advantage of using a weighting function when counting at stations is that smoothly varying histograms are produced. The histograms were calculated and plotted using a Turbo-Pascal microcomputer program written by Dr. R.M. Stesky. The details of the calculations are given in Stesky and Bailey-Kryklywy (1988).

COUNTING FUNCTION

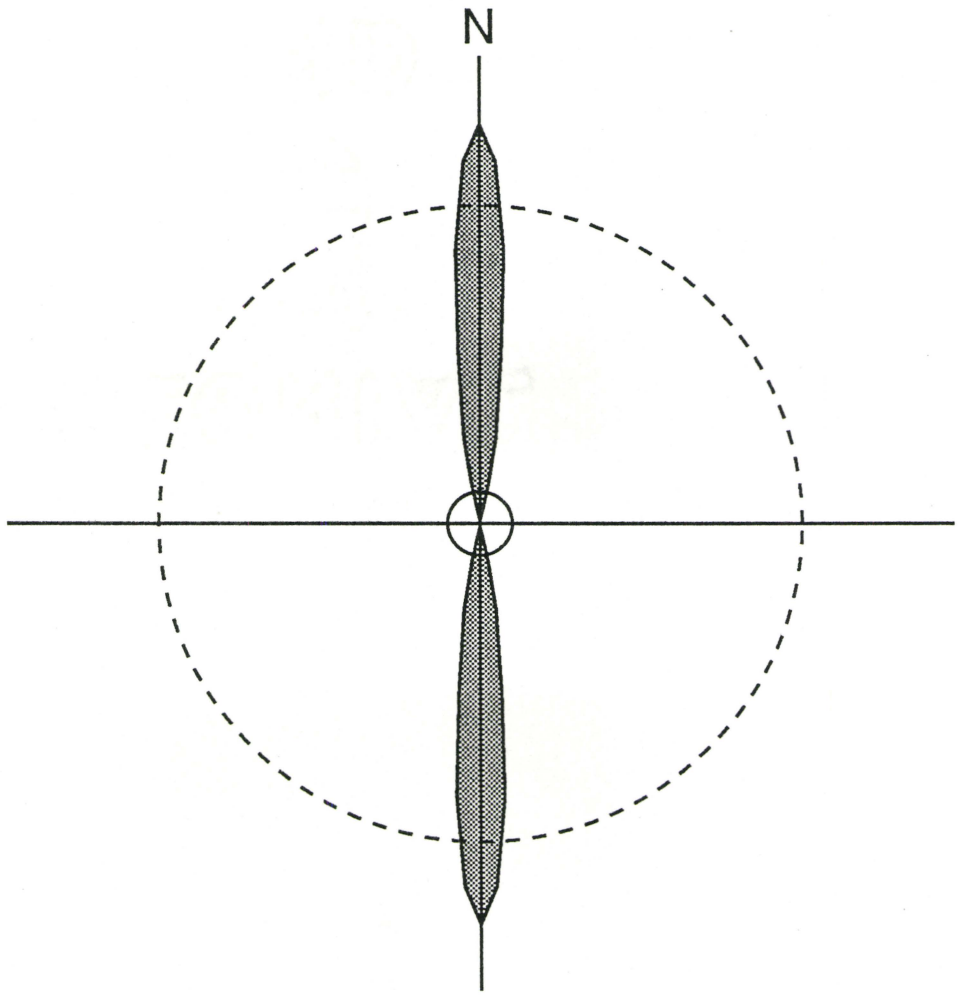

n = 1 E = 0.08 σ = 0.40 k = 100

Peak value = 1.00 Peak Orientation = 0.0°

——— E - - - - E ± 1.8σ

Appendix D

Circular Histograms of Echelon Fracture and Zone Orientations by Station Location

STATION 22

right-stepping fractures

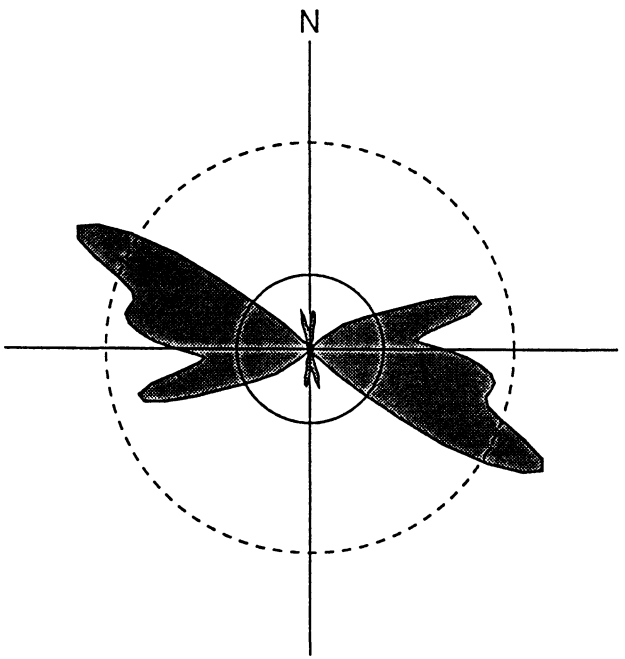

n = 25 E = 2.00 σ = 1.98 k = 100

Peak value = 7.14 Peak Orientation = 117.5°

—— E - - - - E ± 1.8σ

STATION 22

right-stepping zones

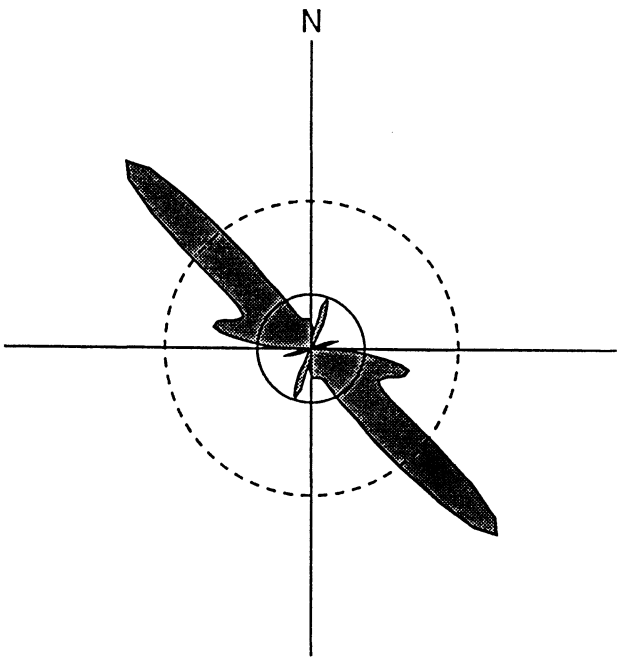

n = 26 E = 2.08 σ = 2.02 k = 100

Peak value = 10.20 Peak Orientation = 135.0°

—— E - - - - E ± 1.8σ

STATION 23

right-stepping fractures

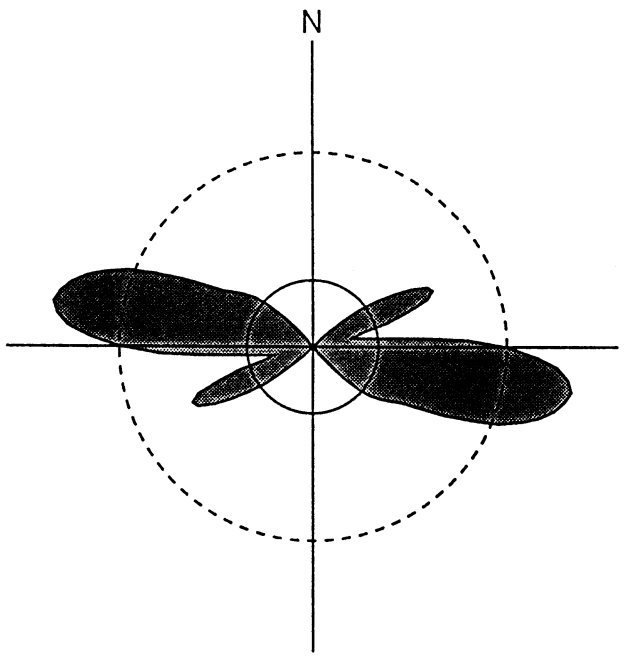

n = 22 E = 1.76 σ = 1.86 k = 100

Peak value = 6.92 Peak Orientation = 100.0°

—— E - - - - E ± 1.8σ

STATION 23

right-stepping zones

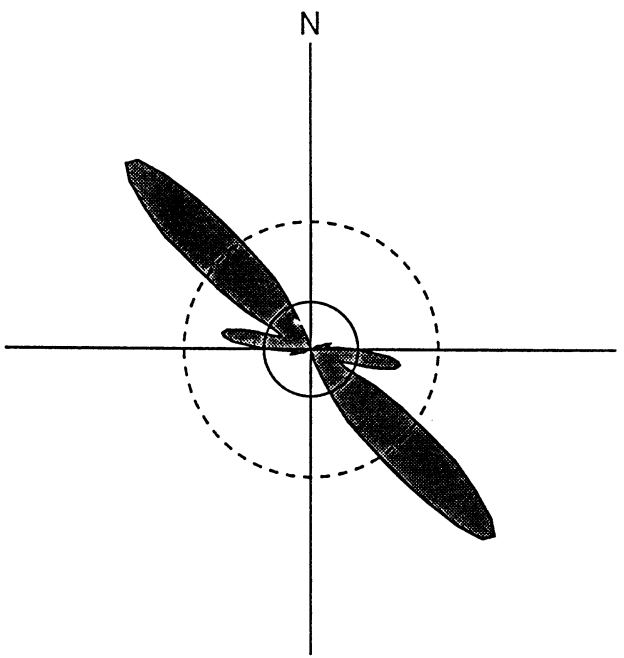

n = 29 E = 2.32 σ = 2.14 k = 100

Peak value = 12.75 Peak Orientation = 135.0°

—— E - - - - E ± 1.8σ

STATION 20

right-stepping fractures

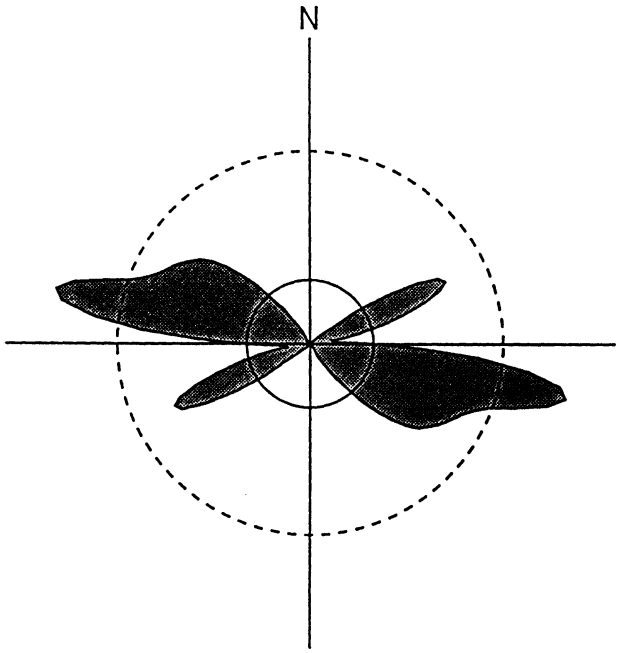

n = 20 E = 1.60 σ = 1.77 k = 100

Peak value = 6.46 Peak Orientation = 102.5°

—— E ---- E ± 1.8σ

STATION 20

right-stepping zones

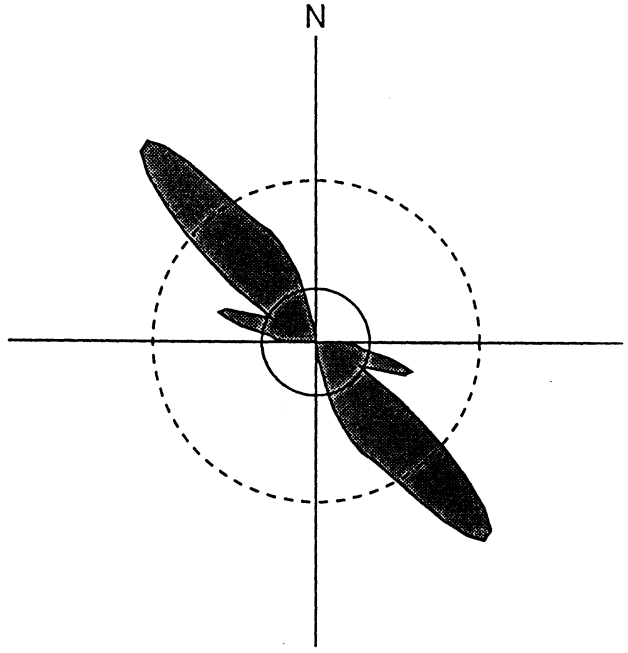

n = 20 E = 1.60 σ = 1.77 k = 100

Peak value = 7.76 Peak Orientation = 140.0°

—— E ---- E ± 1.8σ

STATION 21

right-stepping fractures

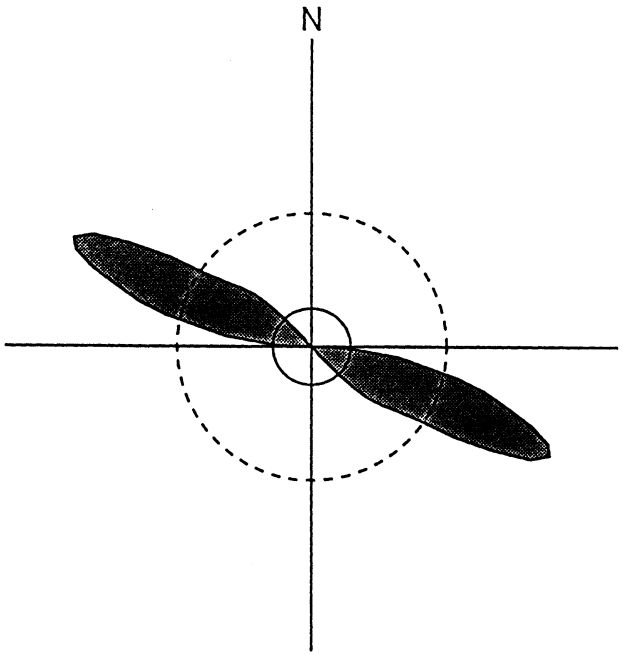

n = 13 E = 1.04 σ = 1.43 k = 100

Peak value = 7.03 Peak Orientation = 115.0°

—— E - - - - E ± 1.8σ

STATION 21

right-stepping zones

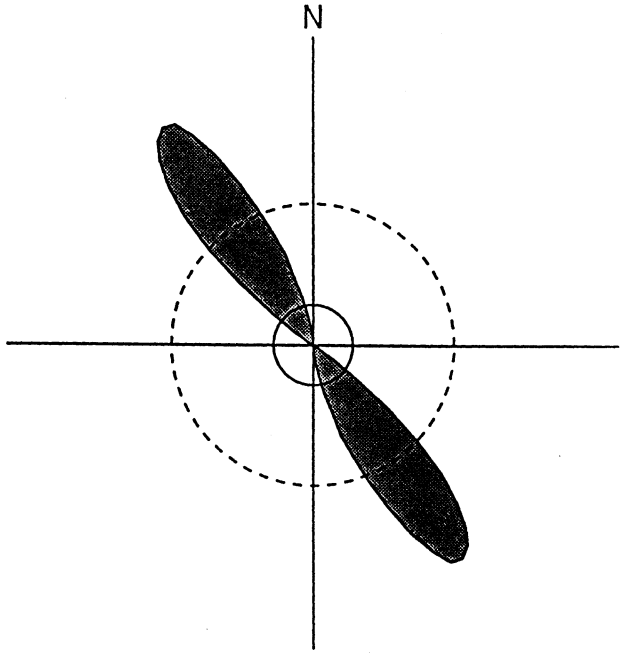

n = 13 E = 1.04 σ = 1.43 k = 100

Peak value = 6.70 Peak Orientation = 145.0°

—— E - - - - E ± 1.8σ

STATION 6

right-stepping fractures

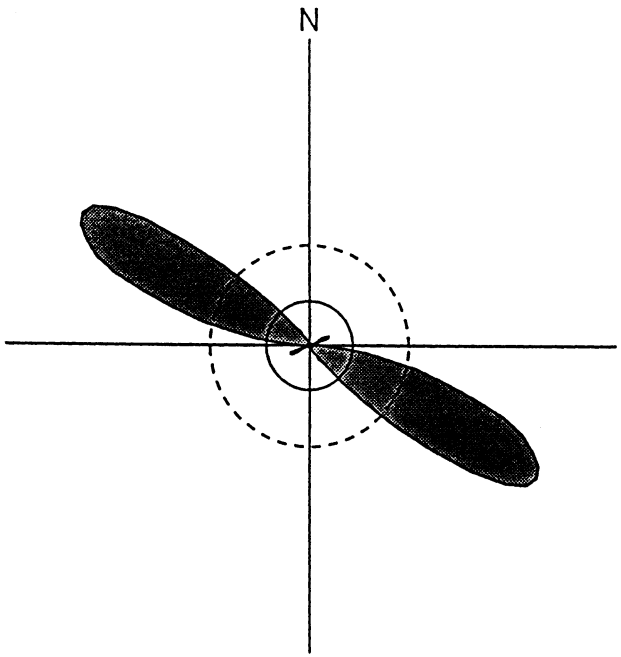

n = 51 E = 4.07 σ = 2.83 k = 100

Peak value = 24.21 Peak Orientation = 120.0°

—— E - - - - E ± 1.8σ

STATION 6

right-stepping zones

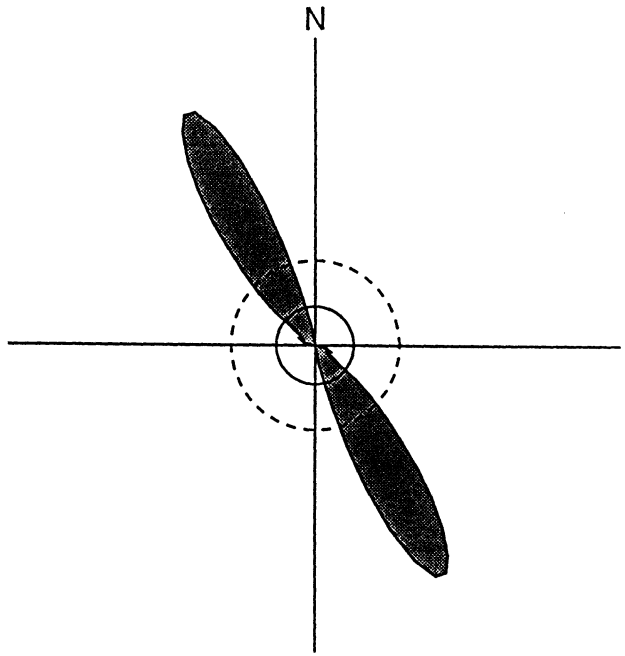

n = 51 E = 4.07 σ = 2.83 k = 100

Peak value = 28.42 Peak Orientation = 150.0°

—— E - - - - E ± 1.8σ

STATION 2

right-stepping fractures

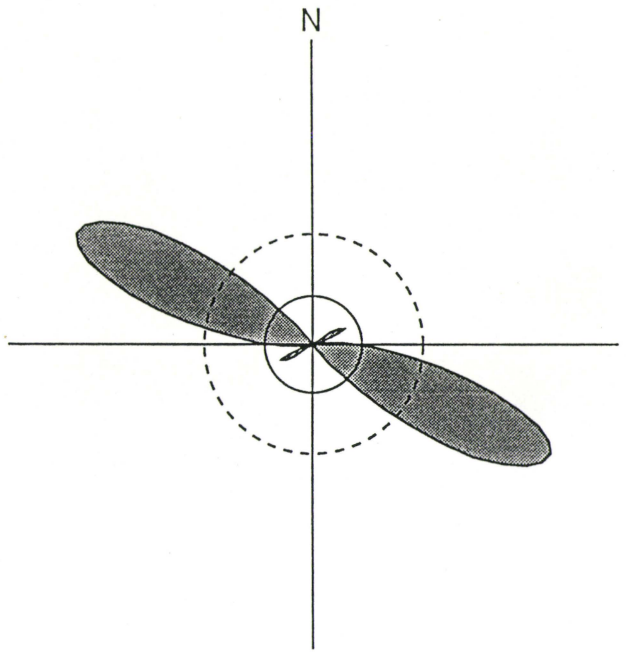

n = 51 E = 4.07 σ = 2.83 k = 100

Peak value = 21.99 Peak Orientation = 115.0°

—— E - - - - E ± 1.8σ

STATION 2

right-stepping zones

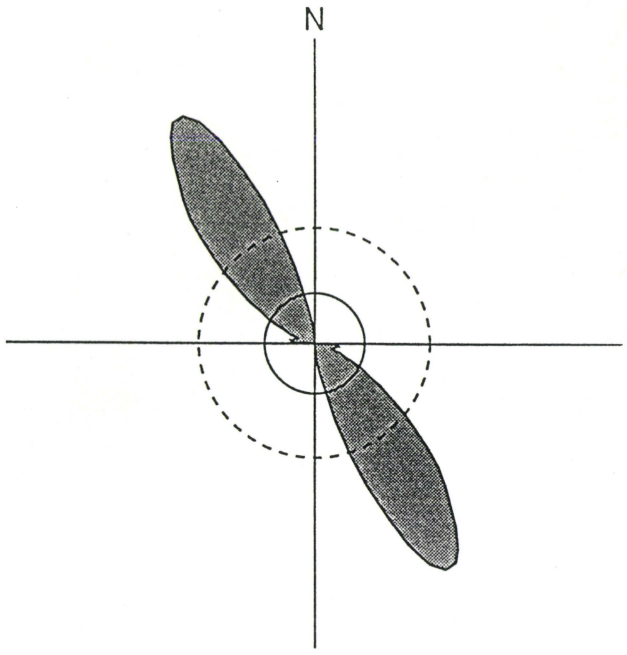

n = 51 E = 4.07 σ = 2.83 k = 100

Peak value = 20.85 Peak Orientation = 150.0°

—— E - - - - E ± 1.8σ

WEST STATIONS [7,18]

right-stepping fractures

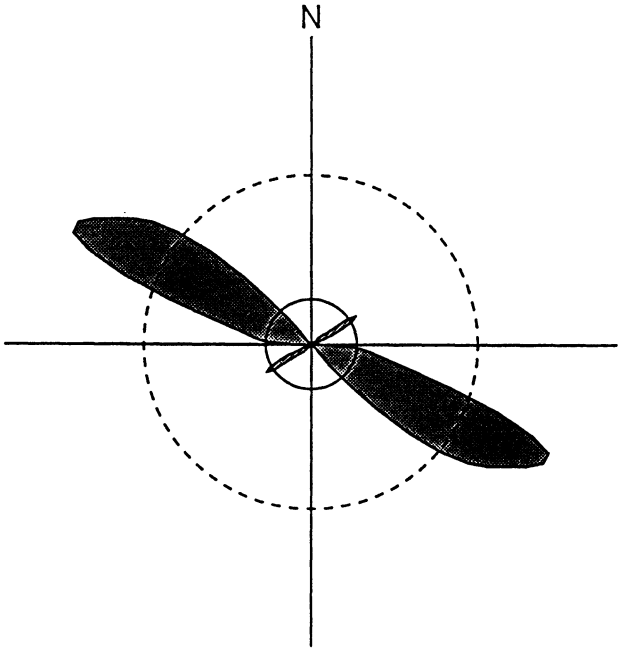

n = 11 E = 0.88 σ = 1.32 k = 100

Peak value = 5.10 Peak Orientation = 115.0°

—— E - - - - E ± 1.8σ

WEST STATIONS [7,18]

right-stepping zones

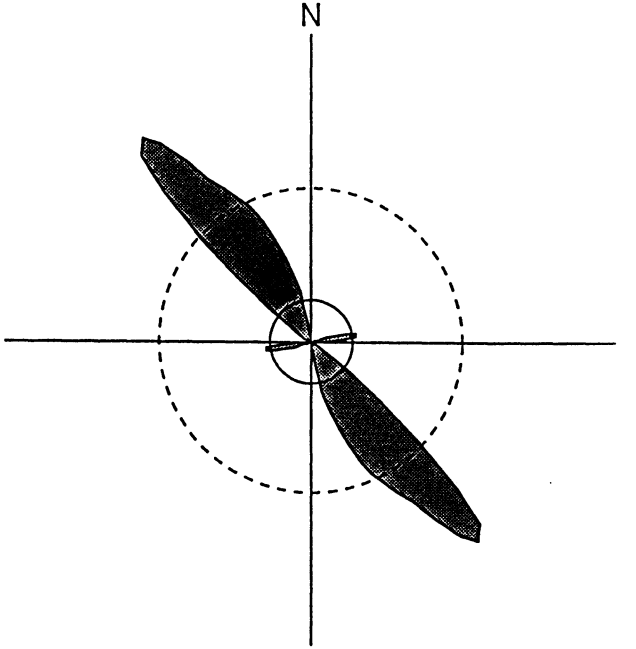

n = 11 E = 0.88 σ = 1.32 k = 100

Peak value = 5.60 Peak Orientation = 140.0°

—— E - - - - E ± 1.8σ

STATION 17

right-stepping fractures

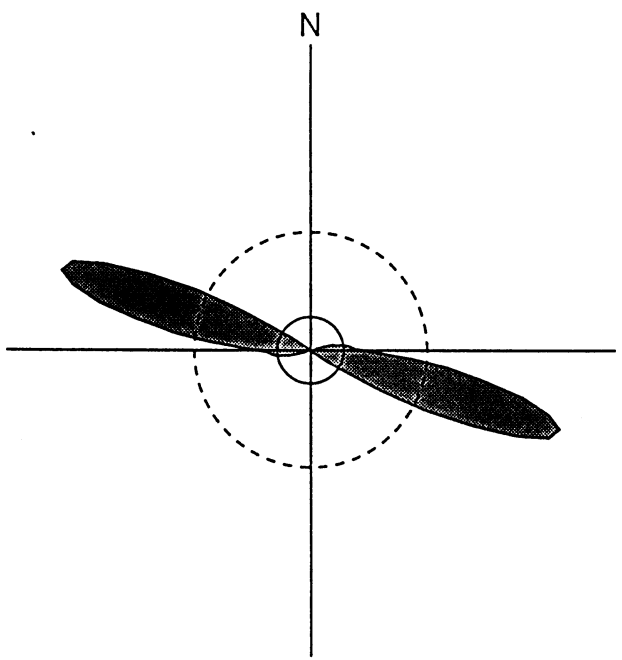

n = 13 E = 1.04 σ = 1.43 k = 100

Peak value = 8.11 Peak Orientation = 107.5°

—— E - - - - E ± 1.8σ

STATION 17

right-stepping zones

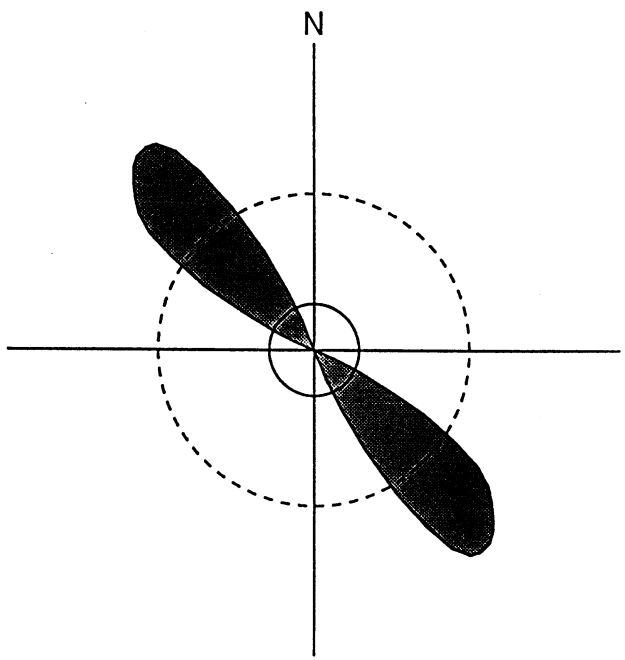

n = 13 E = 1.04 σ = 1.43 k = 100

Peak value = 6.06 Peak Orientation = 140.0°

—— E - - - - E ± 1.8σ

STATION 19

right-stepping fractures

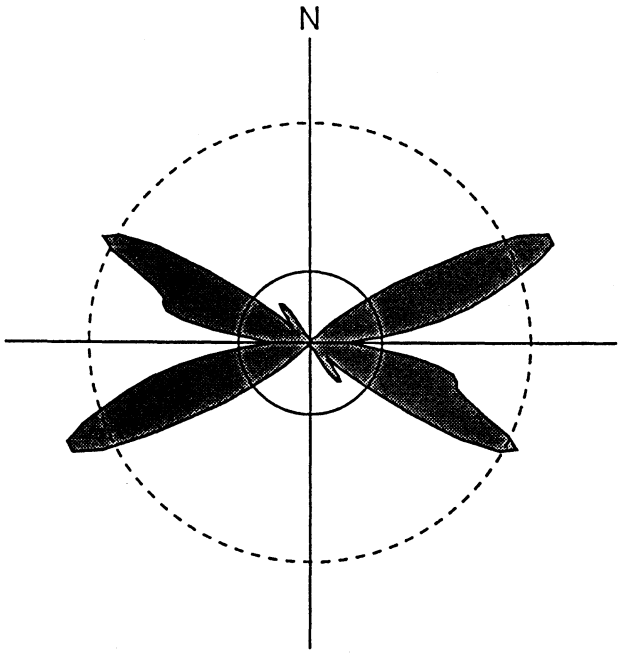

n = 18 E = 1.44 σ = 1.68 k = 100

Peak value = 5.30 Peak Orientation = 67.5°

—— E - - - - E ± 1.8σ

STATION 19

right-stepping zones

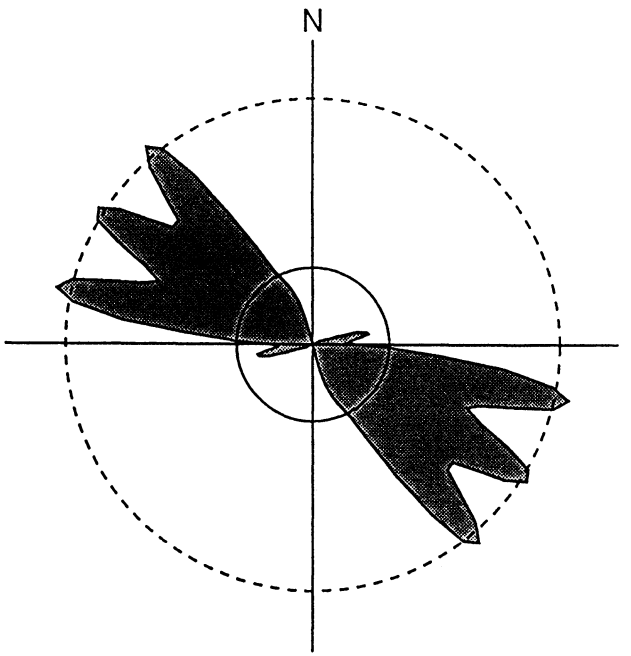

n = 17 E = 1.36 σ = 1.64 k = 100

Peak value = 4.58 Peak Orientation = 102.5°

—— E - - - - E ± 1.8σ

EAST STATIONS [1,8]

right-stepping fractures

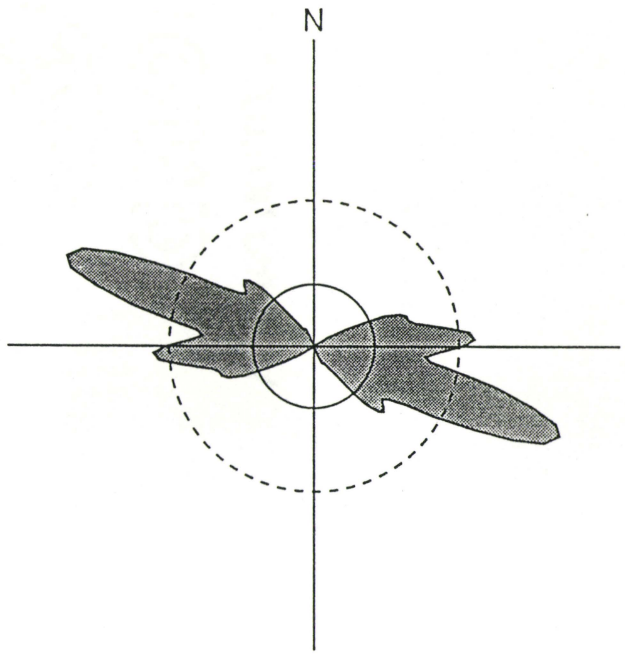

n = 43 E = 3.44 σ = 2.60 k = 100

Peak value = 14.74 Peak Orientation = 110.0°

——— E - - - - E ± 1.8σ

EAST STATIONS [1,8]

right-stepping zones

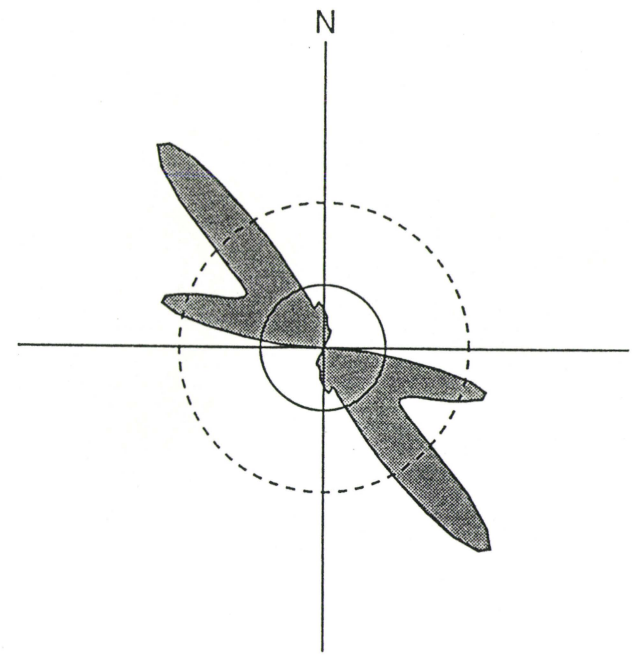

n = 44 E = 3.52 σ = 2.63 k = 100

Peak value = 14.85 Peak Orientation = 140.0°

——— E - - - - E ± 1.8σ

EAST STATIONS [11,13,14]

right-stepping fractures

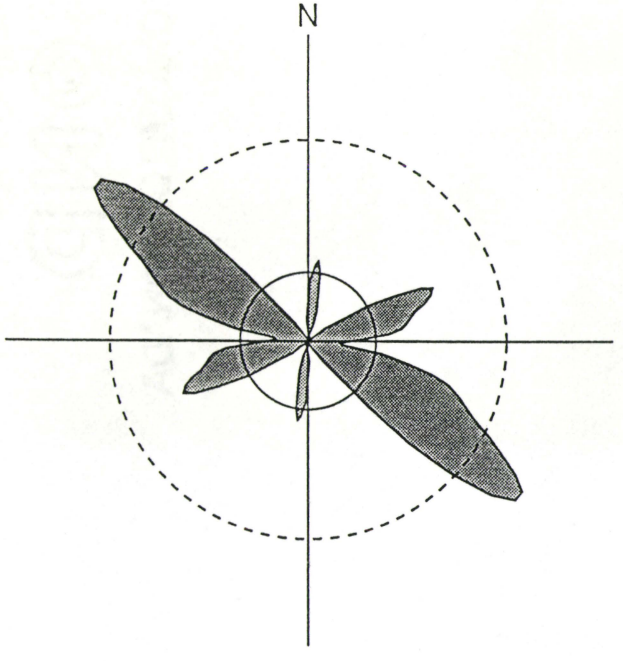

n = 21 E = 1.68 σ = 1.82 k = 100

Peak value = 6.51 Peak Orientation = 127.5°

——— E - - - - E ± 1.8σ

EAST STATIONS [11,13,14]

right-stepping zones

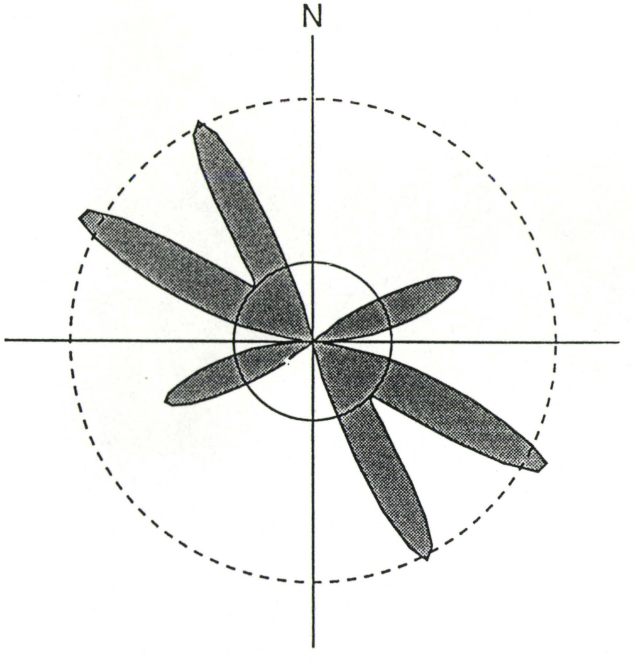

n = 19 E = 1.52 σ = 1.73 k = 100

Peak value = 5.05 Peak Orientation = 117.5°

——— E - - - - E ± 1.8σ

EAST STATIONS [15,16,25]

right-stepping fractures

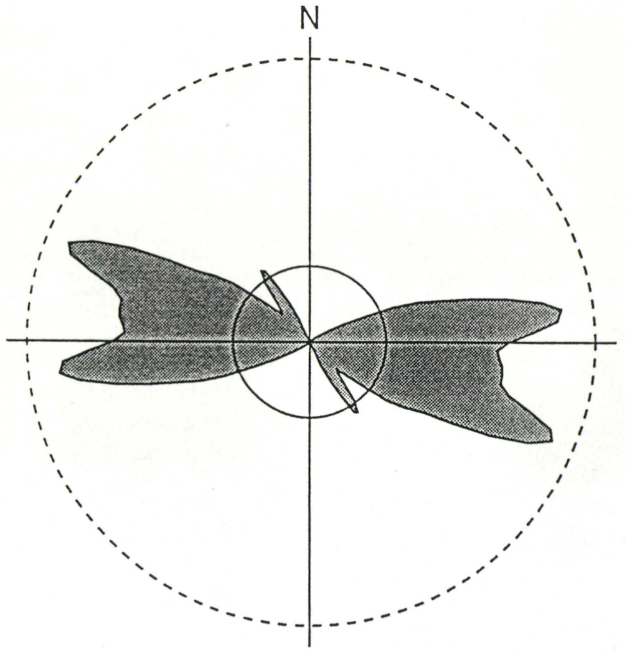

n = 11 E = 0.88 σ = 1.32 k = 100

Peak value = 2.99 Peak Orientation = 112.5°

—— E - - - - E ± 1.8σ

EAST STATIONS [15,16,25]

right-stepping zones

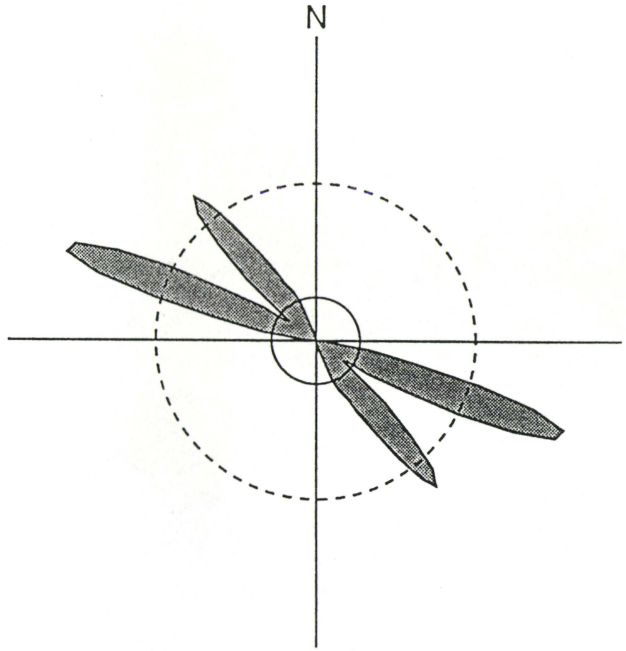

n = 11 E = 0.88 σ = 1.32 k = 100

Peak value = 5.37 Peak Orientation = 110.0°

—— E - - - - E ± 1.8σ

STATION 24

right-stepping fractures

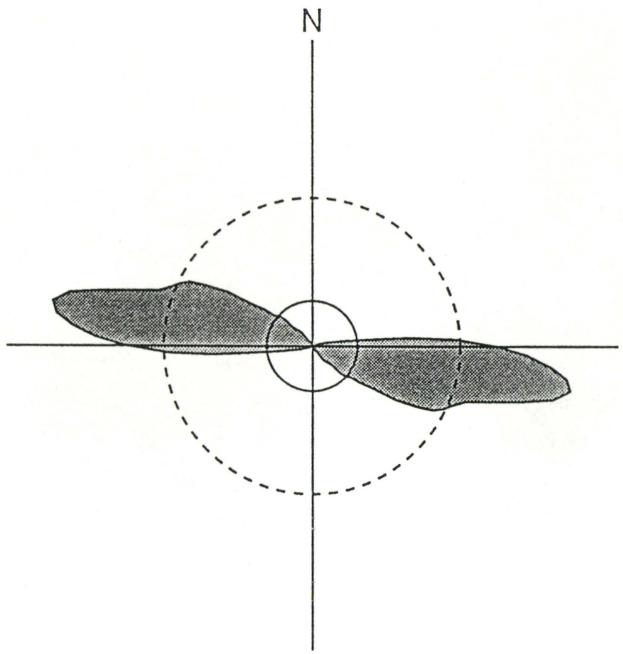

n = 16 E = 1.28 σ = 1.59 k = 100

Peak value = 7.28 Peak Orientation = 100.0°

——— E - - - - E ± 1.8σ

STATION 24

right-stepping zones

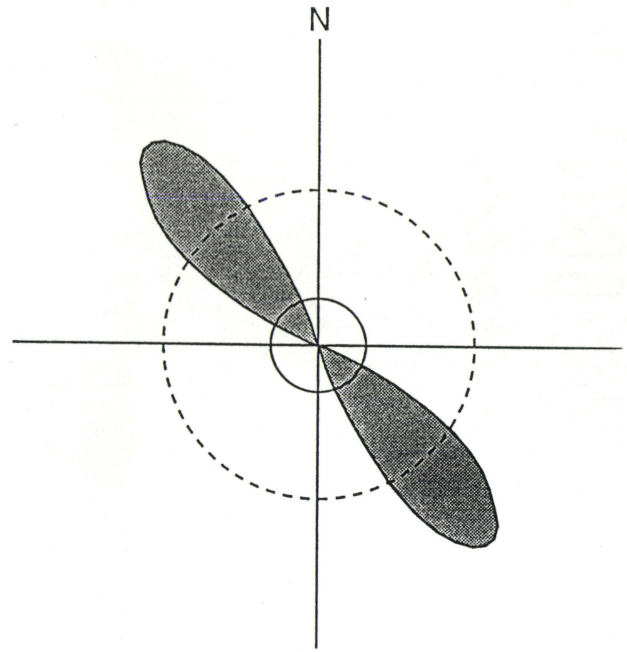

n = 16 E = 1.28 σ = 1.59 k = 100

Peak value = 7.00 Peak Orientation = 137.5°

——— E - - - - E ± 1.8σ

STATION 22

left-stepping fractures

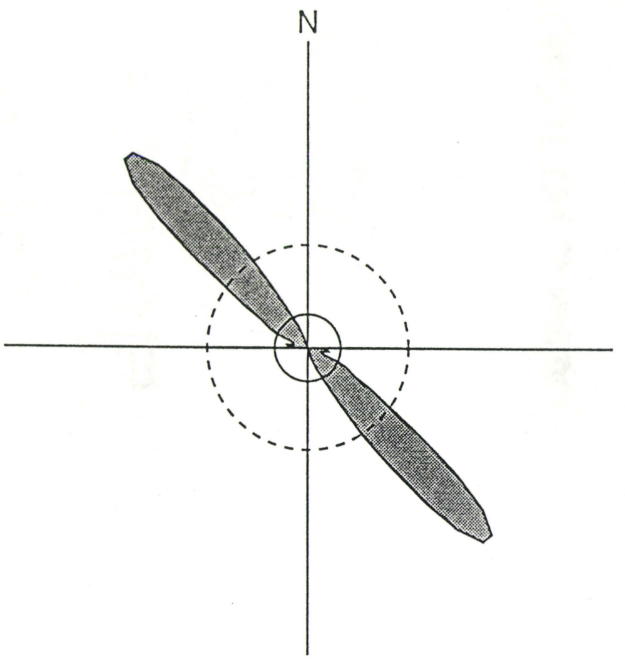

n = 20 E = 1.60 σ = 1.77 k = 100

Peak value = 12.41 Peak Orientation = 135.0°

——— E - - - - E ± 1.8σ

STATION 22

left-stepping zones

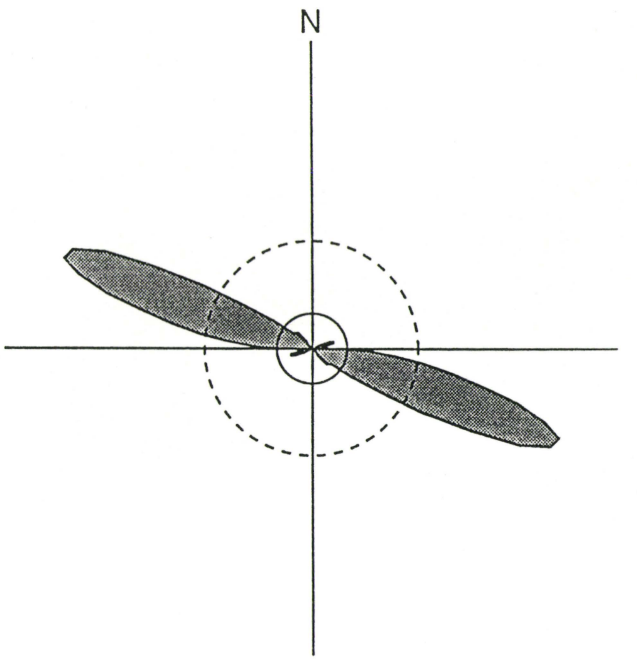

n = 20 E = 1.60 σ = 1.77 k = 100

Peak value = 11.86 Peak Orientation = 110.0°

——— E - - - - E ± 1.8σ

STATION 23

left-stepping fractures

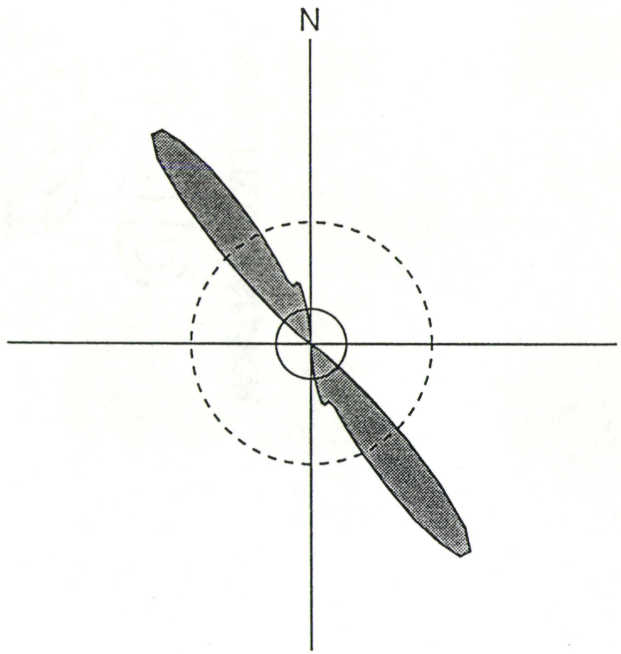

n = 13 E = 1.04 σ = 1.43 k = 100

Peak value = 7.91 Peak Orientation = 142.5°

——— E - - - - E ± 1.8σ

STATION 23

left-stepping zones

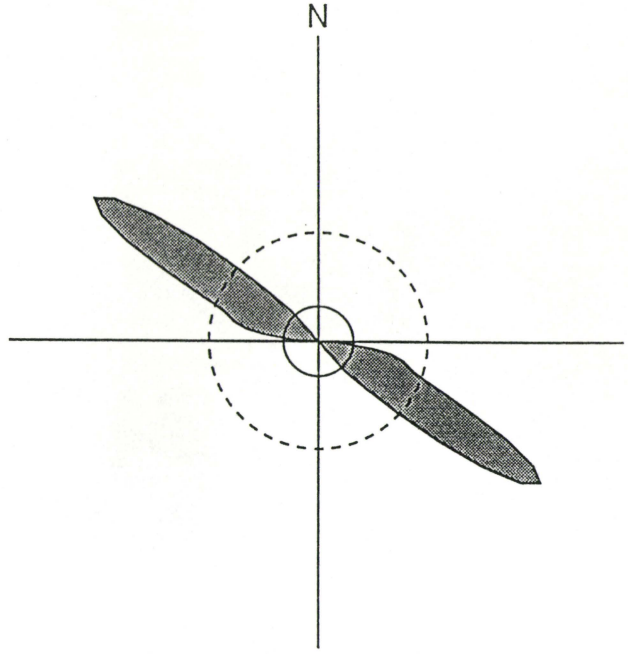

n = 17 E = 1.36 σ = 1.64 k = 100

Peak value = 10.37 Peak Orientation = 122.5°

——— E - - - - E ± 1.8σ

WEST STATIONS [2,6,7,20]

left-stepping fractures

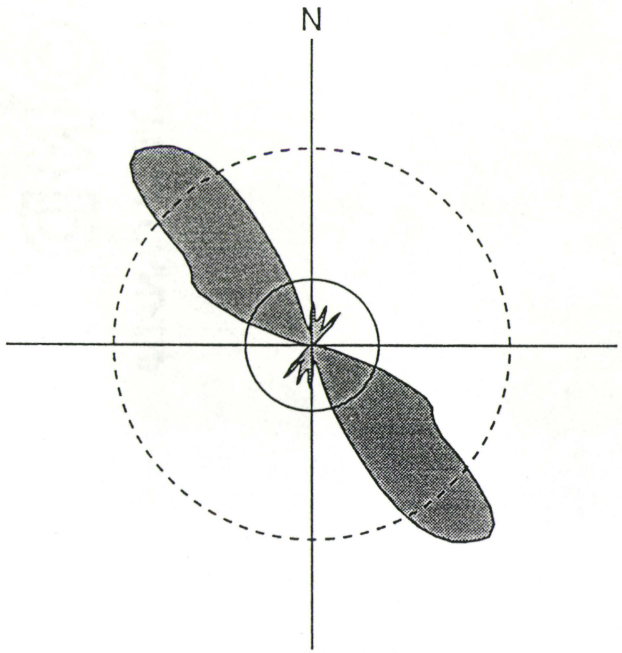

n = 20 E = 1.60 σ = 1.77 k = 100

Peak value = 6.37 Peak Orientation = 137.5°

—— E - - - - E ± 1.8σ

WEST STATIONS [2,6,7,20]

left-stepping zones

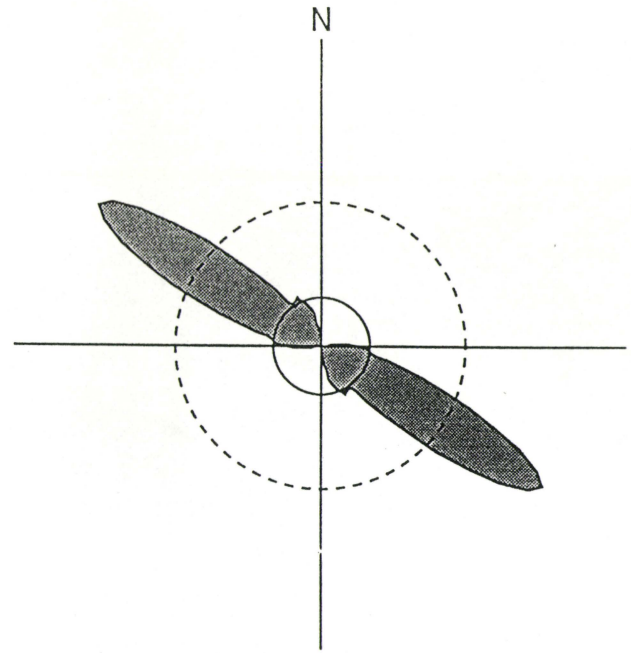

n = 20 E = 1.60 σ = 1.77 k = 100

Peak value = 8.64 Peak Orientation = 122.5°

—— E - - - - E ± 1.8σ

STATION 19

left-stepping fractures

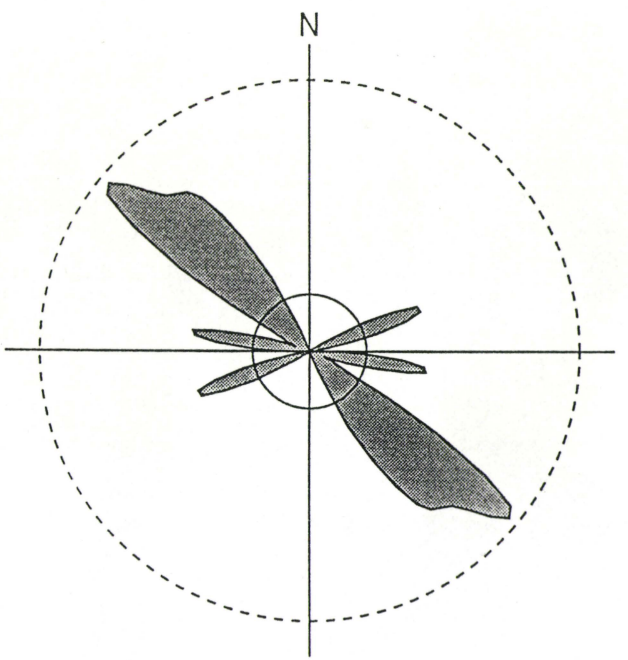

n = 6 E = 0.48 σ = 0.97 k = 100

Peak value = 2.16 Peak Orientation = 130.0°

——— E - - - - E ± 1.8σ

STATION 19

left-stepping zones

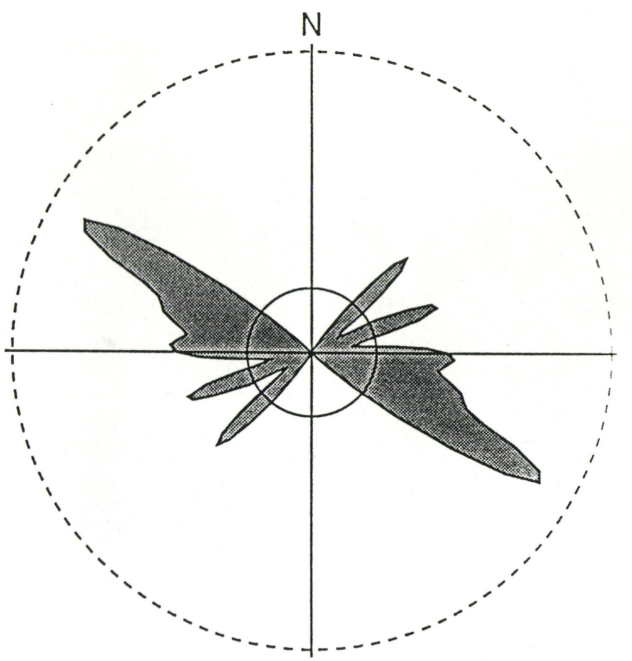

n = 6 E = 0.48 σ = 0.97 k = 100

Peak value = 1.96 Peak Orientation = 120.0°

——— E - - - - E ± 1.8σ

EAST STATIONS [1,8,10,11]

left-stepping fractures

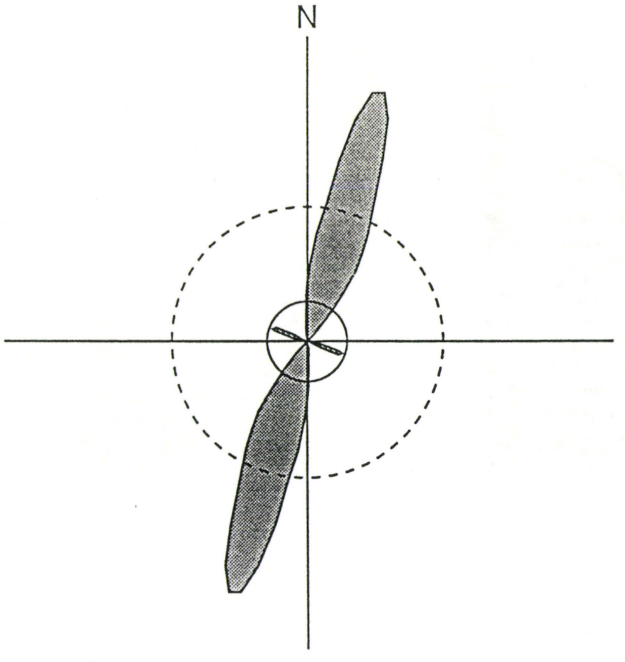

n = 13 E = 1.04 σ = 1.43 k = 100

Peak value = 6.92 Peak Orientation = 17.5°

——— E - - - - E ± 1.8σ

EAST STATIONS [1,8,10,11]

left-stepping zones

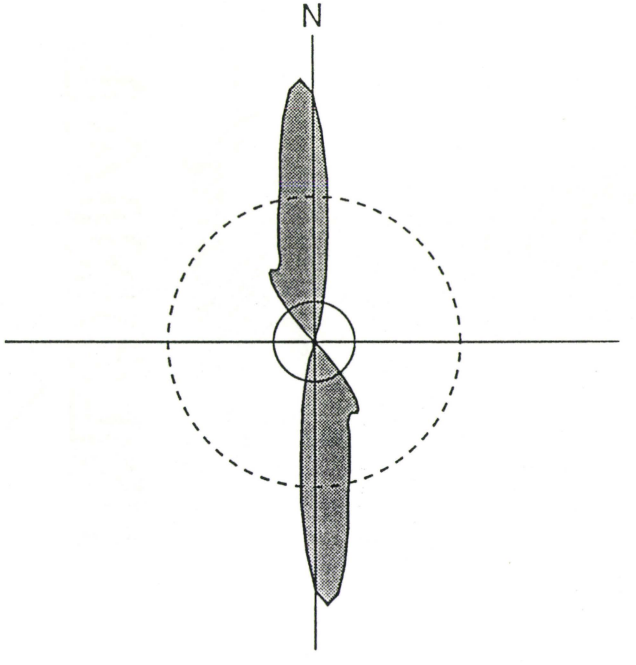

n = 12 E = 0.96 σ = 1.37 k = 100

Peak value = 6.21 Peak Orientation = 177.5°

——— E - - - - E ± 1.8σ

STATION 25

left-stepping fractures

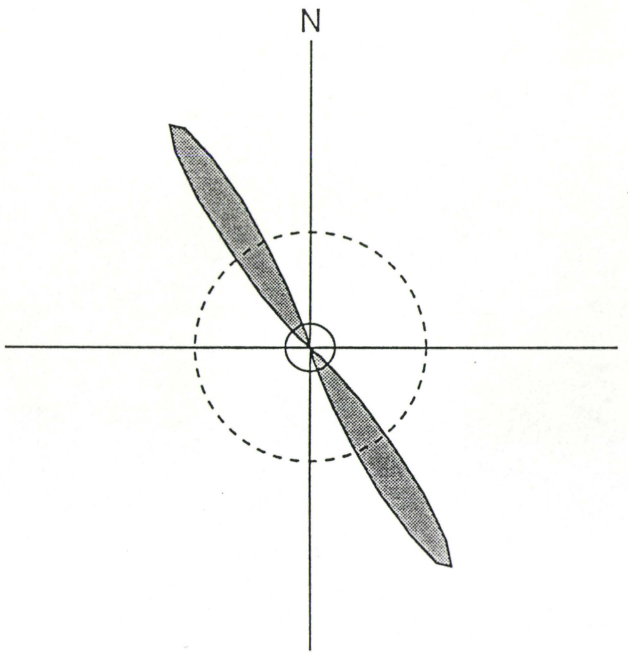

n = 6 E = 0.48 σ = 0.97 k = 100

Peak value = 5.03 Peak Orientation = 147.5°

——— E - - - - E ± 1.8σ

STATION 25

left-stepping zones

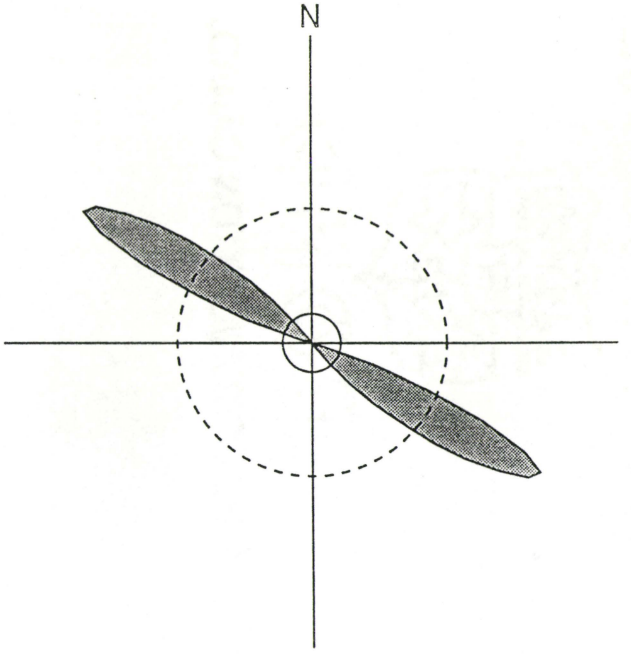

n = 6 E = 0.48 σ = 0.97 k = 100

Peak value = 4.36 Peak Orientation = 120.0°

——— E - - - - E ± 1.8σ

STATION 24

left-stepping fractures

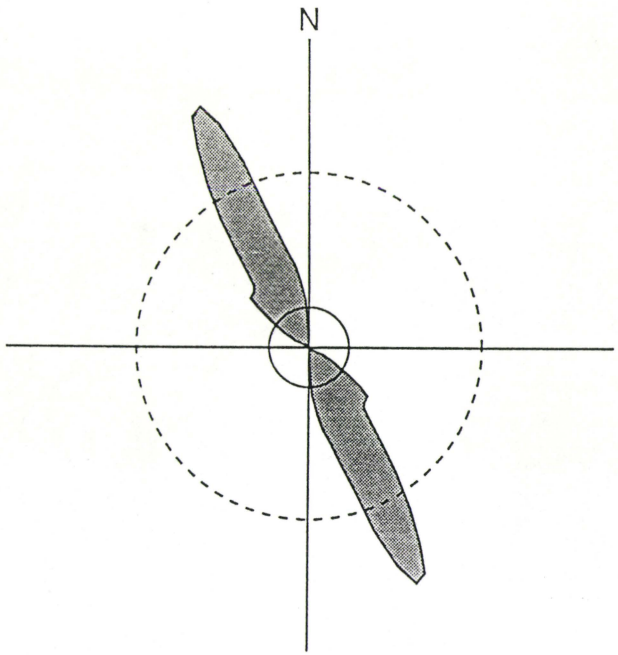

n = 7 E = 0.56 σ = 1.05 k = 100

Peak value = 3.70 Peak Orientation = 155.0°

——— E - - - - E ± 1.8σ

STATION 24

left-stepping zones

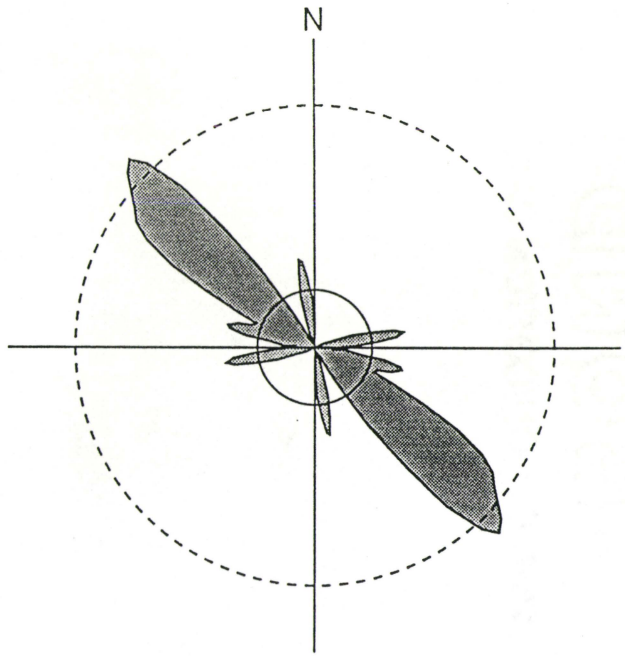

n = 8 E = 0.64 σ = 1.12 k = 100

Peak value = 2.90 Peak Orientation = 135.0°

——— E - - - - E ± 1.8σ

Appendix E

Orientations of Shear Zones, Shear Fractures and Isolated Fractures by Station

STATION 23

shear zones

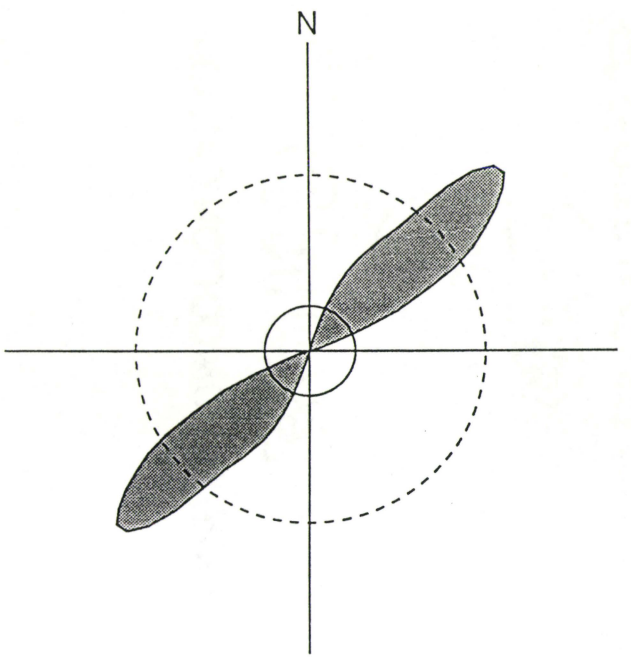

n = 10 E = 0.80 σ = 1.25 k = 100

Peak value = 4.58 Peak Orientation = 47.5°

——— E - - - - E ± 1.8σ

STATION 9

shear zones

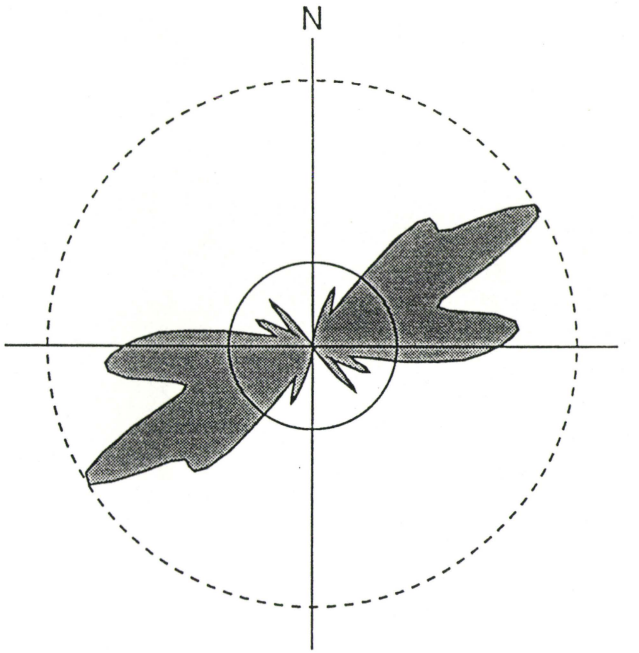

n = 17 E = 1.36 σ = 1.64 k = 100

Peak value = 4.27 Peak Orientation = 57.5°

——— E - - - - E ± 1.8σ

STATION 8

shear zones

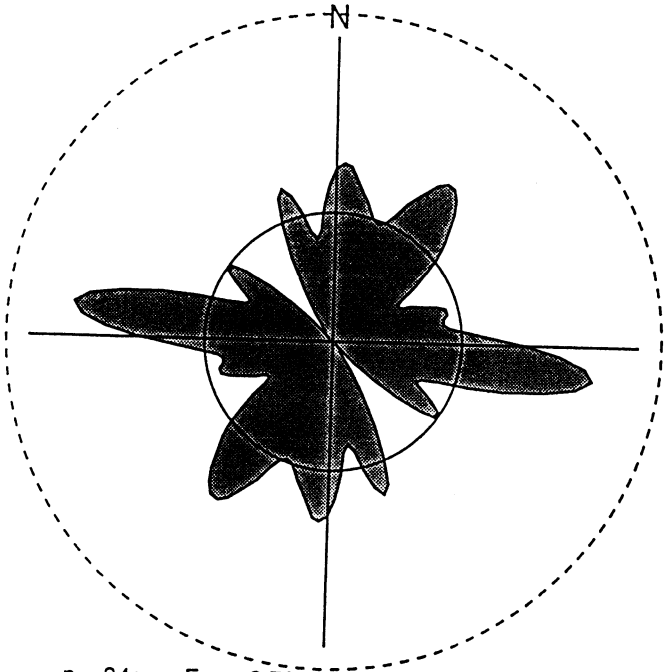

n = 34 E = 2.72 σ = 2.31 k = 100

Peak value = 5.50 Peak Orientation = 97.5°

—— E ---- E ± 1.8σ

STATIONS 12,13,14

shear zones

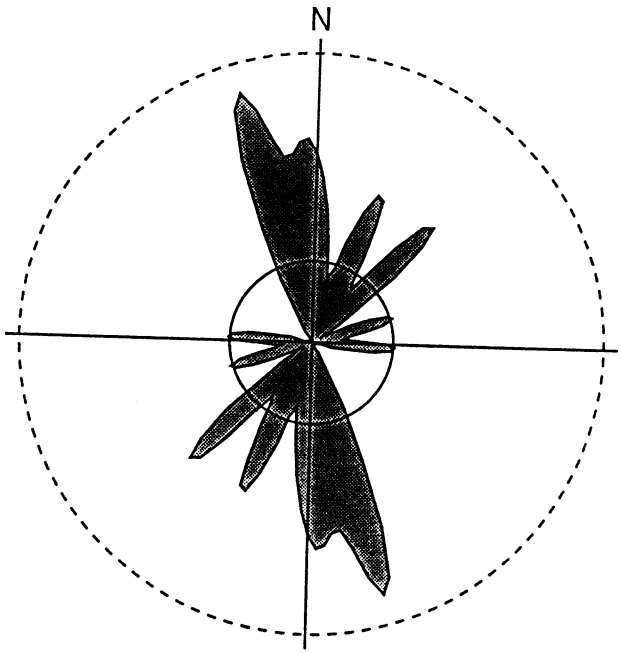

n = 12 E = 0.96 σ = 1.37 k = 100

Peak value = 3.09 Peak Orientation = 162.5°

—— E ---- E ± 1.8σ

STATION 17

shear zones

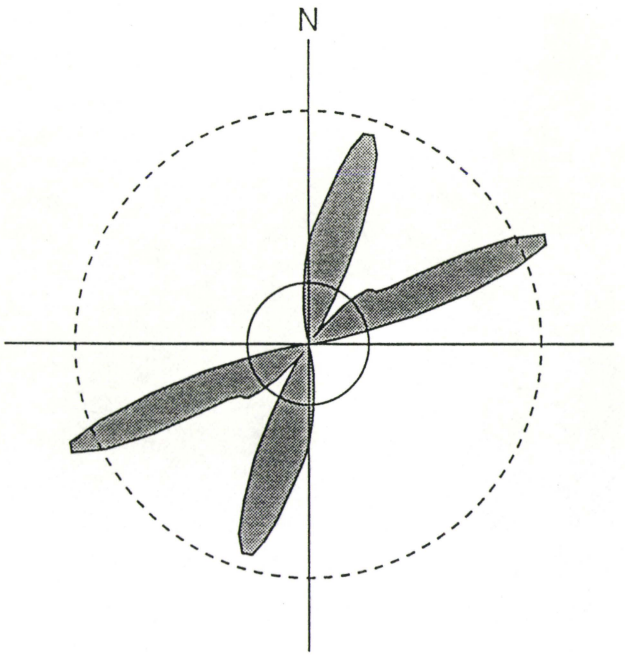

n = 10 E = 0.80 σ = 1.25 k = 100

Peak value = 3.43 Peak Orientation = 65.0°

——— E - - - - E ± 1.8σ

STATION 1

shear zones

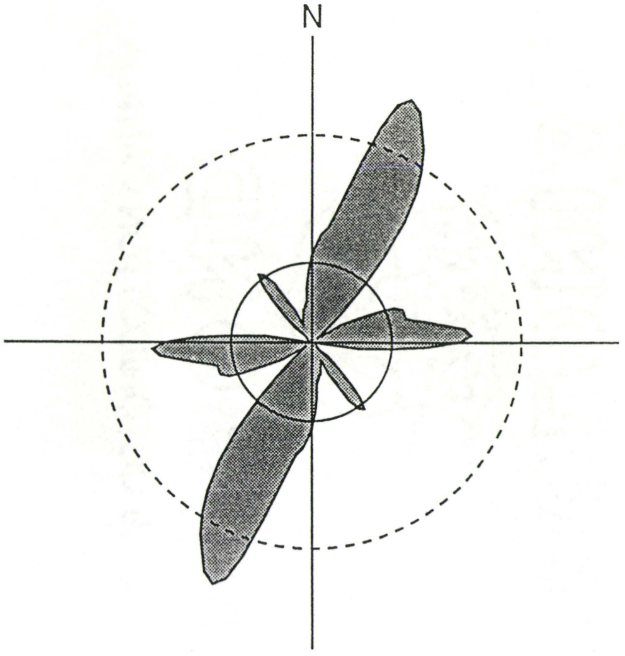

n = 31 E = 2.48 σ = 2.21 k = 100

Peak value = 8.14 Peak Orientation = 22.5°

——— E - - - - E ± 1.8σ

STATION 23

shear fractures

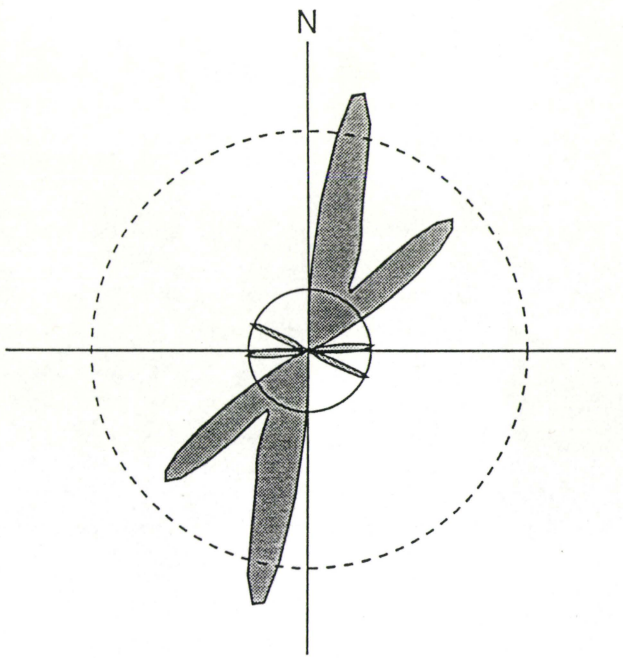

n = 12 E = 0.96 σ = 1.37 k = 100

Peak value = 4.12 Peak Orientation = 12.5°

—— E - - - - E ± 1.8σ

WEST STATIONS [6,20]

shear fractures

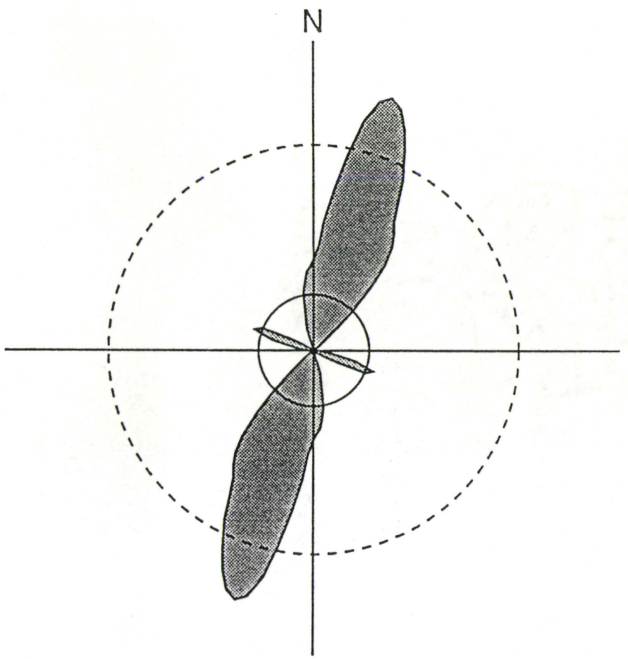

n = 11 E = 0.88 σ = 1.32 k = 100

Peak value = 4.17 Peak Orientation = 17.5°

—— E - - - - E ± 1.8σ

EAST STATIONS [1,8,9,10]

shear fractures

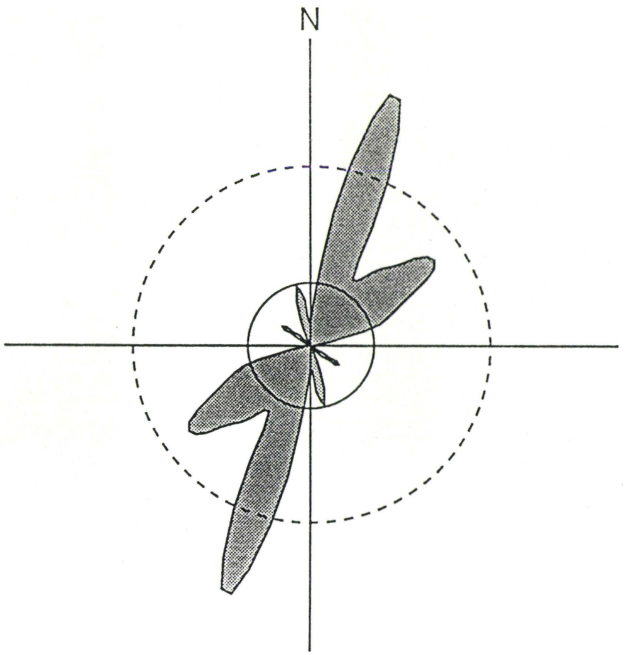

n = 23 E = 1.84 σ = 1.90 k = 100

Peak value = 7.75 Peak Orientation = 17.5°

——— E - - - - E ± 1.8σ

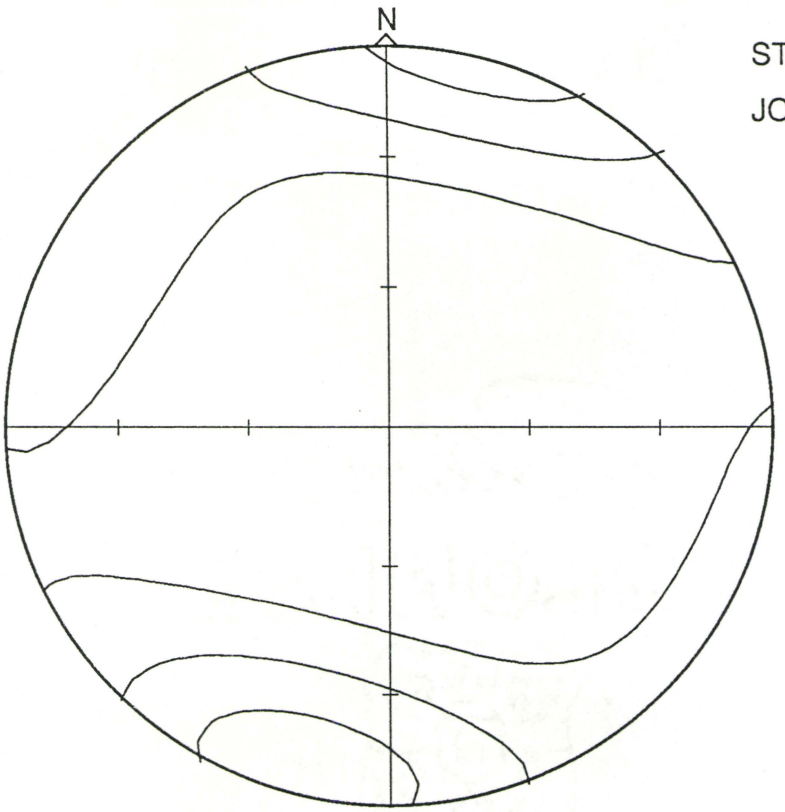

STATION 1

JOINTS

N 11
k 4.4
E 2.5
s 0.8
Peak: value 6.8
position 196°/ 4°

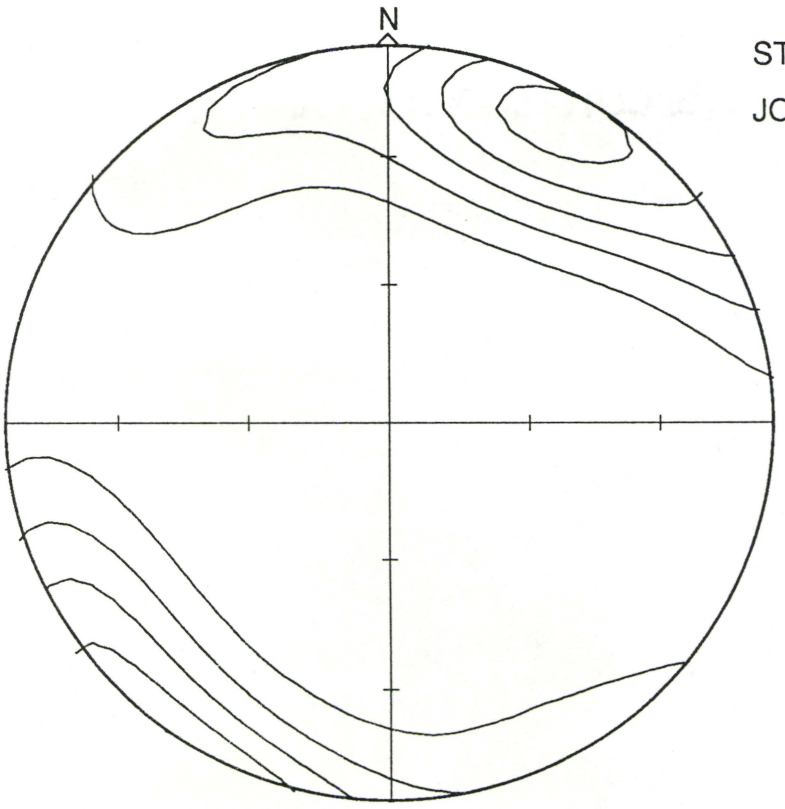

STATION 2

JOINTS

N 33
k 9.3
E 3.5
s 1.2
Peak: value 14.1
position 28°/ 8°

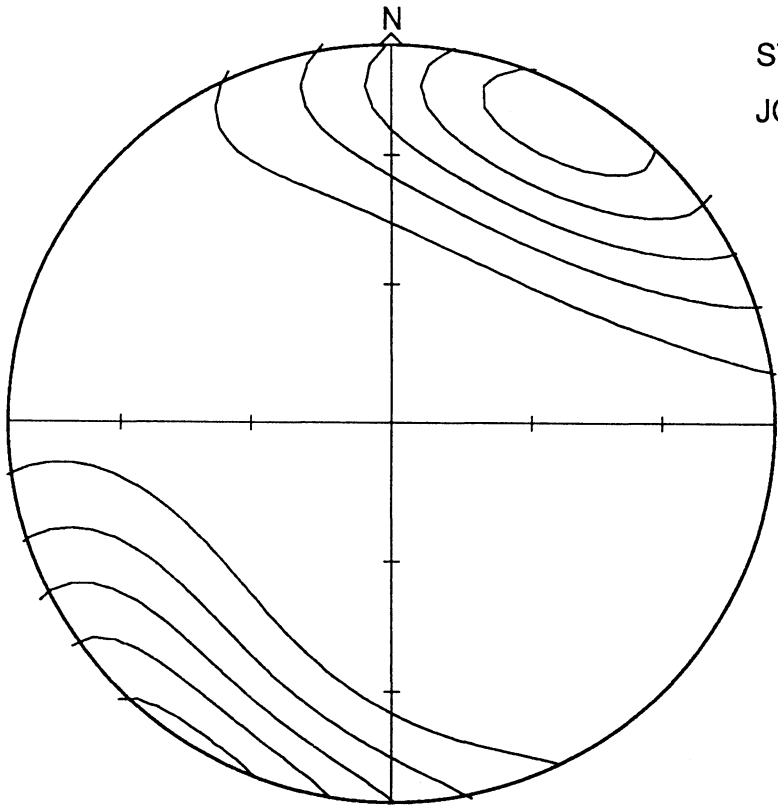

STATION 6

JOINTS

N 20
k 6.4
E 3.1
s 1.0
Peak: value 12.7
position 28°/ 8°

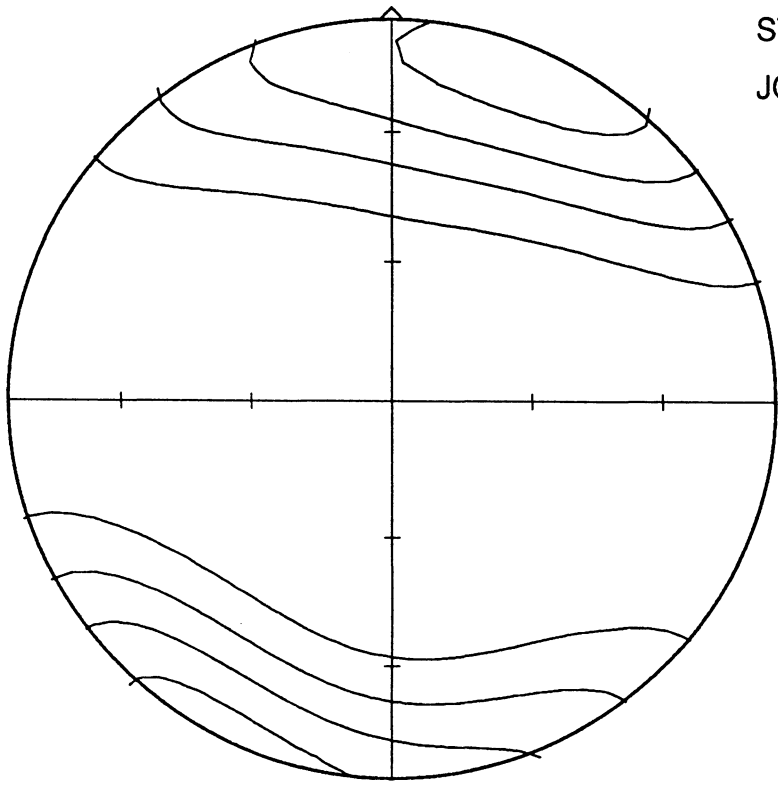

STATION 7

JOINTS

N 18
k 6.0
E 3.0
s 1.0
Peak: value 10.3
position 25°/ 5°

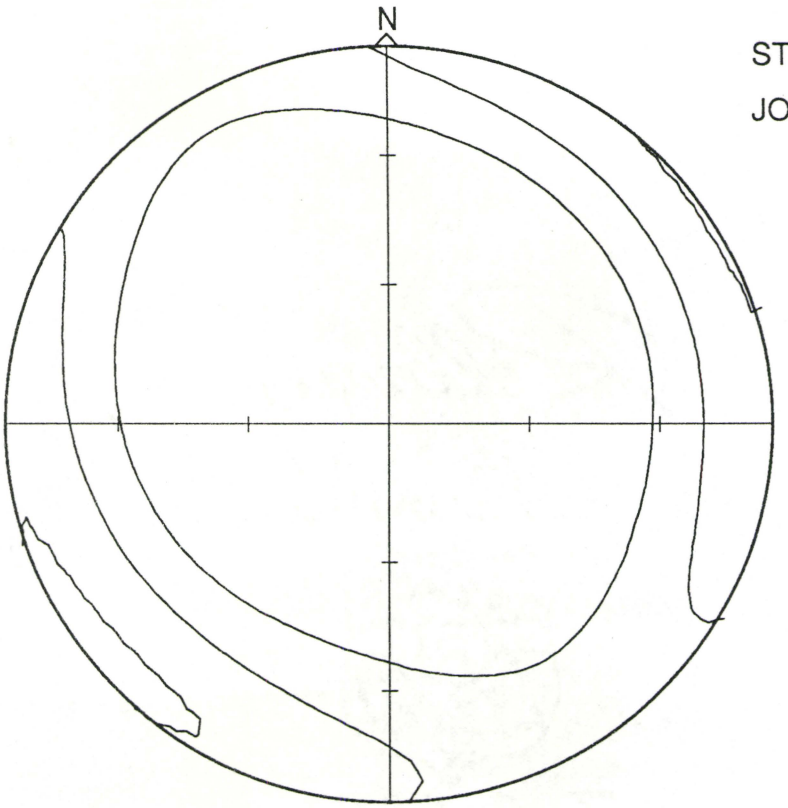

STATION 8

JOINTS

N 21
k 6.7
E 3.2
s 1.0
Peak: value 7.6
position 234°/ 4°

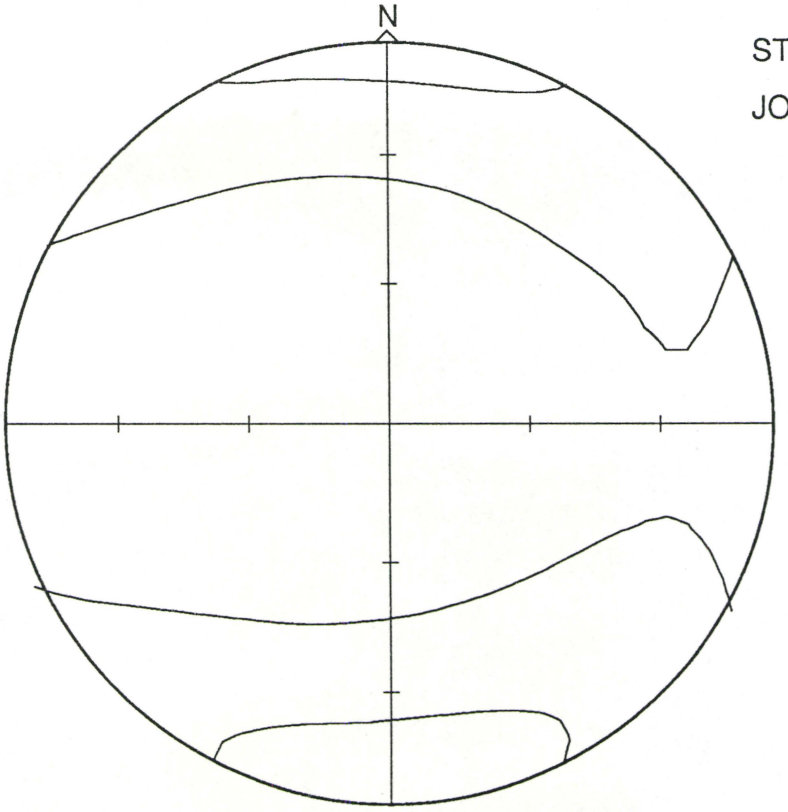

STATION 10

JOINTS

N 5
k 3.1
E 1.6
s 0.5
Peak: value 3.0
position 180°/ 6°

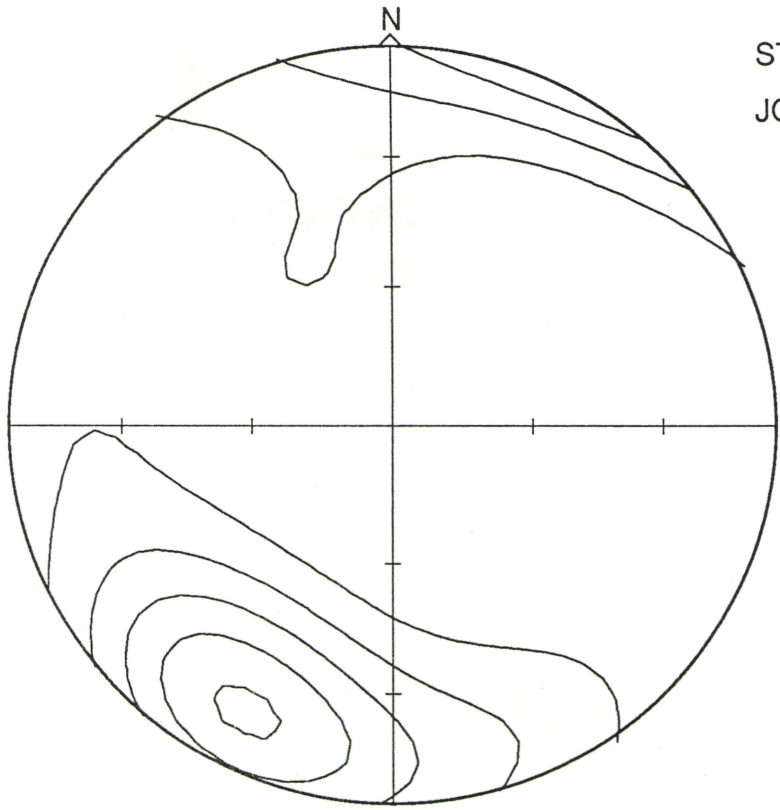

STATION 14

JOINTS

N 27
k 8.0
E 3.4
s 1.1
Peak: value 12.8
position 207°/ 14°

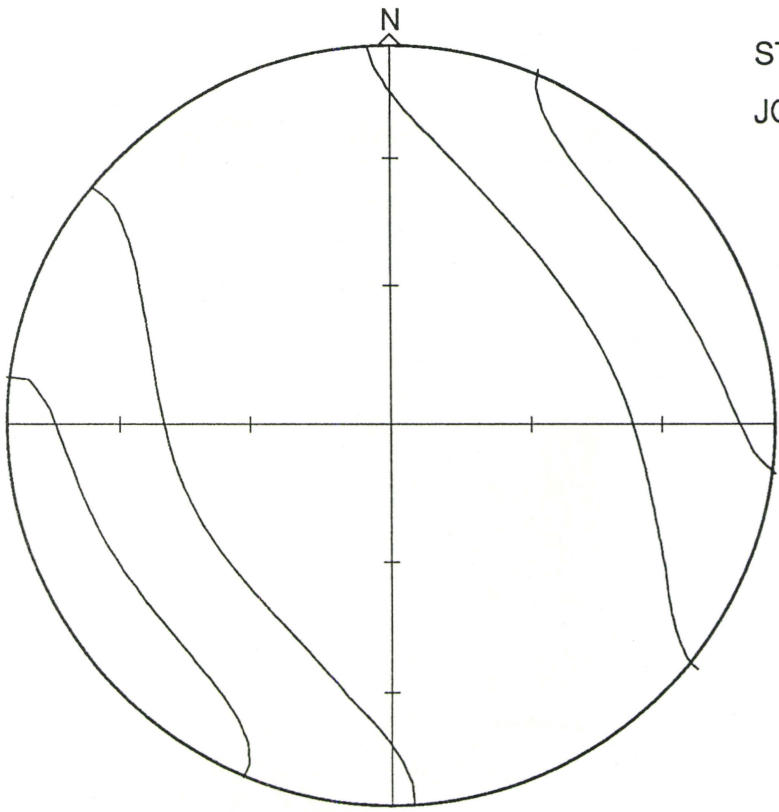

STATION 17

JOINTS

N 5
k 3.1
E 1.6
s 0.5
Peak: value 3.2
position 232°/ 1°

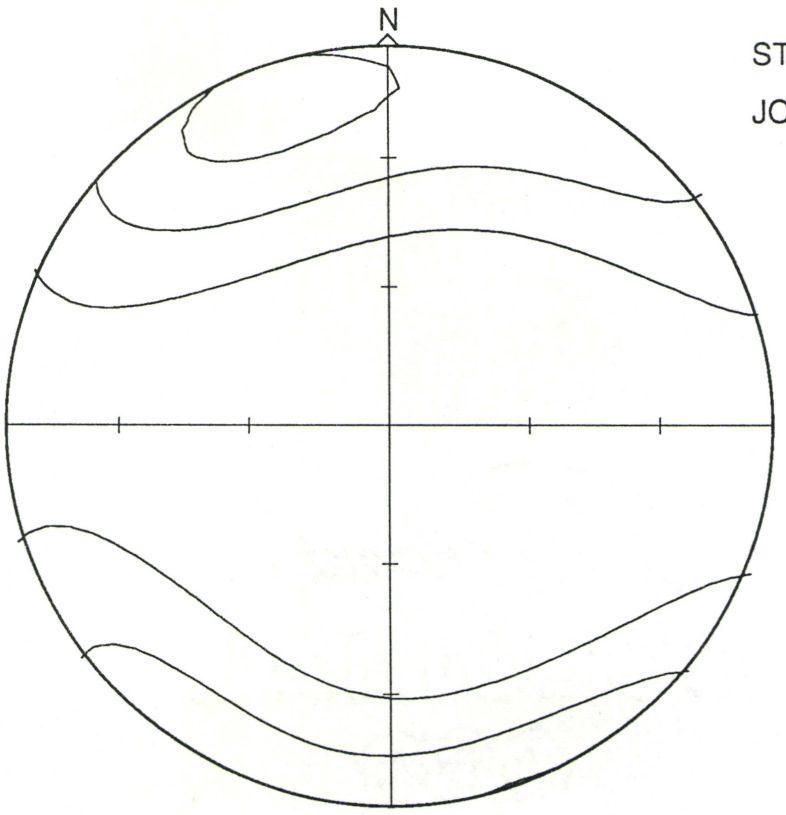

STATION 18

JOINTS

N 12
k 4.7
E 2.6
s 0.9
Peak: value 6.6
position 338°/ 11°

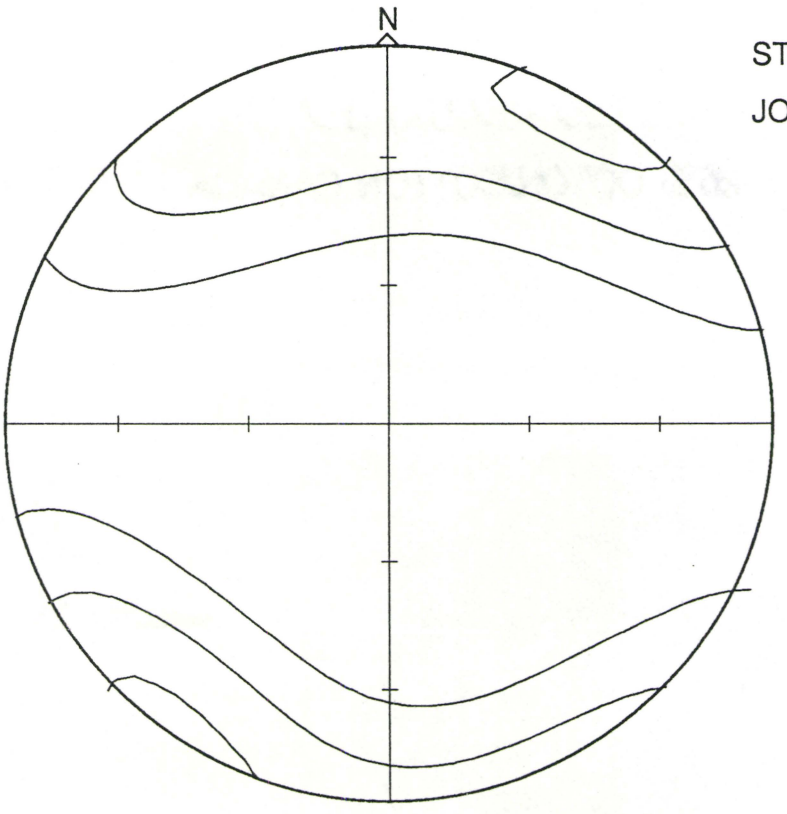

STATION 19

JOINTS

N 14
k 5.1
E 2.7
s 0.9
Peak: value 6.9
position 214°/ 0°

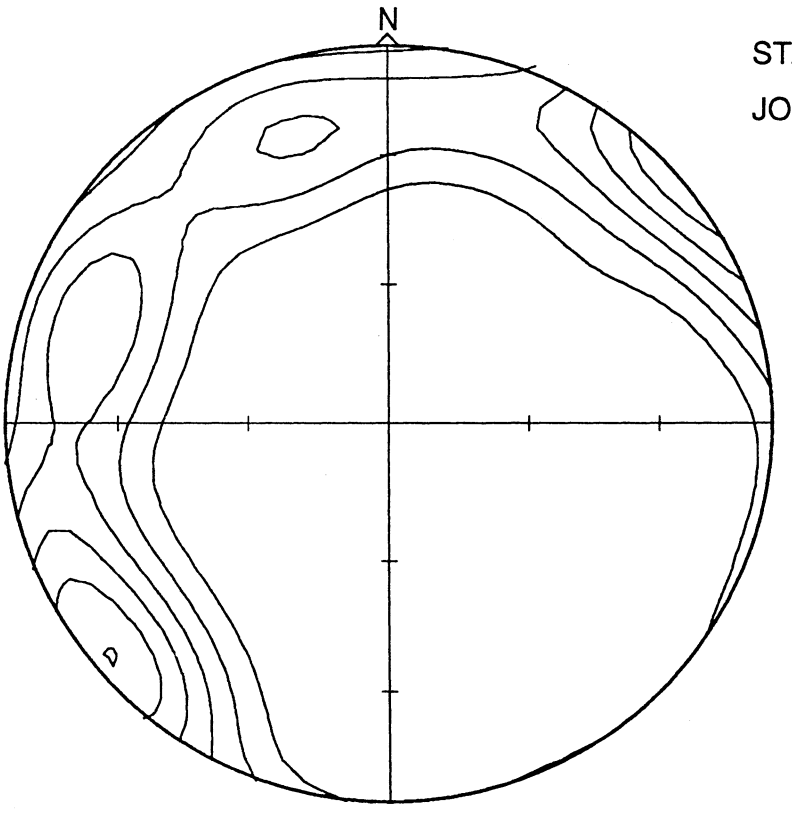

STATION 20

JOINTS

N 77
k 19.1
E 4.0
s 1.3
Peak: value 17.6
position 230°/ 6°

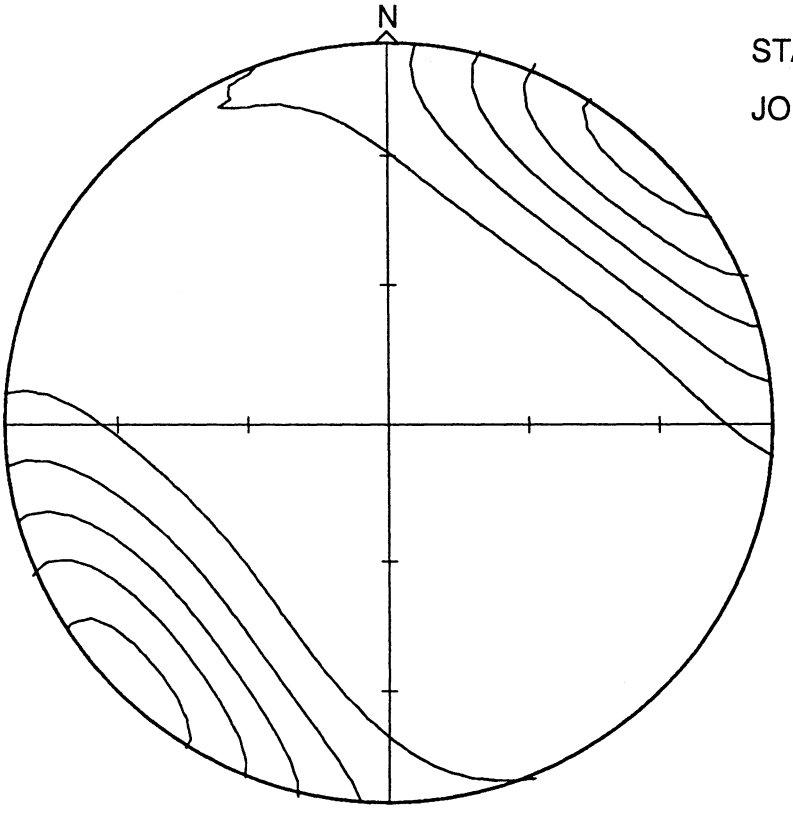

STATION 21

JOINTS

N 21
k 6.7
E 3.2
s 1.0
Peak: value 12.8
position 225°/ 2°

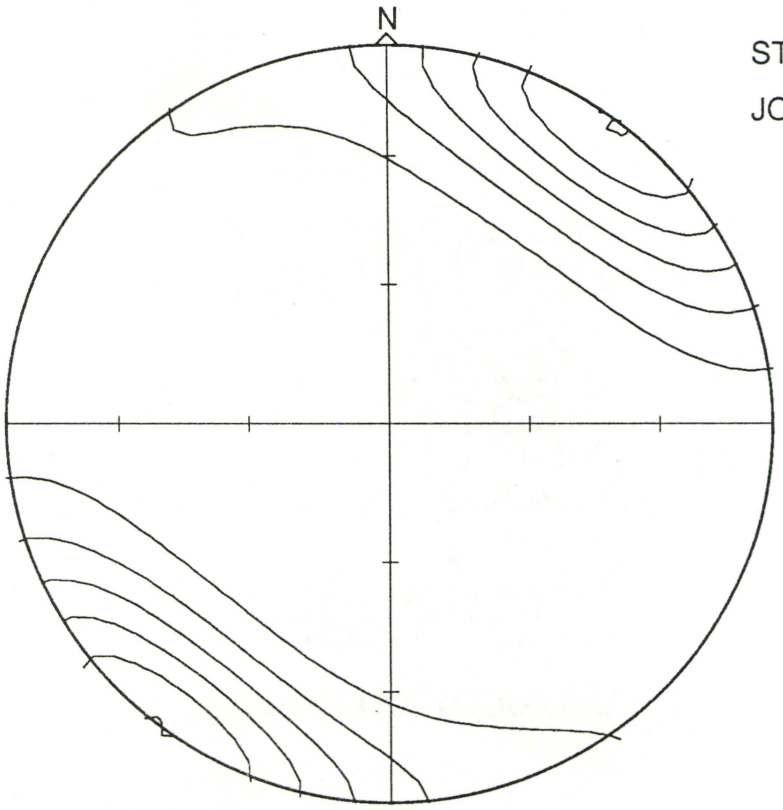

STATION 22

JOINTS

N 25
k 7.6
E 3.3
s 1.1
Peak: value 14.5
position 38°/ 1°

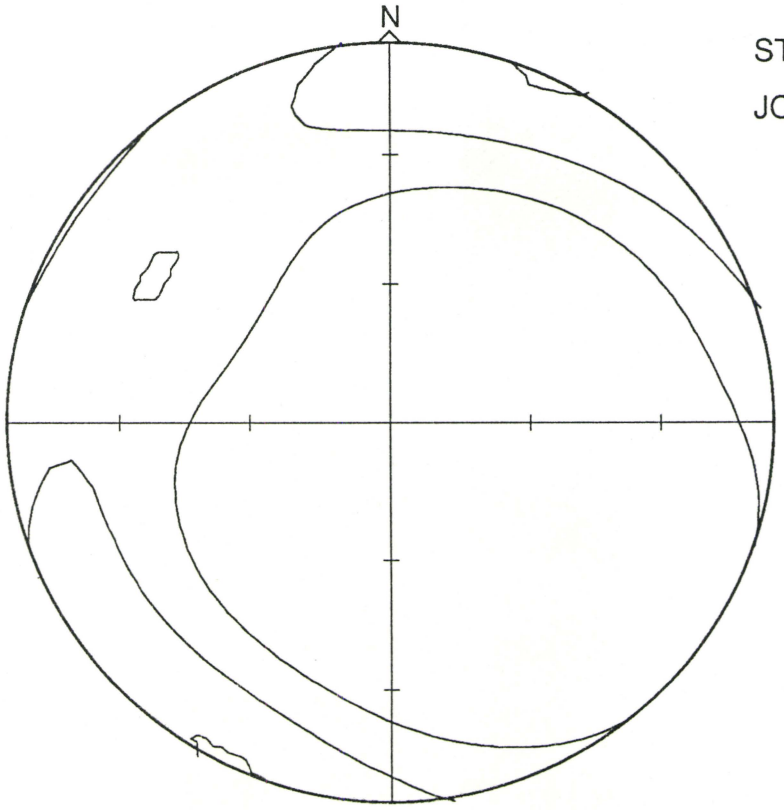

STATION 23

JOINTS

N 23
k 7.1
E 3.2
s 1.1
Peak: value 7.7
position 207°/ 1°

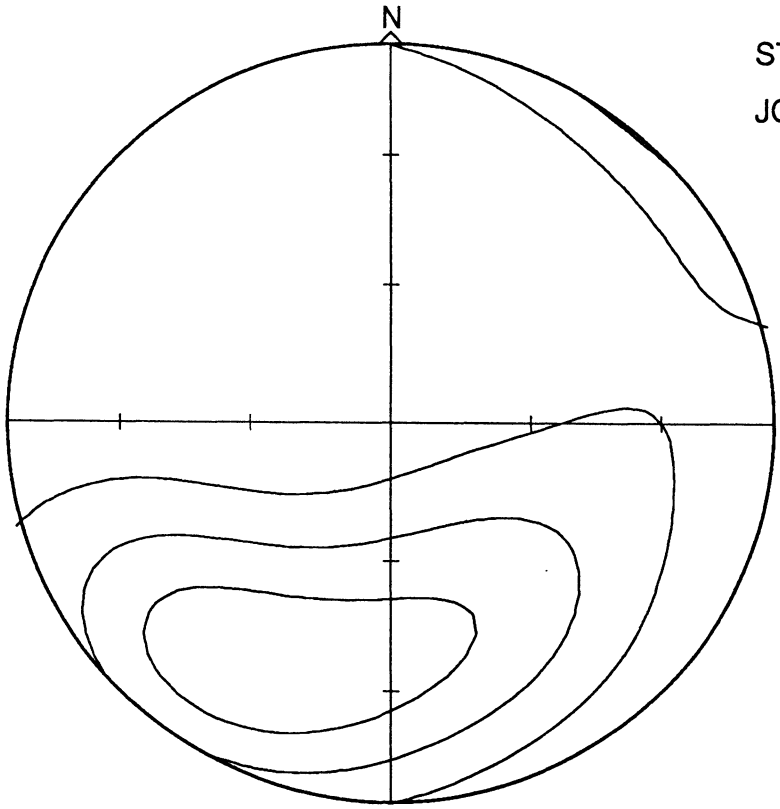

STATION 24

JOINTS

N 18
k 6.0
E 3.0
s 1.0
Peak: value 8.6
position 207°/ 26°

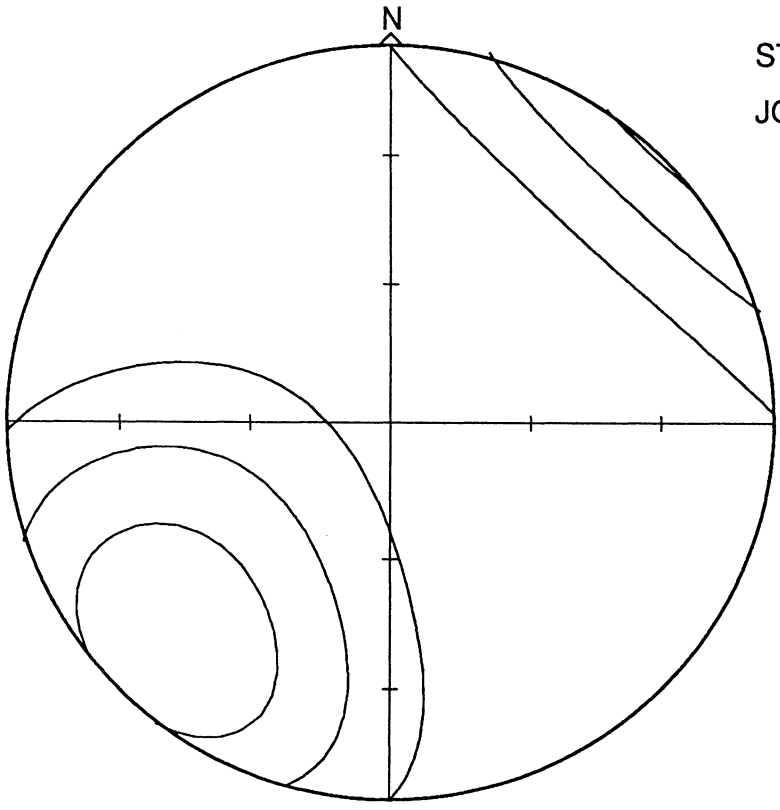

STATION 25

JOINTS

N 7
k 3.6
E 2.0
s 0.7
Peak: value 5.6
position 225°/ 23°